COMPUTER SIMULATION OF ONE-HANDED BACKHAND GROUNDSTROKES IN TENNIS

by

Behzat Bahadır Kentel

A Doctoral Thesis

Submitted in partial fulfilment of the requirements for the award of Doctor of Philosophy of Loughborough University

October 2008

ABSTRACT

Computer Simulation of One-handed Backhand Groundstrokes in Tennis

Behzat Bahadır Kentel, Loughborough University, 2008

A subject-specific, torque-driven, 3D computer simulation model with eight segments was developed to investigate the effects of different variables belonging to the racket and player on the wrist and elbow loadings in one-handed tennis backhand groundstrokes. Wobbling masses were included to represent soft tissue movement. The stringbed was represented by nine point masses connected to each other and the racket frame with elastic springs. There were twelve rotational degrees of freedom: three at the shoulder, two at the elbow, two at the wrist, three at the grip and two between the racket handle and racket head. Seven pairs of torque generators were used to control (via activation profiles) the joint angle changes in the model. An elite player was chosen to perform consistent and high standard backhand topspin strokes and a Vicon System was used to record the performances. The simulation model was matched to a typical performance by varying the activation profiles to minimize the difference between simulation and performance in terms of joint and racket angles. Once matched, the model variables in question were perturbed using single simulations with fixed activation profiles and the effect on the loading at the wrist and elbow observed along with the changes in kinematics. The results showed that off-centre impacts substantially increase the risk of injury by increasing the net torques at wrist by up to seven times. For a centre impact, maximum wrist flexion torque increased by up to 20% and 11% for a 20% decrease in moment of inertia and for a 20% increase in mass, respectively. Maximum wrist extension torque for an off-centre impact increased by 11% when the grip stiffness values were doubled. In contrast, the racket frame flexibility and soft tissue movement in the arm had negligible influence on the wrist and elbow. This study suggests that due to high torques obtained in the wrist extensors, the off-centre impacts below the longitudinal axis of the racket may be a substantial contributing factor for 'tennis elbow'. In the future, the model can be used for further investigations on the technique of the backhand stroke.

Keywords: backhand, simulation model, activation profiles, wrist loading, off-centre impacts, tennis elbow

ACKNOWLEDGEMENTS

I would like to express my gratitude to my supervisors Dr Mark King and Dr Sean Mitchell for their guidance and support throughout this study. I am also grateful to Head AG, Austria for their financial support.

I would like to thank past and present members of biomechanics research group (Fred, Matt, Veni, Jono, Pete, Andy, Sam, Lesley, Mike, Chris, Emma, Steph, Felix, Monique, Phil, Neil, Martin, Mickael) for their friendship. Special thanks to Sam and Lesley for proof-reading my thesis and to Jim May for participating in this study.

I also would like to thank Volkan and Bilge for their friendship and making an enjoyable life in Loughborough.

Finally, I wish to thank Aysu and my family for their never-ending love and constant support.

PUBLICATIONS AND AWARD

Conference Presentations:

Kentel, B. B., Mitchell, S. R., and King, M. A. (2006). "A muscle driven computer simulation model of the backhand shot in tennis". In M. Hiley, M. King, M. Pain, F. Yeadon (Ed.), *Proceedings of the Biomechanics Interest Group of the British Association of Sport and Exercise Sciences*, 22, Loughborough University, 2006, 8.

Kentel, B. B., King, M. A. and Mitchell, S. R., (2008). "The effect of off-centre impacts on loading at the wrist and elbow in tennis backhand strokes". *Gait & Posture*, Volume 28, Supplement 2, September 2008, Pages S38-S39. Abstracts of the XVII. Annual Meeting of ESMAC Antalya, Turkey.

Award:

Prof Tansu Arasil Best Presentation Award, XVII. Annual Meeting of ESMAC, 2008

DEDICATION

To Aysu

and

my family

Aysu' ya

ve

aileme

TABLE OF CONTENTS

LIST OF FIGURES

LIST OF TABLES

1 INTRODUCTION

1.1 Overview

Tennis is one of the most popular sports in the world. It is played and watched by millions of people throughout the world. The tennis industry is growing bigger and bigger every year. As the industry grows, more people begin to play tennis as a recreational sport and it turns out to be a more competitive game among professional tennis players. The Lawn Tennis Championship at Wimbledon in 2005 had more than 500,000 spectators and millions more watched on television and the total prize money was more than £10 million.

Many scientists work on developing new tennis equipment and new techniques to improve the performances of tennis players. Besides performance improvement, injury prevention is another area that researchers study extensively. Tennis injuries are very common; fortunately, most of the injuries in tennis do not affect the normal life of the players. Researchers investigate these injuries' pathology and aetiology to help tennis players avoid injuries or to find effective treatment methods.

Lateral epycondylitis, commonly known as 'tennis elbow', is one of the most frequent injuries in tennis. As such, it is a concern for tennis players, researchers and tennis equipment manufacturers. The incidence of tennis elbow among recreational players is very high, affecting nearly 50% of those players at some point (Carroll, 1981; Giangarra et al., 1993; Kelley et al., 1994). In addition, less acute elbow pain is experienced by nearly all tennis players in their tennis life to some extent. Tennis equipment manufacturers advertise their products by claiming their designs reduce the incidence of the injury, however, these claims generally lack scientific proof.

The cause and effects of tennis elbow have been studied by researchers for some considerable time. Despite decades of research, the aetiology of tennis elbow is still an enigma. Nevertheless, there is a general agreement on its pathology. Microtears and microtrauma, caused by excessive loading or overuse, occur in the wrist extensor muscle tendons where they attach to the lateral epycondyle of the humerus.

It is believed that technique has an important role on the incidence of 'tennis elbow'. Poorly performed one-handed backhand strokes of recreational players provoke the occurrence of 'tennis elbow' within these players (McLaughlin and Miller, 1980; Blackwell and Cole, 1994). Another factor that may contribute to the incidence of 'tennis elbow' is the off-centre impacts that cause high joint loadings (Hennig et al., 1992; Nesbit et al., 2006; Glynn, 2007). Since the generally accepted cause of tennis elbow is the overload of associated muscle groups (Kibler, 2002), the effects of the racket moment of inertia (Nesbit et al., 2006; Glynn, 2007) and grip tightness (Hatze, 1976) on the joint loadings were also investigated.

The factors that may increase the likelihood of injury may be classified into three groups: technique, equipment factors and physiology of the player. This study makes a substantial contribution to the ongoing investigation of equipment factors and technique in tennis elbow injuries by computer simulation modelling of backhand strokes.

1.2 Aim

The aim of this study was to investigate the effect of several variables of the equipment and the player on the wrist and elbow loadings in one-handed tennis backhand groundstrokes. It is also hoped that this study will contribute to understanding the causes of tennis elbow. To achieve this aim, a subject-specific 3D computer simulation model was developed. After evaluating the model, the variables considered were perturbed to observe their effects on the wrist and elbow loadings.

1.3 Research Questions

In connection with the aim of the study, a number of research questions were formulated:

What is the effect of ball impact location on the kinetics and kinematics of the wrist and elbow in one-handed tennis backhand groundstrokes?

The location of ball impact with the racket has a direct influence on the joint internal forces and torques as well as the joint kinematics. Hennig et al. (1992) stated off-centre impacts resulted in approximately three times increased load onto the arm which may contribute to the development of 'tennis elbow'. Glynn (2007) compared the effects of different variables such as stringbed tension, racket frame inertia and stiffness on elbow loading and found that among all variables impact location affected the loading at the elbow most. In addition, Nesbit et al. (2006) investigated more than one off-centre location on the longitudinal and the vertical axes of the racket for a forehand stroke. However, the simulation models used by Glynn (2007) and Nesbit et al. (2006) were angle-driven and therefore could not demonstrate the effect of impact on the kinematics of the arm for an impact location for which they lacked motion data. In addition, due to constraining the motion it is likely that angle-driven models over estimate internal loadings due to noisy kinematic data. Moreover, Nesbit et al. (2006) used a rigid connection between racket and hand which might give unrealistic results as the rotation of the racket and the impact force is directly transferred to the hand.

Therefore, a simulation model using forward dynamics with a satisfactory hand-racket interaction is needed to investigate the effects of the off-centre impacts on the kinetics and kinematics of the wrist and elbow.

What is the effect of the physical properties of the racket on the kinetics and kinematics of the wrist and elbow in one-handed tennis backhand groundstrokes?

It is well known that physical properties of the racket, including mass, moment of inertia, viscoelastic parameters of the racket frame and stringbed tension, affect the behaviour of the racket and therefore the tennis player. Racket companies produce rackets with different inertial properties for elite players and recreational players. Although there are several studies investigating the effects of the physical properties of the racket on the game (Mitchell et al., 2000a), the effects on the wrist and elbow loadings are documented in the literature only in limited numbers.

Nesbit et al. (2006) stated that inertia values had a moderate effect on pronation / supination torques for forehand motion. In addition, Glynn (2007) compared two rackets with different inertial properties; although consistent results were found with the study of Nesbit et al (2006), relatively small effects on elbow

and wrist loadings were presented. It is generally accepted that using lower string tensions in the racket results in higher outbound ball velocity and higher contact time with lower maximum impact force. Glynn (2007) reported that low-tension rackets had lower elbow loadings. Miller (2006) stated that modern rackets are stiffer than the old wooden ones to consume less energy at impact for bending the racket but increased stiffness causes the racket to vibrate faster which has been proposed to be one of the causes of 'tennis elbow'. However, Glynn (2007) showed that there was no substantial relation between the racket frame stiffness and joint loadings. This study will aim to address these effects with a torque-driven simulation model.

What is the effect of the soft tissue movement on the kinetics and kinematics of the wrist and elbow in one-handed tennis backhand groundstrokes?

Multibody models generally consist of rigid link segments connected with revolute joints. However, since the human body is not rigid this assumption might give unrealistic results. Wobbling mass and rigid body models of drop jumping have been compared by Gruber et al. (1998) and Pain and Challis (2006). Considerably less joint torques were found for the wobbling mass model than the rigid body model in both studies. Glynn (2007) recently used wobbling masses in a backhand simulation model to increase the accuracy of the model. Therefore, wobbling masses will be used in this study in order to have better accuracy and the effects of wobbling masses on the joint loadings will be investigated.

What is the effect of the grip tightness on the kinetics and kinematics of the wrist and elbow in one-handed tennis backhand groundstrokes?

Hatze (1976) investigated the effects of the grip tightness and reported that a tight grip will increase the power of the stroke and the magnitude of the vibrations transmitted through the hand while for a loose grip, the power of the stroke and the vibrations transmitted to the hand are decreased. He stated that with players using a tight grip and complaining of lateral pain, there might be a connection between having a tight grip and the development of 'tennis elbow'.

Snijders et al. (1987) develop a biomechanical model of the forearm and hand to investigate the effects of the power grip on provocation of 'tennis elbow'. They

concluded both the finger flexors and the wrist and finger extensors were activated during grasping and these activations increased with increasing grasping forces.

In this study, the effects of the grip on the wrist flexion / extension torque during a backhand stroke will be investigated in order to consider whether grip tightness may be a contributing factor for 'tennis elbow'.

What is the effect of the wrist configuration at impact on the kinetics and kinematics of the wrist and elbow in one-handed tennis backhand groundstrokes?

It is generally accepted that bad technique or improper backhand strokes may provoke the incidence of 'tennis elbow' by causing high loading on wrist extensors. Since wrist extensors are responsible for wrist extension, many studies have been focussed on the wrist motion during the backhand stroke (Blackwell and Cole, 1994; Knudson and Blackwell, 1997). Although investigation of the wrist flexion / extension motion during backhand strokes have generally been accompanied by EMG of wrist extensors in the literature, the wrist and elbow kinetics have not been involved most of the time. In this study, the loadings on the wrist and elbow will be investigated for different wrist flexion angles at impact. In the future, the effect of not only the wrist but also other joint angles may be considered using the simulation model.

What is the effect of the inbound ball velocity on loadings at the wrist and elbow?

In the literature, there is little published work on the effects of ball velocity on joint kinetics and kinematics. Chow et al. (1999) showed that muscle activation increases with increased ball incoming velocity. This increase in activation may result in a faster backhand stroke as well as a tighter grip. A faster stroke results in much higher ball velocity relative to the racket. Since higher impact forces are obtained from higher ball incoming velocity (Cross, 1999b), it is believed that higher joint torques and forces occur during an impact with a faster incoming ball velocity. This study will address this statement and investigate the effect of inbound velocity on wrist, and elbow loading.

1.4 Thesis Outline

This study consists of eight chapters. After the introduction chapter the outline of the thesis is as follows:

Chapter 2 covers an extensive review of literature in three main parts. Firstly, tennis-related subjects are presented, secondly examples of upper extremity models found in the literature are described, finally, the investigation of different techniques is considered.

The development of the simulation model is presented in Chapter 3. After an overview of the simulation model presenting the main features of the model, details of the development of the model elements including player, racket and ball are described.

Chapter 4 describes the performance data collection of tennis backhand strokes and their analysis. The methods and protocol used during the performance data collection and the extraction of joint angles from the collected motion data are presented in detail.

The determination of the subject-specific model parameters and equipment parameters are described in Chapter 5. The subject-specific parameters including torque-strength, inertia and wobbling mass viscoelastic parameters are determined either from experimental results or from an angle-driven version of the model developed in Chapter 3.

In Chapter 6, the torque-driven model of backhand strokes developed in Chapter 3 is evaluated using kinematic data analysed in Chapter 4. This includes matching the performance data of an elite tennis player with the computer simulation results. The evaluation process is completed after finding a set of parameters which give good matching results for both centre and off-centre impacts.

Chapter 7 presents the applications of the model evaluated in Chapter 6. To fulfil the research questions mentioned in Chapter 1, results of the perturbations of the model variables are presented.

Finally, in Chapter 8 a discussion of the results of the study is provided. A general discussion about the study and the conclusions derived are presented with the recommendations for future studies.

2 LITERATURE SURVEY

The literature review is divided into three main parts. The first part includes tennis related subjects: modelling tennis equipment and tennis strokes, upper extremity muscle groups used during playing tennis and 'tennis elbow'. In the second part, after a brief summary of anatomy and physiology of upper extremity its models are presented. Finally, in the last section, the development and evaluation of simulation models and parameter determination are considered.

2.1 Tennis Related Literature

To improve performance of the players and injury prevention researchers have conducted many studies on players and tennis equipment. Characteristics of the tennis racket and ball and their effect on the game have been examined in numerous studies. The impact of the tennis racket and ball is a complicated phenomenon, but can be analysed in a relatively simple way by modelling the racket and ball. The following sections give a brief summary of previous studies on kinematics and kinetics of tennis strokes and explanations of tennis racket characteristics and modelling techniques of ball and racket.

2.1.1 Kinetics and Kinematics of Tennis Strokes – Brief Summary

Many studies have been performed on the kinetics and kinematics of tennis strokes. Giangarra et al. (1993) detailed the anatomical positions of the elbow and wrist during single- and double-handed backhand strokes from preparation phase to late follow-through phase with cinematographic analysis.

Kelley et al. (1994) performed another cinematographic analysis to compare the strokes of normal players and injured players with tennis elbow. Kelley et al. (1994) observed some deviations in the injured players. These deviations were as follows: a 'leading elbow' with the olecranon pointing at the net and the shoulder elevated and internally rotated, wrist flexion in the early phases with an abrupt change to extension at ball impact, exaggerated wrist pronation that produces an

'upward tilting' racket face at ball impact. (Refer to section 2.2.2 for the anatomical detail.)

Players with and without tennis elbow were also compared by Knudson and Blackwell (1997). They measured wrist and elbow angular kinematics at impact in one-handed backhand strokes. The players were divided into three groups: professionals with no tennis elbow history, intermediates with no tennis elbow history, and intermediates with a history of tennis elbow. No substantial differences were found in elbow angular kinematics before or after impact, but a substantial difference was observed in wrist angular velocity after impact between professional players (4.04 rad/s extension direction) and intermediates with tennis elbow (0.42 rad/s flexion direction).

Blackwell and Cole (1994) investigated the difference in backhand technique of novice and expert players. It was stated that during impact of the tennis ball with the racket, expert players extend their wrist at an average of 0.41 rad. On the other hand, novice players hit the ball with their wrist flexed at an average of 0.22 rad. During impact, the direction of wrist rotation is opposite for the two groups, as well. The impact occurred with a wrist angular velocity of 1.69 ± 1.41 rad/s in the extension direction for expert players and a wrist angular velocity of 2.76 ± 2.5 rad/s in the flexion for the novice players.

In another study comparing expert and novice players, Riek et al. (1999) found similar results to Blackwell and Cole (1994). During impact, both groups began movement with the wrist extended. The novice group moved their wrist into flexion before impact whereas the wrist position of expert players remained extended. The radial/ulnar deviation showed differences between the two groups as well. Novice players kept their wrist ulnar deviated during the whole impact period and had a higher peak of ulnar deviation after impact. Expert players had their wrist radially deviated before impact. At the moment of impact they moved their wrist towards ulna but never reached the value of the novice players at any time after the impact.

Hatze (1976) investigated forces on the racket during and after the ball and racket impact by means of a mathematical model of the racket system. A relationship between ball velocity and impulsive forces on the racket was found experimentally (Equation 2.1):

$$F(v) = 14.4v^{1.221} \text{ N}, \quad \text{for} \quad 0 \leq v \leq 34.1 \text{ m/s} \qquad (2.1)$$

However, this relationship was said to be true only if the torque applied to the handle of the racket was assumed to be zero.

Loads on the forearm prior to impact in tennis strokes were investigated by McLaughlin and Miller (1980). The backhand strokes of a professional player were recorded in the study. The player performed backhand strokes with his regular style and also simulated a beginner's style. Within these two types of strokes, the magnitude of the linear acceleration of the racket mass centre was found to be greater for the regular stroke style of the player in all directions. As a consequence of this, magnitudes of wrist moments in extension, radial/ulnar deviation and supination directions were found to be larger for the regular style backhand stroke.

The forces on the thenar and hypothenar eminences of the hand were examined by Knudson (1991). Advanced and intermediate players were used in the study. There was no significant difference found between the mean post impact peak forces on both thenar and hypothenar of the hand of these groups. However, forces in the thenar eminence in preparation for impact were significantly larger for advanced players (40 ±11 N) than intermediate players (21 ± 5 N). Knudson (1991) claimed that this lower thenar forces of intermediate subjects may provide less resistance to the acceleration of the racket created by the ball impact.

2.1.2 Upper Extremity Muscles Predominantly Used in Tennis

As muscles are responsible for human movement, their strength and endurance is very important in sports where higher levels of motion of the body or its parts are needed. Different muscle groups work for different movements and determination of these muscles can provide useful information to both coaches and players.

To be a good tennis player strength, muscular endurance, flexibility, coordination and agility are all necessary (Roetert, 2000). Throughout a tennis match, players run on the court and make hundreds of strokes. During these strokes, their body moves in various ways with different muscular actions. Determining the

major muscle groups, which are involved in different kinds of strokes, can be used to increase performance and help injury prevention.

Generally, the muscle groups used in trunk rotation and push-off actions for each stroke are the same. However, according to the stroke, muscles used in the swing phase can be different. For instance in a forehand drive and volley, anterior deltoid, pectoralis major, shoulder internal rotators, biceps and serratus anterior are the major muscle groups that are used. Muscles used in backhand drive and volleys are rhomboids, middle trapezius, posterior and middle deltoid, shoulder external rotators, triceps and serratus anterior. In addition to these, in the non-dominant side of a two-handed backhand drive pectoralis major, anterior deltoid and shoulder internal rotators are used (Roetert, 2000). Van Gheluwe and Hebbelinck (1986) added latissimus dorsi and infrasupinatus in forehand drive and volley, especially during impact. Chow et al. (1999) stated that pectoralis major and triceps activated during the forward swing phase of both forehand and backhand strokes in order to help move the arm forward. However, of these muscles, triceps is much more active in backhand whereas, pectoralis major is more active in forehand strokes.

The above muscle groups are responsible for the motion of the pectoral girdle and the arm. For the motion of the wrist and gripping the racket during the strokes, wrist and finger extensors and flexors are activated as well as pronator teres and supinator, which make the pronation/supination motion. In general, the extensor carpi radialis is more active than the flexor carpi radialis during the backhand strokes (Giangarra et al., 1993; Blackwell and Cole, 1994; Kelley et al., 1994; Chow et al., 1999). Increased activity of extensor carpi radialis brevis, extensor carpi radialis longus and extensor digitorum communis muscles during the acceleration phase of both one and two-handed backhand strokes is shown by Giangarra et al. (1993) and Kelley et al. (1994).

2.1.3 Tennis Elbow

Introduction

Millions of people play tennis around the world. It is played by all age groups and generally no severe medical problems occur during playing tennis. However, injury occurrence in competitive tennis players is quite common. Up to 90% of

players reported an injury in the 12 months prior to interview in different studies performed on injury patterns (Kibler, 2002). The major cause of these injuries in the aforementioned studies seemed to be microtrauma repetitive overload. Occurrence of upper extremity injuries is reported as 20% by Reece et al., (1986), and as 27% by Hutchinson et al. (1995).

Shoulder injuries are very common in tennis. The common cause of all shoulder injuries is repetitive microtrauma. Rotator cuff injuries and shoulder instability are the most common injuries occurring at the shoulder (Altchek, 2002). Hand and wrist injuries are less common than shoulder and elbow injuries, but there can be tendon injuries, extensor carpi ulnaris problems, ulnar carpal impingement and hook of the hamate fractures in wrist and hand during tennis (Retlig, 2002).

The incidence of injuries at the elbow were reported from 4% to 15% of all tennis injuries in four different studies (Kibler, 2002), although nearly 50% of players suffer from elbow pain (Carroll, 1981; Giangarra et al., 1993; Kelley et al., 1994). Elbow injuries are generally of overuse type. Lateral epicondylitis, medial epicondylitis, posterior tennis elbow and elbow instability are some of the injuries that occur in the elbow (Renstrom, 2002). The most common injury at the elbow is lateral epicondylitis, which is also known as tennis elbow. Up to 85% of elbow injuries arise from the lateral epicondyle (Giangarra et al., 1993; Kelley et al., 1994). The frequency of tennis elbow (and elbow pain) among players makes it very important in the tennis world.

Lateral epicondylitis was first described by Runge in 1873 (Snijders et al., 1987; Renstrom, 2002; Santini and Frostick, 2002) and it was called 'writer's cramp'. Later the name was changed to 'washer woman's elbow' (Snijders et al., 1987; Renstrom, 2002) and 'lawn tennis elbow' (Bauer and Murray, 1999; Nirschl and Ashman, 2003). Since it is clearly associated with tennis, it was soon called 'tennis elbow'. However only 5% of people suffering from tennis elbow are tennis players (Bauer and Murray, 1999; Renstrom, 2002). The symptoms of tennis elbow can occur during screw-driving, writing, wringing of laundry, etc. (Snijders et al., 1987). Besides tennis players, tennis elbow can also be seen in carpenters, dental technicians and computer operators (Bauer and Murray, 1999).

Anatomy

Tennis elbow occurs at the lateral epicondyle, the projection or knuckle at the lateral side of the humerus. Muscles used for wrist extension are connected to the lateral epicondyle via tendons. There is a common attachment point (common extensor origin) for most of the extensors of the wrist and fingers. These wrist extensors are extensor carpi radialis brevis (ECRB), extensor carpi ulnaris (ECU), extensor digitorum communis (EDC) and extensor digiti minimi. Another muscle, extensor carpi radialis longus (ECRL) is often fused with ECRB and attached to the lateral supracondylar ridge, a little above the lateral epicondyle (Snijders et al., 1987; Jenkins, 2002; Shier et al., 2002). All these muscles are located in the forearm. Their long tendons insert on the metacarpals or phalanges. The main actions of these muscles are extension of the wrist and fingers. ECRL and ECU also deviate the wrist in the radial and ulnar direction, respectively.

Aetiology

The exact aetiology of tennis elbow is not understood, but there is a general agreement that excessive or over use of wrist extensors causes microtrauma and microtears on the tendons of these muscles. Although any of the common extensor origin tendons can be affected from overuse and repetitive stress, the ECRB tendon is the most frequently affected one among them (Snijders et al., 1987; Giangarra et al., 1993; Blackwell and Cole, 1994; Kelley et al., 1994; Bauer and Murray, 1999; Riek et al., 1999; Renstrom, 2002; Maffulli et al., 2003; Nirschl and Ashman, 2003). In some cases of tennis elbow, these micro tears occur on the EDC tendon instead of ECRB (Giangarra et al., 1993; Renstrom, 2002; Nirschl and Ashman, 2003). Bauer and Murray (1999) claim that ECRB has a poor biomechanical design with respect to other wrist extensor muscles. The tendon of the ECRB is very short and wide (Blackwell and Cole, 1994). Therefore, ECRB muscle is mostly identified in tennis elbow injury. High tension levels in the ECRB may also cause tennis elbow and morphological changes occur in the ECRB of people with longstanding tennis elbow (Ljung et al., 1999) further strengthening this association.

The symptoms of tennis elbow can be sudden or gradual. Mostly, there is a repetitive activity or overuse. Playing tennis intensively or going back to tennis after a period of no activity can be good examples. A palpable tenderness can be felt over the lateral epicondyle. This tenderness is localized over the origin of the ECRB

tendon. The pain at the elbow persists from 1 week to 18 months with a mean of 36 weeks (Renstrom, 2002).

Diagnosis of tennis elbow is not very hard. The 'coffee cup test' (picking up a full cup of coffee), wrist extension and middle finger extension tests can be used for diagnosis. The wrist extension test produces pain at the elbow when ECRB is involved and middle finger test produces pain at the elbow if EDC is involved (Renstrom, 2002).

Treatment for tennis elbow is generally conservative. Approximately 95% of people suffering from tennis elbow improve with conservative therapy (Nirschl and Ashman, 2003). These conservative methods include rest, strengthening exercises and braces (Renstrom, 2002; Nirschl and Ashman, 2003). Rest means absence from abuse. A player can still play tennis during the healing period if the injured tissue can be protected through a reduction in playing time and intensity. Elbow counterforce bracing can also help by decreasing angular acceleration of the elbow and decreasing the activity of the muscles. Therefore, excessive loads during healing period can be eliminated. Improving performance technique, control of intensity and duration of activity and changing equipment also helps rehabilitation (of tennis players). If the conservative methods fail to cure the symptoms, surgery can be considered. In surgical cases, ECRB is the most commonly involved tendon (Nirschl and Ashman, 2003).

Epidemiology

The incidence of tennis elbow is directly related to the subject's age and intensity of the playing time. A high activity level in tennis, such as playing 3 times per week or more for at least 30 minutes or more per session most likely results in tennis elbow. Tennis elbow is most common over 35 years of age (Renstrom, 2002; Nirschl and Ashman, 2003). However, patients have been diagnosed with tennis elbow at the ages of 12 and 80 (Nirschl and Ashman, 2003). The male to female ratio for the incidence of tennis elbow is generally stated as equal (Bruggeman et al., 2003; Nirschl and Ashman, 2003).

It has been shown that wrist extensor activity increased during ball impact in players with tennis elbow (Kelley et al., 1994; Bauer and Murray, 1999). Kelley et al. (1994) used 22 competitive tennis players, 8 of whom had tennis elbow. Their backhand strokes were investigated and compared. They found that the injured

players had significantly greater activity for the wrist extensors and pronator teres muscles during ball impact and early follow-through. Additionally they stated that ball contact was in the lower portion of the string area. Bauer and Murray (1999) used 16 subjects, 10 having tennis elbow, and their results were consistent with Kelley et al.(1994). According to their study, subjects with tennis elbow were increasing their wrist extensor activity in order to limit the amount of forced wrist flexion during impact in backhand shots and reduce the pain. This strategy is believed to contribute to increased strain and muscle fatigue, and therefore leads to greater damage.

There is a general belief that tennis players using a double-handed backhand rarely develop tennis elbow. Giangarra et al. (1993) compared uninjured competitive tennis players using single- and double-handed backhand strokes. The non-dominant arm prevents the leading wrist from hooking, helps to absorb vibration and provides the driving force for follow-through. Lower wrist and elbow angular velocities and more uniform body rotation can be obtained in a double-handed backhand technique. However, no differences were found in the wrist extensor activity between single- and double-handed backhand strokes. Therefore, the authors stated that the lower incidence of tennis elbow in double-handed backhand may not be caused by extensor activity. Since it is difficult to develop poor stroke mechanics in a double-handed backhand, the difference in the techniques of the two strokes may cause tennis elbow to appear mostly in single-handed backhand (Giangarra et al., 1993).

The differences in technique between expert and novice players also cause an increased incidence of tennis elbow in novice players (Blackwell and Cole, 1994; Riek et al., 1999). Expert players produce the stroke with extended wrist and during impact the angular velocity of the wrist is in the extension direction. Conversely, the novice players produce the strokes with flexed wrist and wrist angular velocity is in the flexion direction during impact. Thus, in the novice players, wrist extensor muscles are forcibly stretched. During the impact, the flexed wrist position of novice players may lengthen the wrist extensor muscles beyond the plateau region of force-length relationship resulting in less force potential from these muscles. Additionally, eccentric contractions of muscles are directly related with muscle injury. Riek et al. (1999) also stated that for expert players the muscle length of the ECRB is shorter than the optimal length at ball impact and any sudden stretch happening during the impact would push the muscle into a more appropriate place in the force-length

relationship. Both studies propose techniques involving wrist extension before impact in order to have an improved force-length condition during impact (Blackwell and Cole, 1994; Riek et al., 1999).

Snijders et al. (1987) introduced a biomechanical model and investigated the effects of grip power or pinching on tennis elbow. From their model they concluded that during grasping and pinching both the finger flexors and the wrist extensors are active. The activity of the flexors and extensors increases with an increase in grasping or pinching force. During ball impact, supplementary extensor activity is required and extreme or repetitive loading of the extensors may lead to over exertion which may cause tennis elbow.

2.1.4 Characteristics of Tennis Rackets

Some of the major characteristics of tennis rackets, considered by player coaches and many researchers, are weight, swingweight, sweetspots, shock and vibration. The ideal racket depends on the physical properties of the racket and player's own style of play (Brody et al., 2002).

Materials used for tennis rackets have changed with advancements in racket technology. Wood, and to a large extent aluminium rackets, have become obsolete and are not used any more by tennis players. They have been replaced by lighter, stiffer and stronger composite rackets with larger heads, although aluminium is still used to make cheap children's rackets (Brody et al., 2002). Nowadays, most rackets consist of carbon fibres complemented with different materials such as glass, boron, ceramics, Kevlar, titanium or copper fibres (Lammer and Kotze, 2003). Head Sports AG has recently developed a tennis racket also containing piezoelectric materials.

Weight of the racket is another important parameter to be considered. It is usually determined by player's individual style and perception. Light rackets are easier to swing, can be swung faster and are more manoeuvrable. However, light rackets can be rotated in an undesirable manner by the ball during the impact with the racket.

Moment of inertia of the racket depends on the total mass of the racket and its distribution along the racket. It determines the resistance felt in the hand and the arm when racket is swung through the air. A racket with a high moment of inertia is

sluggish, hard to swing and less manoeuvrable. However, for a given swing speed, larger moment of inertia may give more ball speed and allow easy control for the rebound angle of the ball (Brody, 2002; Brody et al., 2002).

Design of a tennis racket regarding its weight, size and shape was studied in detail by Brody (1979). In another study, Mitchell et al. (2000b) investigated the effect of racket moment of inertia during the tennis serve. They stated that faster head speeds can be obtained with rackets having a smaller moment of inertia.

Sweetspots are one of the important terms on which racket manufacturers advertise the advantages of their rackets. Brody (1981) defined three different sweetspots on the racket. The location of the first sweetspot is the centre of percussion (COP) of the racket. If the ball hits the COP, less shock is felt in the grip due to the impact. The second location is a vibration node of the racket. At the node, the least vibrations at the lowest natural frequency occur after impact. Therefore, when the ball hits the node, the racket vibrates little at this frequency. The third sweetspot is the impact location, which gives the highest return ball speed. At this point, the racket/ball coefficient of restitution is at a maximum value (Brody et al., 2002).

Besides sweetspots, Cross (1997) defined the deadspot. The deadspot is near the tip and is the place where the ball gives all its energy to the racket, and vice versa, during impact. Therefore, the best place to hit a serve or smash at high speed is at the dead spot. However, when returning a serve or a fast shot the dead spot will be the worst place to hit the ball.

Vibration of the frame is another characteristic of the racket. After a ball hits a tennis racket some of the energy remains in the form of racket frame and string bed vibration. The racket frame vibration, which has lower frequency but higher intensity with respect to the strings, is transmitted to the hand and causes discomfort during impact (Fairley, 1985).

The amplitude of vibration depends on the location of the impact, relative ball-racket velocity and racket mass and stiffness (Brody et al., 2002). Off-centre impacts increase both the amplitude and the frequency of vibration due to the resulting torque (Elliott, 1988).

Vibration caused by ball and racket impact generally stays at the hand level. Vibration levels at the elbow were found to be one fourth of the levels at the wrist and the vibration at the wrist compared to the racket is also much reduced (Hennig et

al., 1992). Therefore most of the vibration associated with the impact is believed to be damped reaching through the elbow. In addition, since the vibration measurements were taken with uniaxial accelerometers attached to protruding bony structures of the elbow and wrist, there was not enough information to determine loading levels in the soft tissues or how much the forearm soft tissues attenuated the vibration as it propagated to the elbow. Vibration due to mishits may intensify the symptoms of elbow injuries, but it is unlikely that vibration alone is a significant factor determining the occurrence of tennis elbow.

2.1.5 Modelling of the Tennis Ball and Racket

Modelling of tennis equipment has been attempted by many researchers. The tennis ball is generally modelled as a viscoelastic system consisting of a lumped mass with a spring and a dashpot in parallel. The force acting on the centre of mass of the ball is the sum of elastic and damping forces. The spring parameter represents the stiffness of the ball and the dashpot parameter represents the hysteresis loss in the ball. The values of these parameters depend on the type of the ball and are not constant throughout the impact. Generally, to simplify the model, they are assumed to be constant and are determined experimentally.

Goodwill and Haake (2001) modelled the ball as a spring and a dashpot system while modelling the impact between ball and the racket and assumed a linear relationship between the displacement of the centre of mass of the ball and the force on the ball during impact. Leigh and Lu (1992) also used the same viscoelastic system. However, they used a non-linear elastic force as a function of the deformation of the ball when the ball makes contact with the racket. Both studies assumed constant stiffness parameters and a damping coefficient representing the linear relationship between force and velocity of the ball.

An oblique impact of the ball on surfaces was modelled by Haake et al. (2003a). In this model, viscoelastic systems were used again. Additionally, frictional forces and decrease in the moment of inertia of the ball due to the deformation were also included. Davies (2005) modelled the ball impact using viscoelastic systems, as well. He determined the stiffness and damping ratio of the ball at impact as a function of incoming ball velocity.

Apart from viscoelastic systems, Casolo et al. (2000) developed a finite element model of the tennis ball. This model consisted of 20 nodes brick elements with the contribution of the internal air pressure of the ball. More recently, Cordingley et al. (2004) developed a more complex finite element model of pressurised and pressureless tennis balls subject to normal impact. The model predictions showed good agreement with the observed deformation of the tennis ball during impact.

Strings of the racket are generally modelled in the same way as the balls, using viscoelastic systems. Goodwill and Haake (2001) used only a linear spring to represent the stringbed for his model mentioned earlier. Leigh and Lu (1992) determined the stringbed stiffness in a similar way. They also showed experimentally that there was no measurable damping in the string system. On the other hand finite element methods were also used to model a string bed (Widing and Moeinzadeh, 1990; Casolo et al., 2000). Widing and Moeinzadeh (1990) used nonlinear cable elements for the strings.

Modelling of the racket frame is the most complicated part of building the racket and ball impact models. Racket frames are generally modelled in two different ways, namely, rigid body models and flexible beam models. Rigid body models are preferred because of their simplicity and ease of obtaining racket parameters used in these models. Whereas, flexible beam models give more satisfactory results but are much more complex than rigid body models.

Goodwill and Haake (2000), Brody (1997) and Liu (1983) used rigid body models for racket frame in their studies. All models generated in these studies treat the whole racket as a rigid body and do not consider the strings at all.

Leigh and Lu (1992) developed a model in which the ball, strings and racket are all modelled as viscoelastic systems. The racket was modelled as an equivalent lumped mass supported by a linear spring and a linear dashpot. The equivalent lumped mass was calculated from material and inertial properties of the racket. The racket was envisaged as behaving like a cantilever beam and from the load-deflection properties of this structure, racket stiffness was calculated. Lastly, a damping coefficient was chosen arbitrarily based upon previous studies in the literature.

Goodwill and Haake (2003) and Cross (1999a) compared the rigid body and flexible beam models. Cross (1999a) stated that results of a rigid body model were roughly consistent with experimental data. However, the flexible beam model is

superior and its results were in remarkably good agreement with experimental data. In agreement with Cross (1999a), Goodwill and Haake (2003) also showed that the flexible body model matches the experimental results better than rigid body model.

Besides rigid body and flexible beam models, the racket frame was also modelled using finite element methods (Widing and Moeinzadeh, 1990; Casolo et al., 2000). The number of the models employing finite element analysis is quite low in the literature with respect to viscoelastic models. Casolo et al. (2000) developed a finite element model of the racket using 3D beam elements. These were straight elements, with two nodes having six degree of freedom per node. Alternatively, Widing and Moeinzadeh (1990) used linear curved elements for the frame of the racket.

Recently, Glynn (2007) modelled the racket frame as two rigid bodies connected by a pin joint located at the antinode of the fundamental modes of vibration of the racket frame in and out of the racket head plane. Two mutually perpendicular torsional spring-dampers at this joint were used to model the vibration of the racket frame.

The grip or hand-racket interaction has a complex mechanical behaviour since the magnitude of the grip forces and the surface area on which the forces applied are changed with muscle activity time history at hand and forearm. Therefore, there are not so many studies modelling the grip. McLaughlin and Miller (1980) assumed the grip had not changed during the stroke and they treated the hand as a part of the racket. Snijders et al. (1987) used equal but opposite forces acting on the thumb and fingers as the grip force in their grasping model while Knudson (1991) measured forces on the hand by putting two load cells on thenar and hypothenar eminences assuming two- point- contact between hand and racket.

Glynn (2007) modelled the grip as a series of linear spring-dampers and a torsional spring-damper. Both hypothenar and thenar eminences were represented by six different points on the hand. These points were then connected to a fixed point on the racket by a spring-damper. A torsional spring-damper controlled the rotation of the racket around its longitudinal axis.

2.1.6 Summary

In this section, a review of literature in modelling of tennis equipment and tennis backhand strokes was presented. The modelling technique for racket, ball, strings and impact of the ball with the racket are nearly the same for most of the studies. The spring-dashpot system was used to model ball and strings and the racket was assumed as a rigid body. Although there are some different approaches found in the literature such as modelling the racket and the string with the finite element method, the spring-dashpot method gives sufficiently good estimates of real data. Uncomplicated modelling and computation of spring-damper system behaviour bring additional advantages to this method.

Tennis elbow, which is the most common elbow injury in tennis (Kelley et al., 1994), has also been discussed in this section. The anatomy, aetiology and epidemiology of the tennis elbow have been reviewed.

2.2 Anatomy & Physiology of the Upper Extremity

2.2.1 Introduction

The anatomical details of the human muscular system and how muscles achieve locomotion have been the subject of investigation for a considerable period of time.

Galen (129-201 A.D) was the first scientist who defined muscles as the organ of voluntary movement. His detailed studies and discoveries are considered as the first attempts to establish the science of muscles that is myology. His influence on the topic persisted until the Renaissance. Swammerdam, Croone and Stensen made extensive studies of muscle anatomy and physiology in the 17^{th} century. Swammerdam showed that muscular volume was preserved during muscular contraction and Croone stated that a signal from the brain must be sent to muscles in order to contract. Furthermore, Stensen described the muscular and tendinious structures in detail. Van Leeuwenhoek (1632-1723) performed microscopic examinations of muscle tissue using optical instruments and discovered the cross-striation patterns in skeletal muscles (Needham, 1971).

However, the answer to the question how muscles contract and produce forces changed several times, even in the last century. The latest theory was proposed

by A.F. Huxley and Niedergerke (1954) and H. Huxley and Hanson (1954) independently at the same time, using different methods. The sliding filament theory proposes that length changes in a muscle fibre take place by sliding two sets of filaments past one another without appreciable length change in either. However, this theory raised a new unanswered question: What makes the filaments slide? (Huxley, 2000).

Understanding the anatomy and physiology of muscles makes it easier to model them in various studies of human movement. Muscle contraction mechanics explains the relationship of muscular forces with muscular properties such as length or velocity. Various studies have been done using individual muscle models in recent years in order to have a broader view of human movement.

2.2.2 Anatomical Structure of Muscles and Bones – Brief Summary

Bones

Bones give shape, support, and protect body structures. They have tissues that produce blood cells and store various inorganic salts. Bones and muscles interact as levers and aid body movements. Bony projections, called processes, provide sites for attachment of ligaments and tendons; a depression of one bone might articulate with a process of another whereas grooves and openings act as passageways for blood vessels and nerves (Shier et al., 2002).

The skeleton can be separated into two parts: an axial skeleton (skull, ribs, sternum and vertebral column) and an appendicular skeleton (the skeleton of the limbs). Both upper and lower limb skeletons are divided into a girdle and the skeleton of the free limb. The girdle of the upper limb, shoulder girdle, consists of clavicle and scapula; humerus, radius, ulna, carpals, metacarpals and phalanges form the skeleton of the free part of the upper limb (Jenkins, 2002) (Figure 2.1).

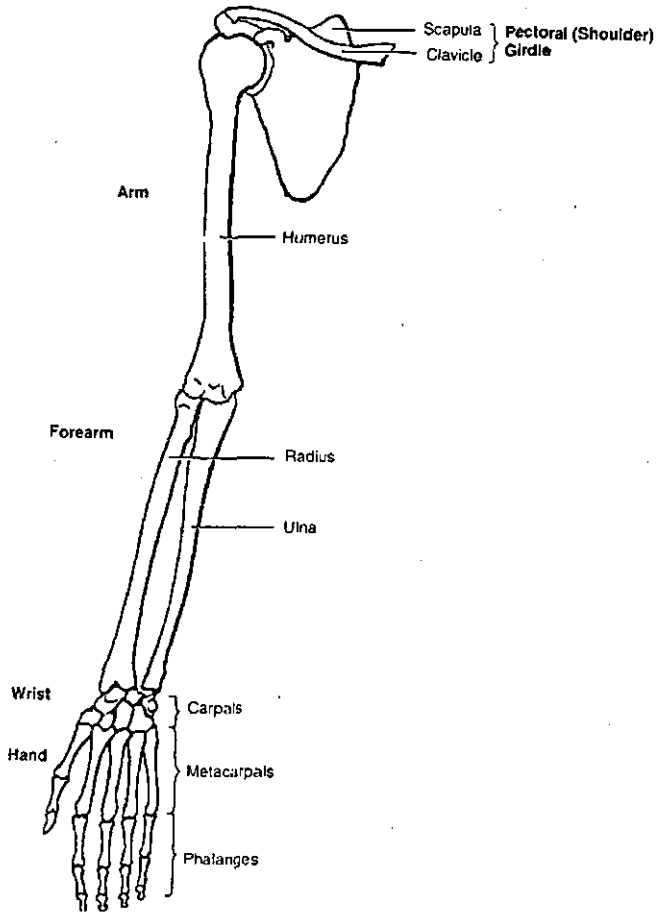

Figure 2.1. The skeleton of the right upper limb [adapted from (Jenkins, 2002), p. 65].

Joints

Joints bind parts of the skeletal system, have a role in bone growth, and enable the body to move in response to skeletal muscle contractions. They vary considerably in structure and function. However, most of the joints of the skeletal system are synovial joints. These types of joints allow free movement and consist of articular cartilage, a joint capsule, and a synovial membrane.

Synovial joints are classified based on their shapes and movements. The shoulder joint, elbow joint and wrist joint are examples of ball and socket, hinge and condyloid types of synovial joints, respectively. Muscle action produces movements at these synovial joints (Shier et al., 2002). The terms describing upper limb movements that occur in different directions and different planes are shown in Figure 2.2.

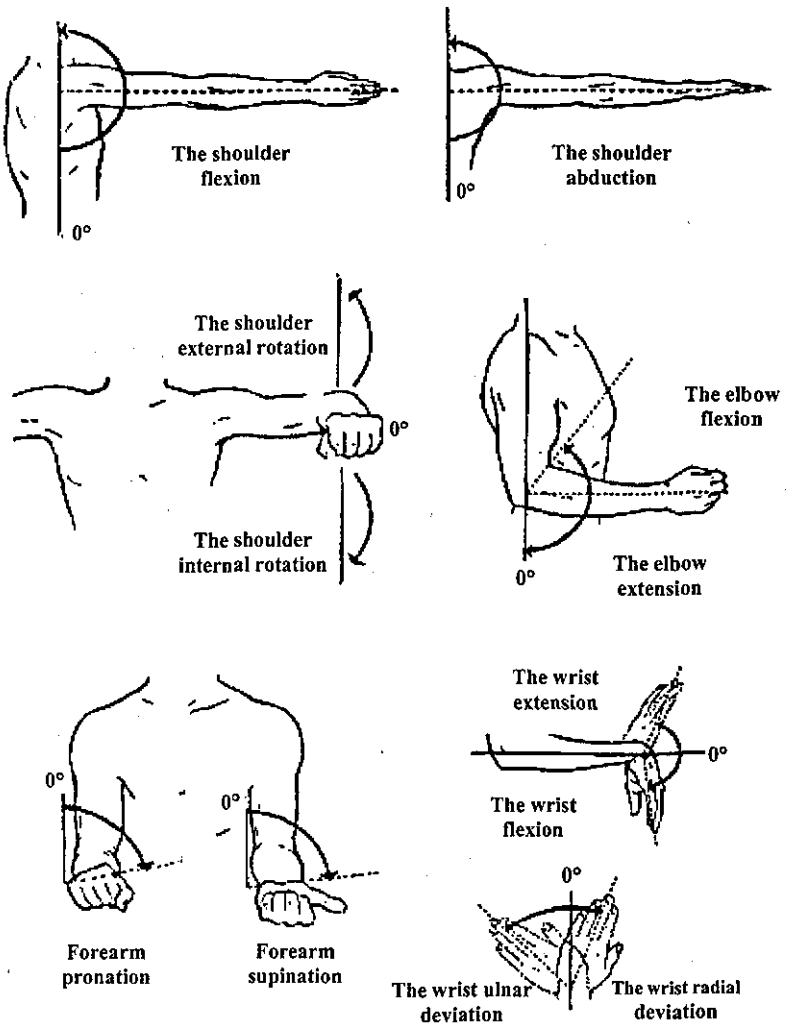

Figure 2.2. Movements of the upper extremity [adapted from (Anonymous, 2008)].

Muscle Anatomy

Skeletal muscles are formed of different layers of structures bundled within each other. These different structures, considered from the most superficial to the deepest, can be identified as the muscle itself, fascicles, muscle fibres, myofibrils and filaments (Figure 2.3).

Many muscles arise by longer connective tissue bundles that are aggregated to form a tendon that connects muscle to the bone. Tendons are much stronger than the muscles that act upon them (Jenkins, 2002).

Each muscle fibre is a single large cell, containing large numbers of mitochondria and as many as several hundreds of nuclei located at regular intervals near the surface of the fibre. The number of the fibres in any muscle is fixed at birth. However, exercise and conditioning increase the size of the fibres (Schnek, 1992).

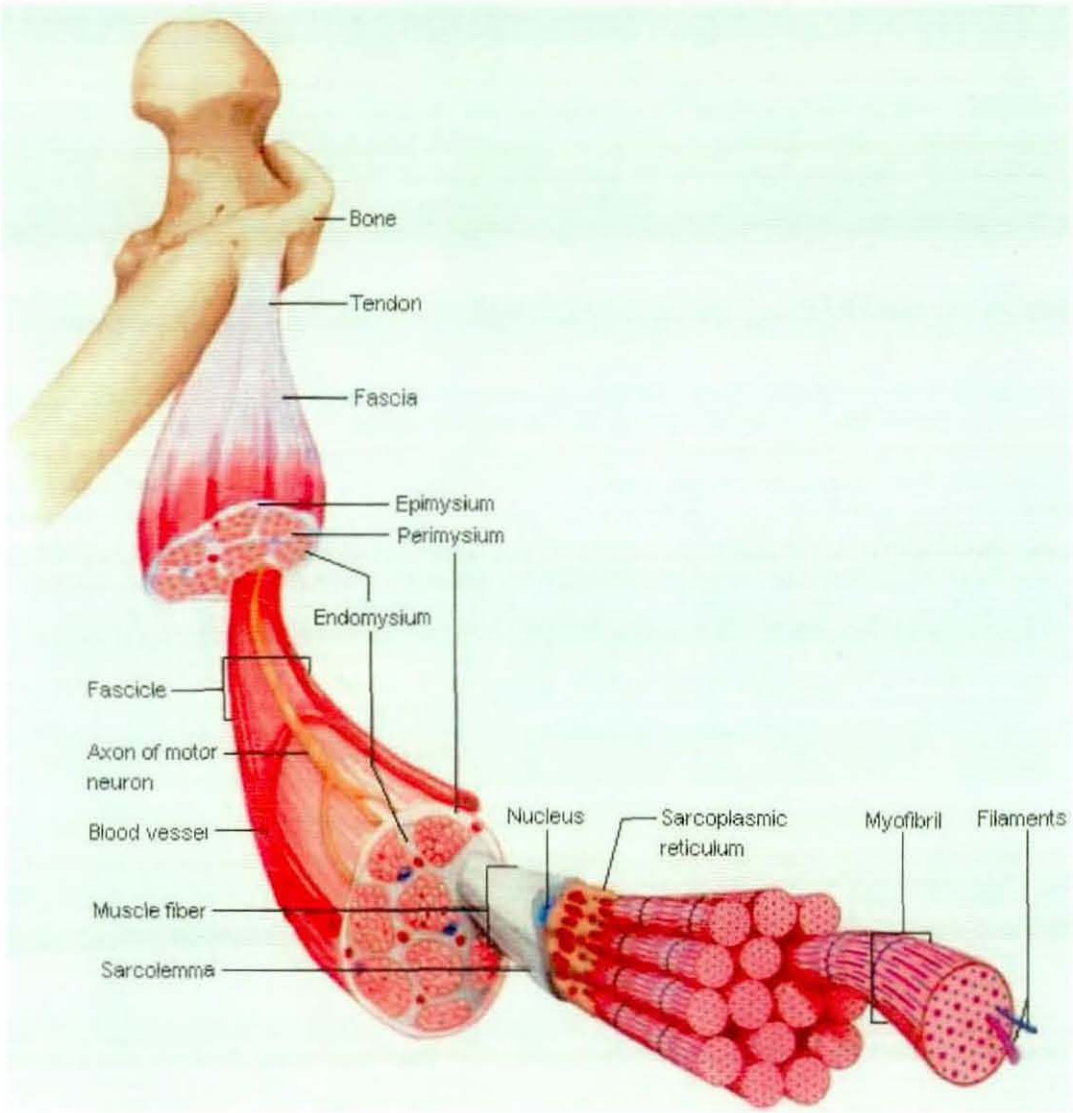

Figure 2.3. Structure of a skeletal muscle [adapted from (Shier et al., 2002), p. 280].

Myofibrils contain myosin (thick) and actin (thin) filaments. The arrangement of these filaments produces alternating light and dark striations, which is the basic characteristic of skeletal muscle fibres. The striations form a repetitive pattern of units called sarcomeres, which are the functional units of muscle contraction (Shier et al., 2002).

The regions of the sarcomere are named according to their appearance. The myosin containing region is known as an A-band whereas the region containing actin is called an I-band. The region of the A-band in which no actin-myosin overlap occurs is the H-zone and the line separating I-bands into two is called the Z-line. Generally, sarcomere length is defined as the distance between two successive Z-lines (Lieber, 2002).

Muscles that move the arm can be separated into four groups according to their primary actions. Coracobrachialis and pectoralis major are flexors; teres major and latissimis dorsi are extensors; suprasipinatus and deltoid are abductors; subscapularis, infrasupinatus and teres minor are rotators. Muscles moving the forearm are grouped into three: biceps brachii, brachialis and brachioradialis are flexors; triceps brachii is extensor; supinator, pronator teres and pronator quadratus are rotators. Muscles moving the hand and fingers have only flexion and extension movements. The flexors are flexor carpi radialis longus, flexor carpi ulanaris, palmaris longus, flexor digitorum profundus and flexor digitorum superficialis. The extensors are extensor carpi radialis, extensor carpi radialis brevis, extensor carpi ulnaris and extensor digitorum (Shier et al., 2002).

Muscle Architecture

Skeletal muscle architecture is the structural property of a whole muscle that dominates its function. It is defined as the arrangement of the muscle fibres within a muscle relative to the axis of force generation (Lieber, 2002). It is one of the most important properties that determines a muscle's force and excursion capability (Lieber and Friden, 2001). There are various arrangements of the fibres in the muscles. However, three general classes of muscle fibre architecture can be listed as:

i. Muscle fibres are arranged parallel to the force-generating axis in parallel or longitudinal architecture.
ii. Muscles with fibres that are arranged at a specific angle relative to the force-generating axis have unipennate architecture.
iii. Finally, in multipennate architecture there are several angles relative to the force-generating axis. This angle is called pennation angle (θ) and varies from about 0° to 30° in mammalian muscles (Lieber and Friden, 2000).

In general, muscles of the arm and forearm have pennation angles of not more than 15° (Lieber et al., 1990; Lieber et al., 1992; Murray, 1997). A comparison of three different pennation angle assumptions (neglecting pennation, assuming a fixed pennation and assuming pennation angle is dependent on fibre length) showed

that a fixed pennation angle assumption provided the worst estimate of muscle force whereas pennation angle change with fibre length provided the best (Scott and Winter, 1991).

Muscle length is defined as the distance from the origin of the most proximal muscle fibres to the insertion of the most distal fibres. However, muscle fibre length must be determined experimentally by microdissection of individual fibres (Lieber and Friden, 2001). Another architectural parameter, physiological cross-sectional area (PCSA) is derived from the other parameters. This is not the actual cross-sectional area of the muscle measured in anatomical planes. Theoretically, PCSA is the sum of the cross-sectional areas of all muscle fibres within the muscle. It is defined as:

$$PCSA(\mathrm{cm}^2) = \frac{Muscle\ mass(\mathrm{g}) \times cos\theta}{\rho(\mathrm{g/cm}^3) \times Fiber\ length(\mathrm{cm})} \tag{2.2}$$

where ρ represents muscle density (1.056 g/cm^3 for mammalian muscle) and θ represents pennation angle (Lieber, 2002).

The relationship between muscle architecture and muscle function is that muscle velocity and excursion are proportional to muscle fibre length, and muscle force is proportional to total fibre cross-sectional area (PCSA) (Lieber and Bodine-Fowler, 1993). Therefore, it can be said that muscles with short fibres and large PCSA are specialized for force production and muscles with long fibres and relatively small PCSA are suitable for high excursions and velocity. However, muscle moment arm (the perpendicular distance from axis of joint rotation to the point of force application) plays an important role in making inferences about the physiologic usage of muscles from their architectural design.

A single architectural difference index δ_{ij}, which represents a comparison between the architectural parameters of two different muscles was presented by Lieber and Brown (1992). Analysis showed that the best discriminators were: fibre length, PCSA, muscle length, FL/ML ratio, and muscle mass. The difference index δ_{ij} was calculated as:

$$\delta_{ij} = \sqrt{\sum_{k=1}^{n} \left(\frac{P_{i,k} - P_{j,k}}{P_{max,k} - P_{min,k}} \right)^2} \qquad (2.3)$$

where $P_{i,k}$ and $P_{j,k}$ represent the k^{th} discriminating parameters for muscles *i* and *j* respectively; $P_{min,k}$ and $P_{max,k}$ represent the minimum and maximum values for the k^{th} discriminating parameter and n is the number of discriminating patterns (Lieber and Brown, 1992).

2.2.3 Muscle Physiology

A muscle fibre contraction is composed of several cellular and chemical reactions. The final result is a movement within the myofibrils in which actin and myosin filaments slide past one another, shortening the sarcomers. According to sliding filament theory, lengths of these filaments do not change. When sarcomers shorten, the H-zones and the I-bands get narrower and the Z-lines move closer together; thus, the muscle fibre shortens and pulls on its attachments.

Acetylcholine (ACh), the neurotransmitter that motor neurons use to control skeletal muscle, is released in the synaptic cleft of the neuromuscular junction. It diffuses rapidly, combines with ACh receptors, and stimulates the muscle fibre. This impulse resembles nerve impulse and propagates in all directions along and around the cell.

The force that shortens the sarcomers comes from cross-bridges pulling on actin. Cross-bridges are the globular parts of the two twisted proteins on myosin, which project outward along myosin's length. A myosin cross-bridge can attach to an actin-binding site and pull the actin. Attachment, pull, release and reattachment of the actin form the cross-bridge cycling, which pulls the actin toward the centre of the sarcomere and shortens the muscle. Myosin cross-bridges contain ATPase enzyme which catalyses breakdown of ATP to ADP in order to release energy to provide force for the muscle contraction (Shier et al., 2002).

2.2.4 Muscle Mechanics

Length-tension relationship: isometric muscle contraction

The isometric length-tension curve is generated by maximally stimulating a skeletal muscle at different lengths and measuring the tension generated by the muscle at each length (Lieber, 1993). When maximum tension is plotted at each length, the relationship between length and tension is obtained (Figure 2.4). There is a direct relationship between myofilament overlap and tension generation. The tension on a fibre is a function of the magnitude of overlap between actin and myosin filaments. For the frog skeletal muscle in Figure 2.4, at sarcomere lengths greater than 3.65 μm no tension is generated because there is no overlap between actin and myosin since the lengths of the actin and myosin filaments are 1.65 μm and 2.0 μm, respectively. There is a region on the curve where length change results in no change in tension (2.0μm-2,2 μm). This region is called the 'plateau region'. Maximum interaction between filaments occurs in this region and maximum tension is generated. Both sides of the plateau region have less tension. Depending on the increasing or decreasing sarcomere length from plateau region, these regions are called descending and ascending limb, respectively. Sarcomere length-tension relationship is directly related to the fibre length-tension relationship.

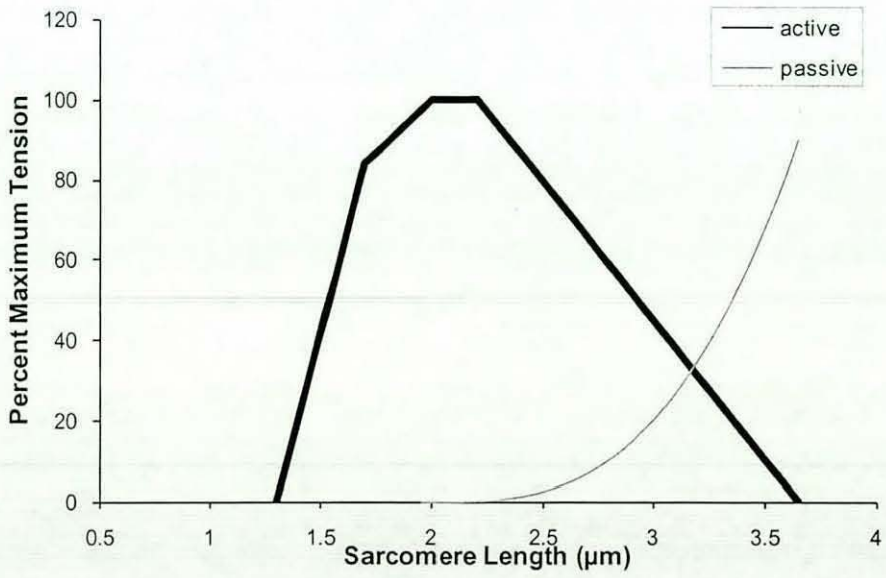

Figure 2.4. Sarcomere length – tension relationship for a frog skeletal muscle[adapted from (Lieber, 2002), p. 52].

The fibre length at which maximum tension is obtained is the optimal length of that muscle fibre, L^M_o. If a muscle is stretched to various lengths without stimulation, passive tension is obtained. The source of the passive tension is the large protein, titin, which connects the thick myosin filaments end to end (Lieber and Bodine-Fowler, 1993; Lieber, 2002). Active muscle force is generated in the region of $0.5\ L^M_o < L^M < 1.5\ L^M_o$, where L^M is the muscle fibre length (Zajac, 1989; Pandy and Barr, 2002).

Force-velocity relationship: isotonic muscle contraction

The 'force-velocity relationship' describes the force generated by a muscle as a *function of velocity under constant load conditions. The force-velocity curve is* generated by the results of many experiments plotted on the same graph as in the case of length-tension curve. In the experiments, a muscle is maximally stimulated and allowed to shorten/lengthen under constant load. Then, the muscle velocity during shortening/lengthening is measured (Lieber et al., 1992). The force-velocity curve determines the mechanical power output of the muscle while it is active (Zajac, 1989) (Figure 2.5).

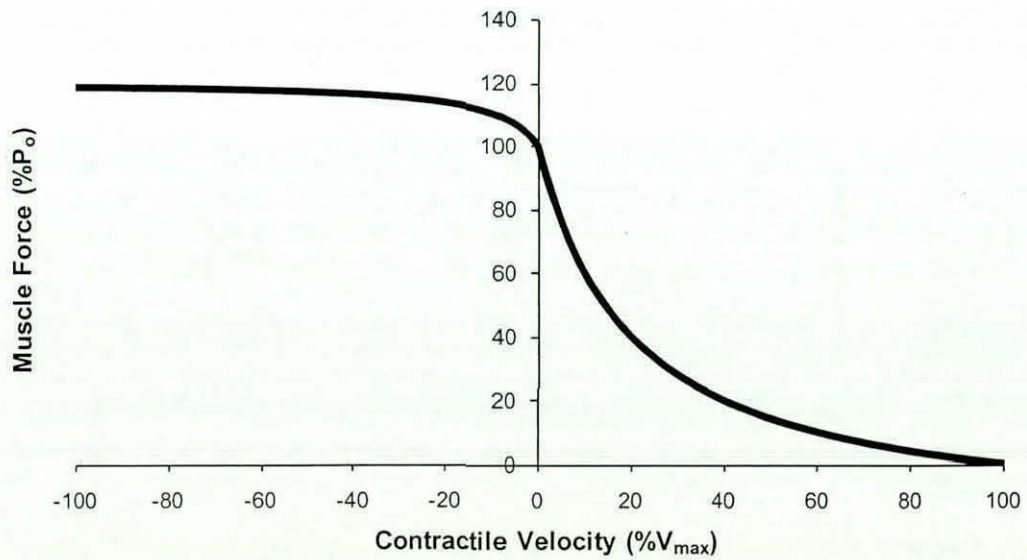

Figure 2.5. Force – velocity relationship.

When a muscle is maximally stimulated and a constant load, which is less than the maximum isometric force developed by the muscle at that length, is applied the muscle begins to shorten (concentric contraction) (Lieber et al., 1992; Pandy and

Barr, 2002). In concentric contractions as the load on the muscle decreases, contraction velocity increases up to a maximum contraction velocity V_{max}. At this velocity, muscle cannot resist any load even it is fully activated (Pandy and Barr, 2002). The force-velocity relationship is characterized by a rectangular parabola and expressed firstly by Hill (1938) with his famous formula as:

$$(P + a)(V + b) = (P_o + a)b \tag{2.4}$$

where P is the load on the muscle, V is the velocity of shortening, P_o is the measured isometric force, and, a and b are constants determined empirically.

Edman (1988) found that this relationship is more complex while studying fibres instead of whole muscle as Hill did. Edman (1988) showed the force-velocity relation had two distinct curves located in the 0-78 and 78-100% of the measured isometric force, P_o.

When the load on the muscle is greater than the maximum isometric force developed by the muscle at that length, the muscle lengthens (eccentric contraction) (Pandy and Barr, 2002). The absolute tensions are very high relative to the muscle's maximum tension generating capacity. Apart from concentric contractions, tension is relatively independent of the velocity. Therefore, muscles are very resistant to lengthening. Muscle injury and soreness are directly associated with eccentric contraction (Lieber et al., 1992; Lieber, 2002). Edman (1988) expressed the characteristic of the force-velocity relationship as a smooth sigmoid function with inflection point at P_o.

Yeadon et al. (2006) define 'differential activation' as the activation level of muscle during voluntary contractions. They stated that maximum voluntary force is a function of the theoretical maximum force (Hill's formula) and a differential activation function which increases from a depressed level for high eccentric velocities to full activation for high concentric velocities. The product of these two functions gives a better estimate for force-velocity relationship for voluntary contractions.

Modelling of contraction dynamics

A mechanical model of human muscle was first introduced by Hill (1938). This was a simple mechanical model of the muscle tissue. Huxley (1957) developed

and formulated the 'cross-bridge theory' of muscle. This is a complex model explaining the structural changes at the sarcomere level and can be thought as more physiologically relevant. Cross-bridge models have not been used widely in biomechanical applications due to their complexity and the subsequent increase in numerical computation time (Herzog, 2000). In contrast, due to its simplicity and that it yields adequate representation of muscle contraction dynamics, Hill-type muscle models are extensively used in various studies involving muscle modelling. Almost all models found in the literature are derived from the Hill's mechanical muscle model. The big disadvantage of Hill-type models is that history dependent effects are generally ignored (Herzog, 2000).

Hill-type muscle models are generally composed of three different elements: contractile, series elastic and parallel elastic elements (Figure 2.6).

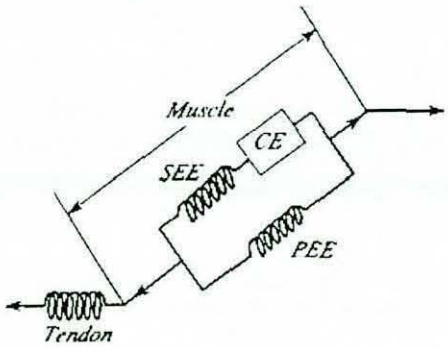

Figure 2.6. Schematic diagram of a Hill-type muscle model [adapted from (Pandy and Barr, 2002), p. 6.23].

The contractile element (CE) of the model is in series with a series elastic element (SEE) and both are in parallel with a passive elastic element (PEE). Together these elements represent the muscle and are in series with the tendon (Zajac, 1989; Pandy and Barr, 2002). The pennation angle is the angle between tendon and the muscle fibres (Delp and Loan, 2000; Pandy and Barr, 2002).

The contractile element models the force-length-velocity relationship of the muscle. This element plays the major part in the model since the others can be neglected in some situations. Peak isometric muscle force, optimal muscle fibre length, maximum shortening velocity of the muscle and muscle activation are the parameters that scale the active force-length relation and force-velocity relation

curves of the muscle (Zajac, 1989; Delp and Loan, 2000; Pandy and Barr, 2002). For muscles composed of multiple fibre types multiple CE's may be used in parallel (Brown and Loeb, 2001).

The series elastic element models the active stiffness of the muscle. In most models SEE is neglected with little inaccuracy (Zajac, 1989; Challis and Kerwin, 1994; Delp and Loan, 1995; Delp and Loan, 2000). Furthermore, with a muscle SEE, muscle fibre properties are not proportional to the sarcomere properties. Tendon elasticity and the serial elastic element are not easily separable. Except for short tendon muscles the tendon part is dominant and muscle elasticity can be neglected (Zajac, 1989). Although muscles exhibit elasticity they are not as deformable as the tendons (Challis and Kerwin, 1994). Generally, tendons are represented by a non-linear elastic element, but a linear stress-strain relationship for tendon may be used (Challis and Kerwin, 1994).

The passive elastic element models the passive stiffness of the muscle. Around the optimal length of the muscle, passive forces are very small and usually neglected. When the fibre lengths are longer than the optimal length, the passive force on the muscle increases rapidly. Therefore, PEE is represented as a non-linear elastic element if the passive force on the muscle is high enough with respect to active muscle forces (Delp and Loan, 2000).

2.2.5 Individual Muscle Driven Models

Individual muscle forces are determined in order to gain substantial information about the aetiology of soft tissue injuries and pathological conditions occurring in the soft tissues (Lemay and Crago, 1996; Riek et al., 1999). In most cases, the cause of these injuries is a local trauma in which an extensive or repetitive force is applied to soft tissues. Such information about individual muscle forces helps to understand the endurance limits of muscles and gives the opportunity of using them properly for a predefined task. Estimated muscle forces can also be used in the rehabilitation process of the associated disorders or diseases as a guideline for treatment or as a baseline to keep track of success of rehabilitation.

Muscles are fundamental for moving the body. Motion of the whole body or a part of it at a desired level is essential for many kinds of sport. Therefore, besides

having an idea about sports injury, muscle forces are also determined in different kinds of sports in order to get optimum performance from players. This can be achieved by creating models of the muscles that are used for the required motion of the body to enable analysis of optimal muscle properties and activation timings.

Individual muscle modelling within musculoskeletal models is a relatively new subject in the field of biomechanics. Many unknowns in the physiology of the muscles have kept this subject beyond reach for a long time. However the main hurdle to overcome is the indeterminate problem encountered. Force developed by each muscle cannot be determined individually with analytical solutions since there are more muscles than the number of degrees of freedom of movements at each joint. The degree of indeterminacy increases with the number of the muscles considered in the model. Therefore, an optimisation is necessary to estimate the values of these forces. A suitable optimisation criterion and constraints have to be selected for estimating individual muscle forces by optimisation.

The optimisation procedures and algorithms are generally based on repeated numerical calculations. For this reason, with the advancing technologies in the computer industry, the number of muscle modelling studies reported in the literature is increasing. Moreover, some recently developed commercial software can be found for muscle modelling.

Despite all these factors, muscle modelling has an advantage over net joint torque models. In net joint torques modelling and calculations are much simpler. Depending on the model accuracy, very good kinematic and kinetic results can be obtained from these kinds of models. However, the information gained is limited to the joint level and this limits its usefulness, especially for clinical purposes. In contrast, despite the additional complexity, individual muscle modelling provides an idea of the working conditions of each muscle modelled in the system.

Epstein and Herzog (2003) stated that an ideal muscle model should have at least some of these features:

i. It should be comprehensive
ii. It should be based on scientific principles
iii. It should be consistent with experimental evidence
iv. It should have predictive value
v. It should be amenable to improvement and refinement

2.2.6 Estimation of Muscle Forces

Individual muscle forces are estimated in various studies with a number of different techniques. Challis (1991) listed five of these techniques. The direct measurement of the forces is highly invasive and requires a strain gauge fitted to the tendon. EMG based force estimation requires extensive calibration and has reliability problems. A dynamic optimisation technique may be used to analyse motor control, and the muscle activity can be inferred from the simulation. This technique can be easily validated by comparing the simulated movement with the actual movement, but formulation of a performance criterion is difficult. When using the control model technique, the system to be controlled is assumed to be known. There are no optimisation criteria. The simplest of these models provides only crude approximations. In static optimisation technique, muscle forces are optimised in such a way that some function related to muscle forces is minimised. Validation of this technique may be difficult (Challis, 1991). In addition to these five techniques, muscle forces are also estimated by finite element methods (Van der Helm, 1994a).

Muscle forces are often estimated using optimisation procedures. These optimisation procedures involve the minimization of an objective function relating to the muscle forces. Challis and Kerwin (1993) examined 15 different objective functions and compared their force predictions with the forces estimated using a validated muscle model. However, it was shown that the muscle forces estimated by the objective functions give poor correspondence with the muscle model predicted forces.

Several models have been developed and evaluated which include estimation of individual muscle forces.

- McLaughlin and Miller (1980) estimated the muscle forces in the forearm immediately before the ball and racket impact. Nine individual muscle forces were estimated, two of which are estimated from gripping forces. The remaining 7 muscle forces were estimated by static optimisation. Minimum total stress and total moment of the muscles were considered as the control function of the optimisation procedure.

- Pandy et al. (1990) used 8 muscles in their 4 segment, planar, articulated linkage model. The mechanical behaviour of the muscles was described by a Hill-type muscle model. Dynamic optimisation was utilised and the performance criterion was the height reached by the centre of mass of the body.

- A shoulder model was introduced by Karlsson and Peterson (1992). They used 11 muscles corresponding to 19 forces in their model. Optimisation criteria used for estimating muscle forces was the minimum sum of the squared muscle stresses.

- A whole upper limb model was proposed by Raikova (1992). The Denavit-Hartenberg method is used for the kinematics and dynamics of the system. 30 different muscles with 50 muscle forces may be used within the model. Optimisation with the Lagrange multiplier method was preferred. It was stated that the objective function should depend on joint reactions and should be a non-linear function of unknown muscle forces. An application of this model, flexion-extension motion in the elbow joint, is also shown by Raikova (1996). 5 muscles were used and the optimisation function $\sum c_i \left| F_i^2 \right|$ was solved analytically by the Lagrange multipliers method, where c_i are the weight factors and F_i are the muscle forces.

- Van Soest et al. (1993) used a Hill-type muscle model for the six muscles in their study. Dynamic optimisation was carried out under the predefined constraints. The optimisation problem was reduced to finding the point in the six-dimensional control space that results in maximum jump height.

- Challis and Kerwin (1994) developed a model to compute individual muscle forces during loaded elbow flexion. Three muscles were involved in the study. A Hill-type muscle model and a simulation procedure were used to estimate the muscle forces.

- Runciman and Nicol (1994) developed a biomechanical model of the glenohumeral joint and shoulder. 26 muscles were used in their study. Muscle forces were estimated by linear optimisation. Minimum overall maximum muscle stress was considered in the optimisation.

- A musculoskeletal model of the shoulder mechanism consisting of thorax, clavicle, scapula and humerus was used for the analysis of the kinematic and dynamic behaviour of the shoulder mechanism by Van der Helm (1994b). Muscles are modelled as active truss or curved truss elements. 16 muscles and 3 ligaments were modelled within the system. The optimisation criterion used was the minimization of the sum of the squared muscle stresses.

- The same finite element method was used in another study by Van der Helm (1994a). In this study 20 muscles were modelled. This time four different optimisation criteria were used while estimating individual muscle forces: minimization of the sum of quadratic muscle forces, minimization of the sum of quadratic stresses, minimization of the sum of quadratic muscle forces normalized by maximal muscle force and minimization of the maximal muscle stress in the entire mechanism.

Computational frameworks and software systems have also been used to create and analyse musculoskeletal models. These software packages enable users to develop, alter, and evaluate different musculoskeletal structures with reduced programming effort. For example:

- 'Software for Interactive Musculoskeletal Model' (SIMM) was developed by Delp and Loan (1995; 2000). SIMM is a graphics based software, enabling users to visualise the musculoskeletal geometry and interact with the models. The muscle-tendon model used in SIMM is a Hill-type muscle model. Once muscle-tendon length and velocity is determined, muscle force is estimated by an iterative algorithm (4 iterations maximum). One application of SIMM was a musculoskeletal model of the upper extremity containing 25 muscles

developed by Charlton and Johnson (2000). Neptune and Hull (1999) also used SIMM in their planar two-legged bicycle-rider model with 14 muscles.

- Lemay and Crago (1996) developed a dynamic model of the upper extremity to simulate forearm and wrist movements. 20 muscles were included in the model. Muscle forces were estimated by a Hill-type muscle model. The upper extremity model was implemented by means of the commercially available software 'Automatic Dynamic Analysis of Mechanical Systems' (ADAMS) that analyses and solves the motions and forces of mechanical systems.

- 'Virtual Muscle' is another computational approach for modelling the complex mechanical properties of muscles and tendons (Cheng et al., 2000). It is embodied as a software package for use with Matlab and Simulink. The software employs graphic user interfaces (GUI) and dynamic data exchange (DDE) to build custom muscle model blocks and link them to kinetic analyses of complete musculoskeletal systems. A Hill-type muscle model is used to estimate the muscle forces within the Virtual Muscle.

Although the aims and structures of the overall models are quite different, all studies except Van der Helm used Hill-type muscle models to determine the muscle forces. Different optimisation procedures were performed in all studies. Some objective functions were compared to determine which one was the most appropriate for the model. The results of individual muscle forces were evaluated by comparing them with experiment results and/or electromyography (EMG) results. It is claimed that the results of the models were sufficiently accurate. However, determination of the muscle groups, their attachment points and activation timings were not mentioned clearly and some of the studies used the muscle architectural data of previous studies.

2.2.7 Summary

After a brief review of anatomy and physiology of the human upper limb, biomechanical models of the upper limb have been presented in this section.

Although Hill's model dates back to 1938, it has been the most used for muscle modelling since it is the simplest method that can model the majority of muscle activity with a reasonably good approximation whilst mathematical models using cross-bridge theories are too complicated. There are fewer studies modelling muscle and other soft tissues as finite elements.

Nearly all of the studies modelled muscle as a linear force system applied to different segments of the body with the same magnitude and line of action but opposite directions. This assumption holds for flexor muscles all the time, however, since extensors turn around the joints this model does not work properly. For this reason, while modelling extensor muscles, this should be taken into account.

2.3 Simulation Modelling

Typically, successful simulation models (e.g. Kong (2004), Glynn (2007)) are achieved using four main steps. These steps are development of the model, construction of the model parameters, evaluation of the model and lastly, optimisation/sensitivity analysis. The following section briefly reviews and describes different techniques used in the process of development and evaluation of a subject-specific computer simulation model.

2.3.1 Development of the Simulation Model

Development of the simulation model is one of the main tasks of the simulation modelling process. A model is a representation of a real system of interest and it should be similar to but simpler than the system it represents. Both very simple and very complex models can be found in the literature. Alexander (2003) described different modelling approaches in biomechanics and gave examples from the literature for each type of model. The complexity of the model depends on the features required from the model. Simple models can help understand basic features of the real system, but more complex models may be needed to identify some special characteristics of the system. Pandy (2003) compared a simple and a complex model of walking and he concluded that although the analysis of the simple model was in

agreement with the complex model, the complex model revealed more significant information about walking. At this point, it should be said that the simplest model, which fulfils the research objectives, should be used.

Formulation of the equations of the motion is needed to develop the simulation model. These equations can be determined from first principles or by using software packages. Using first principles gives exact control over the model but the risk of making mistakes while identifying the system and developing the equations of motion is higher. The use of appropriate software packages overcomes this problem provided the accuracy of the package is sufficient and that it works correctly. Therefore, much more complex systems can be modelled with commercial software packages more efficiently. The flexibility of the package and calculation speed are some important features to be considered before using a commercial software package. There are many simulation software packages available on the market. The best package, which satisfies the needs of the simulation model, should be selected.

2.3.2 Determination of Subject-Specific Parameters

Inertia parameters

To build a simulation model of the human body, inertia parameters of the modelled extremity or segment are needed. Various methods have been performed to calculate inertial parameters, some of which are include cadaver data, statistical modelling, geometric modelling, and computer-aided tomography (CT scan) and/or magnetic resonance imaging (MRI).

A cadaver's segmental inertia parameters can be calculated directly and accurately. In addition to inertia parameters, muscle architecture parameters can be measured from the cadavers. However, since the model is generally desired to be subject-specific and the measurements of muscle architecture need to be made in vivo, the use of cadaver data is usually not a preferred solution.

In statistical modelling, regression equations relating anthropometric measurements of the subject and the inertial parameters are used. These regression equations are generally developed from measurements on cadavers.

Body segments are represented as different geometric solids in geometric modelling. The size and shape of these solids depend on the anthropometric measurements of the subject. Density of the geometric solids is taken from cadaver data. Both complex and relatively simple geometrical models can be found in the literature. Hatze (1983) developed a 17 segment hominoid, i.e. human-like model, with segmental parameter values calculated from 242 anthropometric measurements of a subject. More recently, Yeadon (1990a) developed a more efficient 11 segment geometric model requiring 95 anthropometric measurements (less than half of the Hatze's model requirement).

A comparison of different statistical and geometrical models of upper limb inertial parameters found in the literature was made by Challis and Kerwin (1992). They concluded that among the models they examined, Hinrichs' (1985) regression equations gave the most accurate results whereas geometric models offered the greatest flexibility.

CT scans and MRI provide accurate inertial parameters as well as muscle architecture parameters. Measuring in vivo muscle architecture is an advantage of using MRI. In addition, there are software packages available in the market for creating 3D meshes of muscles and bones from MRI and CT scans (e.g. Mimics).

Strength parameters

To develop a Hill-type model contractile element, series elastic element and parallel elastic element model parameters must be determined. Detailed descriptions of these muscle parameters can be found in section 2.2.4.

The muscle parameters can be estimated from the maximum torque measurements on isokinetic dynamometers, such as those produced by Cybex. Isokinetic testing on these dynamometers consists of torque measurement while the subject works maximally against a crank that moves at a constant angular velocity over a range of angles. The effect of angular acceleration is not considered because of the constant angular velocity. Torque - angular velocity relationship can be expressed either independently of joint angle or at a given angle. Since torque is also a function of joint angle, expressing maximum torque independently of joint angle increases the error. When using torque data collected from isokinetic dynamometers, the effect of limb and crank weight, acceleration and deceleration of the crank, and

the difference between crank and joint angles must be taken into account (King and Yeadon, 2002).

Wobbling masses

Most of the previous studies have assumed rigid body approximation for the body segments while modelling the human body. Although this assumption holds with acceptable errors for some cases, the effect of soft tissue movement on the dynamic behaviour of the human body becomes important when the body segments experience high accelerations or impact forces. Pain and Challis (2001) demonstrated the role of the heel pad and shank soft tissue during impact, whilst Yue and Mester (2002) determined the effects of wobbling mass during the whole-body vibration. Wobbling mass and rigid body models of a drop jump have been compared by Gruber et al. (1998) and Pain and Challis (2006). Considerably less joint torques were found for the wobbling mass model than the rigid body model in both studies.

Kong (2004) and Glynn (2007), after geometrically modelling the body segments, separated hard and soft tissues of the segments as rigid and wobbling components. Relative mass of bone and the remaining components were used for separation. They estimated the mass ratio of bone and soft tissue of the segments by using the data from literature (Clarys and Marfell-Jones, 1986). Alternatively, by having 3D meshes of the bones from Magnetic Resonance images, volumes of the bones can be calculated easily and once the density of the bone is estimated bone mass can be found. The separated bone and soft tissue components were modelled as two rigid segments, which were connected to each other with non-linear spring-damper systems to represent soft tissue movement (Kong, 2004; Glynn, 2007). The damping coefficient was set so that the system is near-critically damped (Pain and Challis, 2001).

Equipment parameters

The inertia parameters of a tennis racket are needed for the computer simulation model in this study. How to measure these parameters by simple experiments was described by Brody (1985). Glynn (2007) measured the moments of inertia of two tennis rackets around the transverse and frontal axis by the experimental methods described in the literature and compared them with the values

obtained by using a Babolat Racket Diagnostic Centre. Differences of 3.4 to 13.4% were found between the two methods.

As it was mentioned earlier in section 2.1.5, tennis racket-ball impacts were modelled mostly with spring-damper systems. For this reason, viscoelastic parameters have to be determined for the simulation model. The ball is generally modelled as a lumped mass, which is attached to a spring-damper system. The stiffness and damping coefficients of this system were mostly determined by experimental methods in the previous studies. A quasistatic deformation test and simple ball drop test were used to determine the ball stiffness and damping coefficients by Brody (1979) and Leigh and Lu (1992). For the same purpose, Haake et al. (2003b) and Davies (2005) used optimisation procedures to match the experimental data. They also found a linear relationship between ball impact velocity and ball viscoelastic parameters. All these studies mentioned above, assumed constant parameters throughout the impact. On the other hand, Goodwill and Haake (2004) introduced another damping component, momentum flux, besides material damping. In addition, they determined the stiffness coefficient and both damping coefficients as a function of ball displacement. However, they used Euler's method to solve the equation of motion of the ball, which might not have very accurate results.

For the viscoelastic parameters of the stringbed models, Goodwill and Haake (2001) determined the stiffness coefficient by applying a force over a circular area, which is perpendicular to stringbed, and measuring the resulting deflection for different loads. Leigh and Lu (1992) determined the string stiffness in a similar way. To determine damping coefficient they dropped a pool ball on the stringbed, which was clamped in place. No loss in the rebound velocity of the pool ball was found so they concluded there was no damping in the string system. For this reason, a damping coefficient was not used in the stringbed model (Leigh and Lu, 1992).

2.3.3 Evaluation

Evaluation of the model is the next step after developing the simulation model and determining the model parameters. It ensures that the assumptions made in the modelling phase are correct and enhances the reliability of the model.

However, it is impossible to completely validate models of natural systems. The agreement of the results of the model and real system only supports the probability of representing the real situation by the model (Oreskes et al., 1994).

The model's performance under known conditions is compared with the performance of the real system in order to evaluate the model (Maria, 1997). By determining and using subject-specific parameters, a simulation model is expected to reproduce actual performance of the same subject. For this reason, a performance data collection is necessary to evaluate the simulation model. Most models are evaluated by comparing the motion of the model with the subject's actual motion. An image analysis is needed to measure and analyse the subject's motion. Sometimes additional synchronised data may be necessary such as force plate data, electromyography, etc. depending on the aim of the simulation model.

Image analysis

Motion analysis of actual performance of a tennis player during backhand strokes is needed for generating realistic inputs for the simulation model and for the evaluation of the model. Motion of the body segments as a result of muscle activation can be examined at each instant of the stroke by sequential camera image analysis. Joint angles and motion of joint centres can be determined by different techniques including cinematography and automatic motion analysis systems.

Cinematography is used extensively in measuring motion in sport. Giangarra et al. (1993) and Kelley et al. (1994) used cinematography for analysing backhand strokes in their studies. The high image resolution associated with this technique is a big advantage but analysing and digitising the film is a very time consuming process and subject to human error.

High-speed video cameras are generally used for capturing fast motions such as the impact of tennis balls with rackets. The high frame rates associated with these cameras allows users to record motions occurring during very small time intervals. The resolution of high-speed cameras is not as good as cine films, but decreasing sampling rate improves the quality of the image and the difference between the resolutions of images has further decreased with the development of new technologies in high-speed cameras. However, since the sampling frequencies can be very high, and the memory required for high-resolution frame images is very large, it is not practical to use high-speed cameras for long duration events.

Automatic motion analysis systems have become popular in recent years. These systems use active or passive markers attached to the body. The position and motion of these markers determine the joint kinematics and therefore the motion of the body. Although there are successful examples (Mitchell et al., 2000a) of using motion analysis systems with active markers (e.g. CODA), generally passive markers are used in motion analysis systems (e.g. VICON, ELITE) since they do not need the wires and power sources necessary for active markers. Typically, strobes emitting infrared light are attached to each camera of the system. The passive markers covered with retro-reflective material reflect the infrared light and cameras capture the image of markers with infrared filters. The biggest advantage of these systems is the analysis of the captured images. The system digitises the locations of the markers and creates the 3D view of the image automatically. Required joint kinematics are calculated and presented to the user by the system. The main disadvantage of these systems is the price. Additionally, the system is a 'black box' from which one can only obtain limited outputs that generally do not allow the user internal access. However, there are examples of researchers developing and validating their own bespoke motion analysis system having full control of the system with low cost.

Electromyography (EMG)

EMG is the only tool available to measure muscle activation. It is used in almost every study that is concerned with muscles and their activation. EMG provides useful data, but it has many limitations.

Three different types of electrodes are used to obtain EMG signals: surface electrodes, intramuscular wire electrodes and needle electrodes. The last two are invasive electrodes and mostly used clinically. Although they are non-invasive, using surface electrodes limits the number of muscles that can be monitored since activation of the deep muscles cannot be measured with surface electrodes.

EMG signals provide information about muscle activation timings and the force contribution of individual muscles as well as groups of muscles. In biomechanics, there are mainly three applications of surface EMG signals: they are used as an indicator for the initiation of muscle activation, they are related to the muscle force, and they are used as an index of the fatigue processes occurring within the muscle.

Location and orientation of the electrodes is very important. The electrode should be placed on the midline of the muscle belly between a motor point and the tendon insertion or between two motor points. The detection surfaces should be arranged in such a way that they intersect as many muscle fibres as possible. The reference electrode should be placed as far away as possible and on electrically neutral tissue, which may be a bony prominence.

Crosstalk from other adjacent muscles is another important factor in EMG. It has been shown that in the leg approximately 17% of electrical activity from nearby muscles may be detected. Therefore, if an adjacent muscle is active rather than the one directly below the electrode, a crosstalk signal can be detected and misinterpreted as originating from the muscle of interest. Placing the electrode in the midline of the muscle belly reduces the chance of detecting crosstalk signals.

In the time domain, EMG signals are processed in two ways: root mean squared (rms) value and the average rectified value. For EMG signals detected during voluntarily elicited contractions, the rms value may be appropriate since it represents the signal power (De Luca, 1997).

2.3.4 Optimisation and Sensitivity

Optimisation

Optimisation of the model parameters with respect to some selected criteria is needed in simulation modelling since there are many solutions for the system, some of which are not feasible. At the beginning of the optimisation process, an objective function, which depends on the aim of the model, is formulated. Then, an algorithm is developed to minimise or maximise the objective function by changing the values of the parameters of the model. One of the main difficulties for the optimisation process is to find the global optimum rather than a local optimum.

There are many algorithms available to minimise or maximise a non-linear objective function. The Simplex Method (Nelder and Mead, 1965), which is a local optimisation method, can be iteratively used for global optimising. Genetic algorithms (Man et al., 1996; Mitchell, 1996) are also used for global optimisation. However, the Simulated Annealing algorithm (Corana et al., 1987) has been shown to be more effective than some other commonly used conventional algorithms at the expense of more computing time (Goffe et al., 1994).

The Simulated Annealing algorithm is based on annealing, a thermal process for obtaining low energy states in a material. It tries to minimise energy given by a cost function to find a global minimum (Jensen, 2002).

Sensitivity

Sensitivity analysis shows the sensitivity of the optimum solution to the parameters used in the model. High sensitivity of the solution to a parameter implies that small changes in the value of that parameter cause larger variations in the results. Sensitivity analysis is done by perturbing the values of the questioned parameters of the model.

2.3.7 Summary

In this section, development and evaluation of a subject-specific computer simulation model and techniques for determining both equipment and subject parameters have been described.

2.4 Summary of Literature Review

In the literature, studies about tennis generally focus on modelling of the equipment and kinematics of the tennis shots. There has been almost no prior research on modelling tennis strokes with individual muscles or torque generators. Therefore, there is a lack of information in this area and the intention of this study is to fill this gap in the literature.

In this study, the generally accepted and used methods, e.g. the spring-dashpot method for modelling tennis equipment and a rotational equivalent of Hill's model for torque generators, will be used. Development of these methods and determination of the parameters can be found in the following chapters.

3 DEVELOPMENT OF THE SIMULATION MODEL

In this chapter, the development and the main features of a computer simulation model of one-handed tennis backhand strokes will be discussed. The model consists of an arm and torso with a tennis racket and a tennis ball and it was developed using MSC.ADAMS.

3.1 Model Development

3.1.1 Selection of the Software Package

To develop the simulation model a software package was selected, since writing equations of motion from first principles would be too time consuming for a complex multibody model. There are many software packages available for modelling purposes such as: AUTOLEV, VisualNastran 4D (VN4D) and MSC.ADAMS. Each package has different capabilities and so has advantages and disadvantages. AUTOLEV, for example, lacks a modern object-oriented structure and does not have a graphical user interface. Moreover, it is not easy to use AUTOLEV for the models including individual muscles because complex code needs to be written for muscle wrapping in the model. Testing simple models and having personal communication with researchers who used VN4D revealed that it was not very flexible and the range of allowable parameter types that could be controlled by Simulink was limited. In addition, it was not clear which output of the VN4D block diagram in Simulink corresponded to which parameter in VN4D. Considering the factors such as flexibility, user-friendliness, accuracy, speed, import/export possibilities from/to other software packages, visual graphics it was decided to use MSC.ADAMS (ver. 2005).

3.1.2 Overview of the Simulation Model

To begin with, in order to learn how to use the MSC.ADAMS software, its commands and capabilities efficiently, various simple initial models were created and tested. With these simple models, configuration and design of the model was

studied step by step. By adding more segments, features and structures to one of these initial models, the main model was developed (Figure 3.1).

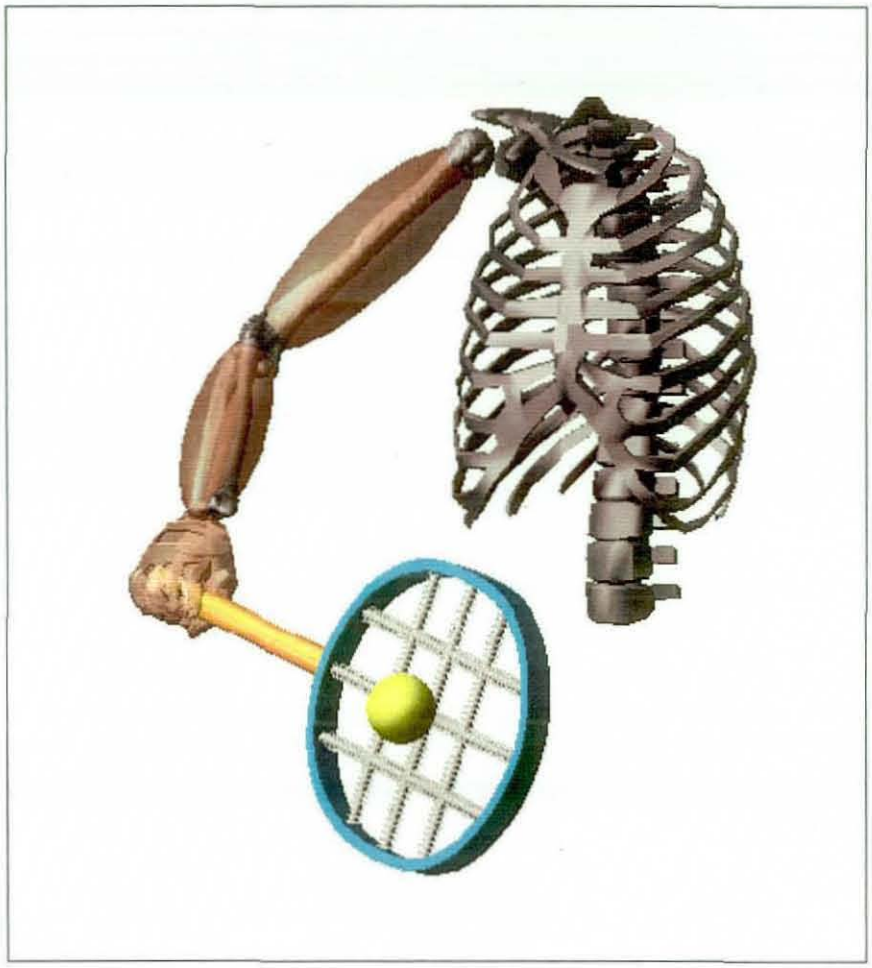

Figure 3.1. 8-segment computer simulation model for one-handed tennis backhand strokes including tennis ball.

The player-racket model has eight segments, named from proximal to distal: humerus, ulna, radius, hand, racket handle, racket head and two more segments for representing upper arm and forearm wobbling masses. The thorax and scapula are not included in this number since their motions are predefined. Additionally, there are nine point masses to represent the stringbed and the ball was modelled as a rigid sphere. There are twelve rotational degrees of freedom in the model: three at the shoulder, two at the elbow, two at the wrist, three at the grip and finally two between the racket handle and racket head. Time histories of the translation and orientation of thorax and scapula were input to the model from performance data collected on a one-handed backhand stroke by an elite tennis player.

The simulation model can be used either as an angle-driven model or as a torque-driven model depending on the aim and the required output from the model. In addition, some of the torque generators may be replaced with individual muscles (e.g. wrist extensor or flexor). The angle-driven model was also used to determine some of the model parameters such as hand-racket interaction and wobbling mass parameters. This was achieved by driving the model with time histories of segmental motion and optimising the required parameters in order to have minimum difference between simulation and performance data. Time histories of the segmental motion during tennis backhand strokes of an elite tennis player were obtained using a Vicon Motion Analysis System. These data were composed of translation and rotation of each body with respect to a global origin or relative to each other and were fitted by quintic splines to reduce the noise in the data.

For the torque-driven model, activation parameters for each of the torque generators were optimised (Chapter 6). The control and the optimisation of the model were done using MATLAB via Simulink. The Simulated Annealing algorithm was used for optimisations (Goffe et al., 1994).

To compare off-centre impacts with centred impacts for a specific simulation, the impact location of the ball on the racket can be arranged. The eight point masses around the racket centre, which were used to model the stringbed with centre point mass, define the different impact locations. The direction and magnitude of the inbound velocity of the ball are kept constant while changing the ball position.

The simulation model can be divided into two parts: player model, and racket model with ball. These parts will be discussed in detail in the following sections.

3.2 Player Model

3.2.1 Body Segments

The player model has four segments: humerus, ulna, radius and hand. The thorax, scapula and clavicle were also added to the model as supplementary segments. The thorax and scapula define the position and orientation of the model with respect to the global origin. Although, the thorax is counted as one segment, it is a combination of ribs, spine and sternum fixed together. The relatively small motions

of these segments with respect to each other were neglected since they were beyond the scope of this study.

3D meshes of the scapula and thorax were obtained from the literature (BRG.LifeMOD™) whereas Magnetic Resonance (MR) images were used to form humerus, radius and ulna segments (Chapter 5). The model was designed so that in the future it will be driven by individual muscles. For this reason, bone shapes are important to determine the muscle attachment points more realistically. The shape of the bones can also be used while dealing with the muscle-wrapping problem.

The motion of the clavicle was not included in the kinematic chain of the model. However, for the sake of visual completeness the clavicle was added to the model as a redundant segment. The time history of clavicle motion was estimated from the performance data, but had no influence on the simulation.

3.2.2 Joints

The joints used in the player model are simplified versions of the anatomical joints at the shoulder, elbow and wrist. Since the scapula and thorax motions were predefined, there was no need to use a joint between these segments.

The joints were formed by 2 or 3 consecutive revolute joints on top of each other. The rotation axis of each consecutive joint is perpendicular to the others and the rotations around these axes correspond to anatomical joint movements (e.g. flexion, abduction) in three perpendicular planes (i.e. sagittal, coronal and transverse planes).

To represent anatomical joint angles the generally accepted notation first used by Grood and Suntay (1983) was used (Figure 3.2). The rotation axes of the joint were determined by considering the anatomical structure. The line joining the proximal and distal joint centres was coincident with the rotation axis normal to the transverse plane. Two anatomical locations such as condyles or processes on the distal end of the bones helped to define the rotation axis normal to the sagittal plane. The cross product of these two rotation axes gives the remaining third axis for the coronal plane. Changing the sequence of rotations affects the joint angle values and singular positions of the joint considerably. The rotational sequence used in each

joint model was initially a rotation in the sagittal plane, then in the coronal plane and finally in the transverse plane.

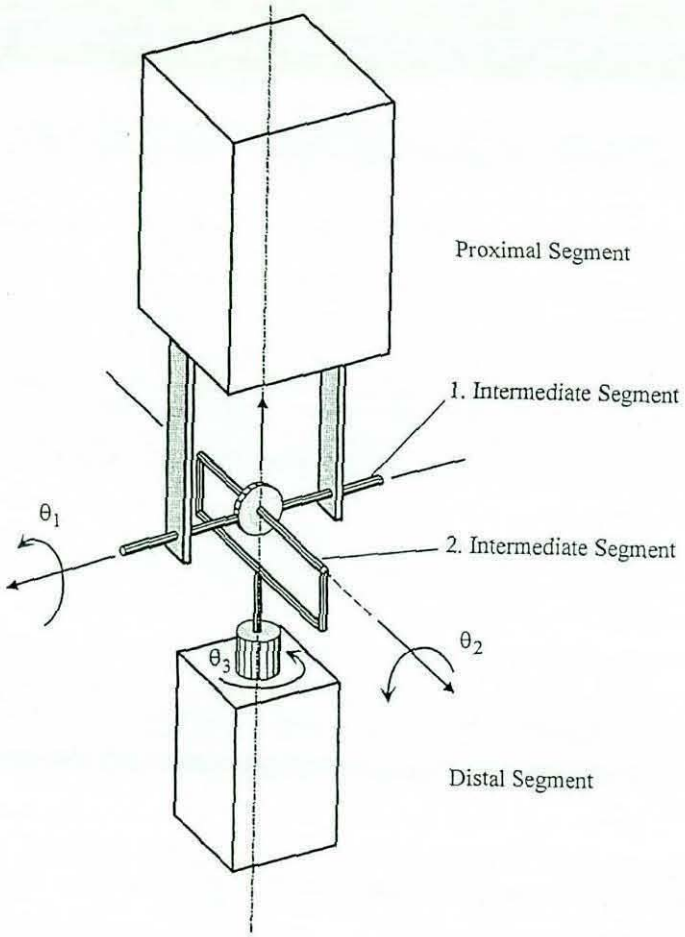

Figure 3.2. *Mechanical model of the joints used in the simulation model.* [adapted from (Guler, 1998), p.31]

Shoulder and wrist joints were defined exactly as in the joint model mentioned above (Figure 3.2). On the other hand, although there are examples in the literature using the same joint model for the elbow joint (Raikova, 1992), it was modified to allow the radius to rotate around the ulna in order to have a more realistic pronation/supination movement of the forearm (Lemay and Crago, 1996; Holzbaur et al., 2005). To achieve this, the location of the third revolute joint was moved to the radial head and the rotation axis was tilted by passing through the centre of the radial head and the centre of the distal end of the ulna (Morrey and Chao, 1976) (Figure 3.3). The results of this modification will be discussed in Chapter 4.2. in detail. Furthermore, the second revolute joint at the elbow was fixed

to represent a constant carry angle since the motion of forearm in the coronal plane is very limited due to the structures of the humerus and ulna at the elbow joint.

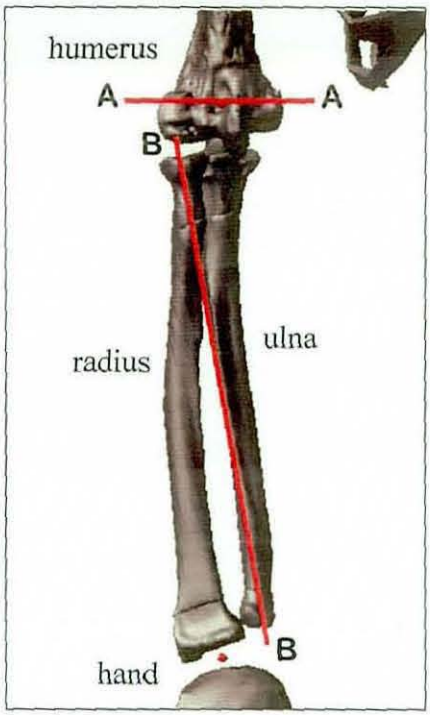

Figure 3.3. The rotation axes of the elbow joint: (A-A) for flexion / extension and (B-B) for pronation / supination

For the wrist joint, the structure of the metacarpal bones does not allow the hand to rotate around the longitudinal axis (Jenkins, 2002). Therefore, the third revolute joint was fixed at the wrist.

The locations of the joint centres were estimated from the bone shapes. Generally the shoulder joint is simplified as a ball and socket joint and the centre of the head of the humerus is estimated as the shoulder joint centre (Van der Helm et al., 1992; Veeger, 2000). The same method was applied in the player model. The location of the elbow joint centre was first estimated as the centre of the line connecting the lateral and medial epicondyles. This location was then translated by a small amount (~1.5 mm) on the line to find a better estimate considering the shape of the humerus and ulna (Figure 3.4a). The wrist joint centre was estimated similarly. First, the midpoint of the line connecting the radial and ulnar condyles was found in the anatomical position. This point was then translated downwards (~23 mm) on the line connecting this point and the elbow joint centre considering the overall forearm link length (Figure 3.4b).

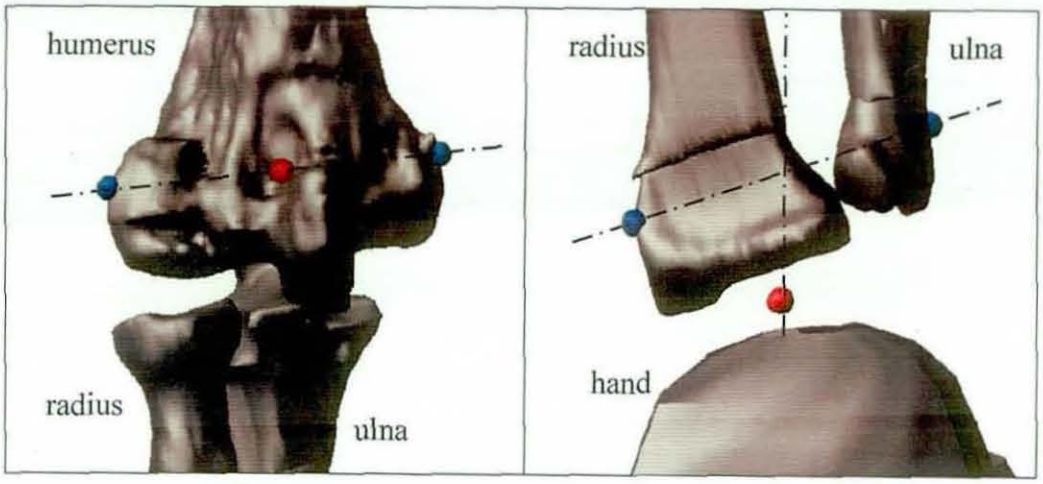

Figure 3.4. The location of the elbow (a) and wrist (b) joint centres. Blue dots represent (epi)condyles and red dots represent joint centres.

The neutral positions of all joints were chosen to be the same as in the anatomical position of the thorax and arm (Figure 3.5). Joint angles were defined as positive in the direction of flexion, adduction / ulnar deviation, and external rotation / supination around the corresponding rotation axes. The initial conditions of each joint were determined from the performance data.

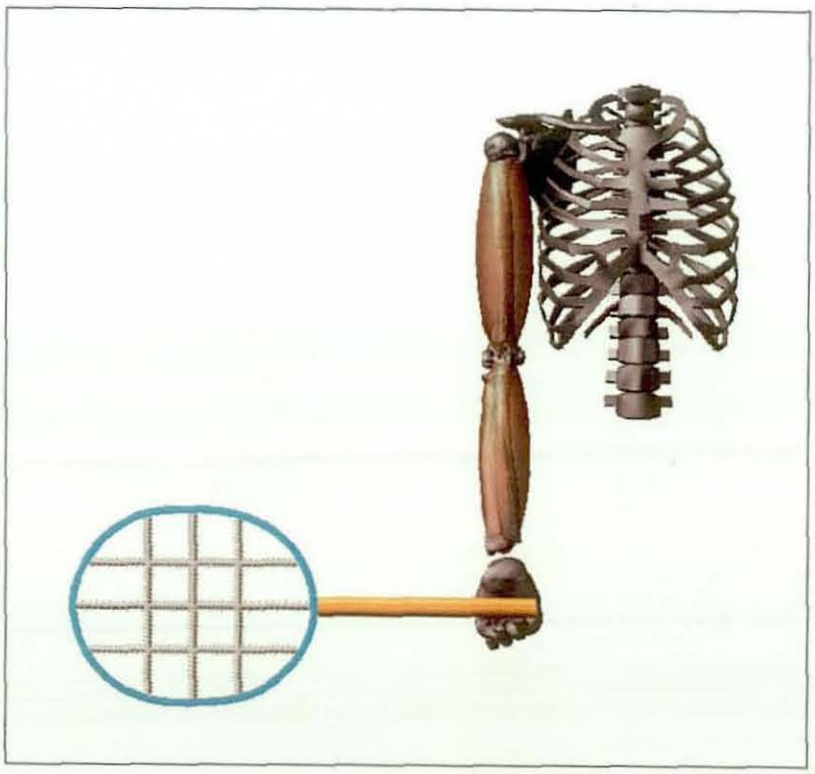

Figure 3.5. Neutral positions of all joints in the model.

3.2.3 Joint Actuators

Angle-driven joints

All segmental motions of the player model were predefined for the angle-driven model and determined from the performance data collection. For the angle-driven model, no actual joint actuators were used since the input motion data constrained the segments of the model to follow the desired motion.

Torque-driven joints

Pairs of torque generators were used at the shoulder, elbow and wrist joints for the torque-driven player model for each different joint movement. These torques applied at each joint centre are the net moments of all muscular forces around the rotation axis of that joint. Necessary torque values for the backhand stroke motion were estimated from the torque-strength parameters (Chapter 5) and torque activation parameters (Chapter 6) as well as from the joint angle and angular velocity.

The torque generators were modelled as a contractile component and a series elastic component adapted from the model of Kong (2004). Each torque generator has extensor and flexor parts that act in opposite directions and represent the agonist-antagonist muscle action. A graphical representation of the torque generators for extensor and flexor torques can be seen in Figure 3.6 where:

θ_j = joint angle
θ_{con} = contractile component angle
θ_{sec} = series elastic component angle

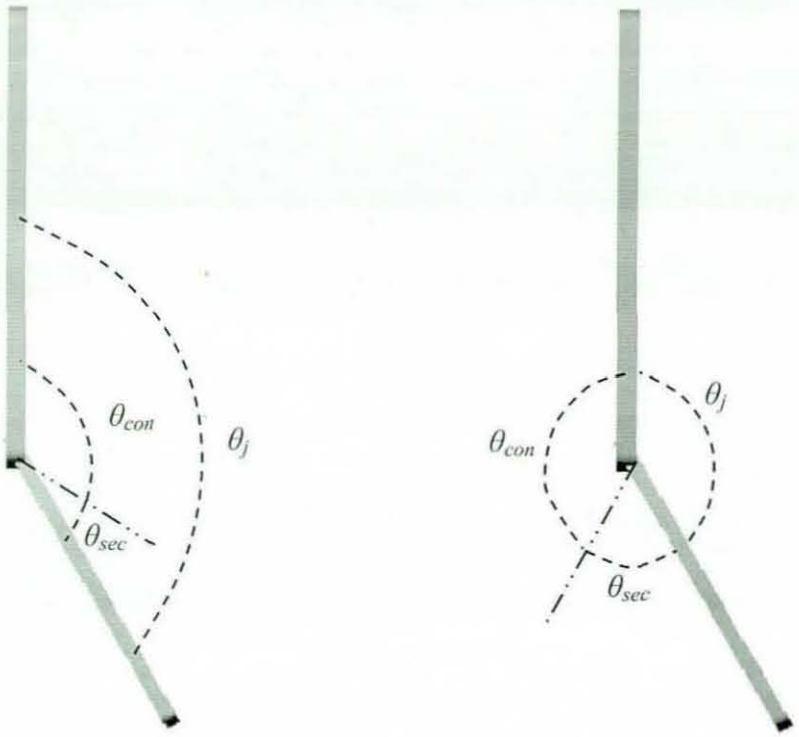

(a) (b)

Figure 3.6. Graphical representation of a torque generator for flexor (a) and extensor (b) torque.

From the Figure 3.6, the geometric relationships can be written as:

$$\theta_j + \theta_{con} + \theta_{sec} = 2\pi \quad \textit{for extensor} \tag{3.1.a}$$

$$\theta_j = \theta_{con} + \theta_{sec} \quad \textit{for flexor} \tag{3.1.b}$$

The contractile component torque (Equation 3.2), which is a function of contractile component angle and angular velocity, was calculated using torque-strength parameters (Chapter 5).

$$T_{con} = T_4(\omega)a(\omega)[1-q(\theta_{con}- \theta_{opt})]^2 \tag{3.2}$$

where, T_{con} = contractile component torque

ω = contractile component angular velocity

$T_4(\omega)$ = four-parameter-fit contractile component torque (Equation 3.3)

$a(\omega)$ = differential activation

q = rate at which torque drops off from the optimum angle

θ_{opt} = optimum angle at which maximum torque occurs

and,

$$T_4 = \frac{T_c(\omega_{max} + \omega_c)}{\omega + \omega_c} - T_c \qquad \textit{for concentric} \qquad (3.3.a)$$

$$T_4 = \frac{-(T_{max} - T_o)\omega_e}{\omega_e - \omega} + T_{max} \qquad \textit{for eccentric} \qquad (3.3.b)$$

(equations taken from Yeadon et al.(2006))

where, T_o = maximum isometric torque

T_{max} = maximum torque, asymptote of torque in eccentric hyperbola

ω_{max} = maximum angular velocity at which torque equals zero

$-T_c$ = asymptote of torque in concentric hyperbola

ω_c / ω_e = asymptote of angular velocity in concentric / eccentric hyperbola

On the other hand, the series elastic component torque was obtained by Equation 3.4.

$$T_{sec} = k\,\theta_{sec} \qquad (3.4)$$

where, T_{sec} = series elastic component torque

k = series elastic component stiffness

Since the contractile component torque calculated from the torque-strength parameters was the maximum possible torque, it was multiplied by a torque activation level and equated to the series elastic component torque (Equation 3.5).

$$T_{con}\ a(t) = T_{sec} \qquad (3.5)$$

where, T_{con} = contractile component torque

T_{sec} = series elastic component torque

$a(t)$ = torque activation level

At the beginning of the simulation, the initial contractile component angle was calculated (Equations 3.1-3.5). For the next time step, the contractile component angle was updated using a 4th order Runge-Kutta approximation. In this process, the contractile component angular velocity was needed at specific times for particular contractile component angles. Equations 3.1-3.5 were combined and converted into a cubic polynomial (in terms of angular velocity) and the root that satisfied Equation 3.5 was selected in order to calculate the required angular velocity. After determining the contractile component angle from the Runge-Kutta approximation, Equations 3.1.b and 3.4 were used to determine the flexor or extensor torque. The same procedure was applied for the subsequent time steps in the simulation.

The torque activation level takes values between 0 (no activation) and 1 (full activation). Quintic functions (Yeadon, 1984) (Equation 3.6) were used to ramp up or down the activation level instead of an abrupt change in the activation.

$$Q(x) = x^3(6x^2-15x+10) \tag{3.6}$$

3.2.4 Wobbling Masses

Soft tissue motions within the upper arm and forearm were represented using wobbling masses. The wobbling masses were assumed to be rigid bodies which were attached to the segments by spring-damper systems as can be seen in Figure 3.7. Since there are two segments in the forearm, the proximal end of the wobbling mass was attached to the ulna and distal end to the radius (radius and ulna together form the forearm segment). Identical springs were used for each wobbling mass and the spring force was calculated by Equation 3.7 (Pain and Challis, 2001):

$$F = -kx^3 - c\dot{x} \tag{3.7}$$

where, F = spring force

k = stiffness coefficient

c = damping coefficient

x = displacement between wobbling mass and bone

$\dot{x}$ = time derivative of x

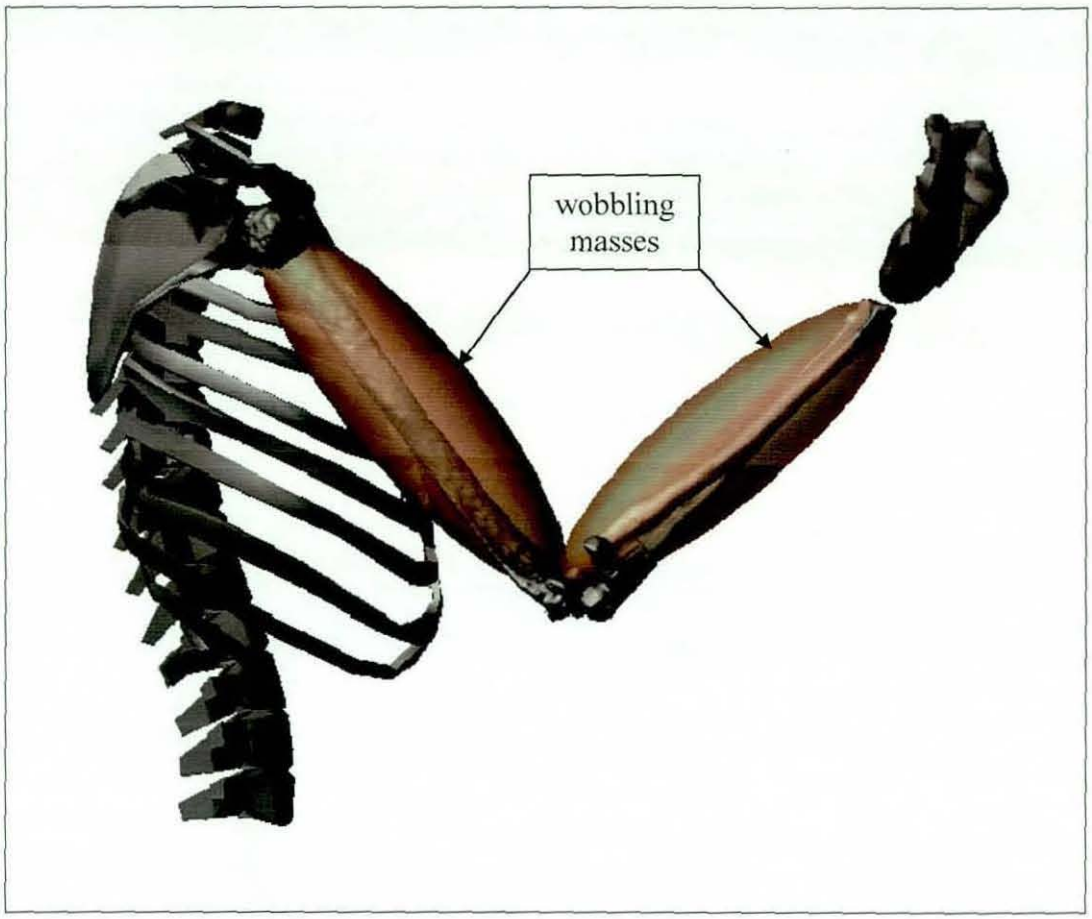

Figure 3.7. Upper arm and forearm wobbling masses.

3.2.5 Hand-racket Interaction

It was seen from the performance data (Chapter 4) that there was little linear motion of the racket with respect to the hand since the player holds the racket firmly during a backhand stroke. For this reason, a ball and socket joint with three rotational degrees of freedom was used to connect the hand and the racket handle. Three pairs of equal and opposite torques between the hand and the racket were used to represent the gripping torque around the principal axes of the tennis racket. The resistance of the racket motion within the hand after the impact was represented by three torsional springs around the rotation axes of the racket with respect to the hand (Equation 3.8).

$$T_G = T(t) \qquad \textit{before impact} \qquad (3.8.a)$$

$$T_G = T(t) - k_t(\theta - \theta_o) - c_t(\theta - \theta_o)\dot{\theta} \qquad \textit{after impact} \qquad (3.8.b)$$

where, T_G = gripping torque

$T(t)$ = gripping torque as a function of time only

k_t = torsional stiffness

c_t = torsional damping

θ = angular displacement of racket with respect to hand

θ_o = angular displacement of racket with respect to hand at impact

$\dot{\theta}$ = time derivative of θ

3.3 Racket and Ball Model

The racket model developed by Glynn (2007) was used in this study. The racket frame and stringbed were modelled separately and then combined to give the whole racket. The ball was modelled as a rigid sphere. The simplified model of the ball-racket impact will be discussed after describing the model.

3.3.1 Racket Frame Model

The racket frame was composed of two rigid segments; racket handle and racket head (Figure 3.8). These two segments were joined together with two consecutive revolute joints, which have perpendicular rotating axes. The location of the joint was determined from a vibration analysis of the racket frame in the frontal and transverse planes of the racket (Glynn, 2007). The average location of the antinodes of the fundamental modes of vibration in each plane was selected for the joint location since the displacement of the racket was maximum at the antinodes. The vibration of the racket frame was controlled with two torsional spring-dampers at each revolute joint. The resistive torque at the joints was defined by the spring-damper equation:

$$T = -k_t\theta - c_t\dot{\theta} \tag{3.9}$$

where, T = resistive torque in the torsional spring

k_t = torsional stiffness of the spring

c_t = torsional damping of the spring

θ = angular displacement between racket frame and racket head

$\dot{\theta}$ = time derivative of θ

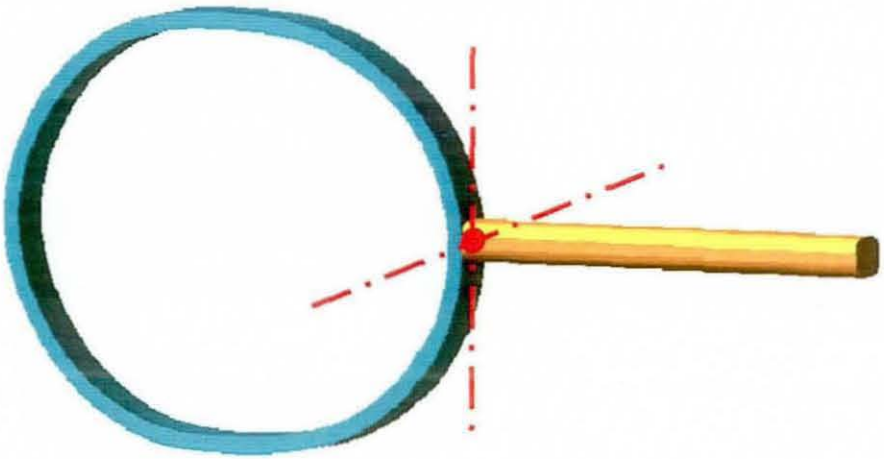

Figure 3.8. Two-segment racket frame model with the rotation axes of the joints between segments.

3.3.2 Stringbed

The stringbed was modelled as nine point masses/particles attached to each other and/or the racket frame by elastic springs (Glynn, 2007) (Figure 3.9). Since only these nine point masses represent the stringbed, the ball impact can only occur at one of these points in a given simulation. The location of the point mass in the middle was chosen as the geometric centre of the stringbed. The remaining point masses were located around the centre point at a distance of one tennis ball diameter away to cover most of the stringbed area. The impact, which occurs at one of these points, represents off-centre impacts. The mass of the strings was equally shared by the nine point masses.

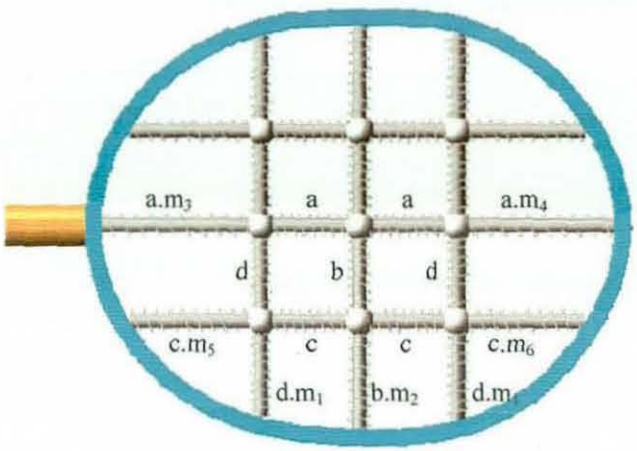

Figure 3.9. The stringbed model with point masses. Stiffness coefficients of the springs are also shown.

The springs around the point masses were preloaded at the beginning of a simulation to represent string tension in the racket. Considering the symmetry and natural length of the springs around the geometric centre of the racket, four different stiffness coefficients (a-d in Figure 3.9) were attributed to these springs. Stiffness coefficients of other springs, which have one end fixed to the racket frame, were assumed to be constant multiples (m_1-m_6 in Figure 3.9) of the previously mentioned four stiffness coefficients. Symmetric springs around the long axis of the stringbed were again assumed to have the same stiffness coefficients. Since strings return around 95% of incoming ball energy to the ball after the impact, no damping was used in the springs while modelling the stringbed (Brody, 1995). Spring forces were calculated by the Equation 3.10.

$$F = -kx - P \tag{3.10}$$

where, F = spring force

k = stiffness coefficient

x = change in the length of the spring

P = preload

3.3.3 Ball-Racket Impact

The impact of the ball and racket was modelled as a normal impact force and a frictional force which were normal and tangential to the racket head plane, respectively (Glynn, 2007).

It was seen after analysing the performance data that relative velocity of the ball with respect to the racket had not only a normal component but also considerable tangential components in the racket reference frame. This was mainly due to the motion of the racket, since the major component of the ball was in the normal direction. For this reason, modelling of a normal impact was not sufficient and oblique impacts were considered. To model the oblique impact, frictional forces that occurred due to tangential relative velocity of the ball were combined with the normal impact force.

For estimating the normal impact force, a spring-damper system was used between the ball and the point mass where impact occurred on the stringbed (Glynn, 2007). The normal impact force in the model is defined by Equation 3.11:

$$N = -kx - c\dot{x}R \tag{3.11}$$

where, N = normal impact force

k = stiffness coefficient

c = damping coefficient

x = normal component of relative displacement between the ball and the point mass in racket head reference frame

$\dot{x}$ = time derivative of x

R = ramp-up quintic function (changes from 0 to 1 over the period from ball impact until the edge of the ball penetrates 1.25 mm into the stringbed)

For frictional forces on the racket head plane a coefficient of friction was determined (Glynn, 2007). Although the tennis ball may slide and/or roll on the stringbed both of which have different coefficients of friction, for simplicity, only one coefficient (μ) was used to estimate the frictional forces at the point of impact. Considering the stringbed stiffness at each impact location and the racket symmetry,

three different values for μ were used in the model. The direction of the frictional forces were opposite to the tangential relative velocity (Equation 3.12).

$$F_f = -\text{sgn}(\dot{x})\mu N \tag{3.12}$$

where, F_f = friction force on the racket head plane

μ = coefficient of friction

N = normal impact force

$\dot{x}$ = time derivative of tangential component of relative displacement between the ball and the point mass in racket head reference frame

3.4 Summary

In this chapter, the development and the main features of a computer simulation model of one-handed tennis backhand strokes have been discussed. The model included a torso, a whole arm and a racket-ball system. The joint motion actuators at the shoulder, elbow and wrist can be angle or torque-driven depending on user selection. Ball impact location on the racket can also be selected by the user to simulate centre and off-centre impacts.

Determination of the required parameters for the model from performance data collection, experimental analysis or optimisation will be discussed in detail in the following chapters.

4 DATA COLLECTION AND ANALYSIS OF TENNIS BACKHAND STROKES

To evaluate the computer simulation model described in the previous chapter, stroke performance data were needed from a subject to compare the simulation output and the actual performance. The first part of this chapter describes the method and protocol for the performance data collection of an elite tennis player performing one-handed tennis backhand strokes and the equipment used in the data collection. The analysis and comparison of two selected trials from the data collected is subsequently presented to explore the effects of the ball-racket impact location on segmental motion and muscle activation.

4.1 Performance Data Collection

A protocol for synchronised kinematic and EMG data collection was established for a number of different studies. An elite tennis player was used as the subject. The subject performed topspin and backspin one-handed tennis backhand strokes. In this study, two trials with the Head LM8 racket, which had centre and off-centre impact locations for topspin backhand strokes, were used. The trial having a centre impact was the main trial used for evaluating the simulation model. The second trial, which had an off-centre impact, was used to ensure that the model behaves realistically for different impact locations.

4.1.1 Method and Protocol

Method

The data collection took place in the Gymnastics Centre at Loughborough University. The Centre has a Vicon Motion Analysis System to collect kinematic data from gymnasts. The same system was also used in this data collection since it was not possible to relocate the Vicon System around a tennis court as the system was not portable at that time. However, there was sufficient space in the gymnastics centre to perform an equivalent stroke to one in real court conditions. Masking tape was used to draw the borders of an imitation tennis court.

The Vicon Motion Analysis System is one of the motion tracking and analysis systems on the market. The system includes a data station that controls the system and stores captured data, a number of different foci cameras with strobes on which near-infrared light emitting diodes (LED) are mounted and passive retro-reflective markers coated with reflecting material.

The motion data captured by the system are the position time histories of the markers in 3D space. To capture data, the strobes around the cameras emit infrared light and the markers reflect this light. Each camera lens potentially receives this reflected light from the markers and locates them in its own 2D frame of reference. The 2D frames from each camera are collected in the data station and reconstructed to obtain a 3D location for the markers with respect to a global coordinate system.

Before motion capturing, two stages of calibration, static and dynamic, are performed. In the static calibration, a calibration object is placed in the calibration volume and the system captures the position data of the markers on it. In dynamic calibration, another calibration object, a wand, is moved through the calibration volume. In both cases, the relative position of the markers with respect to each other, which is known previously, are compared with the captured data and the error for each camera is calculated.

After calibration, the time history of the markers' positions within the calibration volume is captured. The reconstruction is done by using specialized software supplied by Vicon. Markers are labelled and the small gaps in the marker trajectories, if there are any, are generally filled using cubic spline interpolation and visually inspected to ensure that this is sensible.

In the performance data collection, a Vicon 624 System was used to collect all kinematic data with an additional analogue signal for synchronising. Twelve M2 strobe cameras, which were spread around the subject's hitting location, were used. Thirty-three 25 mm retro-reflective markers were attached to the subject's body (Figure 4.1) and six markers were attached to the tennis racket (Figure 4.2). The number and position of the cameras were arranged such that the probability of all markers being captured was maximised through pilot testing. The markers were attached to the bony landmarks and some auxiliary places to help build a 3D orientation of each body segment. The Vicon system sampling frequency was chosen as 250 Hz, which was the maximum possible while still being able to capture all

markers in the calibration volume. Static and dynamic calibration of the volume had a mean reconstruction error of 2.2 mm.

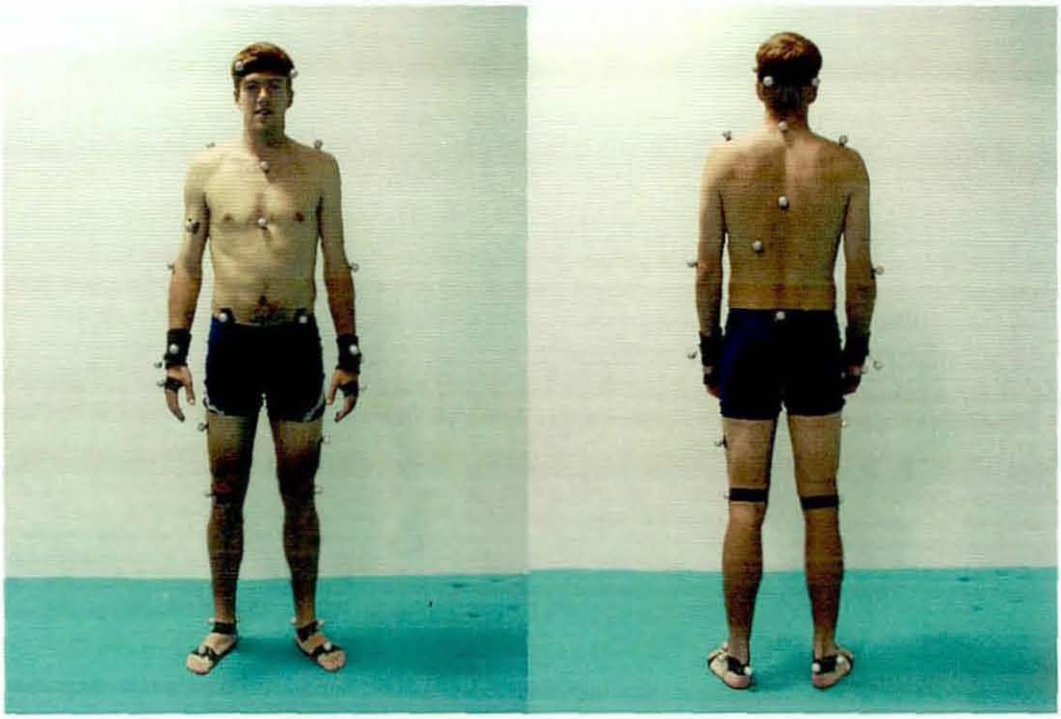

Figure 4.1. Subject with retro-reflective markers.

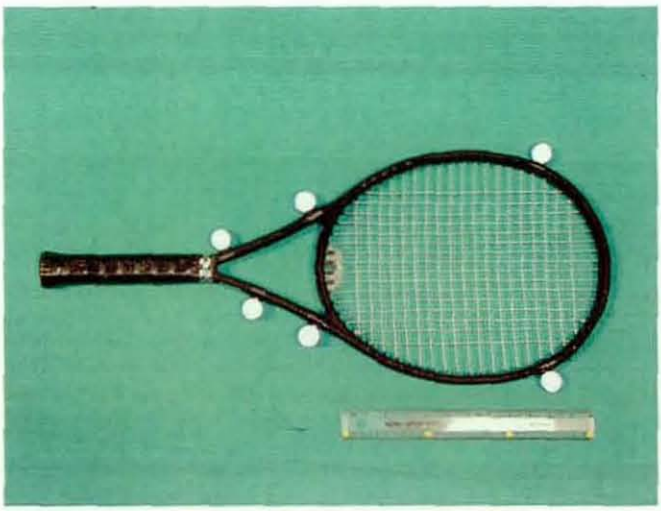

Figure 4.2. Head LM8 tennis racket with retro-reflective markers.

A Biovision EMG system was used to measure the muscle activation during data collection. Nine channels were used: considering motion at the wrist joint, wrist extensors and wrist flexors; motion at the elbow joint, biceps and triceps; motion at the shoulder joint, pectoralis major, latissimus dorsi, anterior, medial and posterior

deltoid muscle groups. Since it was very hard to distinguish between individual forearm muscles, wrist extensors and flexors were considered as muscle groups in the data collection. Nevertheless, the electrodes were aimed to be placed on the extensor carpi radialis brevis and on the flexor carpi radialis for wrist extensors and wrist flexors, respectively. EMG data captured from these muscles were sampled at 1000 Hz. Since the EMG system was initiated manually, data were collected for ten seconds in order to include preparation and follow-through phases of the backhand stroke for each trial. Before collecting data on backhand strokes, maximal voluntary contractions for each muscle group were obtained from a series of resistance exercises in which the subject tried to reach maximum muscle activation.

To measure the ball velocity at impact, impact location, impact time and ball-contact period, two Phantom V4.1 high-speed digital cameras were used. The cameras were genlocked and located to capture impact: one at the left hand side of the subject, approximately in-line with the racket stringbed during impact and one facing the incoming tennis ball, behind the subject. Both cameras operated at 2500 Hz.

The data from the side-on camera were used to determine ball inbound/outbound velocity by digitising ball centre position with the Phantom software. From the same camera, impact time and ball-contact period were also obtained. The high-speed camera behind the subject was used to determine the impact location on the stringbed.

Three uniaxial Brüel and Kjaer piezoelectric accelerometers were mounted on the tennis racket using custom-built brackets, for some of the trials. Accelerometers attached to the right and left sides of the bracket were used to measure racket frame accelerations in the direction parallel to the normal to the stringbed. The other accelerometer, which was attached at the centre, measured the racket frame acceleration in the stringbed plane. The accelerometer data were sampled at 2000 Hz.

A hitting volume of 2.5 m x 2.5 m x 2.5 m was prepared behind the base line of the imitation court. The target area was 4 m^2 adjacent to the other base line. A Bola ball launcher was placed behind this base line (Figure 4.3). The launching velocity and direction of the balls were adjusted according to subject preference. New Penn Titanium tennis balls were used throughout the session.

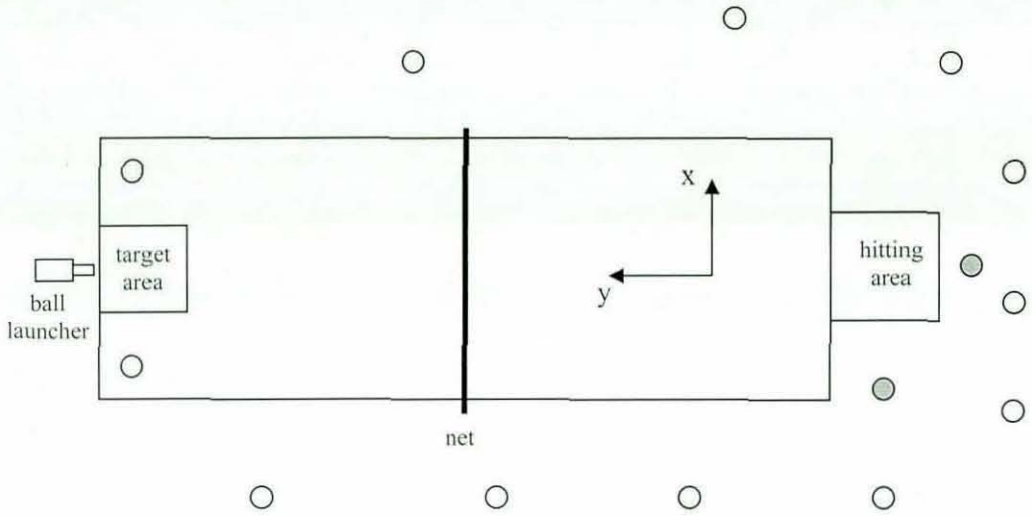

Figure 4.3. Experimental set-up of the performance data collection; white circles represent Vicon cameras and grey circles represent high-speed cameras (figure not drawn to scale).

All the pieces of equipment were synchronised using a trigger system, consisting of a trigger box and remote trigger. The master high-speed camera and EMG system were connected to the trigger box. The remote trigger was used to send a radio signal to the trigger box and to the Vicon system. Vicon received a square pulse on an analogue channel; the trigger box initiated the master high-speed camera and sent a square pulse to the EMG system. The EMG data collection and the Vicon system had been started manually as the ball launched from the ball machine. By using the square pulses sent to them, Vicon and EMG data were synchronised during the analysis of these data.

Protocol

The subject was told about the testing procedure and an informed consent form was signed. The subject hit several one-handed backhand strokes to warm up before the data collection. Then, retro-reflective markers were attached to the subject's body. The surface EMG electrodes were also placed on the subject's appropriate muscle groups (Figure 4.4). In each trial, the Bola machine launched a ball mimicking a baseline rally and the subject returned the ball to land in the target area. Before recording any trial a few pre-trials were done to encourage a consistent backhand stroke.

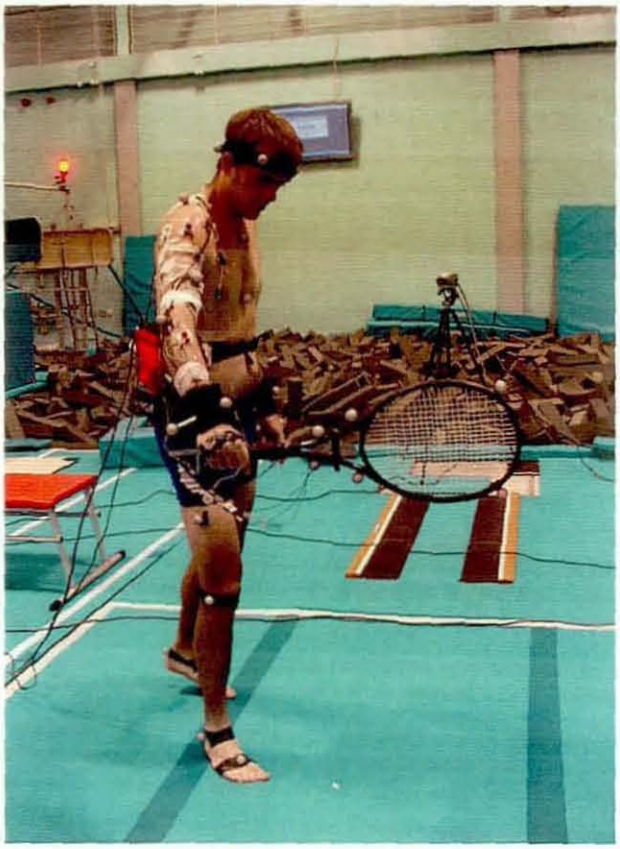

Figure 4.4. EMG electrodes and retro-reflective markers attached to the subject.

Trials were considered successful if the trigger system worked properly and the ball landed in or close to the target area. The subject's opinion about the stroke, either good or bad, was also noted. One good centre impact and one good off-centre impact were selected from the successful trials for top spin backhand strokes.

4.2 Segmental Motion Analysis

To obtain segmental motion data from the marker trajectories obtained by the Vicon System, appropriate segments were formed. This was done using Vicon Body Builder software. A four-segment player model and a racket were formed by using the markers attached to the subject and the racket. The player model included the thorax, upper arm, forearm and the hand segments. Vicon's standard whole-body model, Golem, was customised to form the model and measure the rotation angles.

A reference frame was set on each segment to measure its orientation. The thorax reference frame, whose axes were parallel to the coronal, sagittal and

transverse axes of the torso, was determined by the four markers attached to the subject's torso at the sternum, clavicle, C7, and T10 vertebrae. For the other segments of the player model, the axes of the reference frames were located and oriented such that each axis corresponded to an anatomical rotation axis of that segment. To determine rotation axes of the segments (except the thorax), the line joining the proximal and distal joint centres was assumed to be the rotation axis of the joint in the transverse axis (z-axis). Markers attached to the anatomical locations such as condyles or processes on the distal end of the segment helped to define the rotation axis in the sagittal plane (y-axis). The cross product of these two rotation axes was the rotation axis in the coronal plane (x-axis). In order to be consistent within the model and to visualise rotation angles easily, all reference frames were set in the same way: +z, pointing from the top to the bottom or from the proximal end to the distal end of the segment; +y, pointing to the right or lateral side of the segment; +x, pointing to the segment's front (Figure 4.5).

To estimate the orientation of the anatomical rotation axes and segmental link lengths of the upper arm and forearm, joint centre locations were required. The shoulder, elbow and wrist joint centre locations were calculated using the methodology given in the Golem model (VICON BodyLanguage model, © 1995-1999, Oxford Metrics Ltd.). The shoulder joint centre location was estimated at a suitable distance below the shoulder marker, along the line parallel to the z-axis of the thorax. This distance was taken as 20% of the inter-shoulder distance. The location of the elbow joint centre was calculated in two steps. Firstly, the whole arm plane, which was defined by the shoulder, elbow and wrist markers, was formed and its normal vector was calculated. Secondly, the elbow joint centre was located under the following constraints: the normal vector found in step one should lie on the plane formed by the shoulder joint centre, elbow joint centre and elbow marker; the line connecting the elbow marker and elbow joint centre should be perpendicular to the line connecting the shoulder joint centre and elbow joint centre; the distance between the elbow marker and the elbow joint centre should be half of the elbow width. All these constraints were applied using a special function, CHORD, in the Vicon software. The location of the wrist joint centre was calculated in a similar way. First, the normal vector of the plane which was defined by the two wrist markers and the elbow joint centre was calculated. Then, the wrist joint centre was located half of the

wrist thickness away from the mid-point of the two wrist markers along the line parallel to the normal vector.

The four markers around the racket head were used to set the racket reference frame. The y-axis of the racket reference frame was set parallel to the longitudinal axis of the racket; the x-axis was set parallel to the normal vector of the racket head plane; the z-axis, being perpendicular to the others, was set in the racket head plane (Figure 4.5). The racket orientation was calculated with respect to both global and hand reference frames.

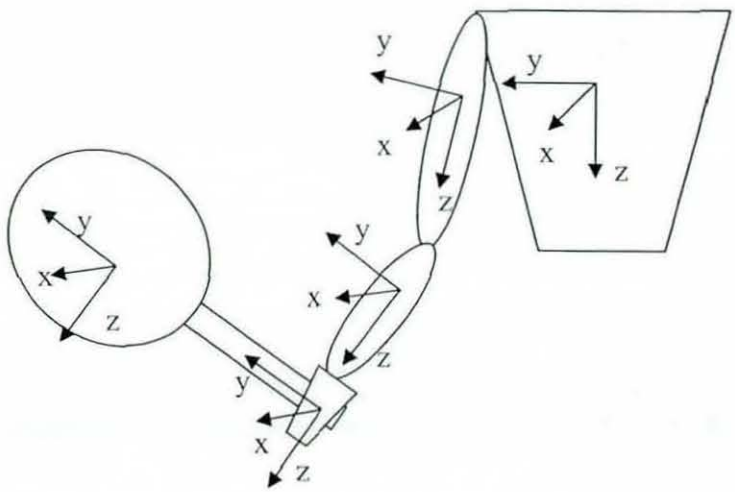

Figure 4.5. Reference frames attached to the body segments (thorax, upper arm, forarm, hand) and the racket when seen from the front of the subject.

An additional clavicle segment was included to estimate the clavicular motion. However, this segment was not used in the kinematic chain of the model. The estimated clavicular motion was used as an input to the clavicle segment in the computer simulation model, which was only used for visual completeness of the whole model (Chapter 3.2.1).

The Euler angles between the proximal and distal segments' reference frames were computed to obtain relative rotation angles. The sequence of rotation in the sagittal, coronal and the transverse plane was used in the calculations. The neutral positions of all segments were chosen to be the anatomical position of the thorax and arm (Figure 3.2).

The rotation angles of the two selected topspin backhand trials, having one centre and one off-centre impact, can be seen in Figures 4.6 - 4.10.

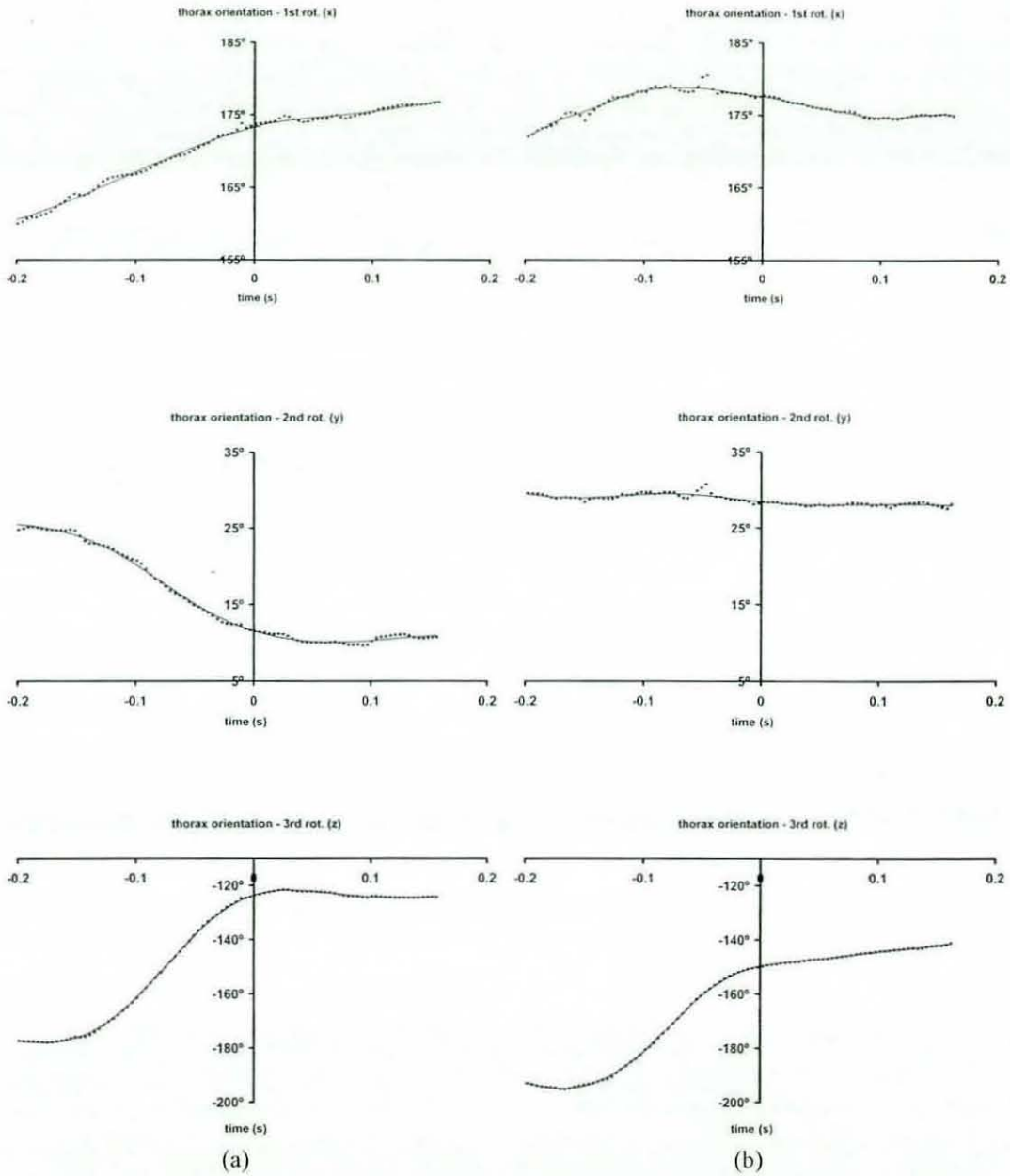

(a) (b)

Figure 4.6. Raw (▪) and smoothed (-) orientation angles of the thorax obtained from the selected topspin backhand strokes for (a) centre and (b) off-centre impact.

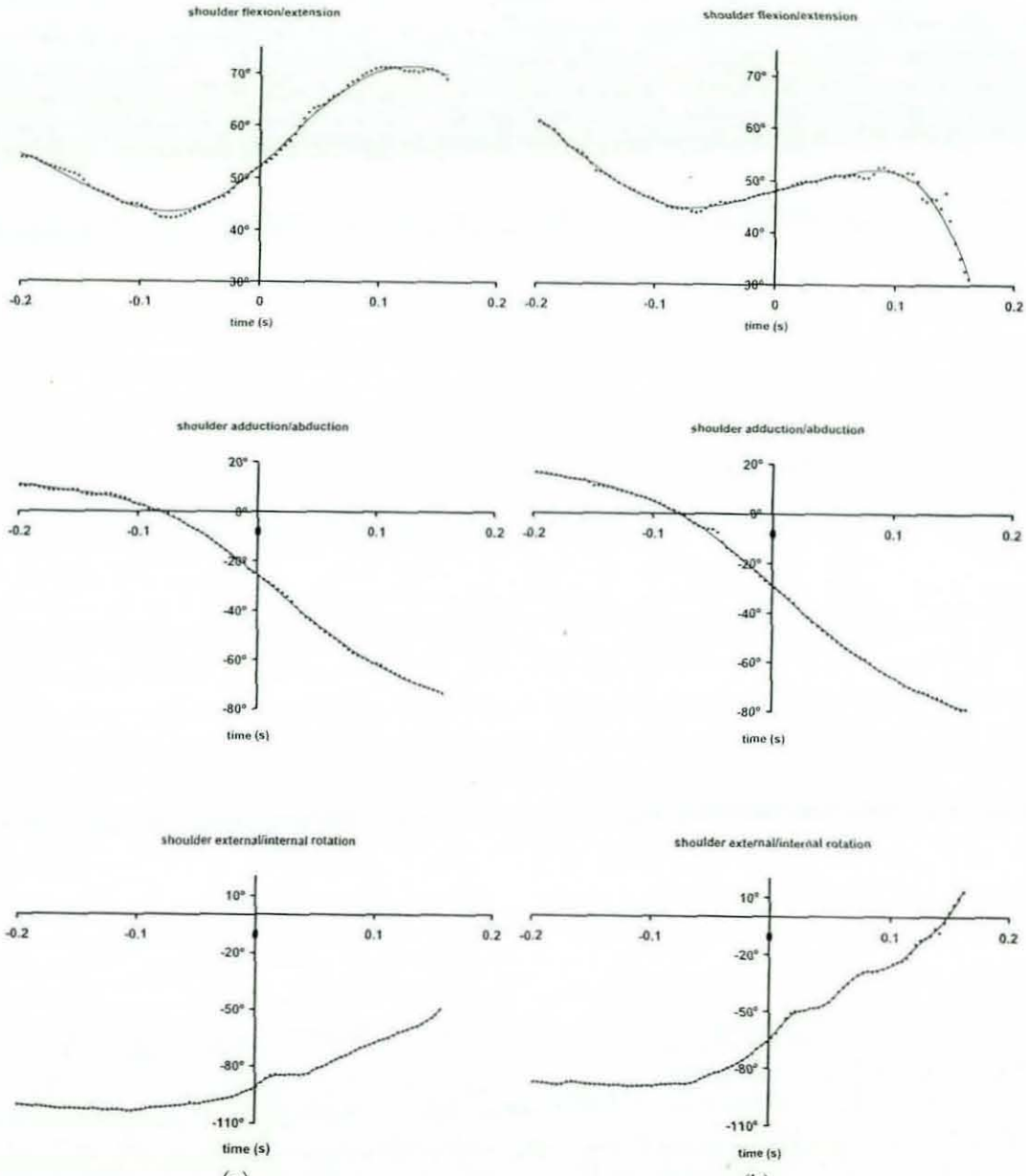

Figure 4.7. Raw (▪) and smoothed (-) shoulder rotation angles obtained from the selected topspin backhand strokes for (a) centre and (b) off-centre impact.

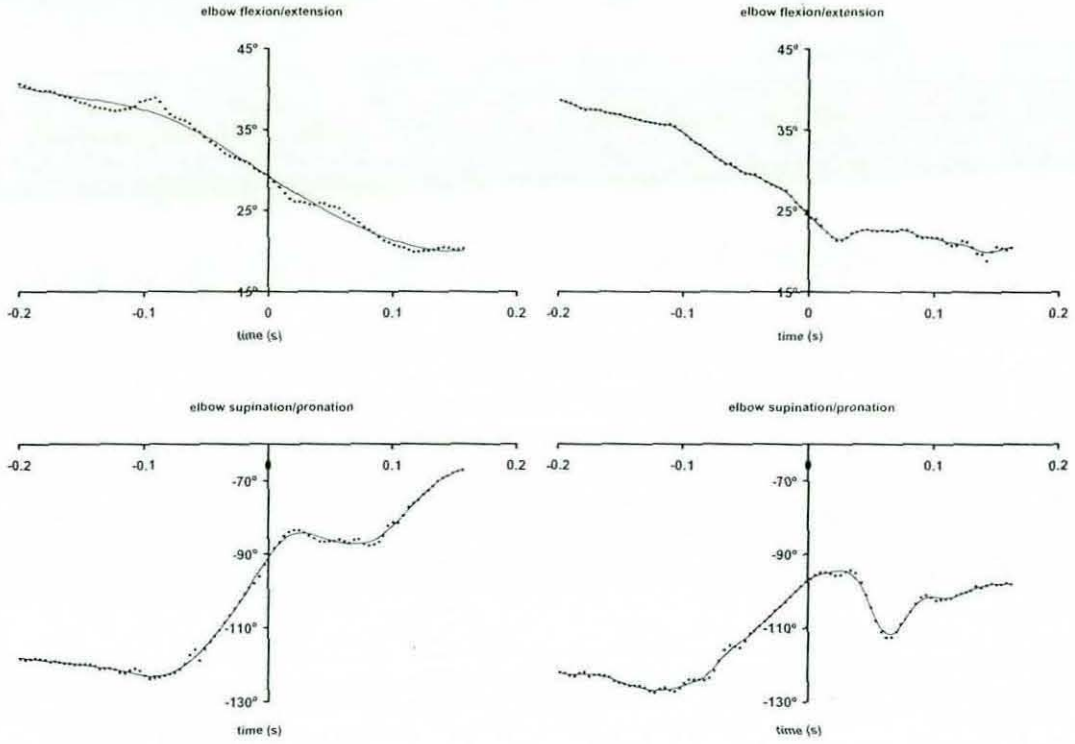

(a) (b)

Figure 4.8. Raw (▪) and smoothed (-) elbow rotation angles obtained from the selected topspin backhand strokes for (a) centre and (b) off-centre impact.

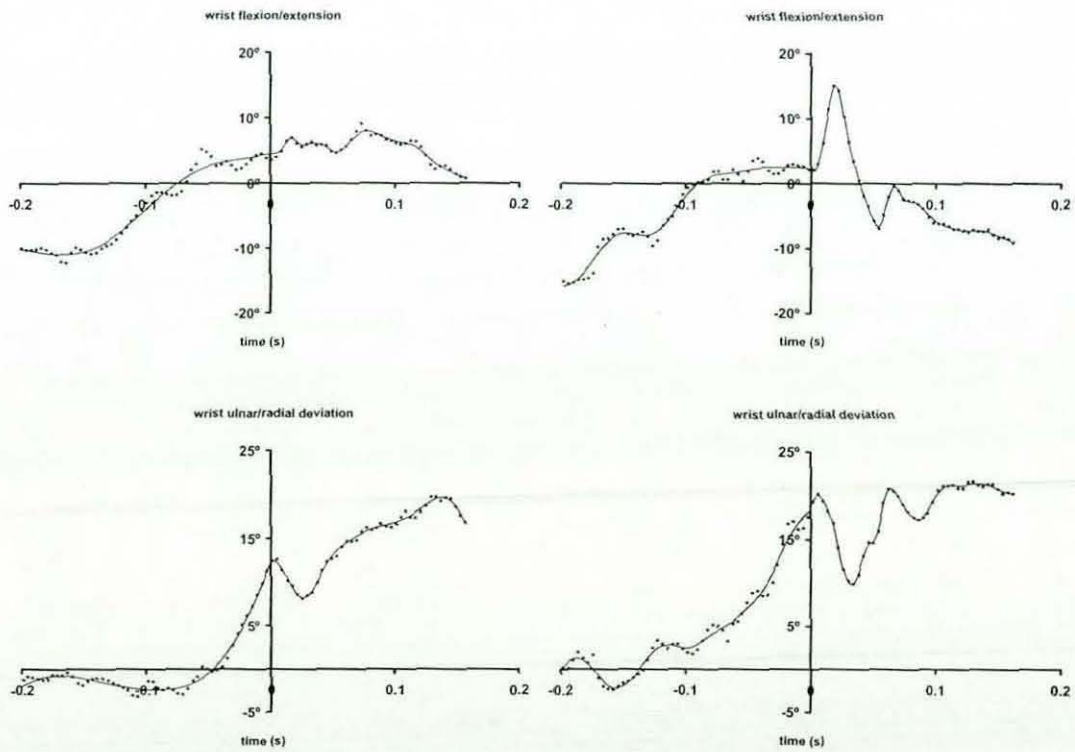

(a) (b)

Figure 4.9. Raw (▪) and smoothed (-) wrist rotation angles obtained from the selected topspin backhand strokes for (a) centre and (b) off-centre impact.

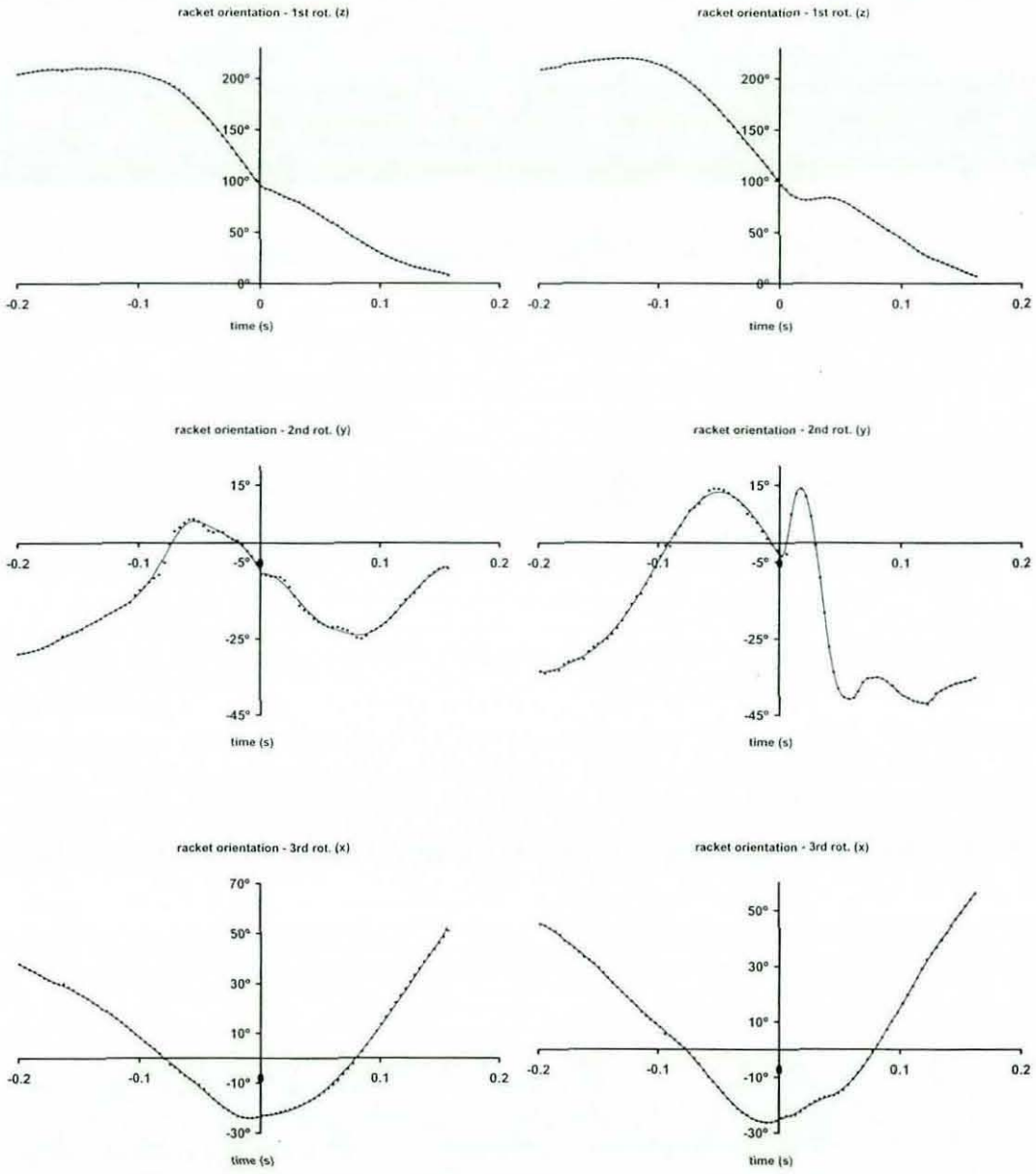

(a) (b)

Figure 4.10. Raw (▪) and smoothed (-) orientation angles of the racket obtained from the selected topspin backhand strokes for (a) centre, (b) off-centre impact.

The thorax angles showed the subject's body-orientation during the backhand stroke. The subject arranged his motion with respect to his initial position, which was not likely to be the same for each trial. Therefore, slight differences in thorax angles were expected between the trials. Although the general tendencies in shoulder and elbow rotation angles were relatively similar in both trials, the wrist rotation angles and racket orientation angles differed considerably after the impact, between the two

trials. The effect of the off-centre impact can be seen as excessive flexion and radial deviation of the hand just after impact, in comparison to the rotation angles for the impact at the centre. The difference in the racket orientation with respect to global reference frame was observed in the second rotation, which was the rotation around the longitudinal axis of the racket. The rapid change in rotation after impact for the off-centre trial was expected since the impact force tends to rotate the racket around its longitudinal axis. This was also seen clearly in the longitudinal rotation of the racket within the hand with respect to the hand reference frame (Figure 4.11).

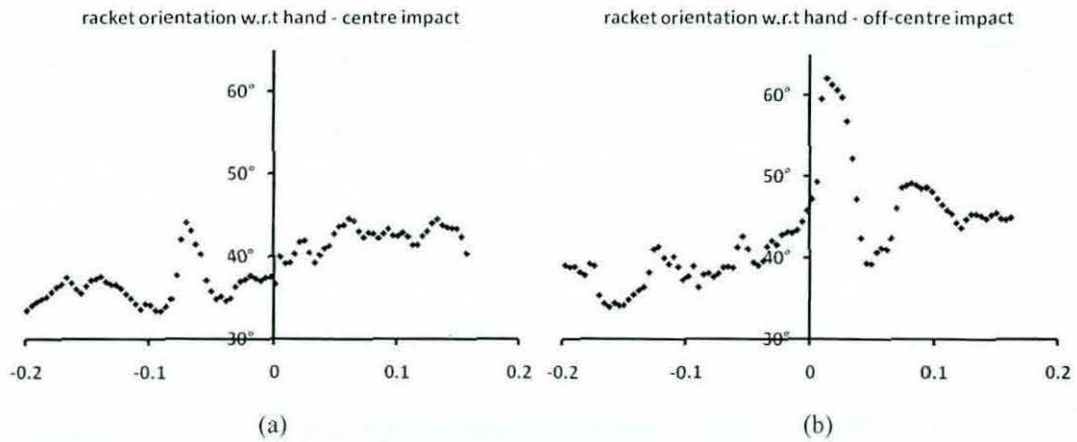

Figure 4.11. Racket orientation with respect to hand around the longitudinal axis of the racket for (a) centre, (b) off-centre impact. Impact is at time zero.

The Conversion of the Elbow and Wrist Angles

The rotation angles of the elbow and wrist joints obtained from the Vicon model were converted for use in the simulation model developed in Adams (Chapter 3.2.2). The reason for conversion was having different reference frames defining the forearm motion in the Vicon and the Adams model. The forearm was composed of two segments, the radius and ulna, in the simulation model as opposed to the Vicon model, which only had one segment. In addition to this, the pronation/supination of the forearm in the simulation model was not perpendicular to the other rotation axes (Figure 3.3). Although the overall rotation matrix of the forearm with respect to the upper arm was the same in both cases, the rotations were expressed differently in each case. The elbow rotation angles of the Vicon model and its conversion to simulation model were compared in Figure 4.12. Since the rotation axes defined in the simulation model were closer to the anatomical rotation axes of the humeroulnar and radioulnar joints, the rotation angles expressed in this model were thought to be

more realistic. The conversion resulted in a relatively constant rotation angle in the coronal plane at the elbow (Figure 4.12a) and an offset of the elbow flexion angle (rotation in the sagittal plane) (Figure 4.12b). Since the rotation axes of the elbow are not perpendicular in the simulation model, the rotation around the pronation/supination axis corresponds not only to pronation/supination but also to flexion/extension rotation in the reference frame used for Vicon model. This is the reason for the offset in the elbow flexion angle (rotation in the sagittal plane) in Figure 4.12b.

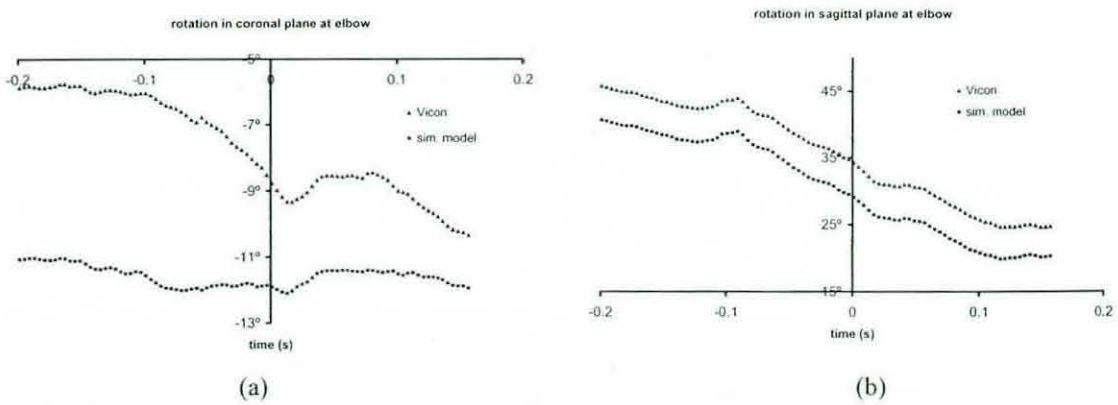

Figure 4.12. Elbow rotation angles in two different planes calculated from the Vicon model and angles converted for the simulation model: (a) coronal plane; (b) sagittal plane. Impact is at time zero.

Data smoothing

In this study, raw angle data taken from the Vicon Motion Analysis System were smoothed by fitting quintic splines (Wood and Jennings, 1979).

In the fitting process, a pseudo data set was generated by averaging data values from adjacent time frames. The error estimate at each data point was a combination of local and global errors, which were calculated from the difference between the real and pseudo data (Yeadon, 1990b; King, 1998). The standard error estimates for position and orientation data were calculated as 50% local and 50% global error. Equal weighting was preferred because 50% local error was sufficient for the splines to smooth the data when the local errors were large and 50% global error gave reasonable error estimates when the local errors were too small.

Since the impact time was a critical point in the mechanical aspect of the backhand strokes, utmost attention had been given not to over-smooth data around the impact time. It was observed from the fitted splines that racket angles and ulnar

deviation had over-smoothing problems. Therefore, these data sets were divided into two subsets at the time of impact to separate before and after impact data. Then, these subsets were smoothed separately.

Figures 4.6-4.10 show the raw and smoothed data sets of rotation angles for the selected topspin trials, which had centre and off-centre impact. In addition, Table 4.1 lists the root-mean-square (RMS) differences between the raw and smoothed data sets for the trials.

Table 4.1. RMS values for the splined rotation angles of the two selected trials having centre and *lower right corner impacts*

Rotation angle	RMS value (deg)	
	Centre	Lower right corner
shoulder flex/ext	0.30	0.43
shoulder add/abd	0.29	0.29
shoulder ext/int rot.	0.14	0.30
elbow flex/ext	0.30	0.10
elbow sup/pron	0.33	0.30
wrist flex/ext	0.39	0.32
wrist ulnar/rad dev.	0.22	0.29
racket ori. 1st rot	0.30	0.21
racket ori. 2nd rot.	0.29	0.26
racket ori. 3rd rot.	0.22	0.14

The joint angles and orientation of the thorax obtained from the performance data collection were comparable to those stated by Wang et al. (1998). In addition, ulnar / radial deviation was consistent with the results of Riek et al. (1999). The characteristics of the wrist flexion / extension angle were also comparable to those found in the literature (Blackwell and Cole, 1994; Knudson and Blackwell, 1997; Riek et al., 1999); the wrist flexes before impact and just prior to impact the flexion stops or slows down and subsequently the wrist starts to extend. However, an offset was observed when comparing the magnitudes of the rotation. This might be due to

different measurement techniques of the wrist flexion. To define the wrist angles the orientation of the hand has to be calculated after fitting a reference frame to hand. However, the method of determining the hand orientation (or hand reference frame) was not explicitly stated in the studies mentioned above.

4.3 Ball-racket Impact and Uniaxial Accelerometers

The x-component of the inbound and outbound velocity was assumed to be zero (refer to Figure 4.2 for global reference frame) since the ball was launched perpendicular to the global x-axis and the relatively narrow target area was in the global y-direction with respect to the hitting area. When determining the impact location, the point mass location (refer to section 3.3.2) closest to the impact point was chosen. For the two top spin trials used in the study, the ball inbound/outbound velocity, contact period and impact location are listed in Table 4.2.

Accelerometer data measured by three uniaxial accelerometers (Figure 4.13) were used to make a comparison of actual and simulation model racket frame acceleration.

Table 4.2. The ball inbound/outbound velocity, contact period and impact location of two topspin backhand strokes

V_{in}^{y} (m/s)	V_{in}^{z} (m/s)	V_{out}^{y} (m/s)	V_{out}^{z} (m/s)	contact period (ms)	impact location
-9.00	-1.35	30.94	6.19	4.0	centre
-8.68	-1.45	24.75	5.06	3.8	upper left

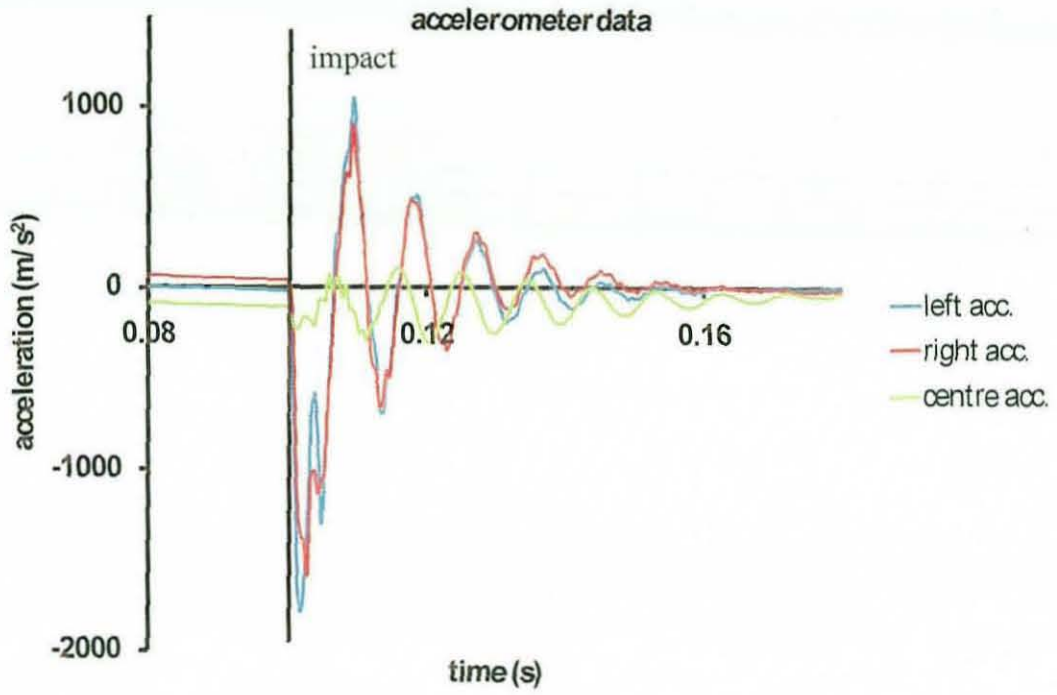

Figure 4.13. Raw acceleration data from the uni-axial accelerometers for a topspin backhand stroke.

4.4 EMG Data Analysis

To start EMG data analysis, the data collected were synchronised with the motion data using the square pulse sent by the trigger box. After synchronising and determining the impact time, the data 500 ms before and after impact were cropped from the whole data set.

The raw EMG signals were full-wave rectified and then filtered using a 4^{th} order low-pass Butterworth filter with 6 Hz cut-off frequency to obtain a linear envelope of the data (Figure 4.14). Cut-off frequencies above 6 Hz allowed unnecessary higher frequencies of the raw data to remain.

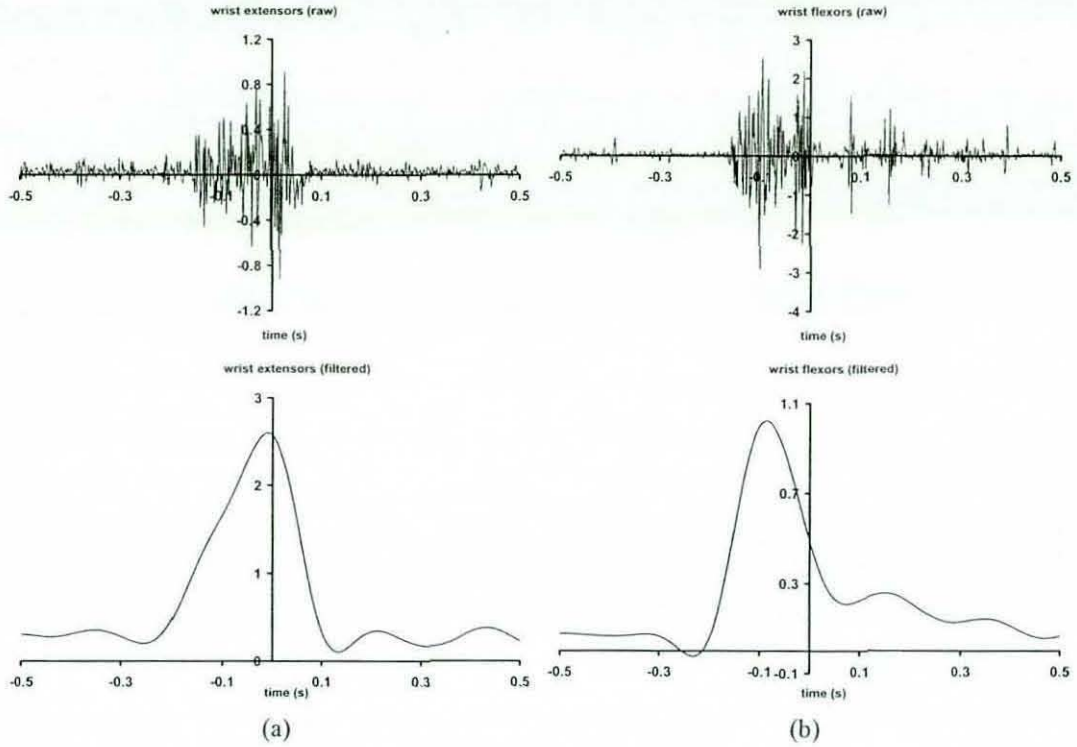

Figure 4.14. Raw and filtered EMG data for (a) wrist extensors, (b) wrist flexors for a topspin backhand trial.

The raw and linear envelope EMG data of the two trials having centre and off-centre impacts are presented in the Figures 4.15-4.18. The wrist extensors, wrist flexors, biceps, triceps, medial deltoid and posterior deltoid were activated maximally before impact and their EMG data were very similar for both trials, except some decrease in the activation of the biceps and triceps. This similarity was expected simply because the subject did not know there would be an off-centre impact beforehand and therefore they repeated the same pattern. When they realized an off-centre impact would occur, there was not sufficient time to react and change their pattern. Whilst going further up from the wrist in the kinematic chain the similarity in the pattern diminished because not only the arm but also the body movement affected the EMG data. Therefore, pectoralis major and latissimus dorsi had considerable differences between the trials.

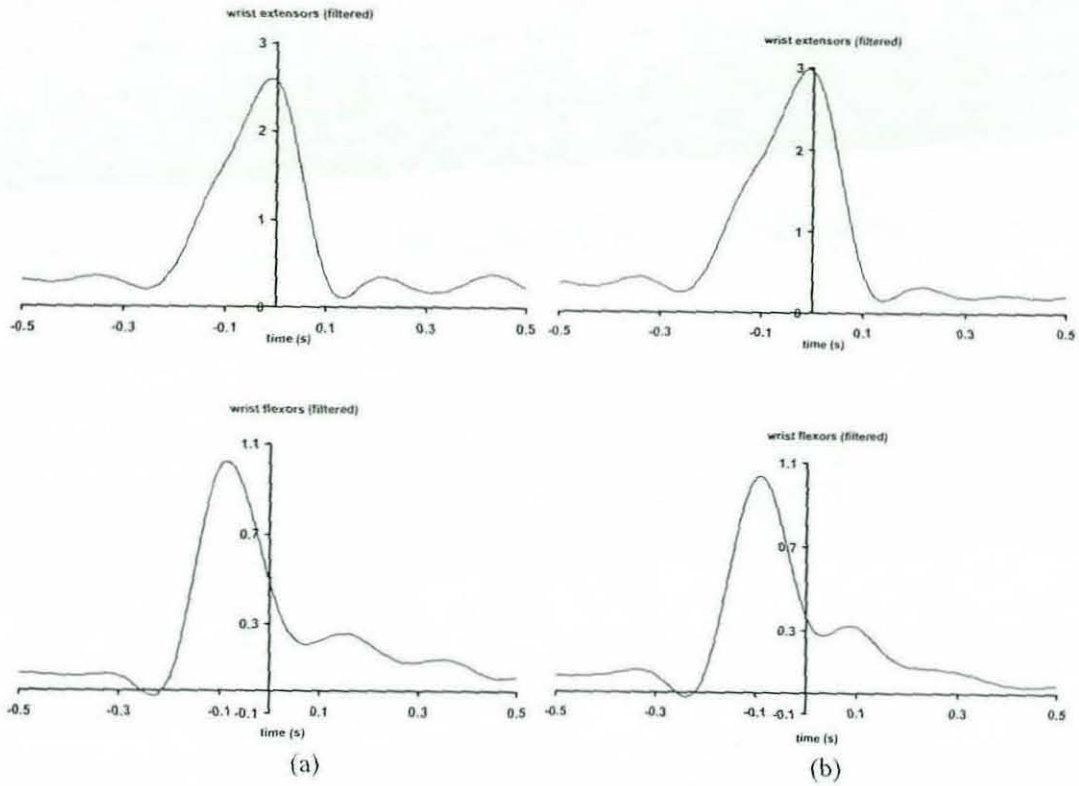

Figure 4.15. Linear envelope EMG data of the wrist extensors and flexors for the selected top spin trials having (a) centre, (b) off-centre impact.

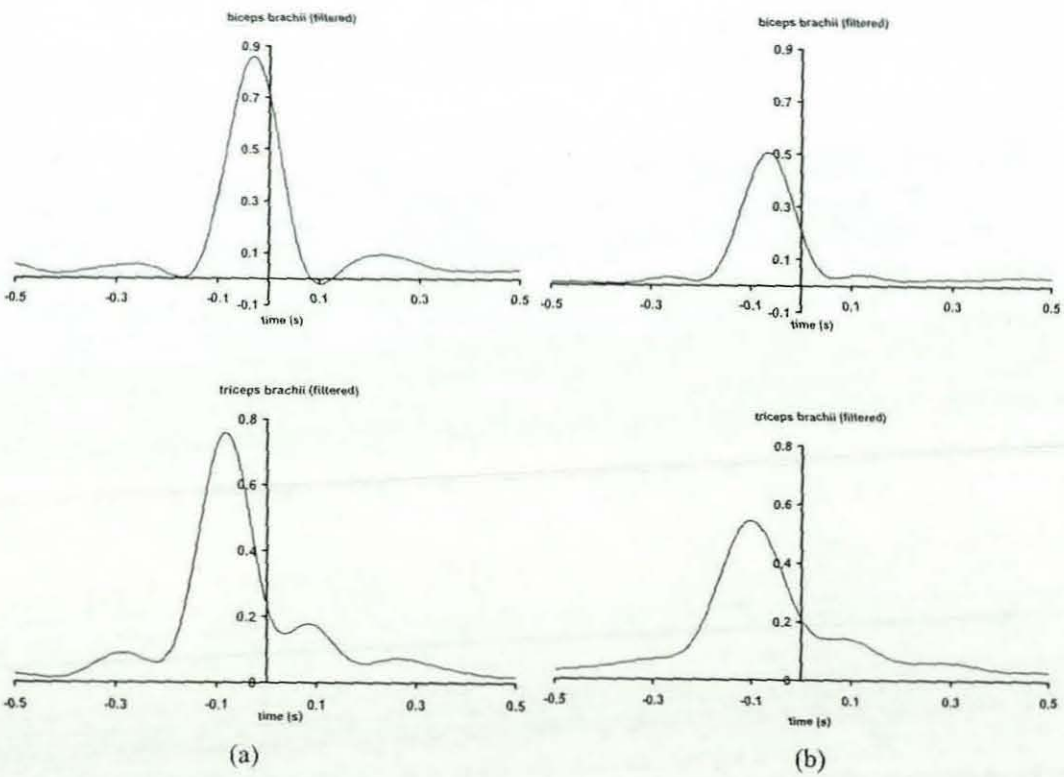

Figure 4.16. Linear envelope EMG data of the biceps and triceps for the selected top spin trials having (a) centre, (b) off-centre impact.

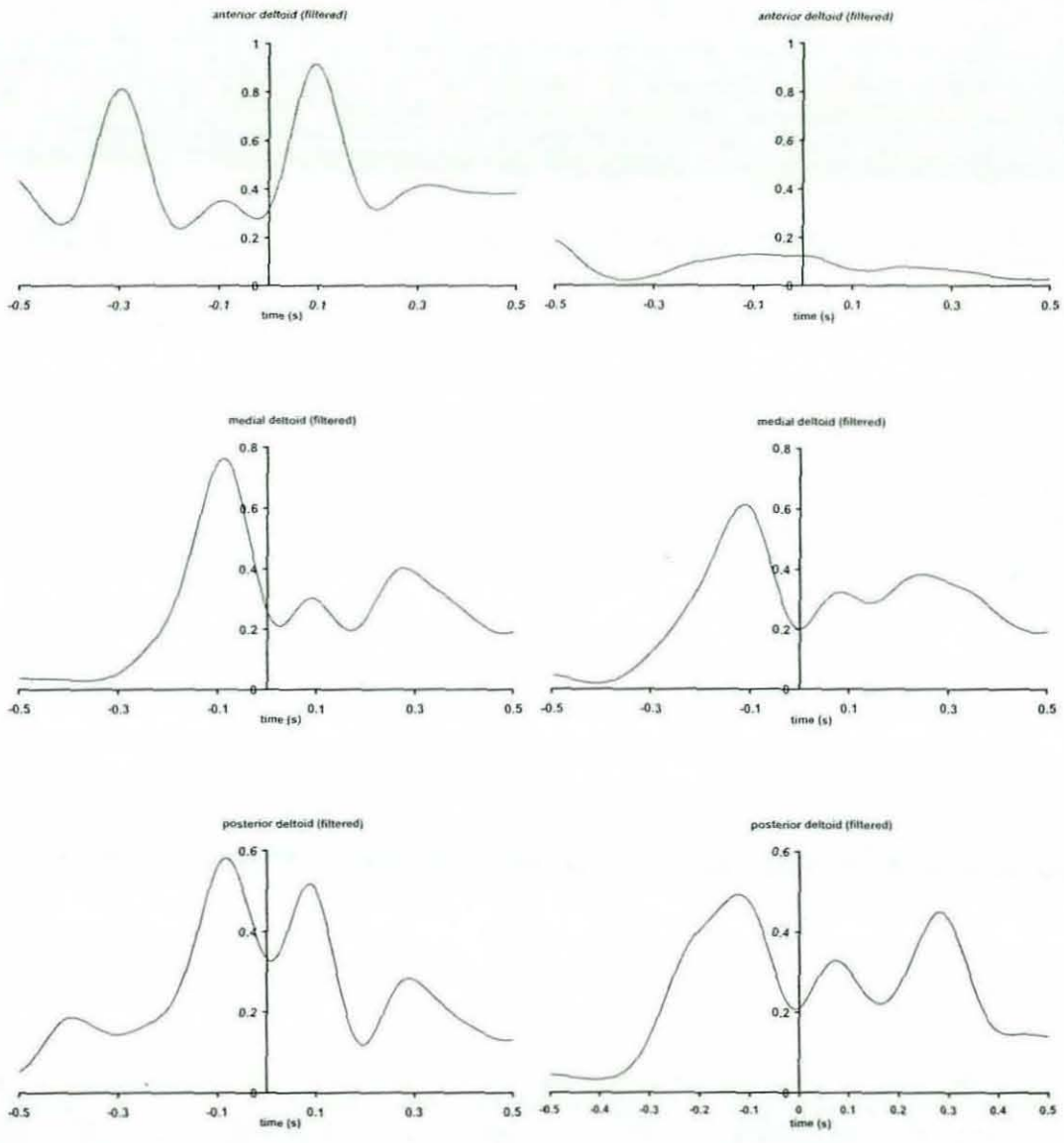

(a) (b)

Figure 4.17. Linear envelope EMG data of the anterior, medial and posterior deltoid for the selected top spin trials having (a) centre, (b) off-centre impact.

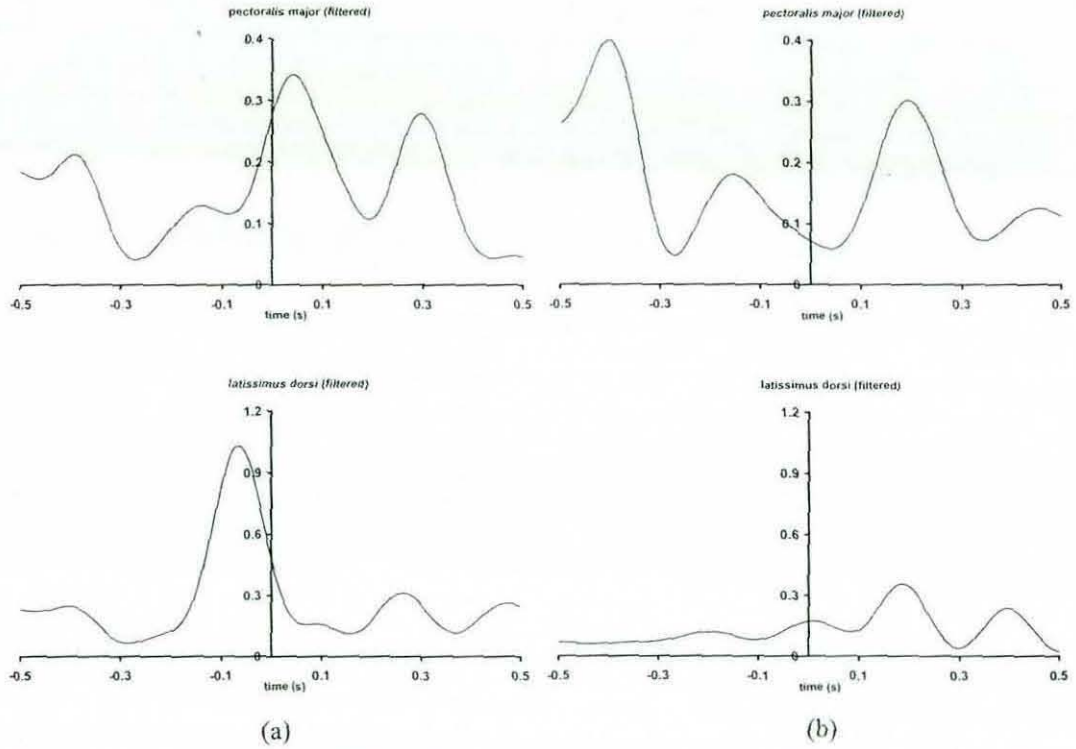

(a) (b)

Figure 4.18. Linear envelope EMG data of the pectoralis major and latissimus dorsi for the selected top spin trials having (a) centre, (b) off-centre impact.

The EMG data for wrist extensors and flexors measured in this study (Figure 4.15) was consistent with the ones reported in the literature (Giangarra et al., 1993; Blackwell and Cole, 1994; Kelley et al., 1994; Riek et al., 1999). Other muscle groups were comparable with the EMG data for a backhand volley presented by Chow et al. (1999).

4.5 Summary

In this chapter, the data collection of one-handed tennis backhand strokes performed by an elite tennis player has been described. The joint angles and racket orientation of two selected trials, which had centre and off-centre impact locations on the racket, have been analysed and compared. Significant differences in wrist kinematics and racket orientation around the longitudinal axis of the racket after ball-racket impact have been found between the two trials. The EMG data of the two trials were compared as well. No substantial difference was found between the muscle groups except pectoralis major and latissimus dorsi which were affected by the body movement.

5 PARAMETER DETERMINATION

Subject-specific parameters and racket parameters were required for the computer simulation model described in Chapter 3. This chapter explains the determination of the torque-strength and inertia parameters of the subject, in addition to the equipment parameters, including: racket frame, tennis ball and string bed parameters.

5.1 Torque - Strength Parameters

5.1.1 Introduction

To utilize a torque-driven simulation, the torque - joint angle - joint angular velocity (T-θ-ω) relationship has to be known or estimated beforehand. This relationship is used to calculate contractile component torque in the torque generator by using Equations 3.2 and 3.3. The contractile component parameters in these equations can be determined by fitting experimental maximum voluntary torque measured by a dynamometer. The series elastic component parameters can be estimated from Magnetic Resonance Imaging or from the literature.

In this study a Cybex Norm isokinetic dynamometer, controlled by an IBM compatible 486 DX2 computer, was used to measure maximum net torques around the shoulder, elbow and wrist joints of the subject who had participated in the performance data collection. To collect data for estimating the T-θ-ω relationship, the subject performed both isometric and isovelocity trials.

In order to estimate series elastic component parameters, data found in the literature were used, with the assumption that the series elastic component stretched by 5% during maximal isometric contraction.

5.1.2 Data Collection

Method

A total of fourteen different joint torques were measured by the Cybex Norm dynamometer: flexion / extension, horizontal abduction / adduction and internal /

external rotation at the shoulder joint; flexion / extension and pronation / supination at the elbow joint; flexion / extension and radial / ulnar deviation at the wrist joint.

The dynamometer was set up according to the user's manual. Time histories of the crank angle and torque applied to the crank were sampled at 1000 Hz and recorded to a laptop computer (connected to the dynamometer via a custom-built interface).

Calibration

To obtain the relation of recorded voltage values with the corresponding torque and angle values, calibration trials were recorded. The crank arm of the dynamometer was set in a horizontal position using a spirit level. The peak torque (T) and voltage output (V_T) for five isometric trials were recorded and then linear regression used (Figure 5.1) to obtain Equation 5.1:

$$T = 73.826\, V_T \qquad (5.1)$$

where, T = peak torque

V_T = voltage output for torque

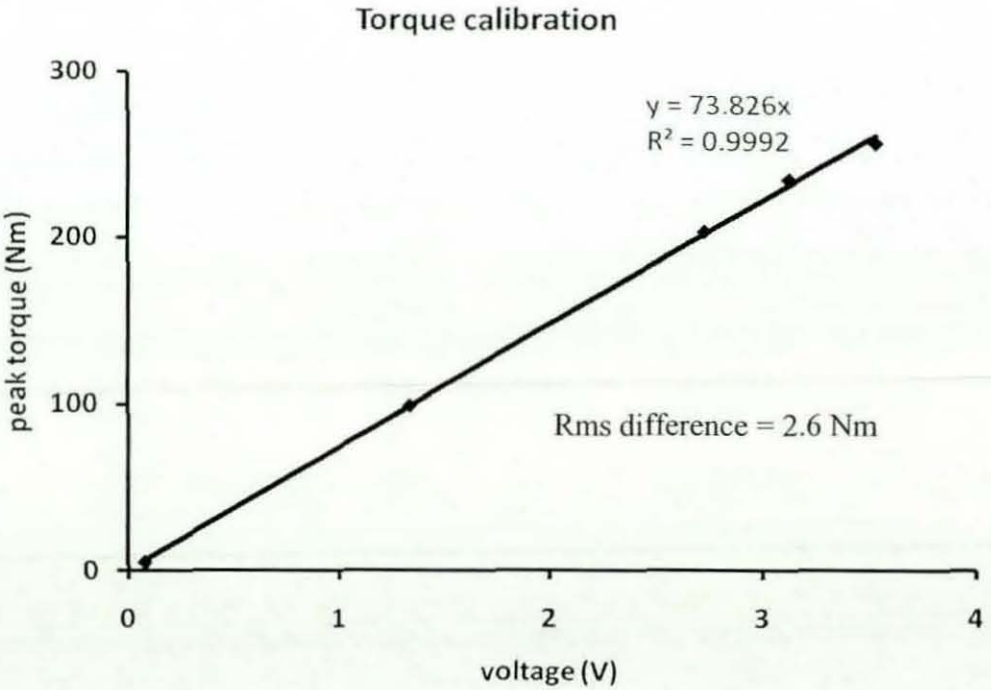

Figure 5.1. Linear regression of peak torque against voltage output.

For crank angle calibration, static trials at different crank angles, every 20° within a full rotation of the crank arm, were measured. The voltage output (V_A) corresponding to each crank angle (A) was recorded and Equation 5.2 was obtained from the linear regression of voltage output against the crank angle (Figure 5.2).

$$A = 61.286\, V_A - 255.69 \tag{5.2}$$

where, A = crank angle

V_A = voltage output for crank angle

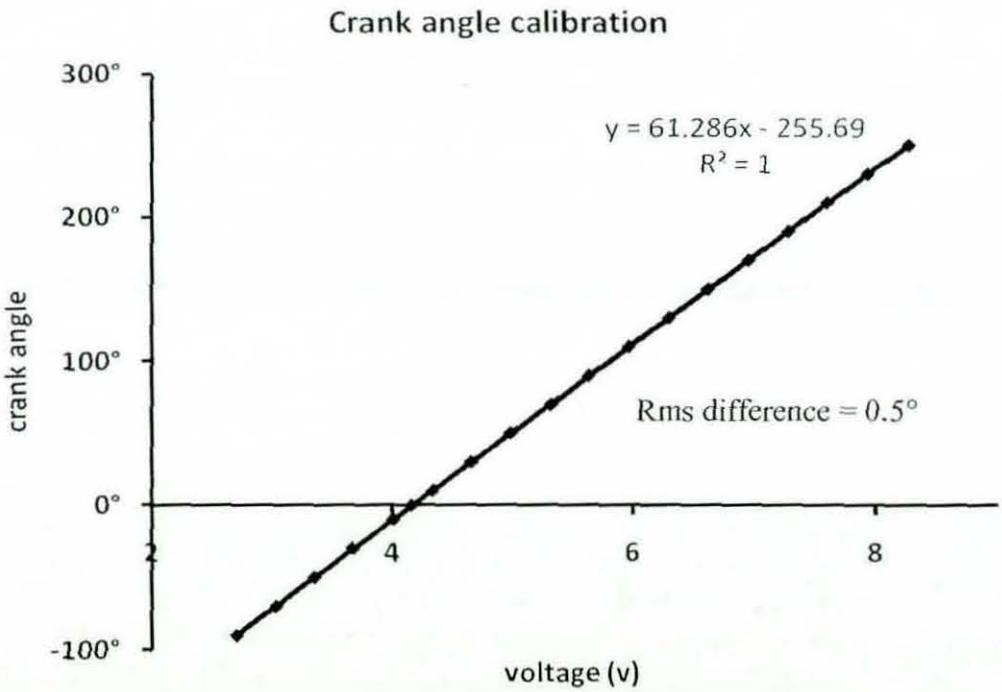

Figure 5.2. Linear regression of crank angle against voltage output.

Protocol

The position of the dynamometer was arranged so that the joint being measured was aligned with the crank joint centre and the rotation axis of the crank coincided with the rotation axis of the joint. To avoid relative motion, the subject was secured tightly to the dynamometer seat with seat belts and the body segments were attached to the crank with the straps provided by the manufacturer (Figure 5.3). At each joint the maximum range of motion (ROM) in which the subject moved

comfortably was determined after the aligning process. The ROM was entered to the dynamometer computer to prevent the crank arm rotating beyond the subject's maximum ROM. Furthermore, mechanical safety locks were put in appropriate places in the dynamometer as an additional safeguard. The subject performed a few sub-maximal warm-up trials before each joint measurement.

For each joint movement, the ROM was divided into eight equal parts and, at each of these joint angles within the ROM, first, passive isometric trials, and then, maximal isometric contraction trials were recorded. From the passive trials, the effect of the weight of the crank arm and body segments were calculated. For the maximal isometric contraction trials, the subject was asked to exert maximum torque. After recording the isometric trials, the isovelocity contraction trials were collected at seven different angular velocities of the crank: 50, 100, 150, 200, 250, 300 and 350°/s (and 400°/s for shoulder flexion). At least two concentric-eccentric contractions were performed at each velocity.

The isometric and isovelocity trials were recorded for 5 and 10 seconds, respectively. The joint movements were tested in the following order: flexion / extension and ulnar / radial deviation at the wrist joint; pronation / supination and flexion / extension at the elbow joint; extension / flexion, horizontal adduction / abduction and external / internal rotation at the shoulder joint.

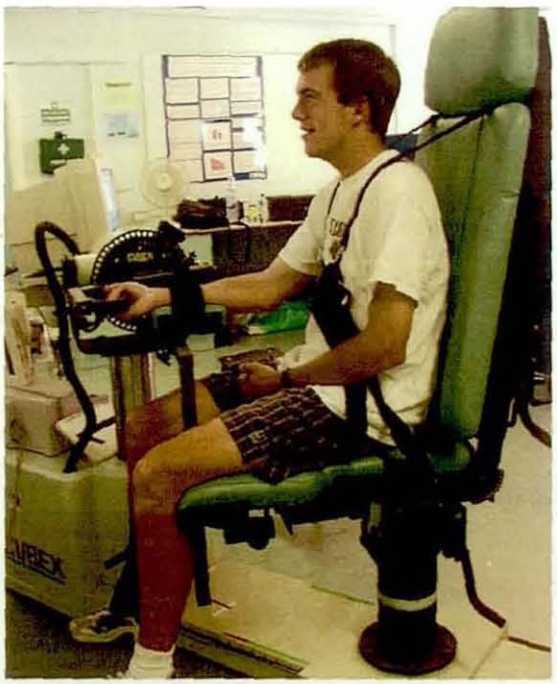

Figure 5.3. The subject and the dynamometer set-up for wrist flexion.

5.1.3 Isometric Data Reduction

Maximum isometric torque

The recorded voltage outputs for each isometric trial were converted to a time history of torque using Equation 5.1. In the time history of torque an isometric period, where a stable isometric torque was observed, was determined (Figure 5.4) and the maximum torque in this period was found. However, due to the noise in the signal, instead of using this maximum torque directly, the average of the torque values within the range of 15 ms before and after maximum torque was calculated as maximum isometric torque.

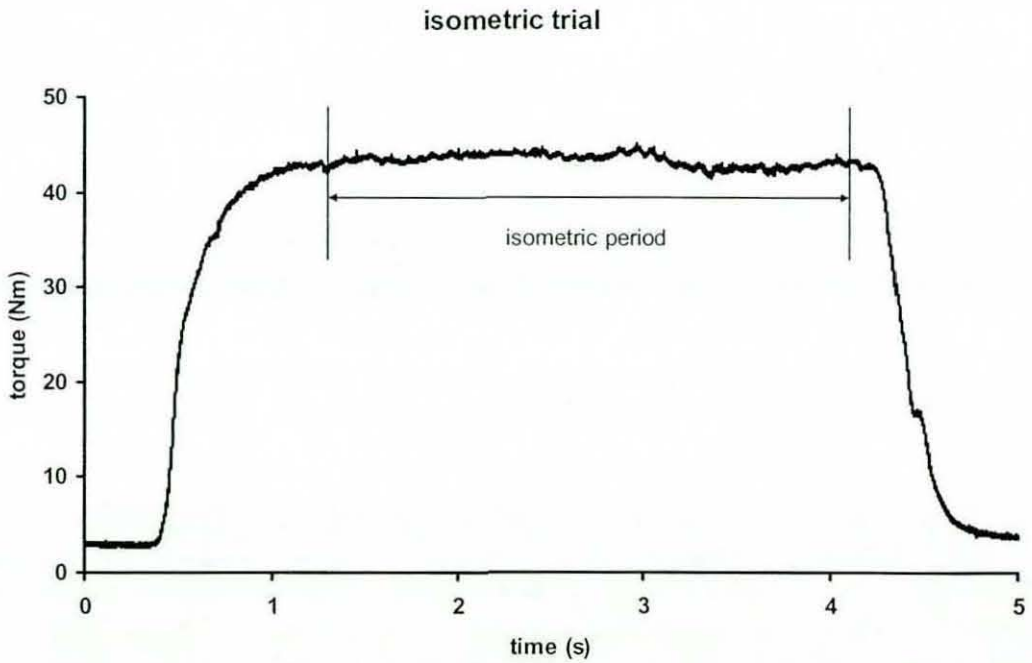

Figure 5.4. Identification of isometric period

Weight correction

The weight of the crank arm and body segments create an additional torque (T_w) at the crank joint centre, either in the same or opposite direction to the isometric torque. Depending on the direction of the movement, the negative or positive contribution of this torque to the measured isometric torque has to be removed. For this purpose, the passive isometric trials at each joint angle were fitted using Equation 5.3.

$$T_w = \pm M\cos(\theta_h) \quad (5.3)$$

where, T_w = torque created by the crank arm and body segment weight

M = maximum possible passive torque

θ_h = the angle between the crank arm and the horizontal

Finally, maximum isometric torque was corrected by using Equation 5.4.

$$T_{ciso} = T \pm T_w \quad (5.4)$$

where, T_{ciso} = corrected maximum isometric torque

T = measured maximum isometric torque

T_w = torque created by the crank arm and body segment weight

Conversion of crank variables into joint variables

During a maximum effort trial, the crank angle and joint angle will be different due to relative movement of the body segment with respect to the crank arm. For this reason, joint angles were measured with a manual goniometer by an experienced researcher for each trial. Then, measured joint angles for a particular joint movement were linearly regressed against crank angles (Equation 5.5).

For wrist flexion / extension, joint angles were estimated by digitising the video images taken. For shoulder internal / external rotation and forearm pronation / supination, the crank and joint angles were assumed to be the same, since the relative movement of the body segments were minimized by the elbow stabiliser pad.

$$\theta_j = m\theta_c + n \quad (5.5)$$

where, θ_j = joint angle

θ_c = crank angle

m, n = constants

The constants 'm' and 'n' for each joint movement are presented in Table 5.1.

Table 5.1. Conversion of crank angles into joint angles

joint movement	m	n
Shoulder flexion	1.05	42.17
Shoulder extension	0.69	60.82
Shoulder horizontal adduction	0.77	1.43
Shoulder horizontal abduction	1.04	-23.73
Shoulder internal / external rotation	-1.00	0.00
Elbow flexion	-0.84	127.80
Elbow extension	-0.93	144.16
Forearm pronation / supination	1.00	15.00
Wrist flexion	0.58	-28.37
Wrist extension	-0.76	8.84
Wrist ulnar deviation	0.75	2.53
Wrist radial deviation	0.81	-1.11

The crank moment arm was constant throughout each trial, but the moment arm for the joint was not due to the relative movement mentioned above. Therefore, the crank torque and the joint torque were different, although the exerted force was the same in both cases. The ratio of the joint torque to crank torque can be estimated as the ratio of the crank angle to joint angle (King, 1998). The constant 'm' in Equation 5.5 was used for this ratio as it gave an average relationship between the crank and joint angles (King, 1998). Finally, the crank torque was converted to the joint torque by using Equation 5.6.

$$T_j = \frac{T_c}{|m|} \tag{5.6}$$

where, T_j = joint torque

T_c = crank torque

m = constant (the same in the Equation 5.5)

Results

Elbow flexion / extension isometric data can be seen in Figure 5.5 as an example of the joint angle – isometric torque relationship. The maximum isometric torque values and corresponding joint angles for each joint movement are listed in the Tables 5.2-5.8.

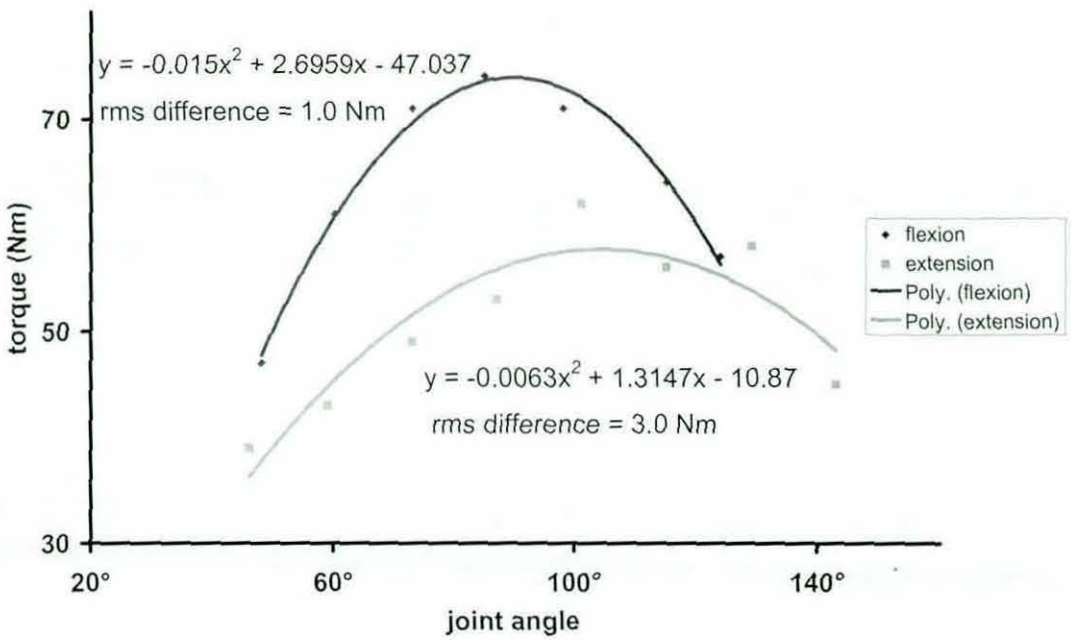

Figure 5.5. Maximum isometric torque value – joint angle relationship for elbow flexion / extension.

Table 5.2. Maximum isometric torque values and corresponding joint angles for shoulder flexion / extension

Shoulder flexion		Shoulder extension	
Joint angle (°)	Torque (Nm)	Joint angle (°)	Torque (Nm)
48	41	65	130
65	44	73	140
80	50	82	148
96	52	91	141
111	51	99	132
127	46	107	124
152	37	123	101

Table 5.3. Maximum isometric torque values and corresponding joint angles for shoulder horizontal adduction / abduction

Horizontal adduction		Horizontal abduction	
Joint angle (°)	Torque (Nm)	Joint angle (°)	Torque (Nm)
44	134	4	47
53	127	25	61
63	105	40	65
72	96	57	62
82	84	71	60
90	67	82	55
108	44	93	51
		103	52

Table 5.4. Maximum isometric torque values and corresponding joint angles for shoulder internal / external rotation

Internal rotation		External rotation	
Joint angle (°)	Torque (Nm)	Joint angle (°)	Torque (Nm)
10	38	10	20
25	38	26	26
35	41	41	28
45	40	56	31
55	36	71	30
65	37	86	31
75	33		
85	30		

Table 5.5. Maximum isometric torque values and corresponding joint angles for elbow flexion / extension

Elbow flexion		Elbow extension	
Joint angle (°)	Torque (Nm)	Joint angle (°)	Torque (Nm)
48	47	46	39
60	61	59	43
73	71	73	49
85	74	87	53
98	71	101	62
115	64	115	56
124	57	129	58
		143	45

Table 5.6. Maximum isometric torque values and corresponding joint angles for pronation / supination

Pronation		Supination	
Joint angle (°)	Torque (Nm)	Joint angle (°)	Torque (Nm)
60	1	55	13
74	2	70	12
90	3	85	10
105	4	100	9
120	6	115	8
136	11	131	8
150	11	145	7
165	13	159	6
180	14		

Table 5.7. Maximum isometric torque values and corresponding joint angles for wrist flexion / extension

Wrist flexion		Wrist extension	
Joint angle (°)	Torque (Nm)	Joint angle (°)	Torque (Nm)
67	42	46	24
73	45	51	24
79	45	59	24
91	42	66	24
96	40	74	26
102	38	81	22
108	37	89	23
		97	19

Table 5.8. Maximum isometric torque values and corresponding joint angles for radial / ulnar deviation

Radial deviation		Ulnar deviation	
Joint angle (°)	Torque (Nm)	Joint angle (°)	Torque (Nm)
66	12	62	18
78	17	70	26
86	23	77	25
93	29	84	33
102	31	92	34
110	26	99	37
118	28	107	41

5.1.4 Isovelocity Data Reduction

Weight correction

After converting the voltage output to torque and crank angle by using Equations 5.1 and 5.2, the same procedure used in the isometric trials was used to remove the effect of the crank arm and the body segmental weights for the isovelocity trials.

Joint angular velocity

For isovelocity trials, the same crank angle range used in the isometric trials was used. For each trial, the subject was asked to produce maximum effort. Therefore, the same relationship between crank and joint angle (Equation 5.5) was assumed for the isometric trials, as well. By taking the derivative of Equation 5.5 with respect to time the crank and joint angular velocity relationship was obtained (Equation 5.7).

$$\omega_j = m\omega_c \qquad (5.7)$$

where, ω_j = joint angular velocity

ω_c = crank angular velocity

m = constant (the same in the Equation 5.5)

Maximum concentric and eccentric torque

For each isovelocity trial, periods that had constant velocity were selected as concentric and eccentric phases by examining the angle data depending on the joint movement. The concentric and eccentric phases, which included the peak eccentric and concentric torques respectively (Figure 5.6), were analysed separately. The torque values in each phase were smoothed against angle values and then maximum torques (T_{max}) were determined. Finally, ten data points equally distributed within the angle range and their corresponding torque values were selected to represent the whole phase. This was done for normalizing all eccentric and concentric phases in a joint movement, since for each angular velocity the phase range and the angle corresponding to maximum torque may differ.

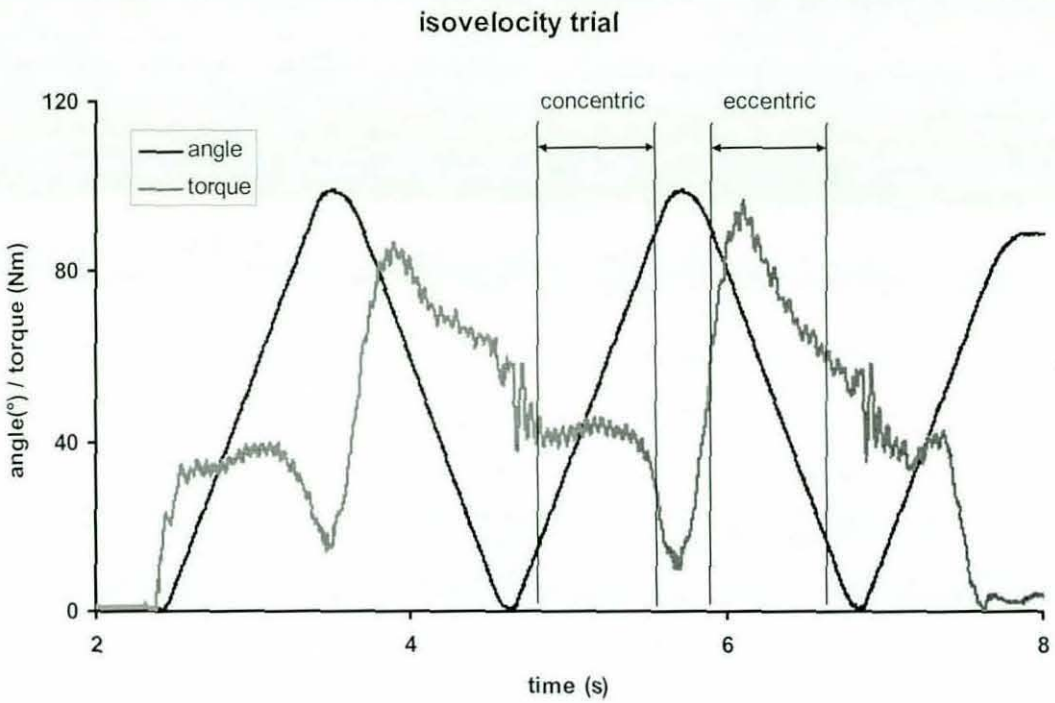

Figure 5.6. Identification of concentric and eccentric phases for an isovelocity trial

Torque value at zero angular velocity (T_o)

To determine the torque value at zero angular velocity, the maximum torque values at the lowest angular velocities in both eccentric and concentric contractions were used. Assuming the ratio of the slopes of the eccentric and concentric phase torque at zero angular velocity was constant, T_o was calculated by the Equation 5.8.

$$T_o = \frac{k\,\omega_e T_c + \omega_c T_e}{k\,\omega_e + \omega_c} \tag{5.8}$$

where, T_o = maximum torque value at zero angular velocity

ω_c = lowest angular velocity in concentric phase

ω_e = lowest angular velocity in eccentric phase

T_c = maximum torque value at the lowest angular velocity in concentric phase

T_e = maximum torque value at the lowest angular velocity in eccentric phase

k = the ratio of the slopes of the eccentric and concentric phase torque at zero angular velocity

The value of the constant 'k' was predicted as 4.3 by Huxley (1957) with his original model; the same value was used in this study.

For different joint movements, a comparison of the calculated T_o and the maximum isometric torque (T_{ciso}) obtained from isometric trials is presented in Table 5.9.

Table 5.9. Isometric torques obtained from isovelocity and isometric data

Joint movement	T_o (Nm)	T_{ciso} (Nm)
Shoulder flexion	51	51
Shoulder extension	118	143
Shoulder horizontal adduction	89	134
Shoulder horizontal abduction	65	63
Shoulder internal rotation	40	40
Shoulder external rotation	31	31
Elbow flexion	78	74
Elbow extension	48	57
Pronation	16	14
Supination	17	13
Wrist flexion	42	43
Wrist extension	23	25
Ulnar deviation	37	41
Radial deviation	29	29

5.1.5 Fitting a Surface to Torque - Angle - Angular Velocity Data

9-Parameter surface function

Since joint torque data is a function of both joint angle and angular velocity, a surface was necessary to express the torque – joint angle – joint angular velocity

relationship. However, the torque generators in the computer simulation model were modelled as a contractile component and a series elastic component (Section 3.2.3). Therefore, joint angle had to be separated into contractile component angle (θ_{con}) and series elastic component angle (θ_{sec}) based on a geometric relationship (Figure 3.3; Equation 3.1).

Throughout the torque-strength data collection, the subject was asked to exert maximum effort. For this reason, it was assumed that the activation level (Equation 3.5) was maximum, i.e. 1.0. Combining the Equations 3.2, 3.4 and 3.5 the 9-parameter surface function (Equation 5.9) was obtained.

$$T_4(\omega)a(\omega)f(\theta_{con}) = k_t\,\theta_{sec} \tag{5.9}$$

where, $T_4(\omega)$ = 4-parameter-fit tetanic torque

$a(\omega)$ = 3-parameter-fit differential activation (Yeadon et al., 2006)

$f(\theta_{con})$ = 2-parameter-fit angle contribution

k_t = series elastic component stiffness

ω = contractile component angular velocity

The nine parameters were distributed into individual functions that constitute the surface function: four parameters were used to define the tetanic torque; three parameters defined the differential activation; finally, angle contribution was obtained from two parameters.

4-parameter-fit tetanic torque

Two rectangular hyperbolas, one of which was inverted, were used to estimate the maximum torque – angular velocity relationship(Yeadon et al., 2006). The hyperbolas joined at zero angular velocity, so each was used only in the concentric or eccentric phase of the muscle contraction (Figure 5.7).

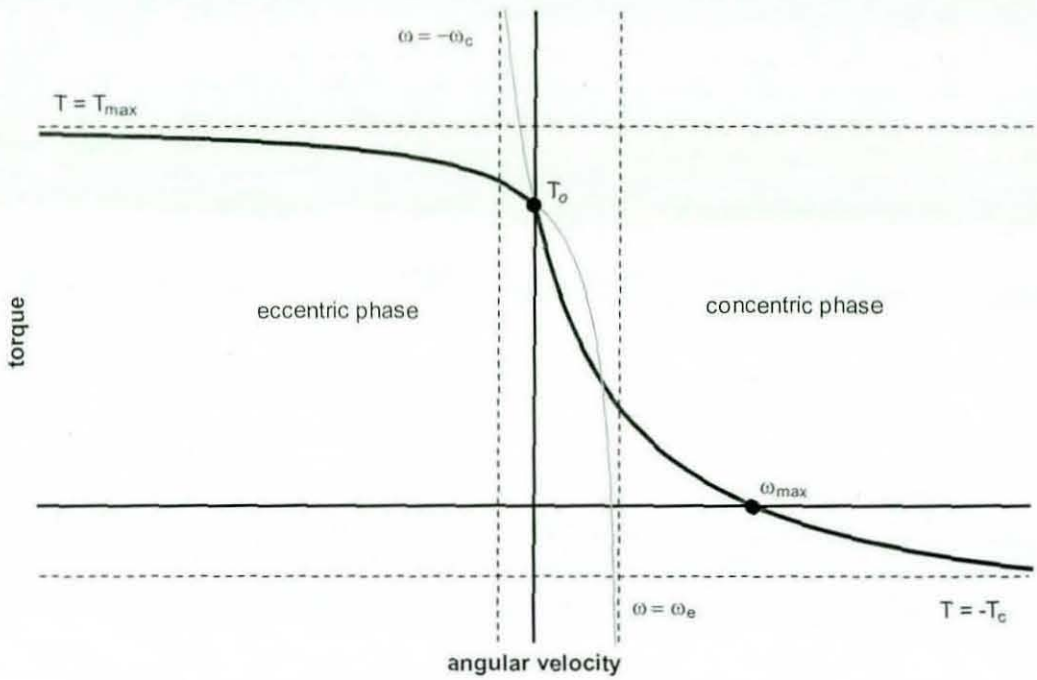

Figure 5.7. Four-parameter hyperbolic function estimating torque – angular velocity relationship.

For the concentric phase, a rotational equivalent of the Hill's (1938) hyperbola for force-velocity relationship was used (Yeadon et al., 2006):

$$(T_4 + T_c)(\omega + \omega_c) = C \qquad (5.10.a)$$

$$T_c = \frac{T_o \omega_c}{\omega_{max}} \qquad (5.10.b)$$

$$C = T_c(\omega_{max} + \omega_c) \qquad (5.10.c)$$

where, T_4 = tetanic torque

ω = contractile component angular velocity

T_o = maximum torque value at zero angular velocity

ω_{max} = maximum angular velocity at which torque equals zero

T_c = asymptote of torque in concentric hyperbola

ω_c = asymptote of angular velocity in concentric hyperbola

Torque in the eccentric phase was estimated by the inverted hyperbola, which is expressed in (Yeadon et al., 2006):

$$(T_e - T_4)(\omega_e - \omega) = -E \quad (5.11.a)$$

$$\omega_e = \frac{(T_{max} - T_o)}{kT_o} \cdot \frac{\omega_{max}\omega_c}{(\omega_{max} + \omega_c)} \quad (5.11.b)$$

$$E = -\omega_e (T_{max} - T_o) \quad (5.11.c)$$

where, T_e = asymptote of torque in eccentric hyperbola

ω_e = asymptote of angular velocity in eccentric hyperbola

T_{max} = maximum torque, asymptote of torque in eccentric hyperbola

k = the ratio of the slopes of the eccentric and concentric phase torque at zero angular velocity

The value of k was set to 4.3, the estimated value in Huxley's (1957) original model, as mentioned earlier. When the Equations 5.10 and 5.11 are examined, it can be seen that four parameters, T_o, T_{max}, ω_{max} and ω_c, completely define both hyperbolas.

Differential activation

Yeadon et al. (2006) showed that in addition to the 4-parameter-fit hyperbolas, a differential activation function was needed in order to obtain a better fit to the experimental data. The differential activation function defines an activation level, which increases from a depressed level for high eccentric velocities to full activation for high concentric velocities (Figure 5.8)(Equation 5.12).

$$\omega - \omega_I = \frac{m(a - 0.5(a_{min} + a_{max}))}{(a_{max} - a)(a - a_{min})} \quad (5.12)$$

where, a = activation level

a_{min} = minimum activation level in eccentric phase

a_{max} = maximum activation level in concentric phase

ω_I = angular velocity at the inflection point

m = maximum slope of activation

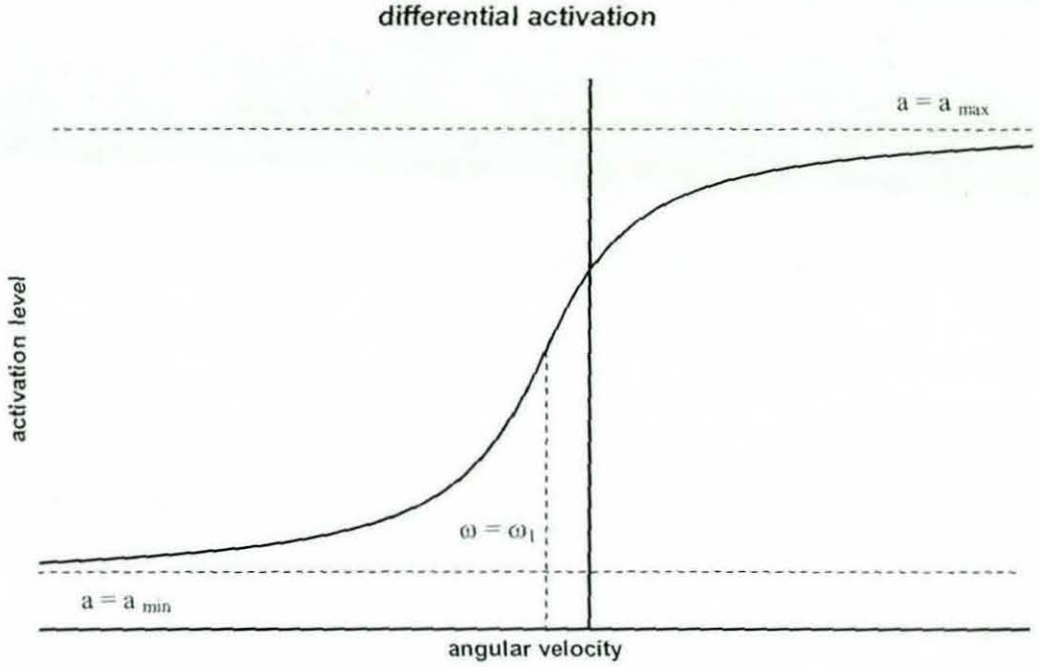

Figure 5.8. Differential activation function

Maximum activation level in the concentric phase was assumed to be 1.0. As a result, the remaining three parameters, a_{min}, ω_1 and m, define the differential activation function.

Angle contribution

The multiplication of the 4-parameter fit hyperbolas and differential activation function estimates the maximum voluntary torque – angular velocity relationship but does not consider the effect of the joint/contractile component angle. However, the torque is dependent on both angle and angular velocity. The angle contribution in the surface function, in other words the torque – angle relationship, was based on rotational equivalent of the force – length relationship. An inverted parabola, which has a maximum at an optimum angle, was used to estimate the torque values at a certain angular velocity (Equation 5.13). Along with the optimum angle, the second parameter that defines angle contribution is the drop-off rate of the maximum torque when going further from the optimum angle.

$$f(\theta_{con}) = 1 - q(\theta_{con} - \theta_{opt})^2 \qquad (5.13)$$

where, θ_{con} = contractile component angle

q = rate at which torque drops off from the optimum angle

θ_{opt} = optimum angle at which maximum torque occurs

Series elastic component stiffness

To optimise the parameters that appear in the left hand side of Equation 5.9, series elastic component (SEC) stiffness has to be estimated beforehand. SEC length, physiological cross-sectional area (PCSA) and moment arm of the major muscle groups contributing to the joint movement are needed to calculate the SEC stiffness.

Pierrynowski (1995) defined the geometric relation between the SEC length and the muscle architecture parameters for pennate and parallel fibred muscles as:

$$SEC\ length = Lb + Lt - Lf\cos(\alpha) \tag{5.14}$$

where, Lb = muscle belly length

Lt = tendon length

Lf = muscle fibre length

α = pennation angle

The architectural parameters and moment arms of the selected muscle groups, which make major contributions to the joint movements in consideration, were found in different sources in the literature. Since the heights of the subjects were often not stated, the data found could not be scaled to the subject in the present study. However, using the average data from different sources might reduce the error encountered. Table 5.9 shows the average of the muscle architecture parameters and moment arms obtained from the literature.

Table 5.10. Average SEC length and moment arm values obtained from the literature.

muscle group	PCSA (mm^2)	α (°)	Lf (mm)	Lt (mm)	Lb (mm)	SEC length (mm)	moment arm (mm)
teres major	816.0	16.0	148.0	41.7	160	59.5	59.0
latissimus dorsi	991.5	31.7	269.4	119.3	225.7	115.7	117.0
anterior deltoid	756.5	22	123.2	26	126	37.8	42.0
pectoralis major (clavicular)	335.0	17	170.3	22.8	177	36.9	62.0
pectoralis major (sternocostal)	440.5	25	203.3	46.8	108.5	48.0	62.0
middle deltoid	655.7	15.0	121.2	15.5	167.8	66.2	42.0
posterior deltoid	433.3	18.0	134.3	40.0	153.0	65.3	53.0
supraspinatus	454.0	7.0	61.9	79.9	91.5	109.9	21.0
infraspinatus	780.3	16.0	85.5	53.3	117.5	88.6	16.0
teres minor	268.3	24.0	67.1	34.4	115.5	88.6	16.0
subscapularis	1238.8	35.6	88.9	42.5	101.0	71.3	28.0
triceps brachii (lateral)	603.8	17.2	84.6	94.5	136.0	149.7	32.1
triceps brachii (medial)	514.0	17.0	83.4	14.9	147.3	82.4	29.5
triceps brachii (long)	528.4	11.0	109.8	136.3	231	259.4	28.1
brachioradialis	128.0	1.2	188.8	58.7	202.5	72.4	57.6
biceps brachii (long)	208.6	0.0	158.9	113.4	254.2	208.7	32.2
biceps brachii (short)	186.8	0.0	171.8	109.8	209.8	147.8	32.0
brachialis	667.0	0.0	96.4	17.5	120.0	41.1	20.1
pronator quadratus	278.5	9.9	23.3	50	39.3	66.3	6.9
pronator teres	361.0	12.9	35.5	115.8	130	211.2	8.7
supinator brevis	535.0	0.0	46.7	24.8	60.0	38.1	6.0

extensor carpi radialis brevis	351.0	8.9	50.4	226.4	127.2	303.8	16.3
extensor carpi radialis longus	230.0	1.3	77.2	226.4	93.7	242.9	18.5
extensor carpi ulnaris	316.7	12.1	47.5	169.2	227.8	303.9	7.7
flexor carpi radialis	306.3	3.1	55.0	127.9	163.7	236.7	8.7
flexor carpi ulnaris	554.0	12.1	42.8	117.9	227.8	303.9	9.1

The SEC stiffness value (k_t) of a joint movement was assumed to be the sum of the stiffness values of the contributing muscles for that movement (Equation 5.15).

$$k_t = \sum_{i=1}^{n} k_i \tag{5.15}$$

where, k_t = SEC stiffness of the joint movement

k_i = SEC stiffness of an individual muscle

n = number of muscles considered

and,

$$k_i = \frac{T_i}{(\Delta\theta_{sec})_i} \tag{5.16}$$

where, T_i = maximum torque generated by an individual muscle

$(\Delta\theta_{sec})_i$ = the change in the SEC angle for an individual muscle

The change in the SEC angle was calculated from the change in the SEC length (ΔSEC length) which was assumed to be 5% of the total SEC length during a maximal isometric contraction (Kong, 2004) (Equation 5.17). The maximum torque generated by an individual muscle was calculated by estimating its contribution to the maximum isometric torque of the whole muscle group. This contribution was

assumed to be the ratio of the product of muscle moment arm (d) and physiological cross-sectional area (PCSA) of an individual muscle to the sum of products for all individual muscles within the muscle group, since the muscle force is directly proportional to the PCSA (Equation 5.18).

$$(\Delta\theta_{sec})_i = \frac{(\Delta \text{SEC length})_i}{d_i} \tag{5.17}$$

$$T_i = T_{ciso} \frac{d_i PCSA_i}{\sum_{i=1}^{n} (d_i PCSA_i)} \tag{5.18}$$

where, d_i = moment arm for an individual muscle

T_{ciso} = maximum isometric torque

$PCSA_i$ = physical cross sectional area for an individual muscle

n = number of muscles considered

The calculated SEC stiffness values and contributing individual muscles for each joint movement are listed in Table 5.11.

Table 5.11. Calculated SEC stiffness values.

muscle group	T_i (Nm)	k_i (Nm/rad)	k_t (Nm/rad)
shoulder extension		(T_{ciso} = 142.6 Nm)	2366.9
teres major	34.5	684.6	
latissimus dorsi	83.2	1682.3	
shoulder flexion		(T_{ciso} = 51.5 Nm)	1386.9
anterior deltoid	20.9	464.2	
pectoralis major (clavicular)	13.7	458.9	
pectoralis major (sternocostal)	18.0	463.9	
shoulder horizontal abduction		(T_{ciso} = 62.9 Nm)	785.9
middle deltoid	28.0	354.7	

posterior deltoid	23.3	378.5	
supraspinatus	9.7	37.0	
teres minor	4.4	15.7	
shoulder horizontal adduction		(T_{ciso} = 134.3 Nm)	1968.5
anterior deltoid	35.5	399.0	
pectoralis major (clavicular)	23.2	780.5	
pectoralis major (sternocostal)	30.5	789.0	
shoulder internal rotation		(T_{ciso} = 39.7 Nm)	603.1
subscapularis	17.0	133.9	
teres major	23.7	469.2	
shoulder external rotation		(T_{ciso} = 31.0 Nm)	113.7
infraspinatus	23.4	84.6	
teres minor	8.1	29.1	
elbow extension		(T_{ciso} = 57.5 Nm)	280.3
triceps brachii (lateral)	24.2	103.8	
triceps brachii (medial)	19.0	136.3	
triceps brachii (long)	18.6	40.3	
elbow flexion		(T_{ciso} = 73.9 Nm)	651.5
brachioradialis	16.3	258.6	
biceps brachii (long)	14.8	45.6	
biceps brachii (short)	13.2	56.9	
brachialis	29.6	290.3	
pronation		(T_{ciso} = 13.8 Nm)	18.0
pronator quadratus	5.2	10.9	
pronator teres	8.6	7.1	
supination		(T_{ciso} = 13.0 Nm)	36.2

supinator brevis	3.4	8.3	
biceps brachii (long)	4.0	12.4	
biceps brachii (short)	3.6	15.5	
wrist extension		(T_{ciso} = 25.1 Nm)	29.2
extensor carpi radialis brevis	11.8	15.8	
extensor carpi radialis longus	8.8	10.7	
extensor carpi ulnaris	5.0	2.7	
wrist flexion		(T_{ciso} = 43.1 Nm)	31.2
flexor carpi radialis	12.7	9.3	
flexor carpi ulnaris	32.1	21.9	
ulnar deviation		(T_{ciso} = 40.7 Nm)	23.3
extensor carpi ulnaris	13.6	7.2	
flexor carpi ulnaris	32.1	16.1	
radial deviation		(T_{ciso} = 29.5 Nm)	30.4
extensor carpi radialis longus	8.8	15.0	
extensor carpi radialis brevis	11.8	15.4	

Optimisation

After determining SEC stiffness, the nine-parameter Equation 5.9 was fitted to the corrected data to obtain a complete torque – angle – angular velocity relationship using the Simulated Annealing (Corana et al., 1987) optimisation algorithm. Among the parameters, the value of T_{max} was assumed to be 1.4 times T_o (Yeadon et al., 2006). The lower and upper bounds of the nine parameters are listed in Table 5.12.

Table 5.12. Lower and upper bounds of the nine parameters

Parameter	Lower Bound	Upper bound
T_o (Nm)	0.9To	1.1To
T_{max} (Nm)	1.4.To	
ω_{max} (rad/s)	18.0	36.0
ω_c/ω_{max}	0.3	0.5
a_{min}	0.2	0.99
m	0.0	3.0
ω_1 (rad/s)	-3.0	3.0
q	0.0	3.0
θ_{opt} (rad)	0.0	6.0

The nine parameters were optimised by minimising a weighted root mean square (RMS) of the difference between the experimental torque data and calculated torque. The reason for using weighted RMS was to obtain a surface representing maximum voluntary torque that is above most of the data points. Another constraint in the optimisation algorithm was to have decreasing torque value with increasing angular velocity. The optimisation results for each joint movement and an example of the nine-parameter surface fit to the experimental data are presented in Tables 5.13 – 5.15 and Figure 5.9, respectively. The isovelocity data for the shoulder external rotation could not be collected for the subject, as the subject could not exert maximum power due to an injury at the time of data collection. Therefore, some of the shoulder external rotation parameters were estimated from the isometric data and moderate values within the upper and lower bounds were assumed for the rest of the parameters.

Table 5.13. Optimisation results for the shoulder joint

Parameter	Flexion	Extension	Horizontal adduction	Horizontal abduction	Internal rotation	External rotation
T_o (Nm)	56.29	119.13	97.48	71.90	42.67	33.75
T_{max} (Nm)	78.81	166.78	136.48	100.66	59.73	47.25
ω_{max} (rad/s)	20.74	31.93	18.05	18.00	19.47	18.00
ω_c (rad/s)	6.70	15.02	6.43	6.93	9.71	7.2
a_{min}	0.99	0.96	0.87	0.85	0.79	0.9
m	3.00	2.98	0.06	0.05	0.17	1.0
ω_1 (rad/s)	-3.00	1.55	-0.69	-0.59	0.39	0.0
q	0.28	0.11	0.24	0.07	0.05	0.1
θ_{opt} (rad)	4.96	0.83	2.41	4.99	5.90	0.90

Table 5.14. Optimisation results for the elbow joint

Parameter	Flexion	Extension	Pronation	Supination
T_o (Nm)	75.82	51.95	17.35	18.30
T_{max} (Nm)	106.14	72.73	24.29	25.62
ω_{max} (rad/s)	18.10	18.45	27.88	35.45
ω_c (rad/s)	5.43	5.55	9.71	16.90
a_{min}	0.96	0.93	0.97	0.86
m	0.16	0.03	0.38	0.09
ω_1 (rad/s)	-1.53	-1.17	2.25	-1.26
q	0.03	0.23	0.40	0.22
θ_{opt} (rad)	0.33	4.64	4.50	1.78

Table 5.15. Optimisation results for the wrist joint

Parameter	Flexion	Extension	Ulnar deviation	Radial deviation
T_o (Nm)	45.78	24.90	41.44	31.63
T_{max} (Nm)	64.10	34.86	58.02	44.28
ω_{max} (rad/s)	21.40	18.08	18.02	21.77
ω_c (rad/s)	10.70	7.78	5.83	7.72
a_{min}	0.99	0.90	0.96	0.93
m	3.0	3.00	0.01	0.03
ω_1 (rad/s)	-2.84	2.59	-1.71	-1.44
q	0.33	0.03	0.18	0.06
θ_{opt} (rad)	4.26	1.27	0.43	5.14

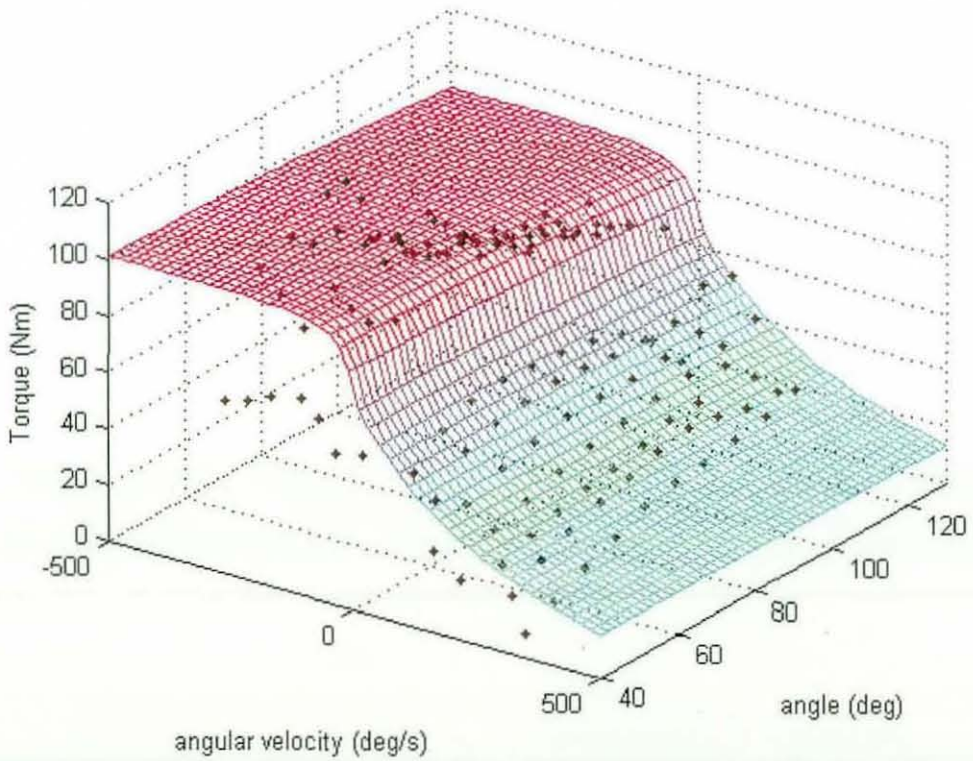

Figure 5.9. Torque – angle – angular velocity relationship for elbow flexion.

5.2 Inertia parameters

5.2.1 Body Segmental Inertia Parameters

The geometric model of Yeadon (1990a) was used to calculate the body segmental inertia parameters. Ninety-five anthropometric measurements were taken from the subject by an experienced researcher (for full data set, see Appendix, A3). For the segmental density values, Dempster's (1955) data were used as a first estimate and these values were then adjusted according to the ratio of the calculated and measured mass of the subject.

Table 5.16 shows the value of segmental mass, distance of centre of mass (CM) from proximal joint and moments of inertia about the frontal (I_x), lateral (I_y) and longitudinal (I_z) axes of the segment.

Table 5.16. Segmental inertia parameters calculated from the inertia model

segment	mass (g)	CM from proximal joint (mm)	I_x (g.mm^2)	I_y (g.mm^2)	I_z (g.mm^2)
right upper arm	2160	126.1	16941000	16939000	2577000
right forearm	1516	124.4	10173000	10088000	1210000
right hand	401	70.2	968000	792000	232000
trunk	33521	299.4	1320106000	1190609000	337162000

5.2.2 Bone and Wobbling Mass Inertia Parameters

Since the upper arm and the forearm were modelled as bones and wobbling masses, inertia parameters for both components were required. The 3D surface meshes of the bones that were created from the MRI scans were imported to MSC.ADAMS environment and each surface mesh defined a 3D object. The MSC.ADAMS software is capable of calculating inertia parameters of an object in its environment. Therefore, the inertia parameters of humerus, ulna and radius were calculated by the MSC.ADAMS software using the geometry of the bones and bone densities. The bone density values were taken from the literature (Clarys and

Marfell-Jones, 1986). However, the playing arms of tennis players have been shown to have significantly higher bone mineral density than the non-playing arms and/or dominant arms of control groups (Pluim et al., 2007), the density value found in the literature was increased by 10% before using it in the inertia parameter calculations.

The inertia parameters of the upper arm and forearm wobbling masses were determined so that the combined system of bone(s) and wobbling mass was equivalent to the whole segment, i.e. they have same total mass, same centre of mass and same moments of inertia (Equations 5.19-5.21, respectively).

$$m_{ua} = m_h + m_{uw} \qquad \textit{for upper arm} \qquad (5.19.a)$$

$$m_f = m_r + m_u + m_{fw} \qquad \textit{for forearm} \qquad (5.19.b)$$

where, m_{ua} = mass of the upper arm segment

m_h = mass of the humerus

m_{uw} = mass of the upper arm wobbling mass

m_f = mass of the forearm segment

m_r = mass of the radius

m_u = mass of the ulna

m_{fw} = mass of the forearm wobbling mass

$$m_h d_h + m_{uw} d_{uw} = 0 \qquad \textit{for upper arm} \qquad (5.20.a)$$

$$m_r d_r + m_u d_u + m_{fw} d_{fw} = 0 \qquad \textit{for forearm} \qquad (5.20.b)$$

where, d_h = the location of the centre of mass of the humerus with respect to the upper arm segment's centre of mass

d_{uw} = the location of the centre of mass of the upper arm wobbling mass with respect to the upper arm segment's centre of mass

d_r = the location of the centre of mass of the radius with respect to the forearm segment's centre of mass

d_u = the location of the centre of mass of the ulna with respect to the forearm segment's centre of mass

d_{fw} = the location of the centre of mass of the forearm wobbling mass with respect to the forearm segment's centre of mass

Although the principal component axes of the bones and the whole segments were slightly skewed, they were assumed to be parallel for simplicity and the total moment of inertia of the upper arm and forearm were calculated using the parallel axis theorem.

$$I_{ua} = I_h + m_h d_h^2 + I_{uw} + m_{uw} d_{uw}^2 \qquad \textit{for upper arm} \quad (5.21.a)$$

$$I_f = I_r + m_r d_r^2 + I_u + m_u d_u^2 + I_{fw} + m_{fw} d_{fw}^2 \qquad \textit{for forearm} \quad (5.21.b)$$

where, I_{ua} = moment of inertia of the upper arm segment

I_h = moment of inertia of the humerus

I_{uw} = moment of inertia of the upper arm wobbling mass

I_f = moment of inertia of the lower arm

I_r = moment of inertia of the radius

I_u = moment of inertia of the ulna

I_{fw} = moment of inertia of the forearm wobbling mass

Tables 5.17-5.18 show the inertia parameters of the bones and wobbling masses of the upper arm and forearm, respectively.

Table 5.17. Inertia parameters of the upper arm.

upper arm	mass(g)	d_x(mm)	d_y(mm)	d_z(mm)	I_x(gmm^2)	I_y(gmm^2)	I_z(gmm^2)
segment	2160	0	0	0	16941000	16939000	2577000
humerus	291	-2.5	4.5	3.5	4340763	4326962	49337
wobbling	1869	0.4	-0.7	-0.6	12593965	12601026	2518789

Table 5.18. Inertia parameters of the forearm.

forearm	mass(g)	d_x(mm)	d_y(mm)	d_z(mm)	I_x(gmm^2)	I_y(gmm^2)	I_z(gmm^2)
segment	1516	0	0	0	10173000	10088000	1210000
radius	110	16.8	-4.4	-46.4	779469	775918	8290
ulna	111	-4.9	-16.5	17.7	751247	749855	8304
wobbling	1295	-1.0	1.8	2.4	8328753	8247357	1122078

5.3 Viscoelastic properties of wobbling masses

The upper arm and forearm wobbling masses were connected to the bone segments with spring-damper systems at the proximal and distal end of the bones. For each wobbling mass, the viscoelastic parameters of the springs at the proximal and distal end were assumed to be the same. The stiffness coefficients were estimated from matching the actual and simulated vibration frequencies of the wobbling masses during the backhand groundstroke in a previous study (Glynn, 2007). The same stiffness parameters were used in this study since the same subject performed the backhand groundstrokes. Near-critical damping coefficients (Pain and Challis, 2001) were selected for use in the spring-damper systems, but the damping values were slightly different to Glynn (2007) due to the rigid / wobbling masses being modelled slightly differently. The simulation model of the arm described in Chapter 3 was used to determine the damping coefficients. The bones of the arm were fixed in the anatomical position and the wobbling masses were allowed to fall due to gravity. The damping coefficients were varied and the motion of the wobbling masses was recorded for each simulation until both wobbling mass systems became near-critically damped and had non-oscillatory behaviour. The stiffness and damping coefficients of the upper arm and forearm wobbling masses are presented in Table 5.19.

Table 5.19. Stiffness and damping coefficients of the upper arm and forearm wobbling masses

wobbling mass	stiffness (N/mm^3)	damping (Ns/mm)
upper arm	0.02	0.085
forearm	0.03	0.110

5.4 MRI Data Collection and Analysis

To obtain some of the muscle parameters such as cross-sectional areas, attachment points of the muscles and build 3D surface images of bones of the arm Magnetic Resonance Imaging (MRI) was used. The MRI data were collected at Churchill Hospital, Oxford under supervision of two radiographers and a doctor. The radiographers were told what was required and they then designed a MRI scan session protocol.

A Genesis Signa MRI machine was used (Figure 5.10) with a maximum magnetic field of 1.5 Tesla. The machine was controlled by a computer out of the scanning room by one of the radiographers while the other radiographer checked the equipment before each scan and helped the subject to locate his arm and body before going into the machine.

The scanning sessions were designed such that the slides had low thickness near the edges of the bones, and high thickness at the shaft of the bones. Since the thickness was low at the edges of the bones, there were more slides at these areas. For this reason the details at and around joints could be seen more easily. The larger number of slides was also required to obtain the bone shape more accurately, since near the joints the shape of the bones of arm is changing rapidly with respect to shaft of these bones.

The sessions started with the shoulder joint and the head of humerus being scanned. After that, the shaft of the humerus was scanned. The scanning of the elbow joint included both the lower part of the humerus and the upper parts of the radius and ulna. Before starting the shafts of the bones of the forearm a short break was given for subject to stand up and move around. Then the shafts of the forearm bones and finally wrist joint and metacarpals were scanned.

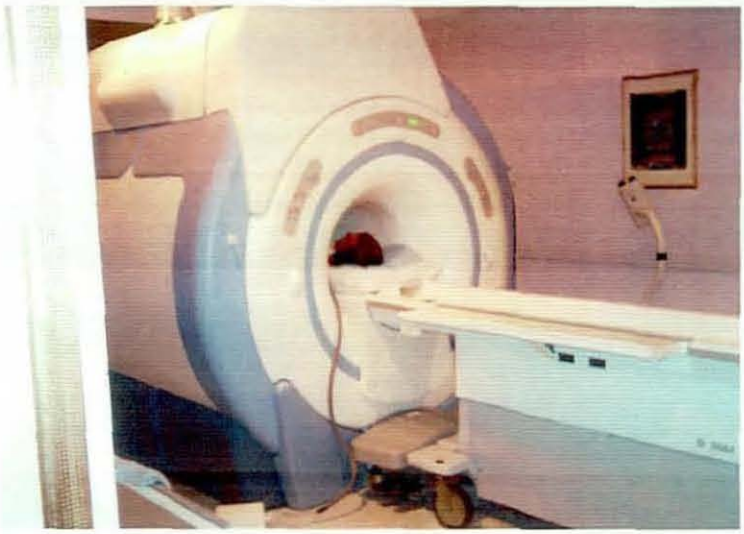

Figure 5.10. Subject within the Genesis Signa MR machine

The things that were expected to be measured from MRI scans were muscle attachment points, cross-sectional area of muscle and bone area on each slide. Of these, bone area was measured, but it was very hard to distinguish between the muscle groups probably due to low resolution of the MR images given from the hospital (Figure 5.11). Therefore, muscle architecture properties could not be obtained from the MRI scans.

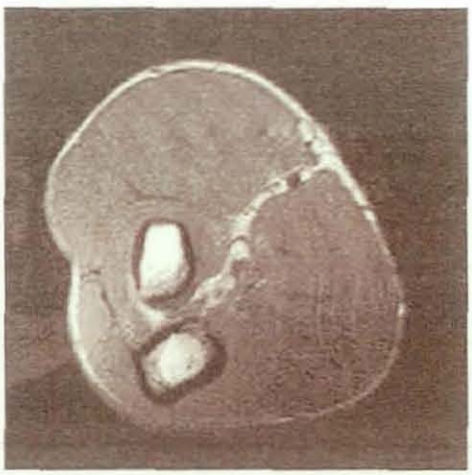

Figure 5.11. MR image of forearm in transverse plane

To process MRI scans Mimics software was used. The bone area was labelled on each slide that had a known thickness and the software estimated the 3D surface mesh of the bones by combining the bone contours on each slide. The 3D meshes of the bones were then exported to the main modelling environment, MSC.ADAMS. A

comparison of the bone surface meshes found from the literature and obtained from the MRI scans is shown in Figure 5.12. The fine mesh of the bones gave additional accuracy to the bone models compared to the ones found in the literature. Therefore, bone inertia parameters were calculated directly from them with a given bone density. In addition, the details on the bone surface obtained from the MRI scans allowed determination of the muscle origin and insertion points / areas more accurately.

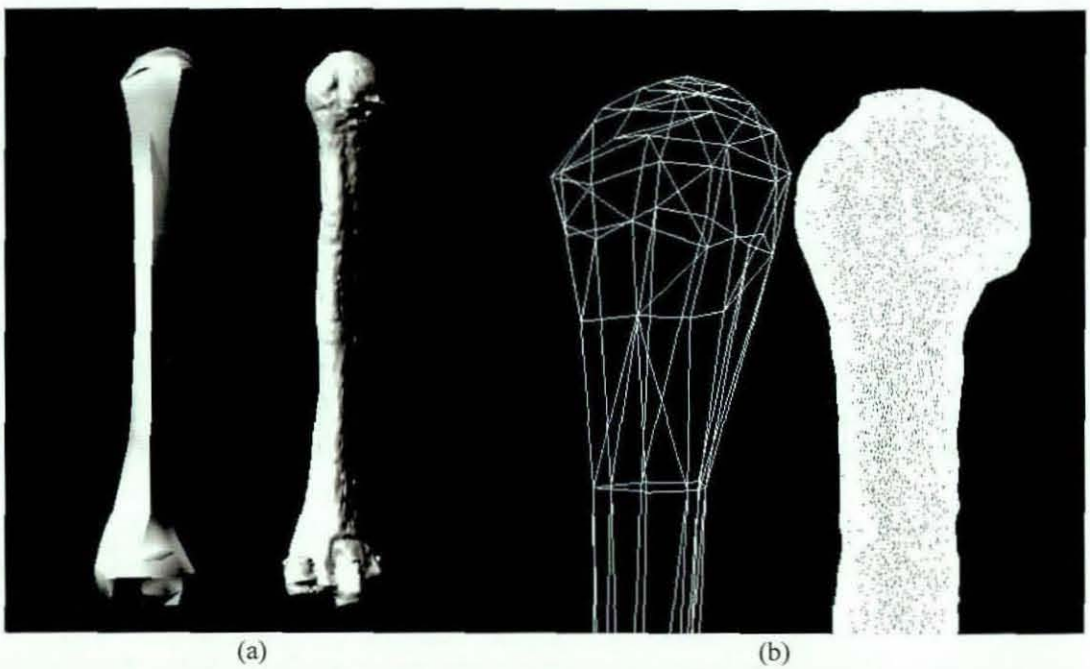

Figure 5.12. The comparison of the rendered surface image of the humerus (a) and a surface mesh of the humeral head (b) found from the literature (left) and obtained from the MRI scan (right)

5.4 Equipment Parameters

The equipment parameters for the tennis racket, stringbed and ball were taken from a previous study in which the same type of racket was used(Glynn, 2007). These were the inertia and elastic parameters of the racket frame; viscoelastic parameters of the stringbed; viscoelastic parameters of the tennis ball for normal and oblique impacts.

Racket parameters

The natural frequencies and the location of the antinodes in the racket head plane and normal to this plane are presented in Table 5.20 (Glynn, 2007).

Table 5.20. Modal analysis of the racket

mode shape	direction	natural frequency(Hz)	antinode location from butt end (mm)
Fundamental mode	normal to racket head plane	149.8	350
	on racket head plane	179.1	375
Second mode	normal to racket head plane	359.4	-
	on racket head plane	375.0	-

The average of the antinode locations in the two planes was assumed to be the location of the joint connecting the racket head and racket handle segment in the simulation model. The racket was cut at that point and the moment of inertia and centre of mass location of both parts were measured (Glynn, 2007) (Table 5.21).

Table 5.21. Inertia parameters of the racket

racket part	mass (g)	CM from butt end (mm)	$I_{long}(gmm^2)$	$I_{front}(gmm^2)$	$I_{trans}(gmm^2)$
whole with strings	255.4	390	1660000	13160000	12520000
whole without strings	240.5	385	1610000	12840000	12000000
racket handle	106.9	195	100000	2030000	2000000
racket head	133.6	187	1510000	3920000	3110000

The optimum torsional stiffness and damping coefficient values of the torsional spring-dampers at the joint between the racket head and racket handle are shown in Table 5.22 (Glynn, 2007).

Table 5.22. Viscoelastic parameters of the racket frame

direction plane	torsional stiffness (Nm/rad)	torsional damping (Nms/rad)
normal to racket head plane	1075	0.04
on racket head plane	1800	0.10

Stringbed parameters

The springs of the stringbed are enumerated in Figure 5.13 and the corresponding optimum stiffness values for these springs are listed in Table 5.23 (Glynn, 2007).

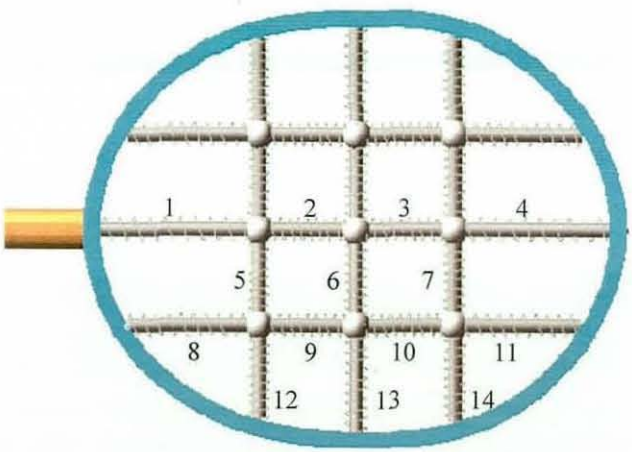

Figure 5.13. The enumeration of the springs in the stringbed model

Table 5.23. Stiffness values of the springs in the stringbed model

spring no.	parameter	stiffness value (N/m)
1	ks1*m3	96969
2	ks1	102170
3	ks1	102170
4	ks1*m4	33042
5	ks4	112630
6	ks2	103380
7	ks4	112630
8	ks3*m5	47660
9	ks3	119780
10	ks3	119780
11	ks3*m6	68933
12	ks4*m1	49129
13	ks2*m2	38964
14	ks4*m1	49129

Besides the spring stiffness values, the preload acting on the springs was also optimised and 967.7 N was found to be the optimum value for the stringbed used in this study (Glynn, 2007).

Ball-racket impact parameters

A linear relationship between the optimum stiffness and damping coefficients and inbound velocity was found for the normal impact force (Glynn, 2007). Therefore, the coefficient values can be determined as a function of inbound velocity within the experimental range (Equation 5.22).

$$k = 1.5491v + 16.522 \quad \textit{for stiffness coefficient} \quad (5.22.a)$$

$$c = 1.1934v - 3.0662 \quad \textit{for damping coefficient} \quad (5.22.b)$$

where, k = stiffness coefficient of the ball

c = damping coefficient of the ball

v = inbound ball velocity

To model the frictional force, three different coefficients of friction (μ) were assigned to the nine impact points on the stringbed (Section 3.3.3). The coefficients of friction at each impact point are shown in Figure 5.16 and the optimum values of the coefficients, μ_1, μ_2, μ_3, are 0.26, 0.30 and 0.35, respectively. (Glynn, 2007).

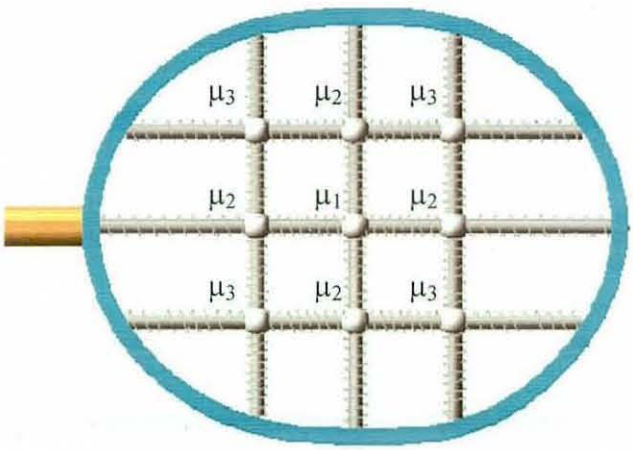

Figure 5.14. Coefficients of friction corresponding to each impact point on the stringbed.

5.5 Summary

In this chapter, the methods used to determine the subject-specific parameters and equipment parameters have been described. The parameters were measured directly from experiments or determined indirectly by matching the experimental results with computer simulations. Maximum voluntary torques were measured using an isovelocity dynamometer. The data collection and analysis of the torque-strength parameters have been explained in detail. The body segmental inertia parameters were calculated using the method of Yeadon (1990a) whereas the inertia parameters of the bones were determined by MSC.ADAMS and wobbling mass inertias were calculated using the parallel axis theorem. The inertia parameters of the racket were measured experimentally. Viscoelastic parameters of the racket frame, stringbed and ball-racket impact were determined indirectly from the experiments by matching the

appropriate experimental and computer simulation results (Glynn, 2007). The parameters determined in this chapter will be used in a torque-driven computer simulation model of the tennis backhand groundstrokes. The next chapter focuses on the evaluation of the simulation model.

6 MODEL EVALUATION

6.1 Introduction

An evaluation of the model is required to use simulation models confidently for further analyses. This chapter describes the evaluation of the simulation model based on comparisons between simulation and performance. Once the simulation model was evaluated for a backhand groundstroke with a ball impact at the centre of the racket, the location of the ball-racket impact was perturbed and the results were compared with the kinematics of a backhand groundstroke with off-centre impact to determine whether the model behaved realistically for off-centre impacts. In addition, comparisons of simulation and performance results of ball outbound velocity and ball contact time are also presented in this chapter.

6.2 Model Evaluation

6.2.1 Overview of Model Evaluation

The torque-driven simulation model has a pair of torque generators for each joint movement (seven in total) and three perpendicular torque components between the hand and the racket representing the gripping torque (Chapter 3). The maximum voluntary torque values for a particular joint angle and joint angular velocity were determined using the torque-strength parameters of the subject (Chapter 5). The torque exerted by each torque generator during a simulation was equal to the maximum voluntary torque multiplied by torque activation level for that torque generator. The gripping torque components between racket and hand were a combination of torque-time profiles (similar to torque activation level) and torsional spring torques (effective after impact). Torque activation levels and torque-time profiles of the gripping torque were parameterized and used as inputs for the model as well as the stiffness and damping coefficients of the torsional springs. As a result, the model was evaluated by optimising the torque-time / viscoelastic parameters of the grip and the activation parameters of the torque generators while minimizing the differences between the joint angles of the arm and global racket angles obtained

from the simulation and performance. The Simulated Annealing algorithm (Corana et al., 1987) was used to vary the model parameters in order to find the best match.

In order to match the conditions at the impact time more accurately, the complete backhand swing was divided into two phases: pre-impact and post impact. The impact period, which is the duration of the ball contact with the stringbed, was considered in the post-impact phase since this phase started when the ball first touched the racket.

During the optimisation of the pre-impact phase, the parameters were divided into four groups and initially optimised individually in the following order: gripping, shoulder, elbow and wrist parameters. The joint motions were angle-driven when the gripping parameters were optimised. After finding acceptable parameters for gripping torque, these parameters were kept constant and the joint motion in consideration was switched to torque-driven to optimise its parameters while keeping the other joint motions angle-driven. The initial optimisation of the parameters in groups was done to find a good initial estimate of the parameters before a final optimisation and to speed up the optimisation process by decreasing the number of parameters. Once initial optimisations of all groups had finished, all parameters were re-optimised altogether. A set of parameters was obtained from this optimisation and used as an initial guess for a last optimisation, whose objective function considered only the last 50 ms of the pre-impact in order to get a better match of the conditions at impact.

The parameters after impact were optimised simultaneously and all joint motions were torque-driven. First, the whole backhand swing was considered and the post-impact phase was optimised. Since the pre-impact and post-impact parameters are independent, the previously optimised pre-impact parameters were held constant throughout the simulations. Then, instead of simulating the whole swing, only the swing after impact was considered in the second optimisation. The simulations started at impact using the initial conditions obtained from the optimised pre-impact simulation. By starting the simulations at impact, it was assured that the pre-impact conditions as well as impact time, ball location in space and other impact conditions would not be affected during sensitivity analyses and other simulations planned. Furthermore, a third optimisation also starting from the impact was also done. However, in this case, the actual performance data were used for initial configuration

of the model and initial torque activation values were also optimised with the post-impact parameters.

An integration step size of 1 ms was used for the initial and final optimisation before impact. To simulate the behaviour of the ball-racket impact more accurately the step size was reduced to 0.1 ms for a period of 10 ms using a customized simulation script, (the ball in contact with the racket for at most 5-6 ms). The integration step size was then changed back to 1 ms after this period. In addition, ADAMS/Solver can decrease the step size up to 10^{-6} of the initial step size in order to converge with the output from the simulation at the period of the initial step size.

6.2.2 Model Parameters

Torque activation profiles for torque generators

The activation level of each torque generator was specified as a function of time and it defined what percentage of the maximum was exerted at the joint at a particular time. The torque activation level takes values from 0 (no activation) to 1 (full activation). The change between the two activation levels was defined by quintic functions (Yeadon, 1984) (Equation 6.1). The quintic function has zero first and second derivatives at the endpoints preventing sudden changes in the activation.

$$Q(x) = x^3(6x^2-15x+10) \qquad (6.1)$$

Two different activation profiles were defined using six activation parameters for each of them (Figure 6.1 and 6.2). The activation profiles represented the activation of the flexor and extensor torques and they were adjusted where necessary. The general extensor profile started with a low pre-activation level to represent the activation before the start of the simulation. During the swing, the activation level ramped up and reached a maximum activation level before impact. After impact, the activation level decreased to zero. The general flexor profile started with a high pre-activation level and ramped down to a minimum level before impact. The ramping up of activations after impact prevented joints from hyper-extension by reducing the effect of the extensor torque. The parameters required to define the extensor and flexor torque activation profiles are listed in Table 6.1 and 6.2, respectively.

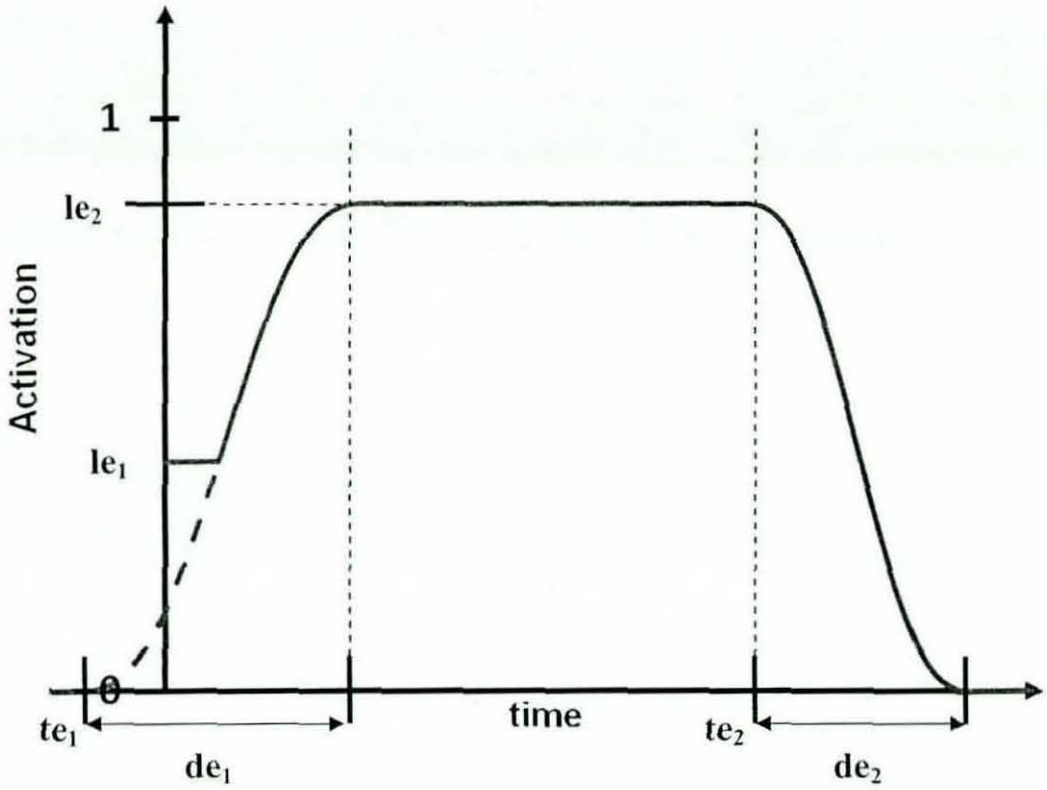

Figure 6.1. Activation profile for extensor torques and its parameters.

Table 6.1. Definition of the parameters used in the extensor activation profiles.

Parameter	Definition
te_1	start time of ramping up
de_1	duration of ramping up
le_1	pre-activation level
te_2	start time of ramping down
de_2	duration of ramping down
le_2	maximum activation level

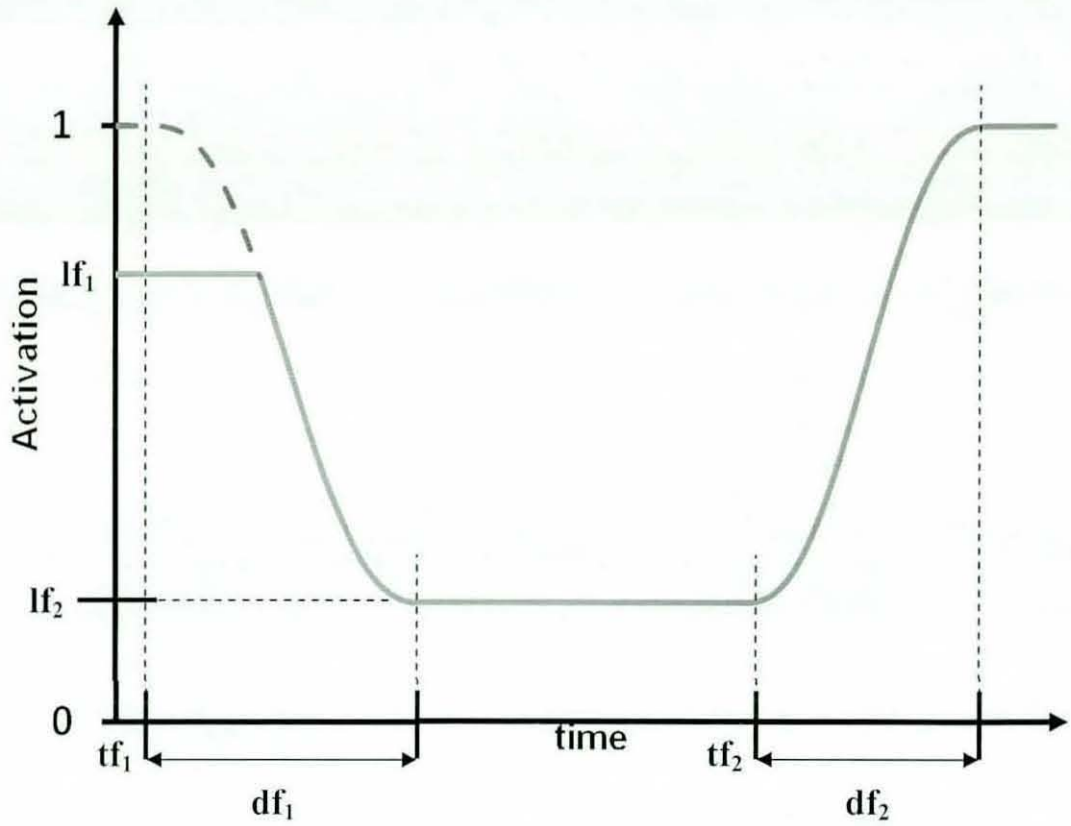

Figure 6.2. Activation profile for flexor torques and its parameters.

Table 6.2. Definition of the parameters used in the flexor activation profiles.

Parameter	Definition
tf_1	start time of ramping down
df_1	duration of ramping down
lf_1	pre-activation level
tf_2	start time of ramping up
df_2	duration of ramping up
lf_2	minimum activation level

Torque-time and viscoelastic parameters of the gripping torque

The time histories of the gripping torque components were estimated using quintic functions similar to the torque activation profiles (Figure 6.3). Each component of the gripping torque started with an initial torque level and either ramped up or down during the swing before impact. After the impact, the gripping torque level used before impact was reduced to zero and replaced with three torsional spring-dampers representing the resistance of the racket motion relative to hand during / after impact. The torque-time and viscoelastic parameters of the gripping torque are presented in Table 6.3.

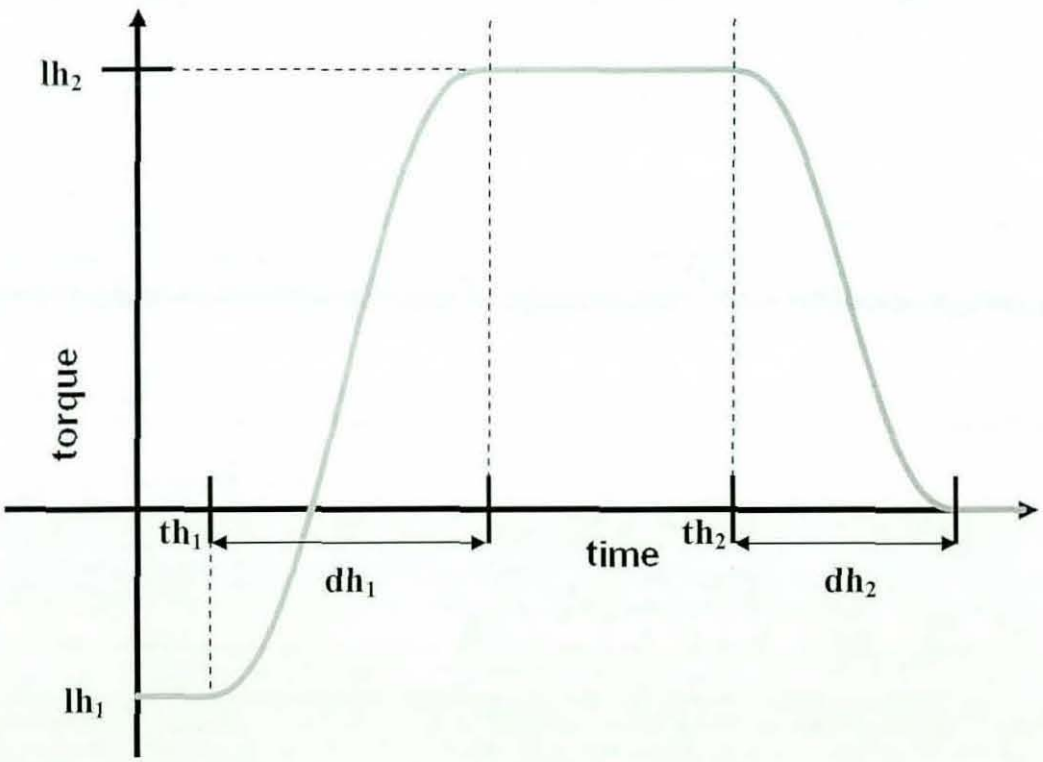

Figure 6.3. Torque profile for the gripping torque components and its parameters.

Table 6.3. Definition of the parameters used in the gripping torque components.

Parameter	Definition
th_1	start time of ramping up
dh_1	duration of ramping up
lh_1	pre-activation level
th_2	start time of ramping down
dh_2	duration of ramping down
lh_2	maximum activation level
kh	stiffness coefficient
ch	damping coefficient

6.2.3 Matching Optimisations

Selecting the torque activation profiles

Initially, for the torque generators defining a joint movement, flexor and extensor torque activation profiles were used considering the joint motion and the description of the torque generators (Section 3.2.3). However, it was observed from the EMG data (Section 4.4) that the activation of the wrist extensors / wrist flexors started concurrently before impact. Therefore, an extensor profile was used for the torque generators for wrist flexion and extension movements. The extensor profiles were also selected for the torque generators for radial and ulnar deviation since these movements were controlled by the wrist extensors and flexors as well. In addition, shoulder flexion and extension movements were both arranged to the extensor profiles after some initial optimisation for the shoulder joint parameters. Table 6.4 lists the joint movement and the corresponding torque activation profile for that movement.

Table 6.4. Joint movements and corresponding torque activation profiles.

Joint movement	Activation profile
shoulder flexion	extensor
shoulder extension	extensor
shoulder abduction	extensor
shoulder adduction	flexor
shoulder internal rotation	flexor
shoulder external rotation	extensor
elbow extension	extensor
elbow flexion	flexor
pronation	flexor
supination	extensor
wrist flexion	extensor
wrist extension	extensor
radial deviation	extensor
ulnar deviation	extensor

Adjustments for torque activation profiles

For each joint motion except wrist flexion, wrist extension and radial deviation, the first four parameters defining the torque activation profile were used in the matching optimisation of the pre- impact phase (Figure 6.4). The activation profiles of wrist flexion, wrist extension and radial deviation before impact were adjusted since no satisfactory results were obtained from the initial optimisation of the four parameters. Reviewing the EMG data (Section 4.4) for the wrist extensors and flexors showed that the maximum activation occurred before impact. Therefore, the activation profiles for these joint motions were estimated by all six parameters; allowing the ramping down of the activation before impact (Figure 6.5). The optimisation of the ramping down after impact remained unchanged so the number of the parameters defining the torque activation profile increased to eight. For the

matching optimisation after impact, the last two parameters of the profiles were used for all joint motions.

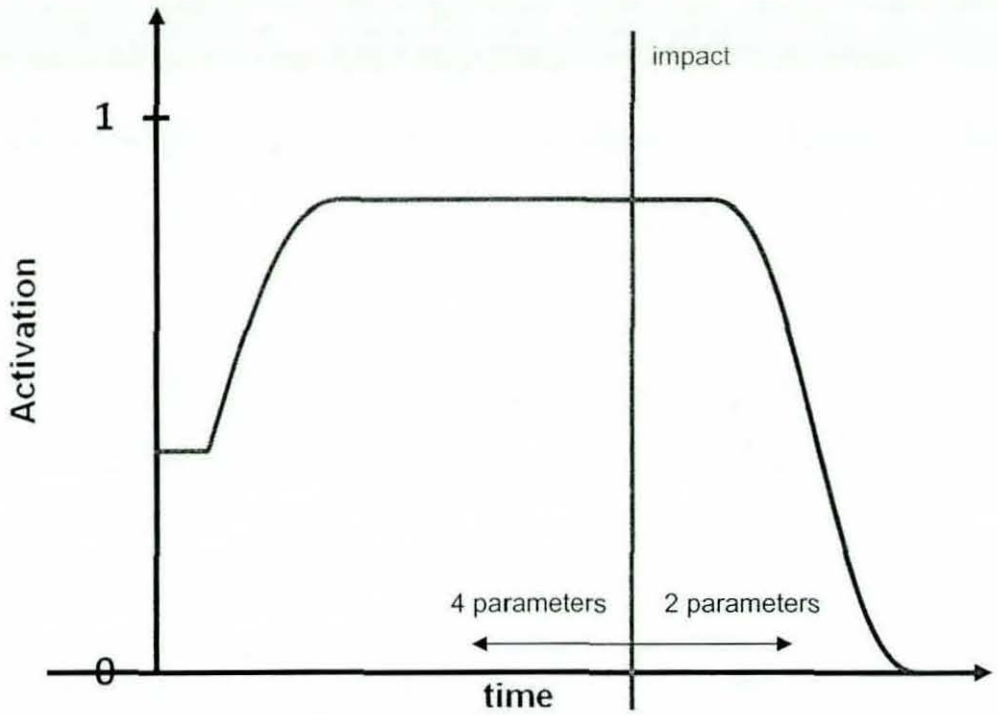

Figure 6.4. Activation profile for extensor torques with respect to impact time.

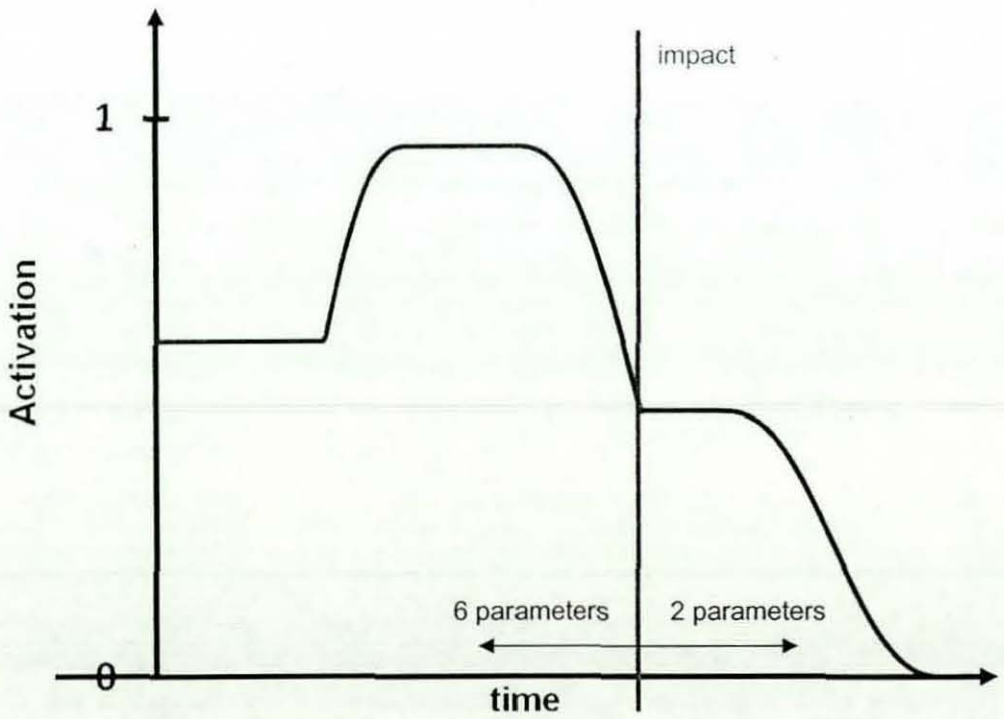

Figure 6.5. Adjusted activation profile for wrist flexion, wrist extension and radial deviation.

Upper and lower bounds of the parameters

The simulation started at an arbitrary instant near the start of the forward motion of the backhand stroke. For this reason, start times of initial ramping up / down activation (te_1 / tf_1) and pre-activation levels (le_1 and lf_1) might have different values within a wide range. Therefore, it was hard to estimate a lower and upper bound for te_1 and tf_1. Although it was obvious that le_1 and lf_1 had to be between 0.01 (minimum allowed activation level) and 1 (full activation), because of the additional constraints ($le_1 < le_2$ and $lf_1 > lf_2$) the upper bound for le_1 and lower bound for lf_1 had to be adjusted. Similarly, le_2 and lf_2 did not have a definite lower bound and upper bound, respectively. The minimum time required from zero to maximum activation level was assumed as 70 ms consistent with the rise (ramping up) times presented in the literature (Freund and Büdingen, 1978). Therefore, for the duration of the ramping up and down (de_1, de_2, df_1 and df_1), considering the change of the activation level, a lower bound proportional to 70 ms was used. For shoulder flexion and ulnar deviation, the lower bound of 70 ms was reduced to 60 and 40 ms, respectively, as the activation profile used was insufficient to give a good match to the performance. The lower bound of the starting time of final ramping down / up activation (te_2 / tf_2) was selected as the impact time since these parameters were used in the optimisation of the swing after impact except wrist extension, wrist flexion and radial deviation.

For the upper and lower bounds, which could not be estimated directly, first, the simulation was manually run several times with different values of the parameter in consideration. Then, by observing the model behaviour, an appropriate value was chosen for the upper and/or lower bound. However, these upper and lower bound values were flexible and they were adjusted during the matching optimisation if the optimum values of the parameters were approaching the bounds.

Objective score

An objective score was calculated and minimised during optimisation of the model parameters. The RMS difference between performance and simulation values of the seven joint angles (shoulder flexion / extension, shoulder abduction / adduction, shoulder internal / external rotation, elbow flexion / extension, pronation / supination, wrist flexion / extension, radial / ulnar deviation) and three racket orientation angles were calculated individually. These ten RMS differences were

then combined into a single score by doing an additional RMS. All angles were equally weighted when calculating RMS differences.

6.3 Results

During the optimisation process, particular importance was given to the impact conditions since it was the most critical instant of the backhand swing. The conditions at impact determine the ball-racket interaction, which is the main cause of the abrupt change in kinetics and kinematics of the racket and arm. For this reason, to match the impact conditions and impact period more accurately, optimisation of the backhand swing was separated into two phases: pre-impact and post-impact. In the optimisation of the pre-impact phase, the main aim was to obtain impact conditions during simulation as close as possible to those during the actual performance. For the post-impact phase, the aim was to match all joint and racket angles of the simulation and the actual performance for at least 40 ms, during which the loadings at the elbow and wrist joints reach a maximum value and then return to normal levels. The parameters of the model were arranged such that the pre-impact phase used only pre-impact parameters and post-impact phase used only post-impact parameters (if simulation started after impact, otherwise pre-impact parameters were used as constants until impact) and there was no crossover between the parameters of the two phases.

6.3.1 The Results of the Pre-impact Phase

The pre-impact phase arbitrarily started from the instant when the arm was swung back and starting to swing forward. It took 237 ms to reach the impact time from the starting point for the trial that was used. A total of 74 parameters (24 at the shoulder + 16 at the elbow + 22 at the wrist + 12 at the hand/racket) were optimised in the pre-impact phase. After initial optimisation of the pre-impact parameters in groups (Section 6.2.1), all parameters were re-optimised altogether. Although the objective score of the optimisation was satisfactory (1.27°), the difference between the simulation and actual performance at impact could have been better. Therefore, a new optimisation was done which considered only the last 50 ms of the pre-impact

while calculating the objective score. The new optimisation resulted in a lower score for the last 50 ms (0.4°; vs. 0.69° for the first optimisation) and a considerably better match of impact conditions for all angles except the 1st rotation of racket orientation (Table 6.5). However, the score for the whole pre-impact period was bigger than the previous optimisation (1.81°). This was due to the larger deviations occurring in the first half of the pre-impact, which had less effect on the impact conditions. Figure 6.6 illustrates this with an example. In the figure, the shoulder external rotation was shown for two different simulations using the parameters from the first and second optimisation. It can easily be seen that the second simulation deviates from the actual performance data much more than the first simulation during the first 120 ms; it then starts to follow the actual data and, especially for the last 40 ms, it matches performance data quite satisfactorily with less deviation at impact.

Table 6.5. A comparison of the optimisation results for pre-impact phase

joint movement	RMS for last 50 ms (deg)		deviation at impact from actual (deg)	
	opt1	opt2	opt1	opt2
shoulder flex/ext	1.10	0.73	2.45	1.74
shoulder abd/add	0.67	0.46	1.68	1.06
shoulder int/ext rot.	0.53	0.32	0.88	0.50
elbow flex/ext	0.41	0.20	0.34	0.21
pron/sup	0.15	0.06	0.25	0.18
wrist flex/ext	0.21	0.15	0.08	0.04
rad/ulnar dev.	0.41	0.23	0.72	0.02
racket ori. 1st rot	0.18	0.22	0.25	0.66
racket ori. 2nd rot.	1.38	0.76	1.84	0.37
racket ori. 3rd rot.	0.68	0.11	0.56	0.02
overall RMS score	0.69	0.40	1.19	0.71

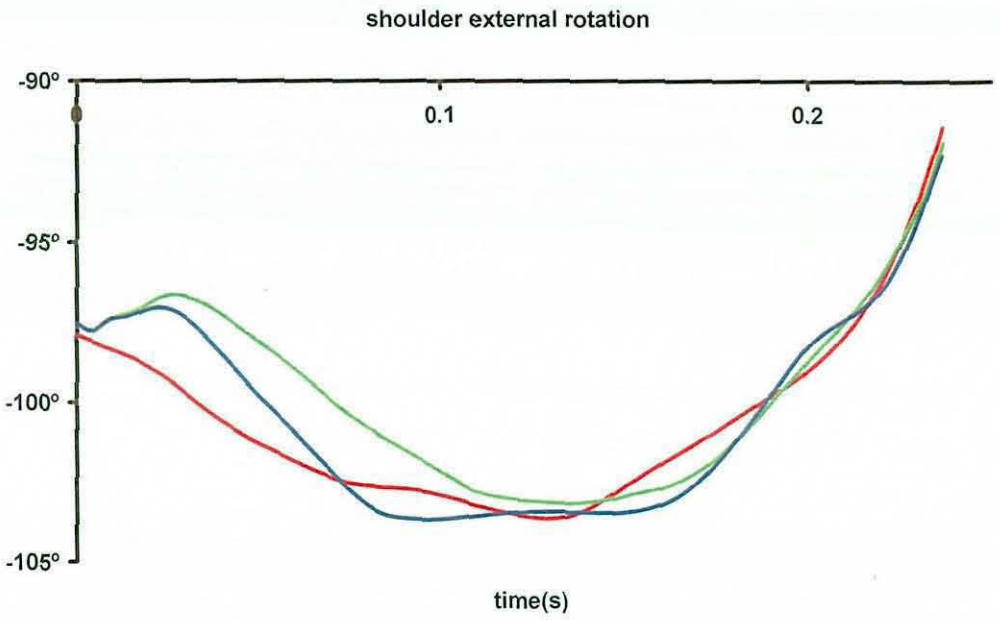

Figure 6.6. A comparison of shoulder external rotation angle obtained from the two optimisation results (*blue first; green second*) and *actual performance (red)*. The simulation ended at impact.

Considering the optimisation results in Table 6.5 and visually inspecting the joint angle graphs, it was decided to use the results of the second optimisation. Table 6.6 lists the parameter values of the second optimisation. Following Table 6.6., Figures 6.7-6.9 show the joint and racket angles from a simulation run by using these values.

Table 6.6. The optimised values of the pre-impact parameters. Refer to Table 6.1-6.3 for the definition of the parameters.

joint mov. / grip torque	$te_1/tf_1/th_1$	$de_1/df_1/dh_1$	$le_1/lf_1/lh_1$	$le_2/lf_2/lh_2$	te_2	de_2
s. flex.	0.14	0.02	0.69	1.00	-	-
s. ext.	0.19	0.06	0.36	0.47	-	-
s. abd	-0.06	0.10	0.41	0.73	-	-
s. add	-0.06	0.11	0.32	0.09	-	-
s. int. rot.	0.05	0.09	0.56	0.31	-	-
s. ext. rot	-0.05	0.13	0.46	0.99	-	-
e. ext	0.02	0.21	0.70	0.93	-	-
e. flex.	0.07	0.20	0.27	0.07	-	-
pron.	-0.02	0.11	0.97	0.15	-	-
sup.	0.03	0.20	0.30	0.61	-	-
w. flex.	0.02	0.15	0.31	1.00	0.16	0.16
w. ext.	-0.03	0.08	0.25	0.99	0.17	0.18
rad. dev.	0.03	0.05	0.37	0.66	0.10	0.24
uln.dev.	0.06	0.02	0.24	0.74	-	-
gr. 1^{st} com.	-0.01	0.02	0.23	0.06	-	-
gr. 2^{nd} com.	0.00	0.06	-7.00	2.28	-	-
gr. 3^{rd} com.	-0.02	0.18	5.14	-4.04	-	-

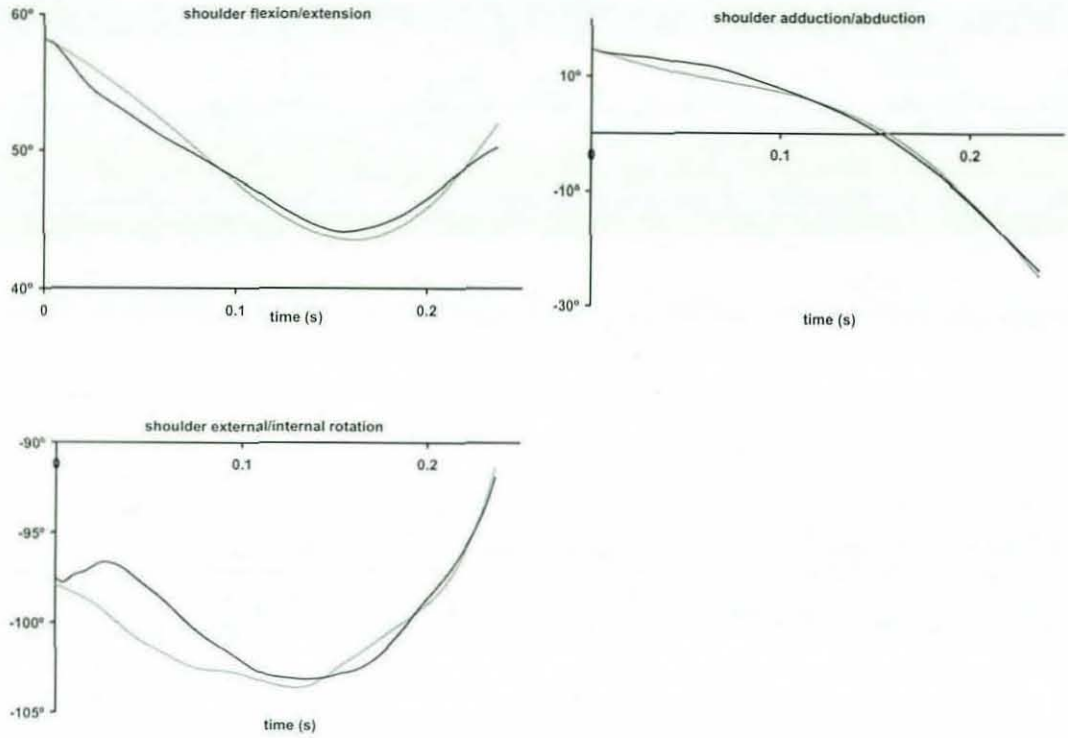

Figure 6.7. Shoulder joint angles with optimised pre-impact parameters: simulation result (black) and actual performance (grey)

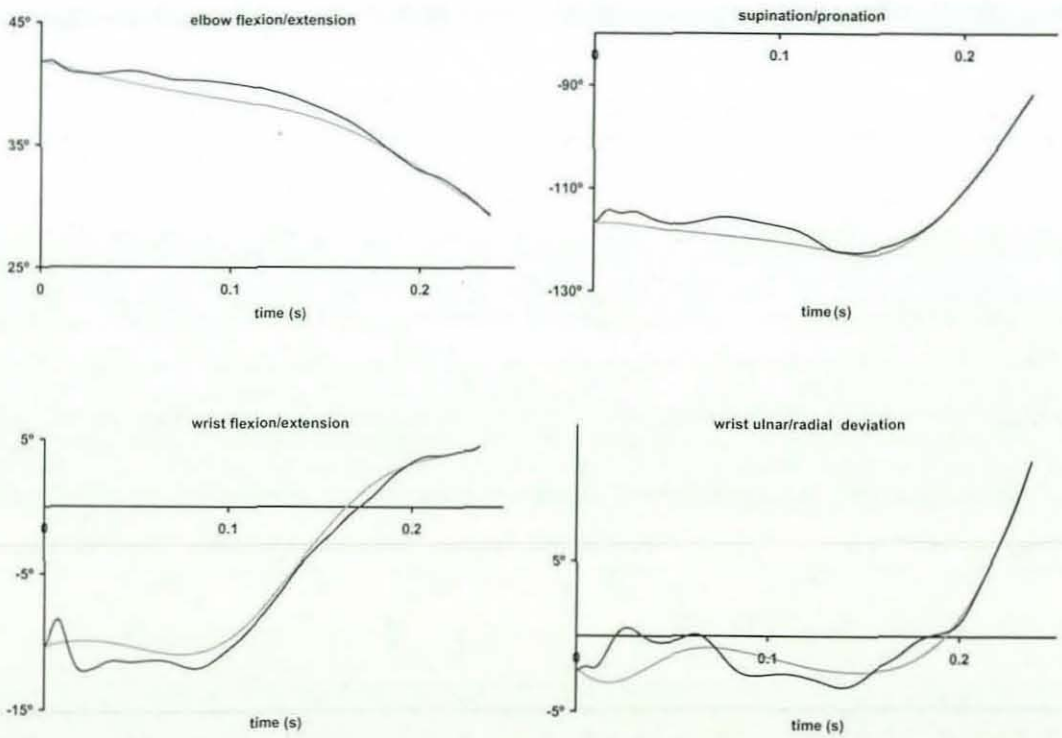

Figure 6.8. Elbow and wrist joint angles with optimised pre-impact parameters: simulation result (black) and actual performance (grey)

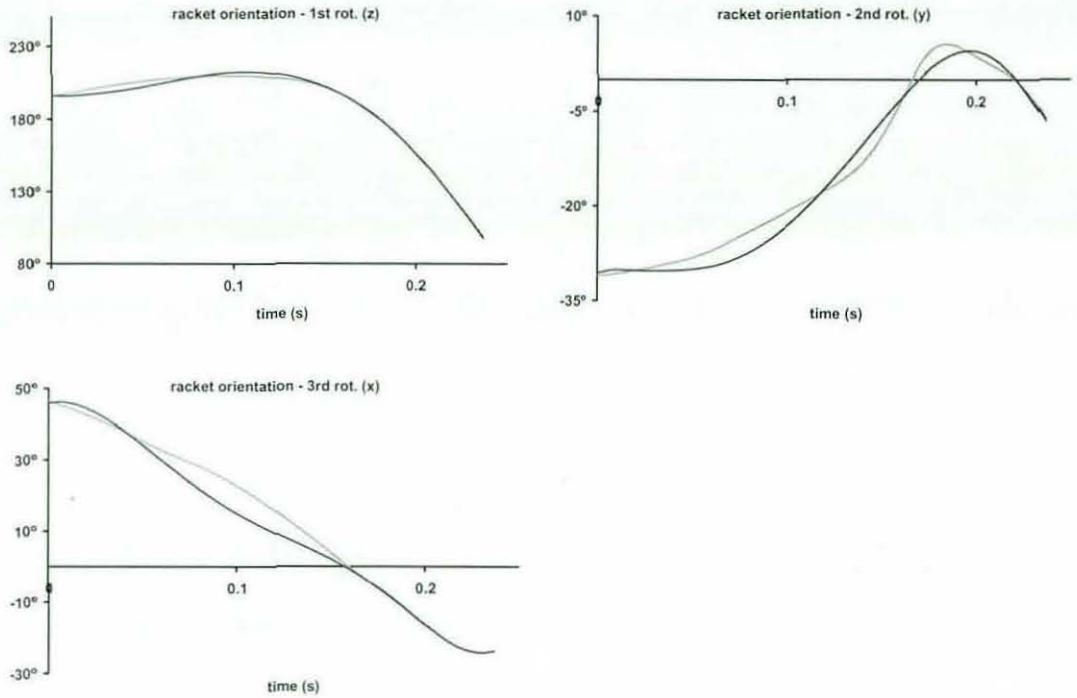

Figure 6.9. Orientation angles of the racket with optimised pre-impact parameters: simulation result (black) and actual performance (grey)

Apart from shoulder flexion/extension, all the angles had excellent matches for the last 30-40 ms before impact. Although maximum shoulder flexion activation was used in the simulation before impact ($le_2 = 1$) it was obvious from the graph that there was not sufficient flexor torque to reach the flexion angle at impact. The reason for this might be that the subject did not exert full power during the strength measurements due to a minor injury of his shoulder.

To follow the motion of the arm and racket easily, still images from the simulation are presented in Figure 6.10 with 40 ms intervals until impact.

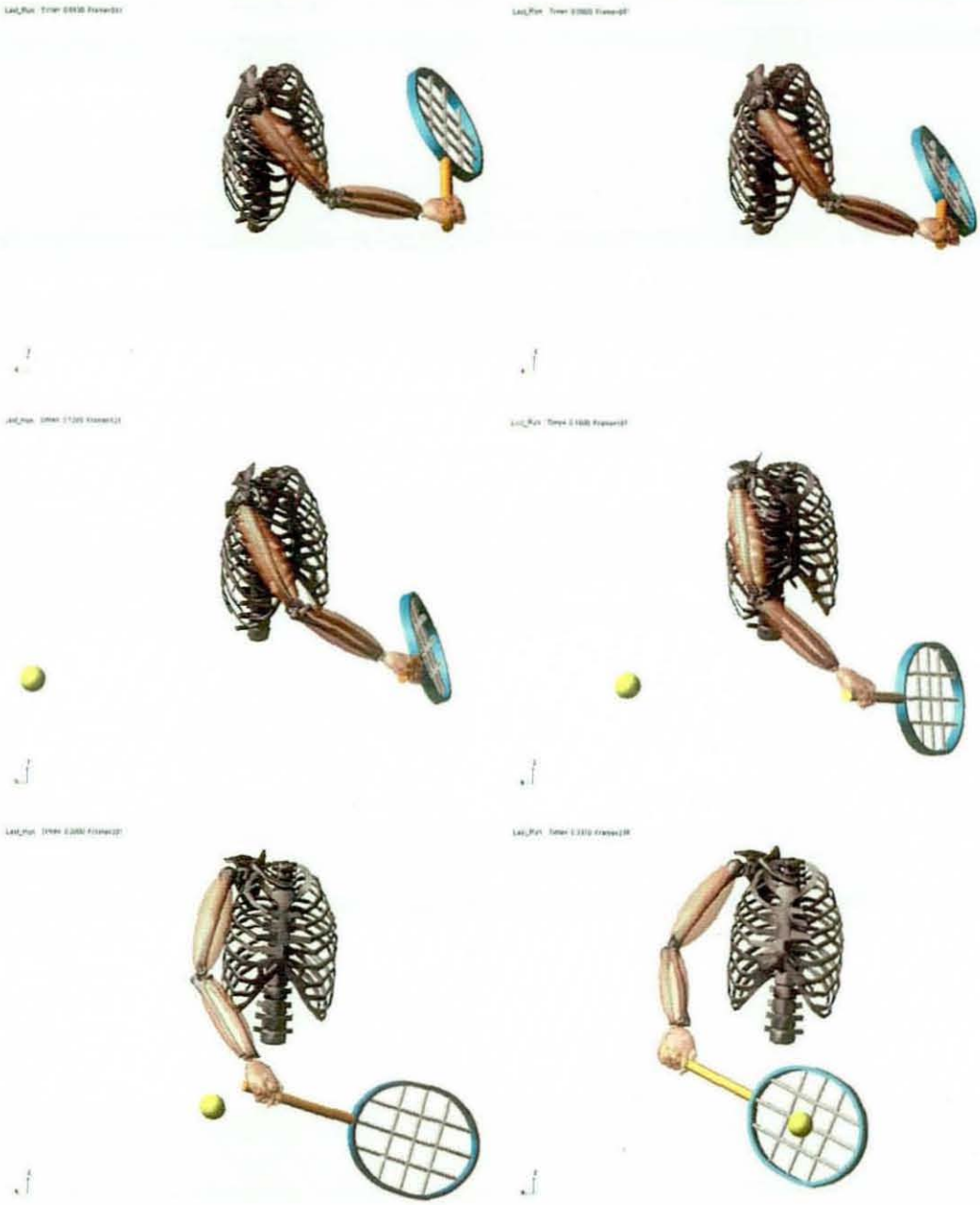

Figure 6.10. Still images from the simulation with optimised pre-impact parameters. There is a 40 ms time difference between each picture.

6.3.2 The results of the Post-impact Phase Matching

The post-impact phase was the main phase of the simulation where the effect of the impact was seen on the kinetics and the kinematics of the arm and racket. To analyse these variables in different conditions (e.g. different string preload, stiffness/damping values) without re-optimising the pre-impact parameters, it was necessary to start the simulation from the impact. Otherwise, if the simulation starts from pre-impact, either incorrect impact conditions would be obtained using the

optimised pre-impact parameters or the pre-impact parameters have to be re-optimised for the new configuration of the model. To avoid re-optimising for every single change in the model, it was decided to start the simulation from impact using the impact conditions obtained from the simulation of the pre-impact phase as initial conditions. Therefore, the post-impact parameters were optimised for the simulations starting from impact and used for further analysis.

The end time of the post-impact phase was arbitrarily selected as 0.3 seconds from the start of the pre-impact phase. This made their post-impact period for the trial used in the optimisations 63 ms. A total of 40 parameters (12 at the shoulder + 8 at the elbow + 8 at the wrist + 12 at the hand/racket) were optimised in the post-impact phase.

A comparison of the optimisation results obtained from the simulations starting from pre-impact (whole swing) and starting from impact (impact onwards) are shown in Table 6.7.

Table 6.7. A comparison of the optimisation results obtained from the whole swing backhand and from impact onwards

joint movement	RMS (deg)		RMS between optimisations (deg)
	whole swing	impact onwards	
shoulder flex/ext	5.77	6.78	1.09
shoulder abd/add	1.16	1.10	0.19
shoulder int/ext rot.	2.94	2.72	0.41
elbow flex/ext	1.20	0.92	0.94
pron/sup	2.53	1.22	2.13
wrist flex/ext	0.94	0.93	0.86
rad/ulnar dev.	1.79	1.57	1.97
racket ori. 1st rot	4.27	1.44	3.52
racket ori. 2nd rot.	1.45	1.22	1.25
racket ori. 3rd rot.	3.52	4.00	0.50
overall RMS score	2.97	2.82	1.60

Although the overall score for the two optimisations (2.97° and 2.83° for whole swing and impact onwards, respectively) are close to each other, some differences for racket orientation first rotation, pronation/supination and radial/ulnar deviation were observed between the two optimisation results. However, the general shapes of the angle curves for both optimisations were similar for all movements including the ones with higher RMS values. The movements with the highest three RMS values are presented in Figure 6.11.

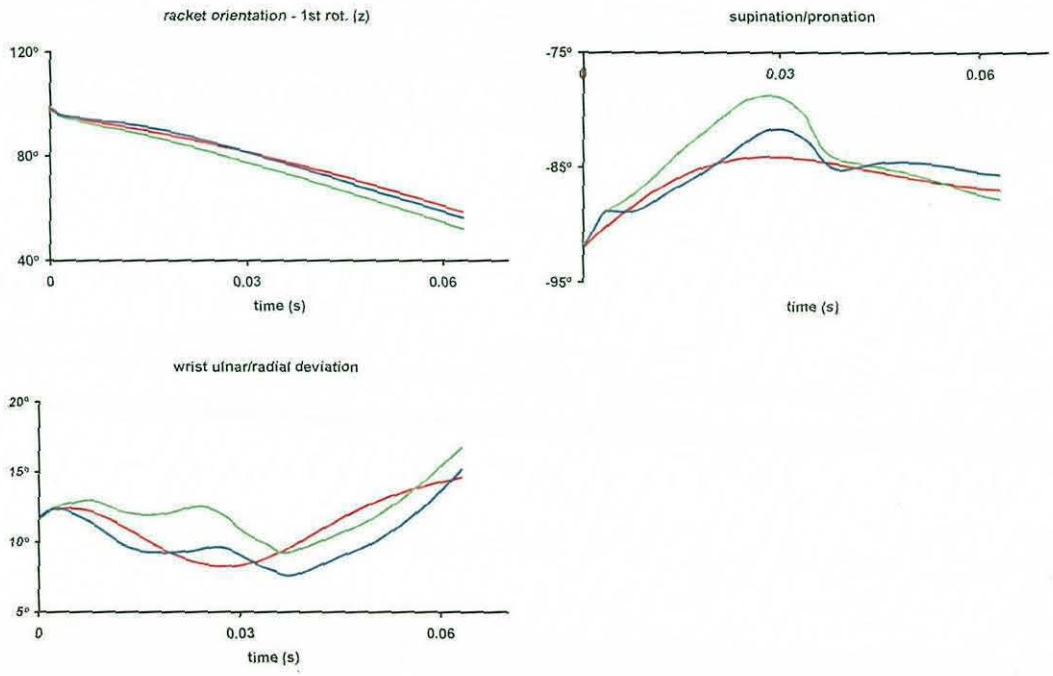

Figure 6.11. *Comparison of* the angles with the highest RMS difference between the optimisations starting from the whole swing backhand (green) and from impact onwards (blue) with the actual performance (red)

It is seen from the figures that although the angle curves are slightly different, they have the same characteristics. However, the smaller RMS values for 8 out of 10 movements made optimisation using the post-impact simulations favourable. Because of the reasons mentioned earlier, the simulations starting from impact were selected for use in further analyses. The result of the comparison of the two optimisations supported this decision.

The optimised values of the post-impact parameters are listed in Table 6.8 and the joint and racket angles obtained by using these parameters are shown in Figures 6.12-6.14.

Table 6.8. The optimised values of the post-impact parameters. Refer to Table 6.1-6.3 for the definition of the parameters.

joint mov.	te_2/tf_2*	de_2/df_2*	joint mov.	te_2/tf_2*	de_2/df_2*
s. flex.	0.24	0.07	s. ext.	0.24	0.04
s. abd	0.27	0.07	s.add	0.29	0.08
s. int. rot.	0.28	0.14	s. ext.rot	0.29	0.08
e. ext	0.26	0.07	e. flex.	0.24	0.08
pron.	0.28	0.10	sup.	0.25	0.07
w. flex.*	0.24	0.06	w. ext.*	0.26	0.05
rad. dev.*	0.28	0.09	uln.dev.	0.24	0.04
grip torque	**th_2**	**dh_2**	**k_t**	**c_t**	
gr. 1st com.	0.27	0.13	82.52	3.25	
gr. 2nd com.	0.28	0.14	348.18	1.50	
gr. 3rd com.	0.27	0.26	44.05	4.53	

* The parameters te_3 and de_3 were listed for wrist flexion, wrist extension and radial deviation. te_2 and de_2 were already used in pre-impact phase.

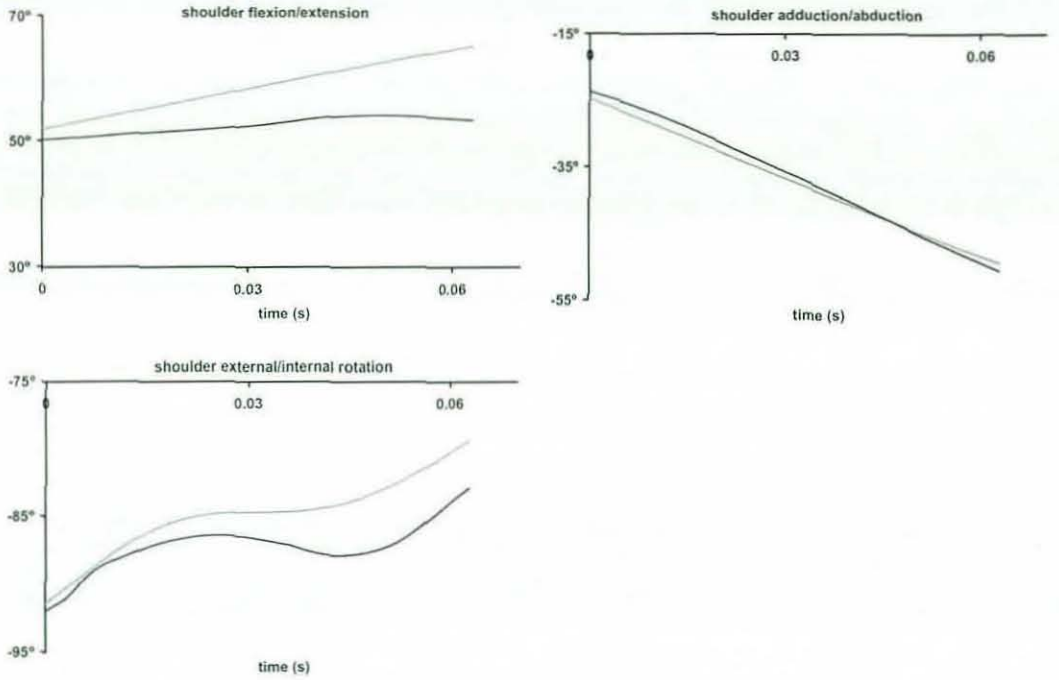

Figure 6.12. Shoulder joint angles with optimised post-impact parameters: simulation result (black) and actual performance (grey)

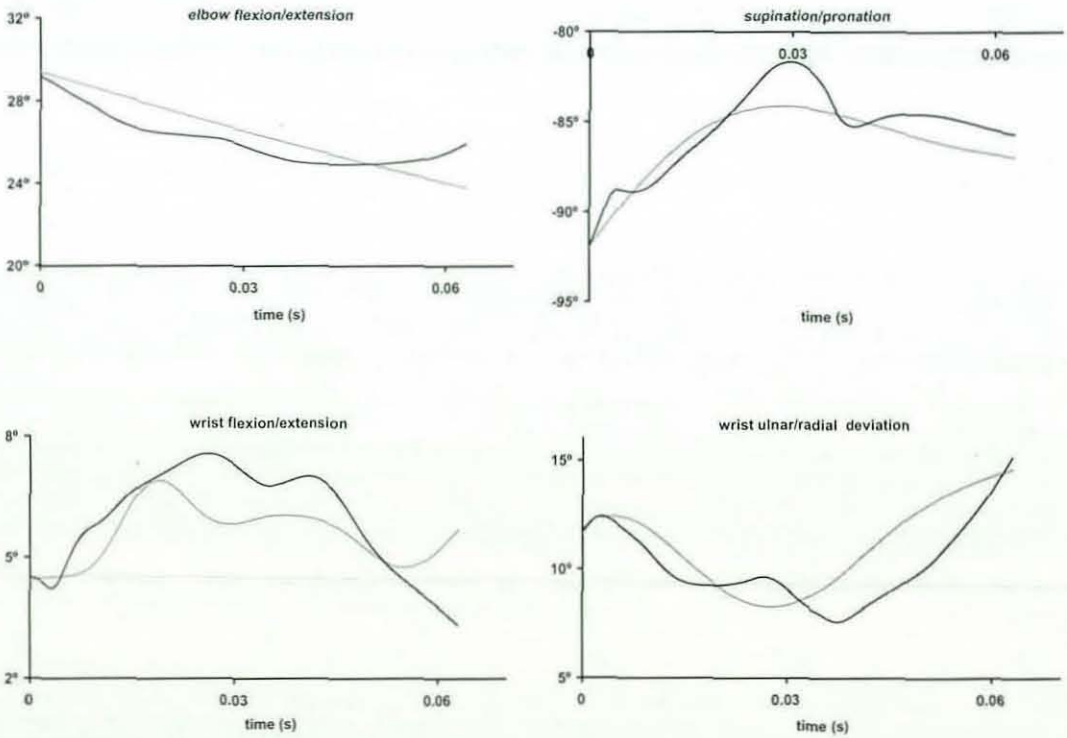

Figure 6.13. Elbow and wrist joint angles with optimised post-impact parameters: simulation result (black) and actual performance (grey)

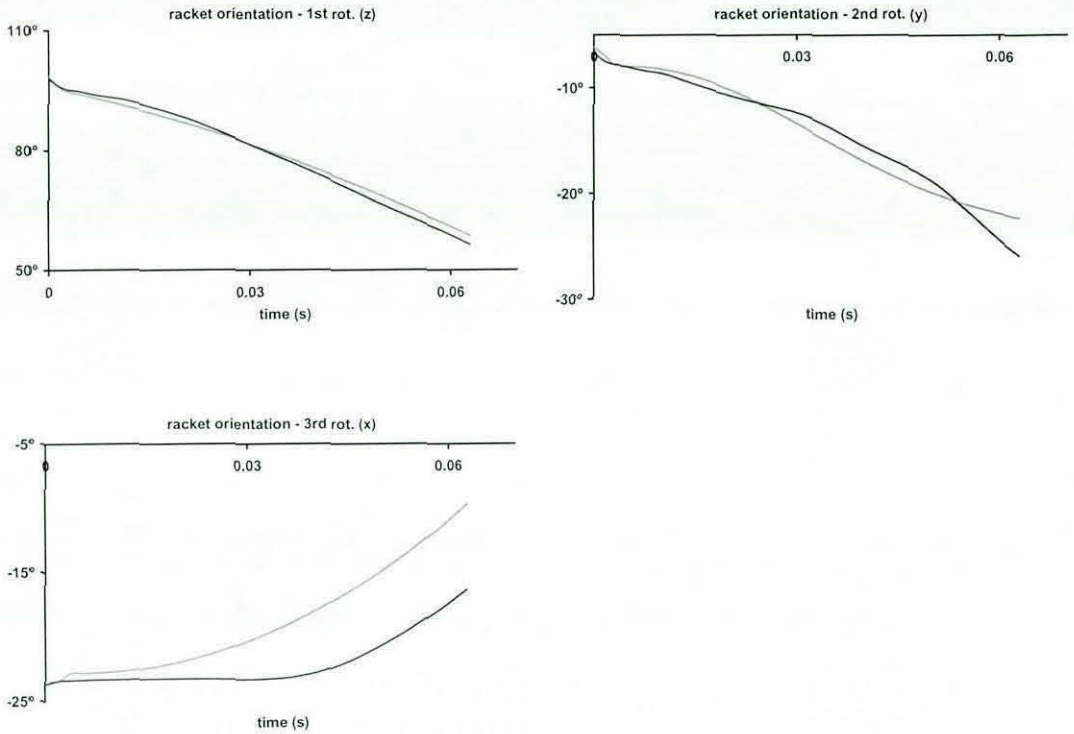

Figure 6.14. Orientation angles of the racket with optimised post-impact parameters: simulation result (black) and actual performance (grey)

Apart from the shoulder flexion/extension angle and 3rd rotation for the racket orientation, all angles matched the actual performance. The inadequateness of shoulder flexor torque at the end of the pre-impact phase was also observed in the post-impact phase. The maximum voluntary shoulder flexor torque obtained from the torque-strength parameters was not sufficient to flex the arm. A possible reason is that a shoulder injury did not allow the subject to exert full torque during the strength test.

The 3rd rotation of the racket orientation corresponds to the rotation around the axis normal to the racket head plane. The deviation of the simulation result from the actual performance might be because the player may exert additional torque around the normal axis during the forward swing of the racket after hitting the ball with topspin.

The still images of the simulation starting from impact can be seen in Figure 6.15 with 10 ms intervals for a 50 ms period.

Considering the joint and racket angles (Figure 6.12-6.14) and overall score of the optimisation, the model was evaluated satisfactorily for the tennis backhand strokes with centre impacts. However, it should also simulate the off-centre impacts

realistically. In the following section, the behaviour of the simulation model during off-centre impacts will be considered.

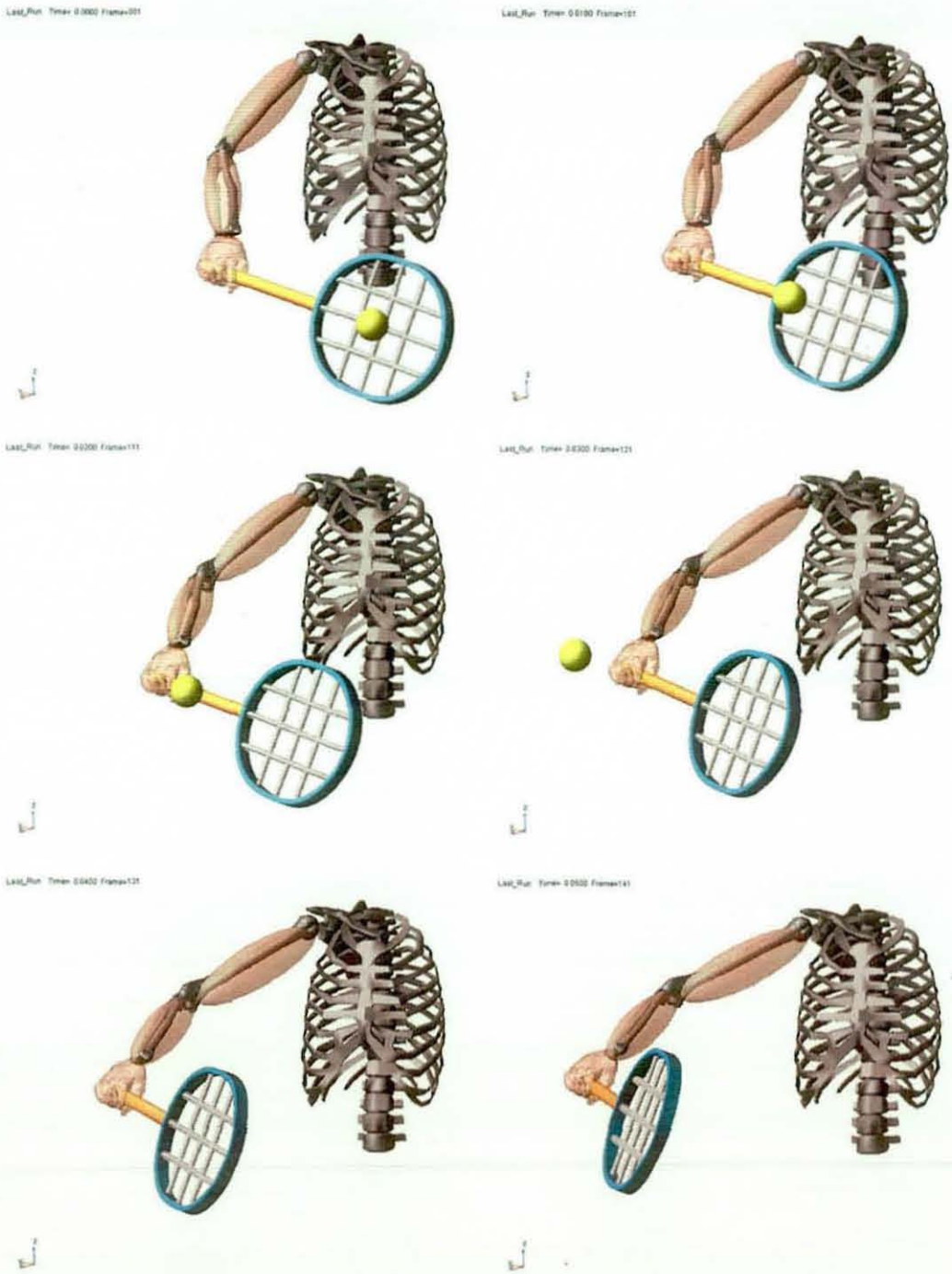

Figure 6.15. Still images from the simulation with optimised post-impact parameters. There is a 10 ms time difference between each picture.

6.4 Simulation of Off-centre Impacts

Overview

The parameters optimised in the previous section were obtained for a tennis backhand trial where the ball contacted the centre of the stringbed. However, the location of the impact is one of the key factors that determine the racket and arm kinematics and kinetics. Although the model was evaluated for centre impacts in the previous section, it should satisfactorily simulate backhand strokes with off-centre impacts as well as the strokes with centre impacts. Therefore, the results of an off-centre impact simulation were compared with the results of actual performance data with an off-centre impact (Section 4.2).

The major effects of the off-centre impacts can be observed within the first 40 ms after impact (Glynn, 2007). They are unlikely to a make change in muscle activations within this period since average premotor reaction time, the time from the presentation of a stimulus until the start of muscle activation, is well over 150 ms (Lewis and Brown, 1994; Flament et al., 1999; de Rugy and Sternad, 2003). Therefore, it was assumed that the players do not change their technique after impact in response to the impact location.

The optimised post-impact parameters (Section 6.3.2) were used in the off-centre impact simulations, assuming no change in technique and grip tightness. After comparing the simulation results with the results of an actual off-centre trial, some substantial differences were observed. Consequently, the post-impact parameters were re-optimised to obtain a good match for both centre and off-centre impact trials with a single parameter set. After re-optimisation, the computer simulation model developed was used to analyse the effects of off-centre impacts.

The following section describes the procedure that was used to find satisfactory results for off-centre impacts in detail.

Comparison of the off-centre impact simulation and actual performance results

The results (joint and racket angles) of an off-centre impact simulation were compared to an actual performance with an off-centre impact. Although the compared results belonged to different trials (a centre impact trial simulation perturbed to have an off-centre impact and an actual off-centre trial), it was expected to have similar results and characteristics since the inbound ball velocity and

kinematic conditions at impact were similar in both cases. In addition, both trials were performed at the same data collection using the same equipment. However, a substantial difference was found for the two most critical angles affected by the off-centre impact, i.e. wrist flexion angle and the rotation of the racket around its longitudinal axis with respect to hand the reference frame after impact (Figure 6.16).

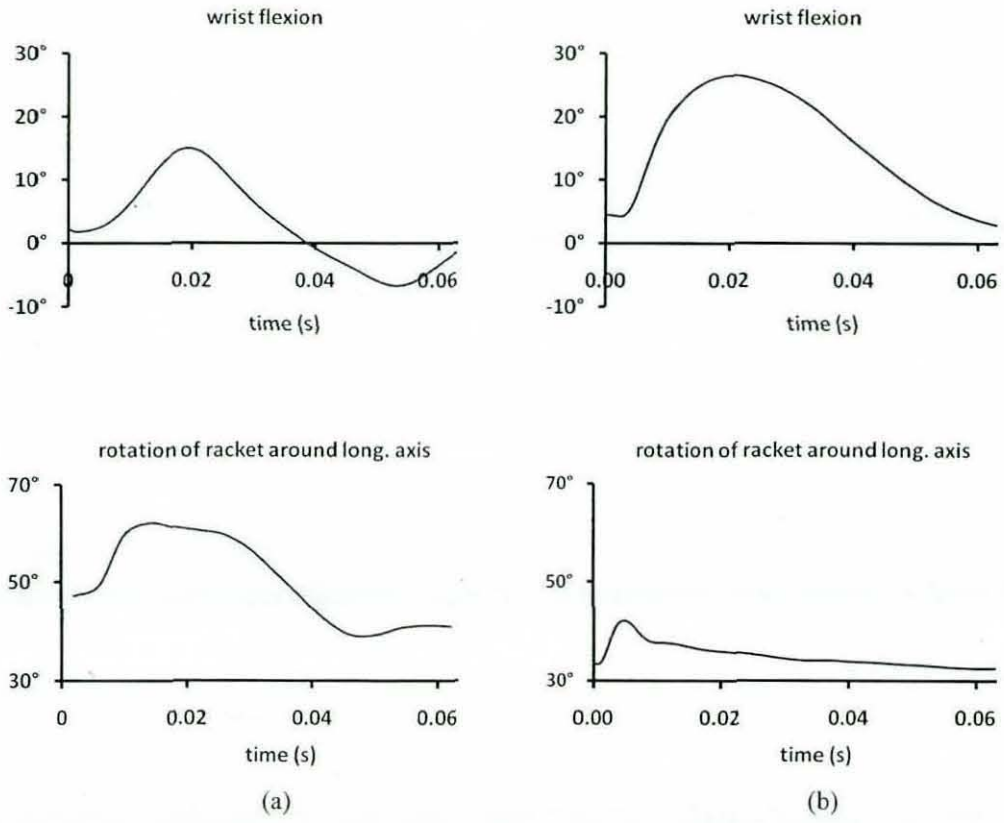

Figure 6.16. A comparison of two different angles from the actual performance (a) and the off-centre impact simulation (b).

The excess wrist flexion and relatively small rotation of the racket around its longitudinal axis with respect to the hand showed that the gripping torque determined by torsional springs was too high in the simulation because of high stiffness values. Therefore, the racket was unable to rotate within the hand as much as it did in the performance and the initial rotation of the racket directly transferred to the wrist causing excess flexion at the wrist. The stiffness values should therefore be decreased to allow the racket to rotate more realistically within the hand. This high stiffness condition was not detected for centre impact simulations since the racket does not rotate (or rotates very little) within the hand in this case.

Re-optimisation of the post-impact parameters

To overcome the high stiffness problem, re-optimisation of the post-impact parameters with smaller stiffness values was necessary. The same set of parameters were used for both centre and off-centre impact simulations. This was due to the assumption that the players do not change technique according to the impact point. Therefore, it was easier to compare centre and off-centre impacts since the only perturbation to the system was the ball impact location.

The two impact conditions should be optimised simultaneously to obtain a satisfactory match for each of them. However, the off-centre impact simulation could only be compared with the actual data subjectively by comparing the range of motion and curve characteristics since the trials were not the same. Therefore, it was not practical to put the off-centre impact results into the objective score function. Without having any terms related to off-centre impact in the objective score, the re-optimisation process was carried out iteratively.

First, a satisfactory match for off-centre impacts was obtained with previously optimised post-impact parameters except stiffness and damping coefficients of the torsional springs representing the grip torque. By trial and error, realistic bounds for the stiffness and damping coefficients of the torsional springs were obtained from off-centre impact simulations. These relatively narrow realistic bounds were used to determine upper and lower bounds of the viscoelastic parameters during the re-optimisation. The post-impact parameters were re-optimised considering only the centre impact. However, while searching for a better match for centre impact, the simulation was forced to keep off-centre impact characteristics using the small intervals determined for the viscoelastic parameters. Apart from the viscoelastic parameters, the upper and lower bounds of the remaining parameters used previously were not changed. After the re-optimisation process, an off-centre simulation using re-optimised parameters was compared with the actual performance. Since satisfactory results were obtained, no adjustments to the interval for the viscoelastic parameters were necessary.

Re-optimisation results

The re-optimised parameters affected the performance of the centre impact simulation. The overall score for centre impact after re-optimisation was found to be 3.56° (2.83° previously) due to the simulation being forced to have lower viscoelastic

parameters. In contrast, the off-centre impact results improved considerably. Therefore, a post-impact parameter set was obtained from the re-optimisation process compromising the results of both centre and off-centre impact simulations.

In order to improve the overall score and to obtain better matches, different torsional spring equations to Equation 3.8.b, for example, torque proportional to the cubic angular displacement, were tried. However, similar results were obtained and no substantial improvement was observed.

The re-optimised values of the post-impact parameters are listed in Table 6.9 and some of the critical joint and racket angles for off-centre impact obtained by using these parameters are shown in Figure 6.17.

Table 6.9. The optimised values of the post-impact parameters. Refer to Table 6.1-6.3 for the definition of the parameters.

joint mov.	te_2/tf_2*	de_2/df_2*	joint mov.	te_2/tf_2*	de_2/df_2*
s. flex.	0.24	0.07	s. ext.	0.24	0.06
s. abd	0.29	0.05	s.add	0.27	0.09
s. int. rot.	0.24	0.11	s. ext.rot	0.29	0.08
e. ext	0.29	0.08	e. flex.	0.24	0.10
pron.	0.24	0.06	sup.	0.27	0.07
w. flex.*	0.25	0.07	w. ext.*	0.26	0.06
rad. dev.*	0.27	0.02	uln.dev.	0.24	0.05
grip torque	th_2	dh_2	k_t	c_t	
gr. 1st com.	0.28	0.18	15.87	0.86	
gr. 2nd com.	0.30	0.16	13.19	13.57	
gr. 3rd com.	0.28	0.30	4.68	0.25	

* The parameters te_3 and de_3 were listed for wrist flexion, wrist extension and radial deviation. te_2 and de_2 were already used in pre-impact phase.

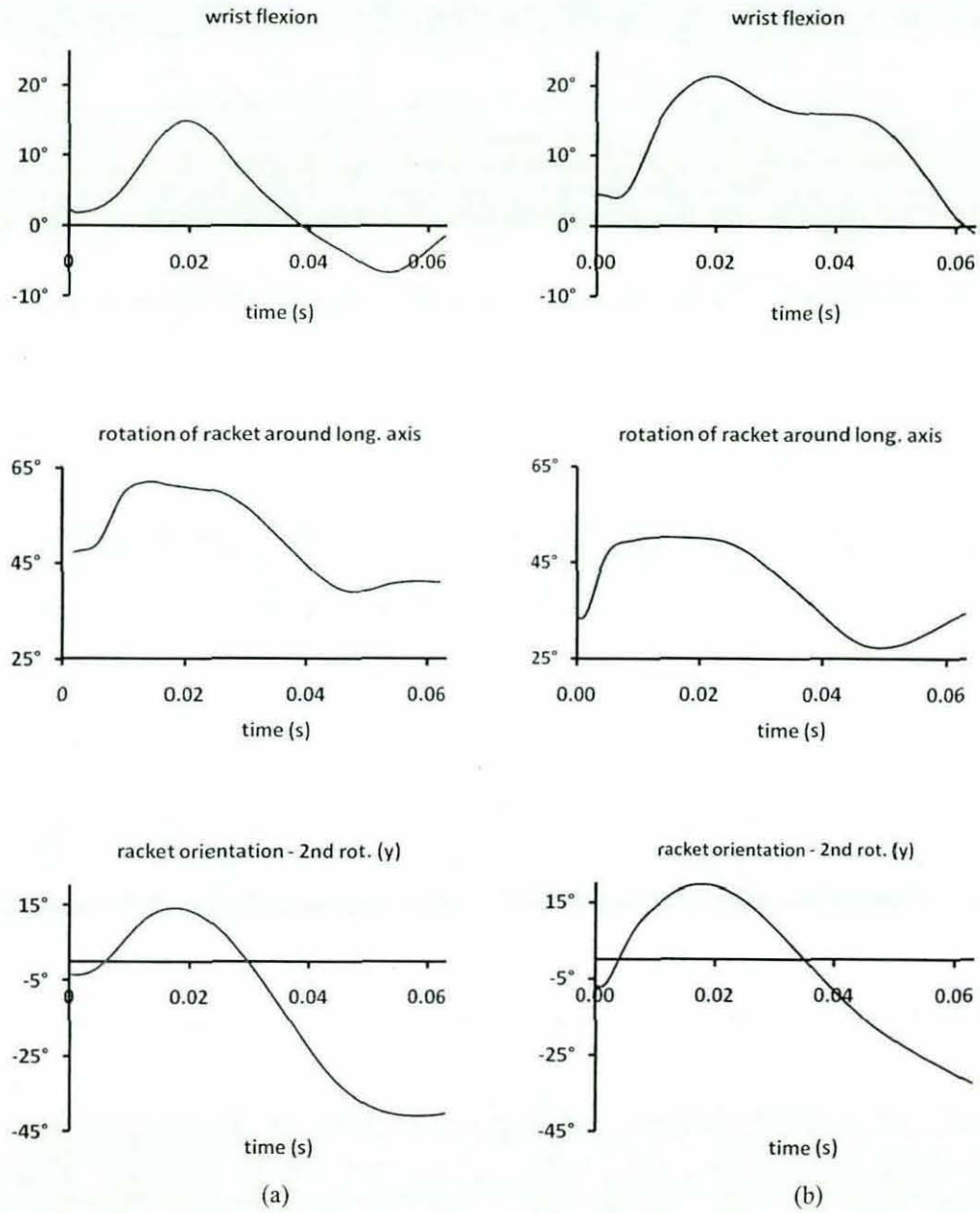

Figure 6.17. A comparison of three different angles from the actual performance (a) and the off-centre impact simulation (b).

When the off-centre simulation results before (Figure 6.16) and after the re-optimisation (Figure 6.17) were compared, it was clear that after re-optimisation the results became more similar to the actual performance data. Especially, the rotation of the racket around its longitudinal axis within the hand with respect to the hand frame improved considerably. Although the initial value was different from the actual data, the characteristics of the curve and the range of motion were very similar. The global orientation of the racket corresponding to the rotation of the

racket around its longitudinal axis for both cases was also similar. The wrist flexion angle of the simulation was larger than the expected values. However, when compared to the results of the simulation before re-optimisation, there was substantial improvement. The maximum wrist flexion angles of the both cases were comparable after the re-optimisation. One should keep in mind that the simulation of the off-centre impact and the actual off-centre impact data belonged to different trials and therefore only the characteristic of the curves and reliability of the model in off-centre impacts were considered during the comparisons.

The joint and racket angles for centre impact simulations using re-optimised post-impact parameters are presented in Figures 6.18-6.20. When compared with the previous results of centre impact simulations (Figure 6.12-6.14) it was seen that previous results were closer to the actual performance. However, the substantial improvement of the off-centre impact simulation encouraged the use of re-optimised parameters despite having a greater objective score for centre impact simulation.

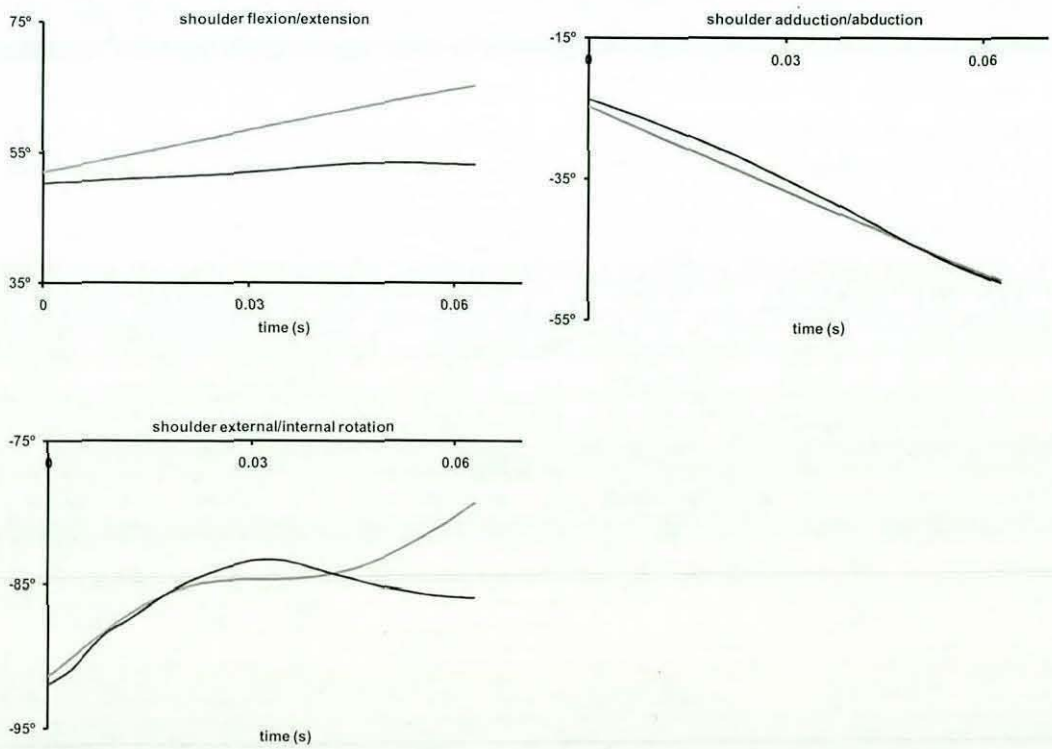

Figure 6.18. Shoulder joint angles with re-optimised post-impact parameters: simulation result (black) and actual performance (grey)

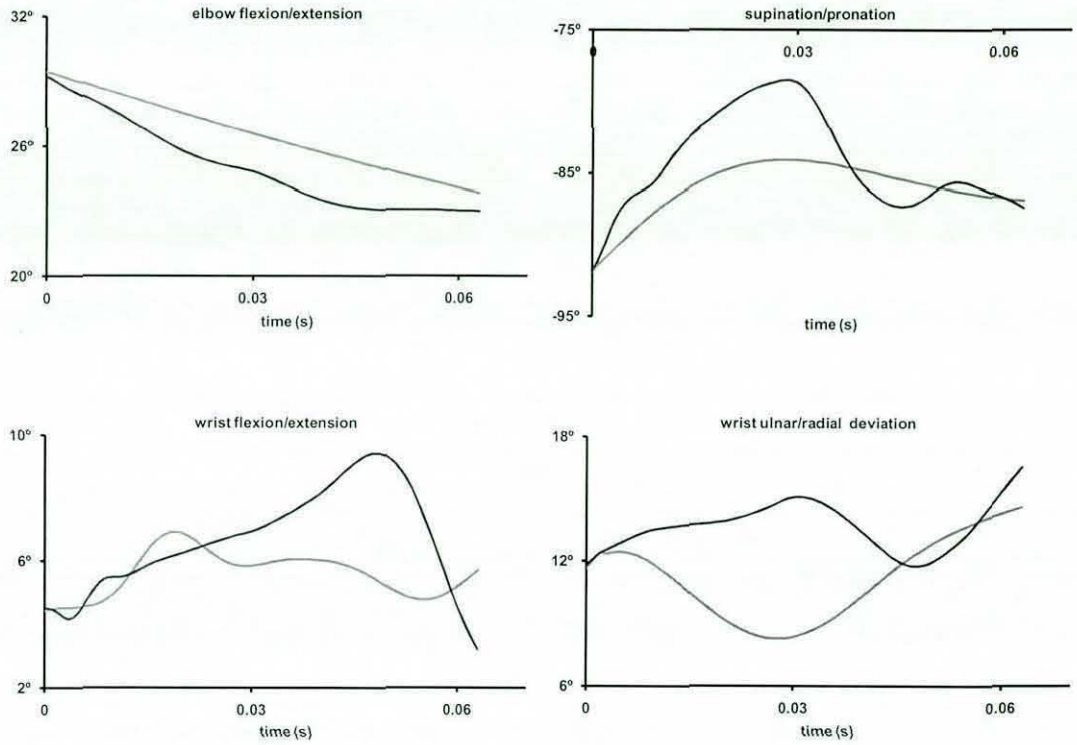

Figure 6.19. Elbow and wrist joint angles with optimised post-impact parameters: simulation result (black) and actual performance (grey)

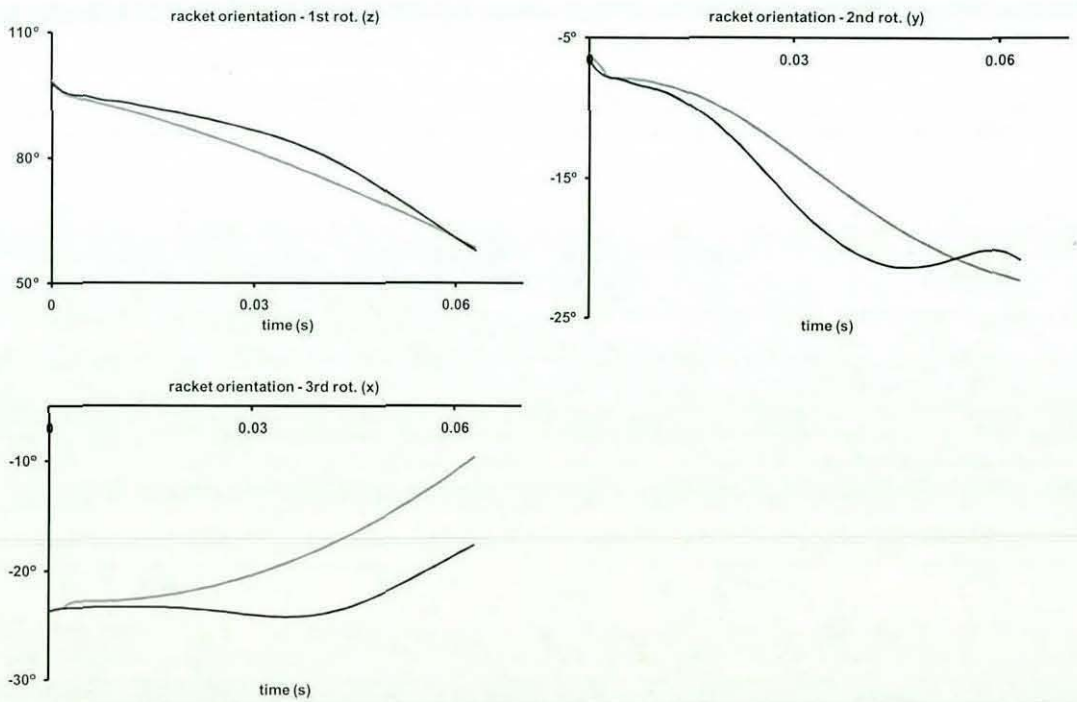

Figure 6.20. Orientation angles of the racket with optimised post-impact parameters: simulation result (black) and actual performance (grey)

6.5 Comparison of Model Variables

6.5.1 Comparison of Joint / Gripping Torques

The maximum joint torques applied to the system by the torque generators were calculated using the torque-strength parameters of the subject. Since these parameters were optimised directly from the strength measurements of the subject with an isokinetic dynamometer, the model was restricted to using realistic joint torque.

In the literature, most of the research has focused on the kinematics of the arm and racket. There are not many examples including kinetic variables. One of them, McLaughlin and Miller (1980) calculated the pronator/supinator, radial/ulnar deviation and wrist flexor/extensor torques during backhand groundstrokes in their study. For a 50 ms period before impact, they found pronator/supinator torque and wrist flexor/extensor torque not greater than 5 Nm. For the radial/ulnar deviation torque, a maximum of 13 Nm was found (McLaughlin and Miller, 1980). The simulation model with optimised pre-impact parameters gave similar results to the findings of McLaughlin and Miller (1980). The maximum torques were less than 4 Nm for pronator/supinator torque and wrist flexion/extension torque. The radial/ulnar deviation torque had a maximum of 7 Nm.

Glynn (2007) calculated the gripping torque about the racket axes at the centre of the handle for 50 ms after impact. The maximum torque values around the longitudinal, transverse and frontal axes were approximately 2 Nm, 7 Nm and 10 Nm, respectively (Glynn, 2007). The magnitudes of the torques from the simulation model using optimised post-impact parameters (1.5 Nm, 6 Nm and 7 Nm, respectively) were comparable to those stated by Glynn (2007).

6.5.2 Comparison of Contact Period and Outbound Velocity

The duration of the impact and outbound velocity were measured during the performance data collection (Table 4.2). The simulation results were then compared to actual values (Table 6.10).

Table 6.10. A comparison of the ball outbound velocity and contact period measured from the actual performance of a backhand stroke and obtained from the computer simulation

source	V_{out}^{y} (m/s)	V_{out}^{z} (m/s)	contact period (ms)
actual performance	30.94	6.19	4.0
simulation result	26.96	6.23	4.1

The contact period and outbound velocity in the vertical direction (z) were matched very successfully. However, there was a slight difference in the forward direction (y). It should be noted that during the measurement of the actual performance it was assumed that the outbound velocity in the side direction (x) was zero. In the simulation model, it was measured as 2.54 m/s.

6.6 Summary

The simulation model developed in previous chapters has been successfully evaluated in this chapter. The evaluation methods were described in detail. It has been showed that there is a good agreement between the simulation results and actual performance before and after impact. The behaviour of the model while simulating off-centre impact has analysed and to improve the model for both centre and off-centre impact simulations, post-impact parameters were re-optimised. Although re-optimisation did not improve the results of the centre impact simulations, substantial improvement for off-centre impact simulations was obtained. Some of the kinetic variables were also compared with the results found in the literature and no substantial differences were observed. Lastly, the successful matching of the outbound velocity of the ball and contact period with the actual performance data added more reliability to the simulation model. In the following chapter, a sensitivity analysis of the model and further analyses will be presented.

7 OFF-CENTRE IMPACTS AND SENSITIVITY ANALYSIS

7.1 Introduction

This chapter focuses on the perturbations of different variables of the computer simulation model evaluated in the previous chapter. These variables include impact location, configuration of the arm at impact, racket frame inertia and stiffness, stringbed tension, inbound ball velocity, and wobbling mass stiffness and damping. The effects of these variables on loadings at the wrist and elbow will be presented since the main cause of the elbow injuries (particularly 'tennis elbow') is the overload of associated muscle groups (Kibler, 2002).

7.2 Perturbation of Impact Location

The location of the impact has a direct influence on the joint internal forces and torques as well as the joint kinematics. Hennig et al. (1992) stated off-centre impacts resulted in an increased loading on the arm by approximately three times. Glynn (2007) compared the effects of different variables such as stringbed tension, racket frame inertia and stiffness on elbow loading and found, that among all variables, impact location affected the loading at the elbow most. Therefore, the location of the impact is one of the key issues to be discussed when considering the loading at the elbow and wrist during a backhand stroke.

To analyse the effects of the impact location, single simulations were run with the same initial conditions for the player and the ball as in the centre impact simulation i.e. the ball inbound velocity, the configuration of the arm and the hitting technique were kept unchanged. The point masses on the stringbed determine the impact locations (Figure 7.1). Therefore, the results of eight different simulations corresponding to an impact at each point mass around the centre were investigated.

The rotation of the racket around its longitudinal axis in the global reference frame showed how the racket behaved with respect to different impact locations (Figure 7.2). The impact location had little effect on the rotations of the racket around the normal and transverse axes.

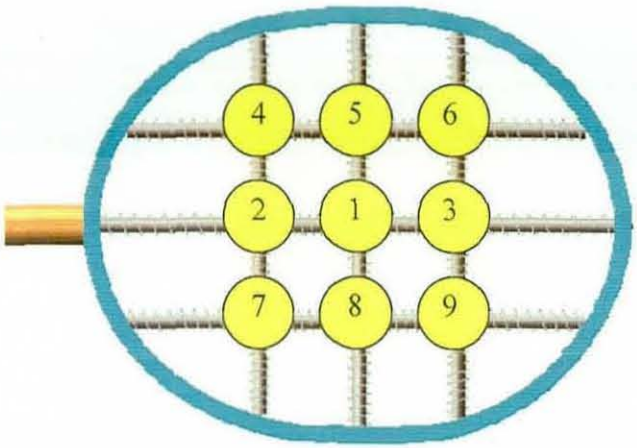

Figure 7.1. The impact locations on the stringbed

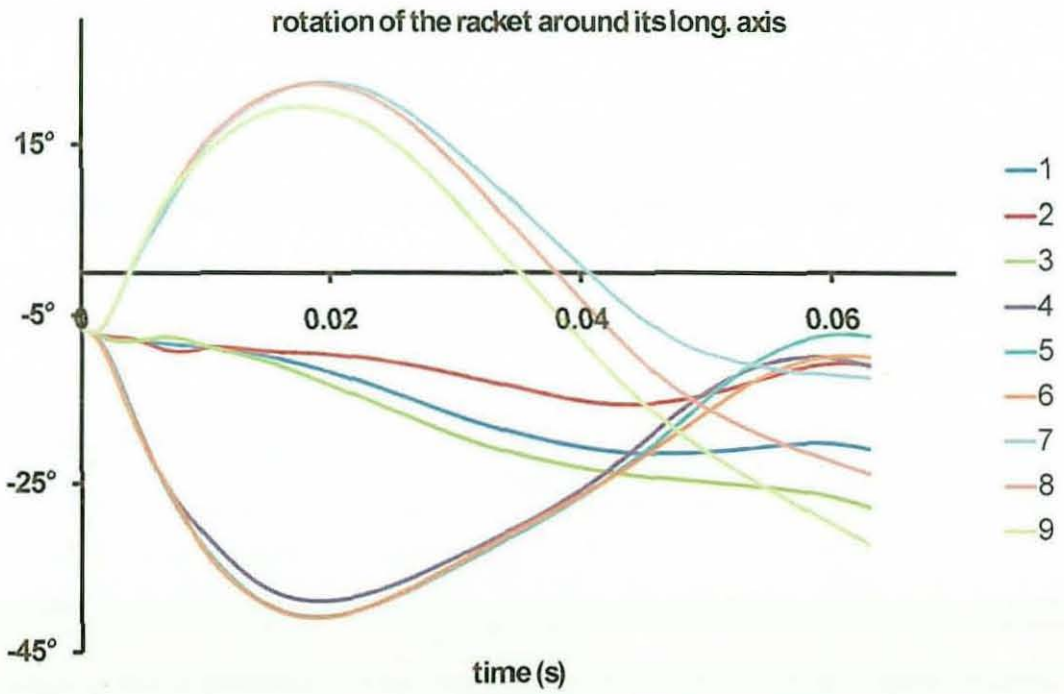

Figure 7.2. The behaviour of the racket for different impact locations. (Refer to Figure 7.1 for the legend)

As expected, the impacts on the locations 4, 5 and 6 caused the racket to rotate backwards and on the locations 7, 8 and 9 caused to rotate forwards. However, due to grip torques it recoiled within 50 ms after impact.

It is clear from the graph that the impact locations on the upper part of the stringbed (4, 5, 6), on the longitudinal axis of the stringbed (1, 2, 3) and on the lower part of the stringbed (7, 8, 9) formed three distinct groups, each showing different characteristics. The same behaviour was also observed in other angles and in the wrist flexor/extensor torque.

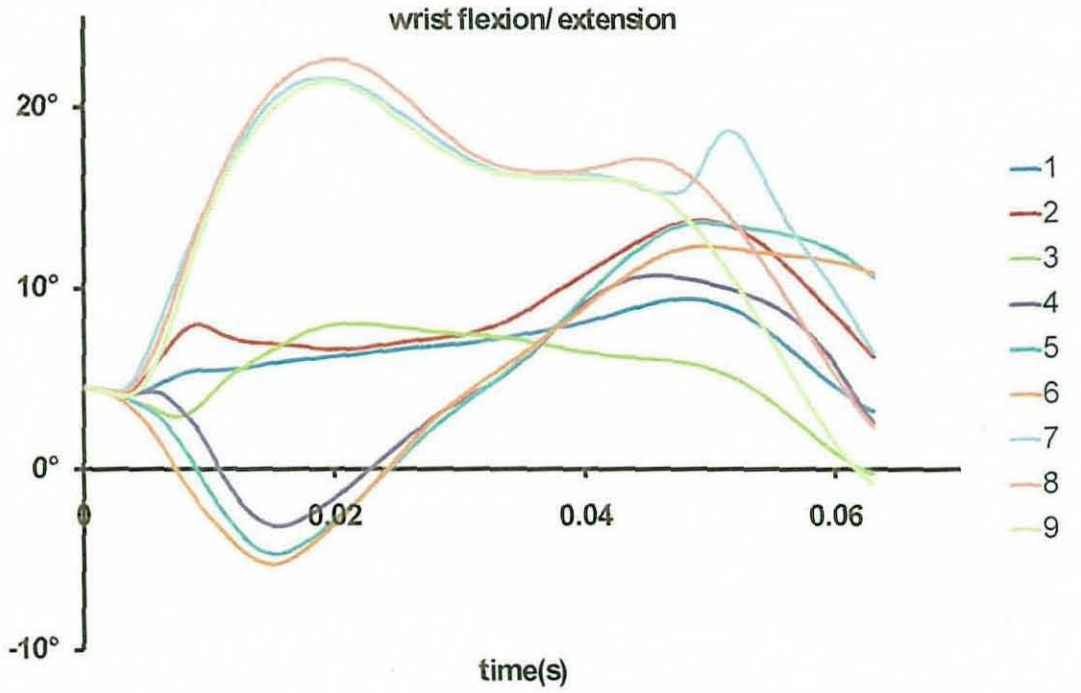

Figure 7.3. Wrist flexion / extension angle corresponding to different impact locations. (Refer to Figure 7.1 for the legend)

The location of the impact affected the wrist kinematics considerably (Figure 7.3). The impact locations on the upper part of the stringbed (4, 5, 6) forced the wrist to extend, whereas impact locations on the lower part (7, 8, 9) forced the wrist to flex with respect to the centre impact results. Considering maximum flexion / extension angles just after impact, the magnitude of additional flexion or extension was approximately 16° or 10°, respectively. Since the longitudinal axis of the racket was not coincident with the rotational axis of the racket, minor differences were observed among the impact locations 1, 2 and 3.

The location of the impact affects the supination / pronation angle, as well (Figure 7.4). When the racket rotates because of an off-centre impact, the rotation axis of the racket is close to the rotation axis of supination / pronation movement due to the configuration of the arm during a backhand stroke. Since the wrist does not

have internal/external motion, the rotation of the racket is transferred to the forearm depending on the grip conditions.

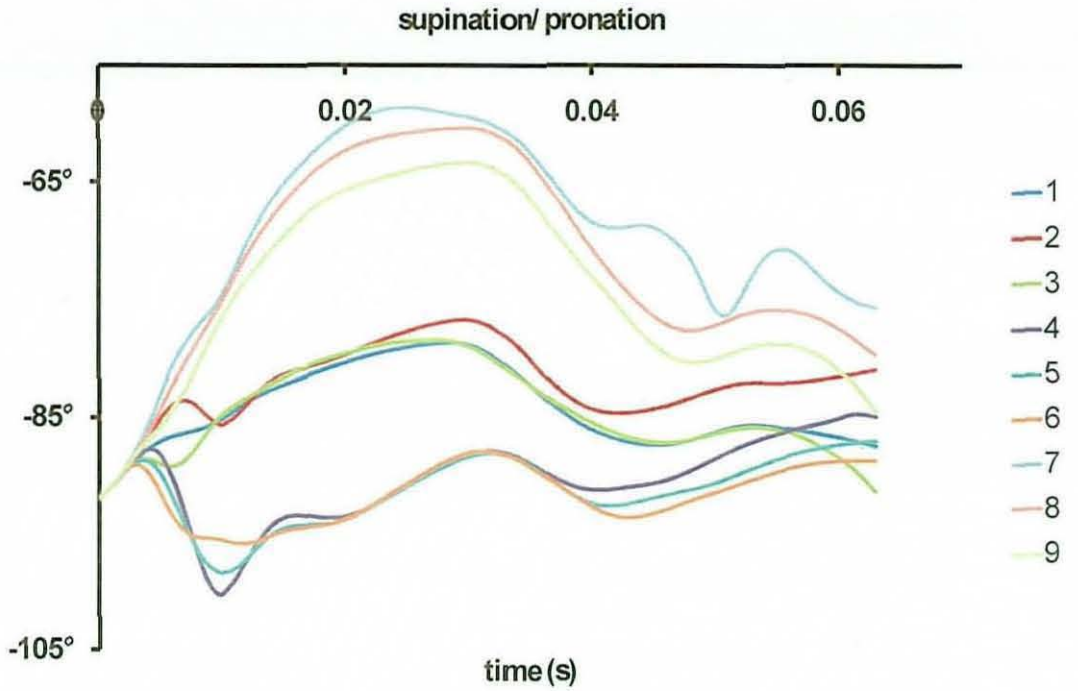

Figure 7.4. Supination / pronation angle corresponding to different impact locations. (Refer to Figure 7.1 for the legend)

Different impact locations on the longitudinal axis showed similar results for supination / pronation angle except relatively small differences just after impact. However, when the ball hit the group located in the upper part of the racket (4, 5, 6), the forearm pronated for about 10 ms and then followed a similar pattern to the centre impact simulations. The forearm had excess supination when the impact occurred in the lower part of the racket (7, 8, 9). The supination / pronation movement was consistent with the forward / backward rotation of the racket. Although the initial motion was different for each group of impact locations, after a certain time similar behaviour was observed for all three groups with an offset between them.

The major effect of the impact location was detected in the wrist flexion / extension torque (Figure 7.5). The centre impact had a relatively small net flexion torque after the impact. However, relatively large flexion or extension torque was observed when the ball hit the upper or lower part of the racket. The maximum

flexion torques for locations 5 and 6 were more than seven times the torque for a centre impact. The torque value for location 4 was slightly less than the other two locations. The reason might be its closeness to the wrist and therefore its smaller moment arm.

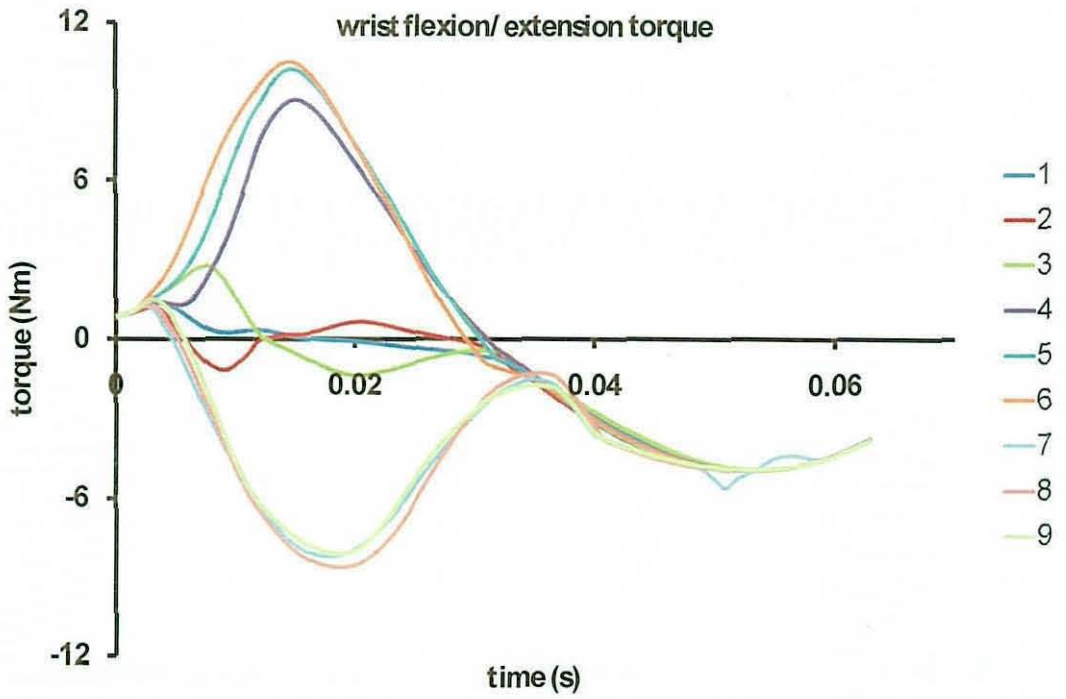

Figure 7.5. Wrist flexion / extension torque corresponding to different impact locations. (Refer to Figure 7.1 for the legend)

The torque profile for impacts at locations 7, 8 and 9 were similar. The maximum extension torque was more than six times the torque for a centre impact. Depending on the motion of the wrist, the concentric / eccentric loading of the wrist flexors / extensors was the main cause of the high torque values observed at the wrist. The wrist flexion / extension motion due to off centre impacts (Figure 7.3) supported this idea. For example, when the ball hits the lower part of the racket, the wrist flexes due to the impact, and during wrist flexion, previously activated wrist extensors are eccentrically loaded while the flexors are loaded concentrically.

The internal joint forces at the elbow and wrist were not affected by the impact location as much as the wrist flexion / extension torque. For each impact location the magnitude of the maximum joint forces after impact are presented in Table 7.1. Maximum differences were observed on the impact locations closer to the tip of the racket (3, 6, 9), especially, when the ball hit impact location 3, a maximum

increase (28%) of loadings was observed for both wrist and elbow with respect to centre impact results. The increases on the internal loadings at the elbow and wrist appeared to be very similar, although the loading at the wrist had higher joint forces.

Table 7.1. Maximum joint forces at the wrist and elbow corresponding to different impact locations and % increase with respect to centre impact simulation. (Refer to Figure 7.1 for the impact location numbers)

impact location	max. loading at wrist (N)	% increase	max. loading at elbow (N)	% increase
1	170	-	145	-
2	175	3	149	3
3	217	28	186	28
4	181	6	154	6
5	176	4	151	4
6	192	13	166	14
7	181	6	154	6
8	183	8	158	9
9	203	19	176	21

7.3 Sensitivity Analyses

Sensitivity analyses were performed for the other variables to investigate their effect on joint forces and torques. Since it has been accepted that the overload in wrist extensors was the major cause of tennis elbow (Kibler, 2002), maximum wrist extension torque (MWET) was considered for off-centre impacts in this section. However, when comparing the centre impact results, maximum wrist flexion was considered (MWFT) since flexion torque was observed just after impact. In addition, the effects on maximum wrist and elbow joint forces (MWJF and MEJF) were analysed. The results of the single simulations with the perturbed values of the variables were compared with the results of the centre and off-centre impact simulations using original values of the variables. For off-centre impact comparison, two impact points were considered. Impact location 3 (on longitudinal axis near tip)

was used when comparing the joint forces since maximum joint forces occurred in that location. For the comparison of wrist extension torque, impact location 9 (in the lower part near the tip) was used. Since the maximum torques in the extension direction were very similar for all three impact locations at the lower part of the racket, that location was selected arbitrarily. The first 40 ms after impact was considered during the simulations since maximum joint forces and torques were observed in this period.

7.3.1 Perturbation of the Mass and Moment of Inertia of the Racket Frame

It is well known that the racket frame mass and inertia affects the behaviour of the racket and therefore the tennis player. Racket companies produce rackets with different inertial properties for elite players and recreational players. However, the effects of the inertial properties of the racket on the wrist and elbow loadings are documented in the literature in limited numbers. Nesbit et al. (2006) stated that inertia values had a moderate effect on pronation / supination torques for forehand motion. In addition, Glynn (2007) compared two rackets with different inertial properties; although consistent results were found with the study of Nesbit et al (2006), relatively small effects on elbow and wrist loadings were presented.

In this study, to investigate the effects of the inertial values of the racket, single simulations of centre impact were used. Centre of mass locations of the racket handle and the racket head were kept unchanged as well as the racket frame stiffness and damping during the perturbation of the inertial properties of the racket.

First, the mass of the handle and racket head were perturbed without changing the moments of inertia. The simulations were run perturbing original mass values by ± 20%. The effect of the mass within the selected perturbation region was found to be negligible on wrist and elbow internal joint forces (Table 7.2).

Table 7.2. The effects of the racket mass (m) on selected joint torques and forces.

simulations	centre impacts			off-centre impacts		
	MWFT (Nm)	MWJF (N)	MEJF (N)	MWET (Nm)	MWJF (N)	MEJF (N)
original	1.36	170	144.5	8.16	217	185.5
0.8*m	1.21	169	143.5	8.36	220	187.5
1.2*m	1.51	170	144	8.01	213	183

MWFT increased by about 11% for an increase of 20% in mass and similarly decreased 11% for a 20% decrease in mass (Figure 7.6). The racket mass influenced MWET in the opposite way although the observed effects were lower (2%).

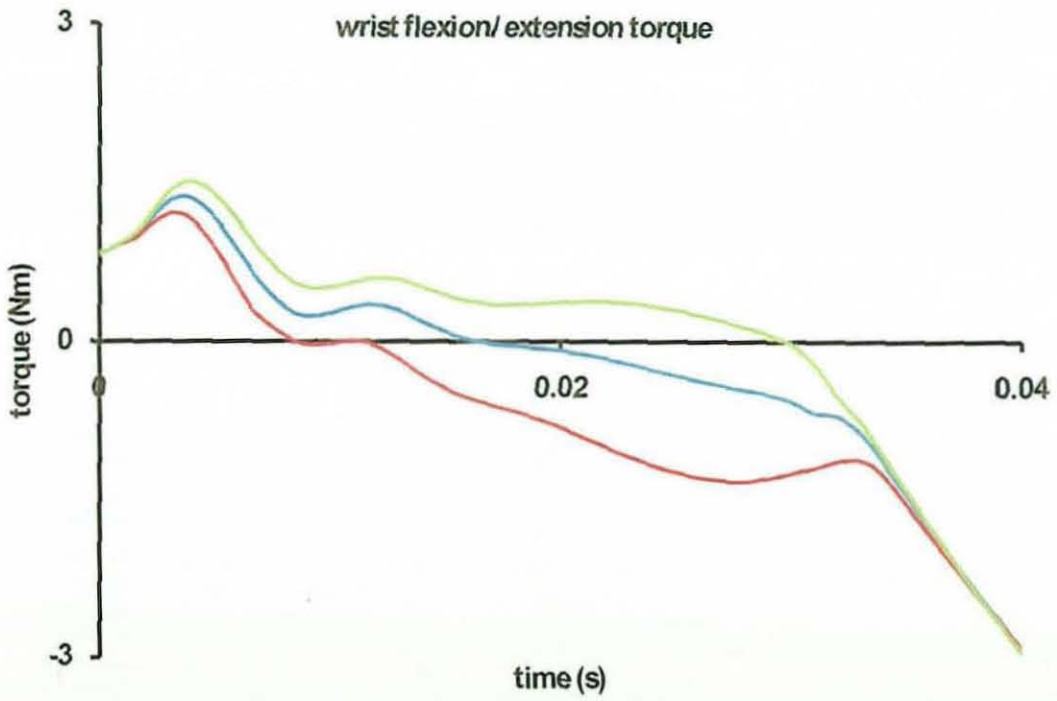

Figure 7.6. The effect of the perturbation of the racket mass on wrist flexion /extension torque for centre impacts. Original (blue), -20% (red), +20% (green).

Considering the kinematics, the wrist tended to flex more, and the forearm supinate more with lower racket mass for both centre and off-centre impact (Figure 7.7). The effect of the increase in wrist flexion angle for lower racket mass caused an increase in the MWET presented in Table 7.2. The effect of the racket mass on the supination was smaller than the effects on the wrist flexion.

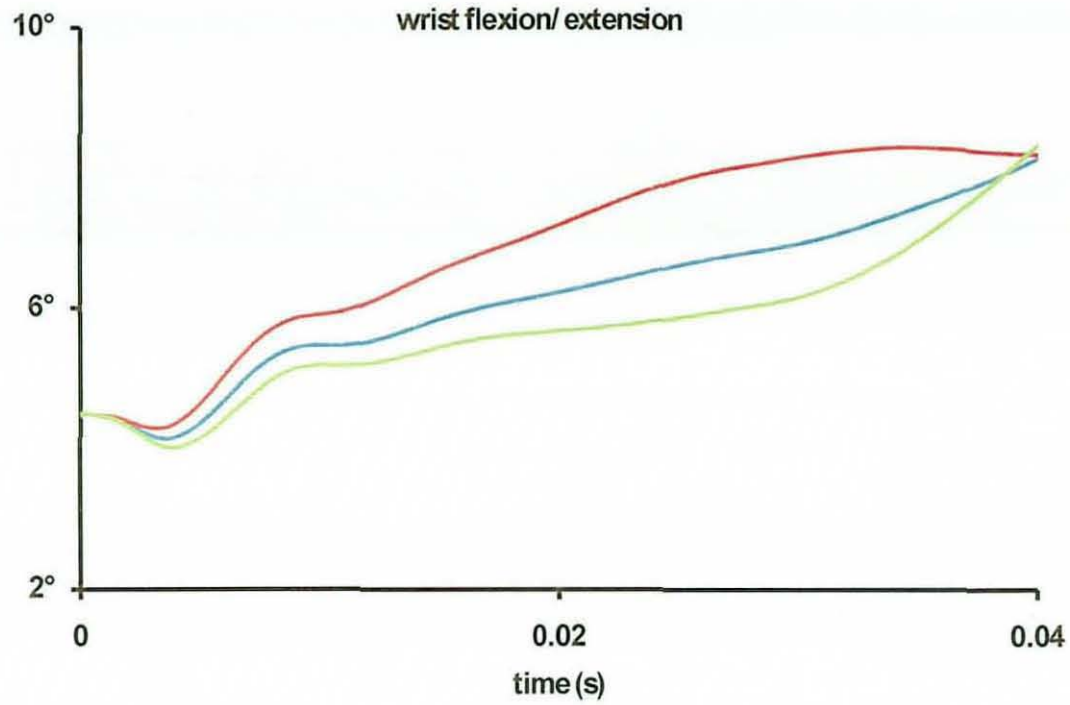

Figure 7.7. The effect of the perturbation of the racket mass on wrist flexion /extension angle for centre impacts. Original (blue), -20% (red), +20% (green).

To analyse the effect of the racket moment of inertia, the frontal (I_{front}), transverse (I_{trans}) and longitudinal (I_{long}) moments of inertia were perturbed by ± 20%.

The racket handle and racket head moments of inertia have perturbed at the same time such that the total moment of inertia of the racket around its centre of mass was perturbed by 20%.

Similar to the perturbation of mass, the wrist flexion / extension and pronation / supination movements were affected only slightly due to the change in moments of inertia of the racket handle and racket head. MWFT was found to be 20% higher using a low moment of inertia racket and found 16% lower using a high moment of inertia for centre impact (Figure 7.8). However, off-centre impact torques had no substantial change. There was a slight increase (3-4%) in the elbow and wrist joint forces while using low moments of inertia for both centre and off-centre impacts whereas a decrease of 4-5% in joint forces as observed with the rackets having high moments of inertia (Table 7.3).

It was believed that the moment of inertia about the longitudinal axis of the racket had a substantial effect on the rotation of the racket within the hand as well as the pronation / supination of the arm during off-centre impacts. Therefore, it was also

perturbed separately by 20% without changing the other moments of inertia of the racket. It was observed that MWET decreased / increased by about 4% for a 20% increase / decrease in the moment of inertia about the longitudinal axis.

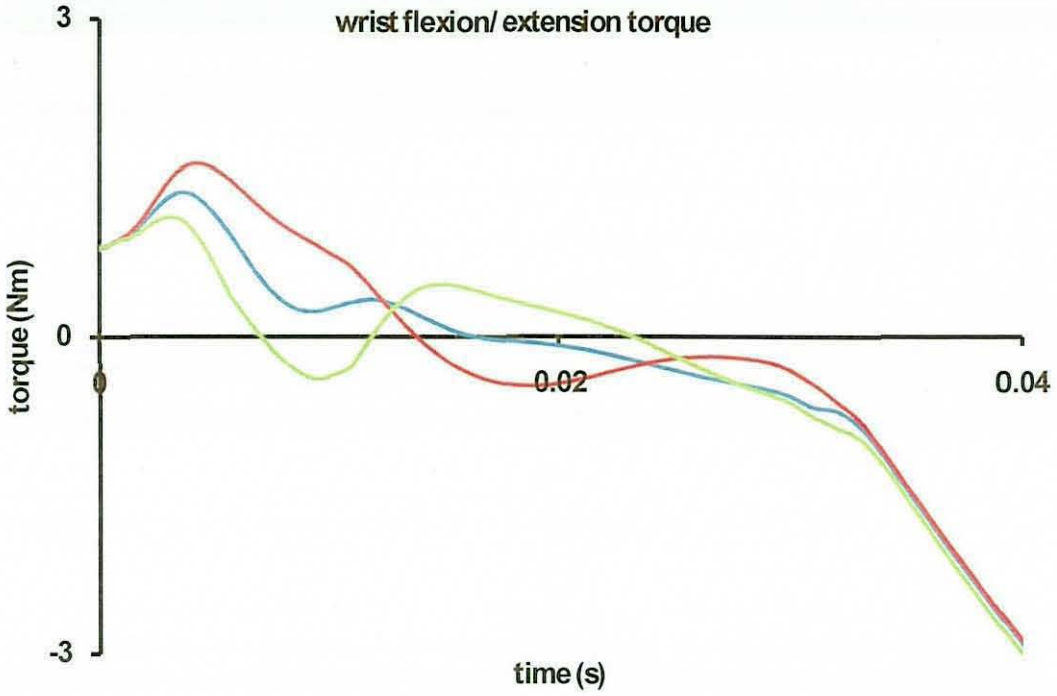

Figure 7.8. The effect of the perturbation of the racket moment of inertia on wrist flexion / extension torque for centre impacts. Original (blue), -20% (red), +20% (green).

Table 7.3. The effects of the racket moment of inertia (MOI) on selected joint torques and forces.

simulations	centre impacts			off-centre impacts		
	MWFT (Nm)	MWJF (N)	MEJF (N)	MWET (Nm)	MWJF (N)	MEJF (N)
original	1.36	170	144.5	8.16	217	185.5
0.8*MOI	1.64	174	149	8.14	225	193
1.2*MOI	1.13	164	139	8.15	209	177

In conclusion, perturbation of the inertial properties of the racket affected the wrist and elbow kinematics by small amounts, whereas the joint forces and wrist flexor / extensor were affected moderately. These result were consistent with the results of Glynn (2007).

7.3.2 Perturbation of the Racket Frame Stiffness and Damping

The torsional springs between the racket head and handle represent the viscoelastic properties of the racket. The racket frame stiffness and damping coefficients were perturbed separately, with each coefficient doubled for the perturbations.

Almost no difference was observed for centre impacts when the racket frame stiffness and damping were perturbed (Table 7.4). Therefore, it can be said that the model was insensitive to the racket frame viscoelastic parameters for centre impact. For off-centre impacts, perturbing damping coefficients caused negligible differences in the results. However, perturbing the stiffness value in the racket plane caused a 3% increase in MWET. In addition, perturbing the stiffness normal to the racket plane resulted in a 3% increase in maximum elbow and wrist joint forces.

Table 7.4. The effects of the racket frame stiffness (k) and damping(c) on selected joint torques and forces.

	centre impacts			off-centre impacts		
simulations	**MWFT (Nm)**	**MWJF (N)**	**MEJF (N)**	**MWET (Nm)**	**MWJF (N)**	**MEJF (N)**
original	1.36	170	144.5	8.16	217	185.5
2*k on plane	1.36	170	144.5	8.42	216	185
2*c on plane	1.36	170	144.5	8.14	217	185.5
2*k normal to plane	1.34	170	144.5	8.22	222.5	191
2*c normal to plane	1.36	170	144.5	8.22	217	186

Since damping of the racket frame had no influence on the loadings at the wrist and elbow, it would appear that the major part of the vibration of the racket attenuates within the hand without reaching the wrist joint.

7.3.3 Perturbation of the Wobbling Mass Parameters

The viscoelastic parameters of the upper arm and forearm wobbling masses were perturbed by ± 20% to observe the effects of the wobbling masses on the joint forces and joint torques. The stiffness and damping coefficients were perturbed separately. For the upper arm wobbling mass, no substantial effect was observed for wrist flexion / extension torque while perturbing the stiffness and damping coefficients (Table 7.5). However, for an increase / decrease in the stiffness value by 20%, the wrist and elbow joint forces increased / decreased by 2% and 3%, respectively for centre impacts. The off-centre impacts were not affected noticeably by the perturbation of both stiffness and damping coefficients.

Table 7.5. The effects of the upper arm wobbling mass stiffness (k) and damping (c) on selected joint torques and forces.

simulations	centre impacts			off-centre impacts		
	MWFT (Nm)	MWJF (N)	MEJF (N)	MWET (Nm)	MWJF (N)	MEJF (N)
original	1.36	170	144.5	8.16	217	185.5
0.8*k	1.35	166.5	140	8.15	215	183
1.2*k	1.38	173	149	8.15	218	188
0.8*c	1.36	169	143	8.16	216	185
1.2*c	1.36	170.5	146	8.14	217	186

Almost no change was observed when the forearm wobbling mass parameters were perturbed by ± 20% for both centre and off-centre impacts (Table 7.6). The only effect observed was a 2-3% increase/decrease in the joint forces with a 20% increase/decrease in stiffness of the forearm wobbling mass for centre impacts.

As a result, the viscoelastic properties of the wobbling masses do not have a substantial effect on the loading of the wrist and elbow. Especially, forearm wobbling mass had almost no effect indicating there was negligible soft tissue movement in the forearm. This result was expected considering the volume of the muscles in the forearm and the co-contraction of the major muscle groups during the backhand stroke.

Table 7.6. The effects of the forearm wobbling mass stiffness (k) and damping (c) on selected joint torques and forces.

simulations	centre impacts			off-centre impacts		
	MWFT (Nm)	MWJF (N)	MEJF (N)	MWET (Nm)	MWJF (N)	MEJF (N)
original	1.36	170	144.5	8.16	217	185.5
0.8*k	1.37	165	141	8.22	214.5	184
1.2*k	1.36	174	148	8.07	219	187
0.8*c	1.34	170	143	8.03	217	185
1.2*c	1.35	171	144	8.03	218	186

7.3.4 Perturbation of the Stringbed Tension

The actual string tension of the racket was measured as 75 lbs (967.7 N) during the performance data collection. This initial tension in the string was used as the preload (Equation 3.10) in the stringbed model. In the market, 75 lbs is accepted as a high tension for the stringbed and 57 lbs is mostly used for a moderate tension in the stringbed. To observe the effects of the stringbed tension on the joint loadings, a low-tension stringbed (57 lbs - 735.8 N) was used in the backhand stroke simulation and the results were compared.

Using low tension for the stringbed decreased the wrist flexion / extension torque by about 5% for a centre impact. However, the most noticeable effect of using low tension for the stringbed was having lower joint forces at the wrist and elbow (11% and 10%, respectively) during off-centre impact simulation (Table 7.7).

Table 7.7. The effects of the stringbed tension on selected joint torques and forces.

simulations	centre impacts			off-centre impacts		
	MWFT (Nm)	MWJF (N)	MEJF (N)	MWET (Nm)	MWJF (N)	MEJF (N)
75 lbs	1.36	170	144.5	8.16	217	185.5
57 lbs	1.29	172	146	8.21	194	167

The stiffness values of the springs used to form the stringbed model were also perturbed by ± 20%. All twenty-four springs composing the stringbed were perturbed at the same time. For a 20% increase in the stiffness values for a centre impact, the wrist and elbow joint forces increased by 5%. For an off-centre impact, the joint forces decreased by 7% and 6% for the wrist and elbow, respectively. However, for a 20% decrease in the stiffness value for centre impacts the joint forces decreased about 3%. In addition, for an off-centre impact the joint forces decreased up to 12% for the wrist and 11% for the elbow (Table 7.8). No substantial difference was observed in wrist flexion / extension torque when perturbing the stiffness values of the springs on the racket head.

Table 7.8. The effects of the stiffness (k) of the springs on stringbed for selected joint torques and forces.

simulations	centre impacts			off-centre impacts		
	MWFT (Nm)	MWJF (N)	MEJF (N)	MWET (Nm)	MWJF (N)	MEJF (N)
original	1.36	170	144.5	8.16	217	185.5
0.8*k	1.38	165	141	8.03	192	166
1.2*k	1.348	180	153	8.10	202	174

The stringbed tension also affected the outbound ball velocity and ball contact time as expected. The ball-racket contact time increased to 4.5 ms. The outbound velocity in the y-direction also increased by about 3%. On the other hand, the perturbation of the stiffness of the springs had no substantial effect on the ball outbound velocity and contact time.

7.3.5 Perturbation of the Grip Stiffness and Damping

The grip conditions determine the rotation of the racket and the wrist flexion. In extreme cases, when there is no interaction between racket and hand, the racket rotates freely after impact and when there is a rigid connection, the rotation of the racket due to the impact is transferred directly to the wrist. Torsional springs representing the grip torques allowed the racket to rotate within the hand and kept wrist flexion to moderate levels. The stiffness and damping coefficients of these torsional springs define the tightness of the grip. Relatively tight and loose grips may be represented by high and low stiffness values.

The effects of the grip tightness, i.e. the stiffness and damping coefficients of the torsional springs between the hand and racket, on the elbow and wrist loading were investigated by perturbing the stiffness and damping values by ± 20%. With the exception of wrist flexion / extension torque almost identical results were obtained when the stiffness and damping were perturbed. For centre impacts, MWFT was not affected by the perturbation; for off-centre impacts MWET increased by 5% for a 20% decrease in stiffness value (Table 7.9).

Table 7.9. The effect of the grip stiffness (k) and damping (c) on selected joint torques and forces.

simulations	centre impacts			off-centre impacts		
	MWFT (Nm)	MWJF (N)	MEJF (N)	MWET (Nm)	MWJF (N)	MEJF (N)
original	1.36	170	144.5	8.16	217	185.5
0.8*k	1.36	170	144.5	7.78	217	185.5
1.2*k	1.36	170	144.5	8.27	217	185.5
0.8*c	1.36	170	144.5	8.04	217	185.5
1.2*c	1.36	170	144.5	8.06	217	185.5

Using stiffness and damping values that were double their original value, the change MWET for off-centre impact rose to 11% without affecting the joint forces. It

was observed that the centre impact simulation was not sensitive to grip stiffness as much as the off-centre impacts. The rotation of the racket within the hand, which is very little for centre impacts, was directly influenced by the grip stiffness. Figure 7.9 illustrates this by showing the results of simulations using a twofold increase in stiffness and damping.

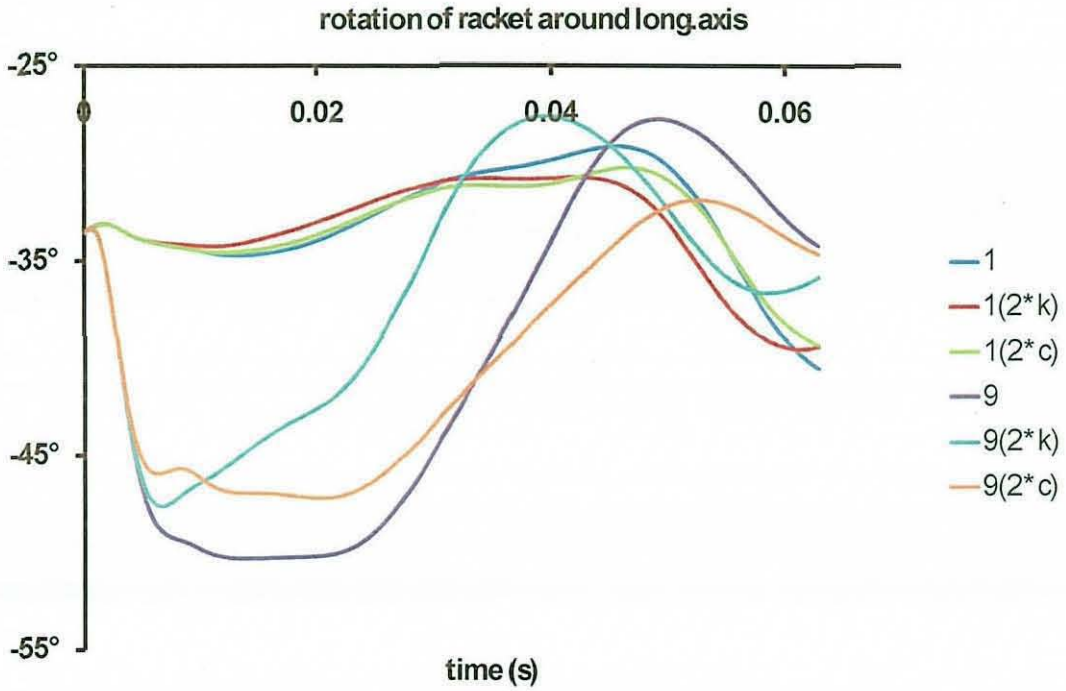

Figure 7.9. The effect of grip stiffness and damping on the rotation of the racket around its longitudinal axis within the hand. Original values and twofold stiffness and damping values were compared for impact locations 1 and 9.

7.3.6 Perturbation of the Inbound Ball Velocity

The inbound velocity was measured as -9 m/s in the y-direction by digitizing high-speed camera captures of the actual performance. The inbound velocity was perturbed by ± 2 m/s to observe its effects on the simulation model.

When the inbound velocity was perturbed to 11 m/s, no substantial difference was observed except a slight increase in MWFT. For off-centre impacts, MWET increased by 5% and wrist and elbow joint forces decreased by 7% (Table 7.10).

The influence of the inbound velocity was higher when it was adjusted to -7 m/s. MWFT decreased by 6% whereas the wrist and elbow joint forces had an increase of more than 2% for centre impact simulation. The off-centre impacts

affected the model slightly more than the centre impacts. A decrease of 10% was observed for MWET. The wrist and elbow joint forces decreased by 8% (Table 7.10).

Table 7.10. The effect of inbound ball velocity on selected joint torques and forces.

simulations	centre impacts			off-centre impacts		
	MWFT (Nm)	MWJF (N)	MEJF (N)	MWET (Nm)	MWJF (N)	MEJF (N)
-9m/s	1.36	170	144.5	8.16	217	185.5
-7m/s	1.27	174	148	7.37	199	171
-11m/s	1.38	170	145	8.56	201	173

The outbound velocity and maximum value of the ball-racket impact force were also compared. When the ball inbound velocity was -7 m/s, the outbound velocity decreased slightly and the contact time increased to 4.2 ms. In addition, the impact force decreased by 2%. For the inbound velocity of -11 m/s, the outbound velocity was found to be 2% faster than the matching simulation result. The most noticeable difference was on the impact force. It increased by about 8% for an increase of 2 m/s in ball inbound velocity

.

7.3.7 Perturbation of the Wrist Flexion Angle at Impact

To observe the effects of wrist flexion at impact, the orientation of the hand was perturbed such that the wrist flexion angle was ± 5° of its initial value. When perturbing the wrist flexion angle, it was assumed that all the kinetic and kinematic variables of the model remained unchanged. The wrist angle time histories for centre and off-centre impact simulations are shown in Figure 7.10.

For a centre impact MWFT increased by about 55% while MWJF and MEJF decreased by 7% and 9%, respectively for an additional 5° flexion at wrist. It should be noted that this 55% increase corresponds to a 0.76 Nm increase in MWFT since the original value of the MWFT was relatively small. When the wrist was initially 5° more extended, MWFT started with a torque value about 15% higher than the original simulation but then reduced without having a local maximum (Figure 7.11).

Wrist and elbow joint forces increased by 10% and 11%, respectively for an extended wrist.

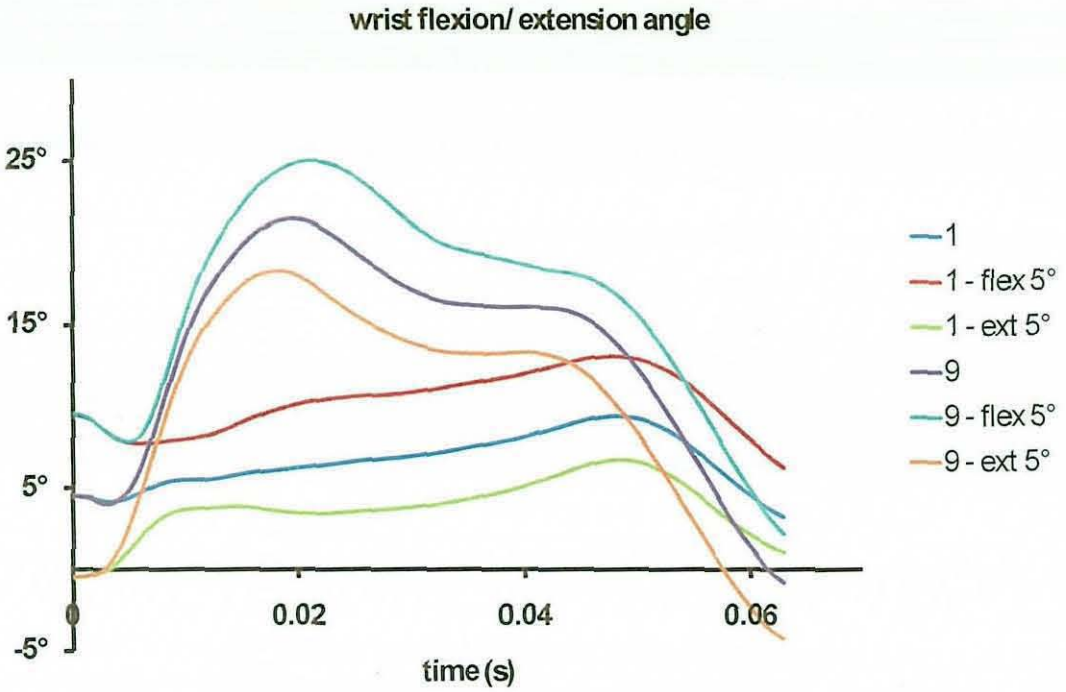

Figure 7.10. Perturbation results of the wrist flexion/extension by 5° for impact locations 1 and 9

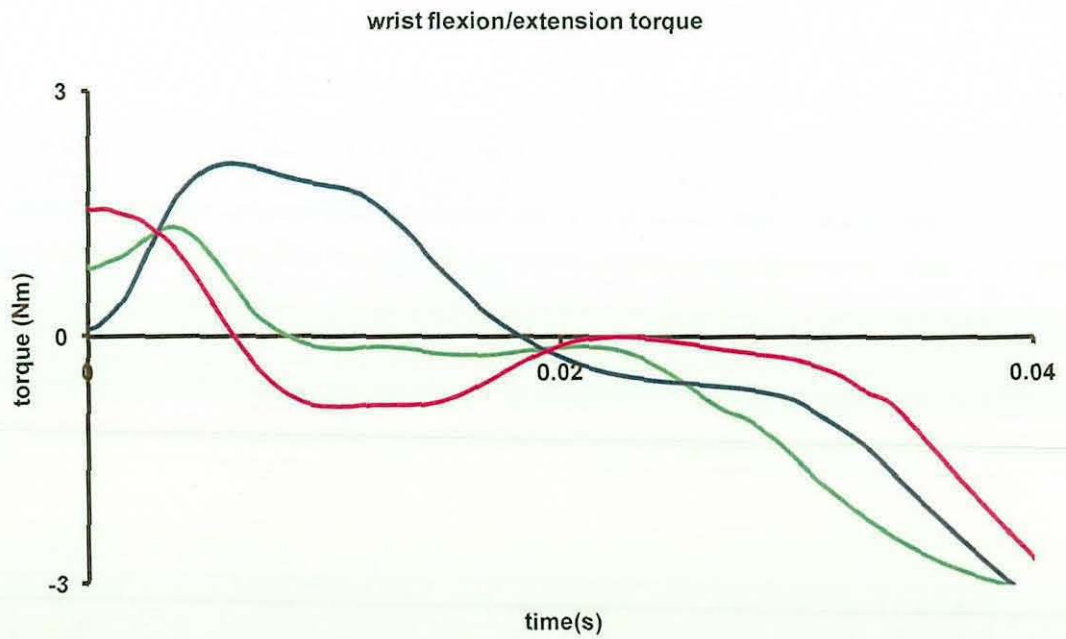

Figure 7.11. The effect of the perturbation of the wrist flexion/extension angle on wrist flexion / extension torque for centre impacts. Original (green), +5° flexed (blue), +5° extended (pink).

For an off-centre impact no substantial difference was observed for MWET except a 2% increase for an additional 5° extension. However, the joint forces were much more affected by the wrist configuration. The wrist and elbow joint forces decreased by 13% and 16%, respectively, when the wrist was initially 5° more flexed. For an extension of 5° MWJF increased by 11% whereas MEJF increased by 13%. The summary of the perturbation results are presented in Table 7.11.

Table 7.11. The effect of wrist flexion/extension configuration at impact on selected joint torques and forces.

simulations	centre impacts			off-centre impacts		
	MWFT (Nm)	MWJF (N)	MEJF (N)	MWET (Nm)	MWJF (N)	MEJF (N)
original	1.36	170	144.5	8.16	217	185.5
flexed +5°	2.12	158	132	8.16	189	156
extended +5°	1.57	185.5	160	8.37	241	210

7.4 Summary

In this chapter, the computer simulation model, which was evaluated in the previous chapter, was used to investigate the effects of the different model variables on wrist and elbow joint forces as well as the wrist flexion / extension torque. First, the location of the impact was analysed, then, a sensitivity analysis was performed by perturbing model variables to observe their effects on the simulation results. Over all variables, the impact location had the most substantial effect on loading at wrist and elbow, while the viscoelastic parameters of the wobbling masses and racket frame had the least effect. The following chapter includes a general summary and discussion of the study.

8 DISCUSSION AND CONCLUSION

8.1 Introduction

This chapter addresses the research questions presented in Chapter 1 while also discussing the limitations and improvements to the techniques used throughout the study. Finally, future studies are suggested for further investigations along with potential improvements of the simulation model.

The aim of this study was to investigate the effect of different variables belonging to racket and player on the wrist and elbow loadings in one-handed tennis backhand groundstrokes. To achieve this aim, a subject-specific, torque-driven, 3D computer simulation model with 8 segments (humerus, ulna, radius, hand, racket handle, racket head and the upper arm and forearm wobbling masses) was developed using MSC.ADAMS.

An elite player was chosen to perform consistent and high standard backhand topspin strokes and a Vicon System was used to record the performances. The orientation of the thorax and other joint angles obtained from the performance data collection were comparable to those stated by Wang et al. (1998). In particular, the characteristics of the wrist flexion / extension angle were also comparable to those found in the literature (Blackwell and Cole, 1994; Knudson and Blackwell, 1997; Riek et al., 1999). The simulation model was matched to the performance for the period from about 200 ms before ball-racket impact to 60 ms after impact by varying the activation profiles in order to minimize the difference between simulation and performance in terms of joint and racket angles. Once matched, the model variables in question were perturbed using single simulations with fixed activation profiles and the effect on the loading at the wrist and elbow observed along with the changes in kinematics.

The methods used to collect subject-specific performance data have been shown to be as good as or superior to those previously published in the literature. The model itself has been shown to incorporate greater levels of complexity and yield deeper insight than other models of tennis strokes reported in the literature. Since the output of the model compares well with both real stroke data and results published in the literature, a high level of confidence in the findings is permissible.

8.2 Research Questions

Specific research questions resulted from the aim of the study and these questions were answered by observing the results of perturbations:

What is the effect of ball impact location on the kinetics and kinematics of the wrist and elbow in one-handed tennis backhand groundstrokes?

The kinematics and kinetics of the wrist and elbow were mostly affected by the location of impact. The results showed that the nine impact locations were separated into three groups that behaved similarly during the simulations: the locations on the upper part of the racket, the locations on the longitudinal axis of the racket and the locations on the lower part of the racket.

Depending on the location of the impact, the racket rotated within the hand and subsequently forced the wrist to either flex or extend. In addition, due to the configuration of the arm at impact, the rotation axis of the racket and supination / pronation movement became close to each other. Since the wrist does not allow internal / external rotation, the rotation of the racket was transferred to the forearm. As a result, when the ball hit the upper part of the racket, the wrist additionally extended by about 10° and pronated by about 12° with respect to the results of centre impact. Conversely, when the ball hit the lower part of the racket, the wrist flexed by about 16° and supinated by about 18° compared to the centre impact results.

The effect of the impact location on wrist and elbow loadings was much more remarkable. The maximum net torques around the wrist flexion / extension axis after the impact were compared for all impact locations. For the ball impact locations above the longitudinal axis of the racket, a net flexion torque more than seven times the torque obtained in the central impact was observed whereas for the impact locations below the longitudinal axis a net extension torque more than six times the central impact torque was obtained. Although a reduction of 12% and twofold increase in torque value were observed for the impact locations close to the throat and tip of the racket, respectively, these changes were relatively small with respect to the other off-centre impact locations. The impact locations on the longitudinal axis resulted in different torque values since the rotation axis of the racket during the backhand stroke was not coincident with the longitudinal axis.

The main reason for high torques at the wrist during off-centre impacts was the eccentric loading of the wrist flexors / extensors. When the wrist was forced into a more flexed / extended position due to the impact, the wrist extensor and flexor torque generators were loaded eccentrically and concentrically depending on the motion of the wrist. Since the model is capable of calculating the wrist flexor and extensor torques separately, the investigation of the torques for each torque generator revealed that the wrist extensor group almost reached the eccentric plateau level for the centre impact. If the ball hit the lower part of the racket, the wrist was forced into a flexion and while the extensor group was loaded eccentrically, the flexor group was loaded concentrically. The extensor torque increased slightly to reach its plateau value and the flexor torque decreased considerably due to concentric loading causing a net effect of extensor torque at the wrist joint.

When the maximum net joint flexion / extension torques were compared, it was observed that the maximum flexion torque (10.5 Nm) was higher than the maximum extension torque (8.2 Nm). Finding a larger flexor torque was surprising considering the fact that the pain or injury due to backhand strokes generally has been located in the lateral epicondyle where the wrist extensors originate. When the torques in the muscle groups were considered separately, the maximum torques for these muscle groups were found to be 24 Nm and 29 Nm for wrist extensors and flexors, respectively. However, the maximum eccentric torque values for extensors and flexors obtained from the isovelocity torque measurements were 31 Nm and 45 Nm, respectively. Although higher torque values were obtained in the wrist flexors during the backhand stroke, when compared with the maximum possible torque, the wrist extensors were subject to a much higher percentage of their maximum values.

The joint forces at the wrist and elbow had similar characteristics just after impact with the wrist forces being slightly higher. Maximum joint forces were observed for impacts closest to the racket tip on the longitudinal axis (28% larger than the centre impact results). It was clear from the results that the impact locations close to tip of the racket produced higher joint forces. This is most likely to be due to the ball impact at these impact locations causing higher moments about the hand-racket interaction.

The results of the off-centre impact simulations were consistent with the studies found in the literature. After comparing the effect of several variables, Glynn (2007) also stated that the location of impact had the highest influence on elbow

loading. Nesbit et al. (2006) investigated more than one off-centre location on the longitudinal and the vertical axes of the racket for a forehand stroke. Although the results of a backhand stroke cannot be compared directly to the results of a forehand stroke, the eccentric loading at the wrist flexors and extensors for off-centre impacts would be symmetrical for both types of strokes and therefore similar results were obtained: Nesbit et al. (2006) found substantial difference between centre and off-centre impacts. It was presented that the impact location close to the tip of the racket had higher elbow flexion / extension and varus / valgus torque. The impact locations above and below the longitudinal axis had higher pronation / supination torque. Hennig et al. (1992) also mentioned the incidence of high loadings due to off-centre impact.

The simulation models used by Glynn (2007) and Nesbit et al. (2006) were angle-driven and therefore could not demonstrate the effect of an impact on the kinematics of the arm for an impact location for which they lacked motion data. In addition, Nesbit et al. (2006) assumed a rigid connection between hand and racket which may cause unrealistic results. The model presented here has been shown to be capable of performing this type of analysis and has shown deeper insight into the kinematics of the arm for impact conditions previously unaddressed by the literature.

Since recreational players are more likely to have more off-centre impacts due to their poor technique, especially under elevated fatigue levels (Brody et al., 2002), there is a greater chance they might be injured by the high loadings observed in wrist and elbow. The high wrist extensor torque occurring in off-centre impacts below the longitudinal axis of the racket indicates that there are high levels of force on the wrist extensor muscles, which include ECRB, the most critical muscle for 'tennis elbow'. In contrast, the off-centre impacts above the longitudinal axis of the racket causes high levels of force in wrist flexor muscles. However, these forces are not very big when compared to their maximum values to provoke an injury at the medial epicondyle where wrist flexors are attached.

What is the effect of the physical properties of the racket on the kinetics and kinematics of the wrist and elbow in one-handed tennis backhand groundstrokes?

The physical properties of the racket that were considered included mass, moment of inertia and viscoelastic parameters of the racket frame, stringbed tension and stiffness of the springs on the stringbed.

Among the racket variables, the moment of inertia had the most substantial effect on wrist and elbow loading. For a 20% decrease of the racket moments of inertia the maximum wrist flexion torque (MWFT) increased by 20% for a centre impact. In addition, a 17% decrease in MWFT was obtained for 20% increase in moment of inertia. No substantial effect was observed in wrist flexion / extension torque for off-centre impacts. However, if the moment of inertia about the longitudinal axis of the racket only was increased by 20%, a 4% decrease in MWET was found. Using a low moment of inertia also resulted in up to 4% higher joint forces whereas high moment of inertia for the racket decreased joint forces by up to 5%.

Although there are several studies investigating the effects of the moment of inertia of the racket on the game (Mitchell et al., 2000a), there are a limited number of studies concentrating on the joint loadings. The effect of moment of inertia on the joint loadings were consistent with the results found in the literature (Nesbit et al., 2006; Glynn, 2007).

It is possible that for the same gripping conditions, rackets having lower moment of inertia have lower resistance to the effects of ball impact and therefore rotate more within the hand compared to the motion of the racket with a higher moment of inertia. Even though this extra rotation was not very big for a 20% decrease in moment of inertia, because of that motion there appears an additional resisting torque at the grip due to the recoil of the racket. It was also observed that the wrist made an extension motion for a short period of time after impact which eccentrically loaded the wrist flexors. These factors contributed to the increase in MWFT for a centre impact.

The perturbation of the mass had negligible effect on the wrist and elbow forces. The only noticeable effect of the racket mass was on the MWFT. A 20% perturbation of the racket mass resulted in an 11% change in MWFT. When the mass of the racket increased, it created an additional torque at the grip due to an increase in

weight. The magnitude of this torque was dependent on the global orientation of the racket. The maximum effect was observed when the transverse axis of the racket was parallel to the global vertical axis so that weight of the racket could have a maximum moment arm. The mass of the racket affected the kinematics of the wrist and elbow slightly. The wrist flexed and supinated more when a low-mass racket was used in the simulations compared with a high-mass racket.

In the literature, generally, the effect of the mass on the game has been investigated. Due to racket companies producing rackets from composite materials and the general tendency towards using lighter rackets by recreational players to produce faster swings, the average racket mass has decreased from about 400 g to 250 g over the past 40 years (Miller, 2006).

The perturbation of the racket frame stiffness and damping in the model had no substantial effect on the wrist and elbow loading even though they were perturbed by doubling their original values. The racket model can be seen to vibrate in its fundamental mode normal to the racket head plane in both centre and off-centre impacts. However, consistent with the results of Glynn (2007), the effect of this vibration was not observed in wrist and elbow even with no damping. Since the damping of the racket frame had no effect on wrist and elbow loadings, it would appear that the vibration of the racket is damped at the grip. The wrist and elbow joints were modelled with no internal damping so the vibration of the racket could only be absorbed in the grip. Since in reality there is damping at each joint due to its anatomical structure, the model can be thought conservative in this respect. Although there is a general belief that the vibration of the racket frame and the transfer of this vibration to arm may be a contributing factor for injuries, particularly tennis elbow, the results of this study showed that the attempts to reduce the vibration of the racket would only increase comfort during impact but not reduce the risk of injury.

To observe the effect of the stringbed tension on the wrist and elbow joint loadings, a low-tension stringbed was used and the results were compared to those of the original matching simulation using a high-tension stringbed. Whilst using low-tension rackets MFWT decreased by 5% for a centre impact and the joint forces decrease by up to 10% for off-centre impacts. Similarly, when the stiffness values of the springs in the stringbed model were perturbed by -20%, the joint forces decreased by up to 12% for off-centre impacts without affecting the wrist extension torque substantially. The results suggest that the benefit of using low-tension rackets is

primarily to reduce the joint internal loading rather than the loading on muscle groups.

Lower wrist and elbow loadings were expected when the stringbed tension and the spring stiffness values were reduced. The stringbed deflected more with low-tension rackets absorbing most of the impact energy. Since the stringbed has very little damping compared to the ball, the deflection of the stringbed, instead of deformation of the ball in high-tension rackets, prevents energy loss during the impact and gives the absorbed energy back to the ball during recoil. The outbound velocity of the ball and the ball-stringbed contact time are therefore higher for low-tension rackets and the effects of the impact are reduced on the racket frame.

Considering the effects of the physical properties of the rackets on loadings at the wrist and elbow listed above, a low-tension racket with low mass and high moment of inertia, especially about the longitudinal axis may be suggested for a recreational player who would like to reduce the chance of the injury or having pain.

What is the effect of the soft tissue movement on the kinetics and kinematics of the wrist and elbow in one-handed tennis backhand groundstrokes?

Soft tissue movement in the forearm and upper arm was modelled as wobbling masses that are rigid segments attached by springs to the link segments of the upper arm and forearm. The stiffness and damping coefficient values of the upper arm and forearm wobbling mass springs were perturbed by ±20% of their original values for both centre and off-centre impacts. No substantial effect of the wobbling mass parameters were observed except a slight (2-3%) decrease / increase in the joint forces obtained when the stiffness of the wobbling masses were decreased / increased. The effects of the wobbling mass parameters on the wrist and elbow kinematics were found to be negligible.

It appeared from the results that the forces and the torques caused by the ball impact at the wrist and elbow were very large compared to the contribution of wobbling masses. Therefore, for the subject used in this study the wobbling masses could be converted into rigid bodies on the bones to reduce the computational load. For most possible subjects, it is unlikely that wobbling masses make a substantial contribution to simulations. For other subjects, according to their age, fitness or

physique, wobbling mass may make a larger contribution to the elbow and wrist joint loadings.

What is the effect of the grip tightness on the kinetics and kinematics of the wrist and elbow in one-handed tennis backhand groundstrokes?

The motion of the racket within the hand was determined by the grip parameters. For a tight grip, which was obtained by increasing the stiffness values at grip, the rotation of the racket within the hand is reduced and transferred to the wrist and elbow. However, for a loose grip, the racket rotates more freely in the hand and therefore reduces the effect on the wrist and elbow.

During the evaluation of the model, a set of viscoelastic parameters for the grip were found by matching the centre impact. However, when using these parameters for an off-centre impact it was observed that the grip was so tight that the racket could not rotate within the hand as much as it did in the actual performance. Therefore, in order to match the off-centre impact as well, the upper bounds for stiffness and damping values were decreased to give a relatively loose grip and a compromised set of parameters were obtained that gave a good match both for centre and off-centre impacts.

The effect of the grip tightness on the wrist kinematics for a central impact was found to be negligible. However, for an off-centre impact, a twofold increase in the stiffness and damping affected the rotation of the racket within the hand considerably.

When the grip stiffness and damping were perturbed by ± 20% from their original values no substantial effect on the wrist and elbow loadings were observed. The only noticeable effect was the 5% decrease in maximum wrist extension torque (MWET) for a 20% decrease in the grip stiffness for an off-centre impact. To see the effects of the grip conditions more clearly the stiffness and damping coefficients were doubled to represent a relatively tight or stiff grip. This time an 11% increase in the MWET was observed for an off-centre impact. This was the maximum MWET obtained among the results of the perturbations of the all variables considering the impact locations. These results showed that a tight grip may contribute to the development of 'tennis elbow' as stated by Hatze (1976) previously.

To obtain high torque from a tight grip was not surprising. If the extreme case of tightness is thought to be a rigid connection between hand and racket, the effects of the ball-racket impact could be transferred directly to the wrist without any damping or reducing effect of the hand. However, too loose a grip might cause problems in controlling the racket after impact and result in unsatisfactory hitting performance (letting go of the racket at impact resulted in up to an eight times decrease in the outbound velocity of the ball); therefore, an optimum grip tightness is needed.

What is the effect of the wrist configuration at impact on the kinetics and kinematics of the wrist and elbow in one-handed tennis backhand groundstrokes?

In order to observe the effects of technique on the wrist and elbow loadings to some extent, the initial wrist flexion angle at the instant of ball impact was perturbed. Although it was possible to perturb the other joint angles as well, the wrist flexion angle was selected since it was one of the most critical angles to consider during a backhand stroke (i.e. most directly associated with the wrist flexors / extensors).

Assuming that all the conditions at impact were unchanged, the initial configuration of the wrist was perturbed by ± 5° around the wrist flexion / extension axis. For a centre impact, a 55% increase in MWFT was observed for an additional 5° flexion at the wrist. It should be noted that since the original value of MWFT was relatively small, this 55% increase corresponds to a 0.76 Nm increase in MWFT. When the initial wrist angle was extended by an additional 5° with respect to the original configuration, MWFT increased by about 15%. However, this increase was observed at the beginning of the impact due to changing the initial length of the torque generators and there was no local MWFT seen later during the swing. Therefore, it might be claimed that no definite increase in torque was observed due to ball impact. The maximum joint forces were affected by the wrist configuration by up to 11% of the original values, so additional wrist flexion resulted in lower joint force values whereas additional wrist extension resulted in higher joint forces. For an off-centre impact, no substantial change was observed for the MWET but there was a 15% increase in joint forces.

The motion of the wrist around the flexion / extension axis expressed the change in the MWFT. When the wrist was perturbed by an additional 5° of flexion, it

resulted in an extension motion for about 10 ms after impact in which the wrist flexors eccentrically loaded and therefore wrist flexion torque substantially increased. When the initial wrist angle was perturbed by 5° in the extension direction, the wrist started flexing just after impact until it reached a maximum at about 20 ms. During this period, the wrist flexors were under concentric conditions and the wrist flexion torque decreased.

What is the effect of the inbound ball velocity on loadings at the wrist and elbow?

The inbound velocity was perturbed by ± 2m/s to observe its effects on wrist and elbow loading. No substantial effect was observed in the joint forces for centre impacts. However, MWFT decreased by about 6% for a slower incoming ball velocity while a faster incoming ball velocity was had a small effect on the MWFT. For off-centre impacts, the effect of the incoming ball velocity became more noticeable. MWET decreased by 10% for the lower inbound velocity and increased by 5% for the higher inbound velocity. The maximum joint forces decreased by up to 8% for both incoming velocities. This is consistent with the results of Chow et al. (1999) who measured the muscle activation for three different incoming ball velocities and found that muscle activation increased to overcome the greater impact forces while hitting a fast incoming ball. In this study, since the activations were kept constant for each ball velocity, the wrist flexed more while hitting a fast incoming ball. Therefore, wrist extensors were loaded eccentrically producing higher MWET.

Since the inbound ball velocity affects the magnitude of the impact force and higher ball velocities create higher impact forces (Cross, 1999b), it was expected to have higher torque values for higher inbound ball velocity.

Recreational players are more likely to have off-centre impacts for higher incoming ball velocity due to poor technique compared with elite players. Therefore, for a fast incoming ball velocity it is very likely they are subject to the combined effects of high velocity and off-centre impacts.

8.3 Limitations and Improvement

8.3.1 Data Collection

The actual performance of the one-handed tennis backhand groundstrokes of an elite tennis player were recorded using a motion analysis system. The sampling frequency of the motion capturing was 250 Hz, which was the maximum possible during the data collection for a 2.5 m^3 calibration volume. Recent studies using the same but upgraded motion analysis system managed to capture data at 480 Hz and for a larger calibration volume. Using this upgraded system would allow more detailed kinematic data to be collected from actual performances of the backhand stroke.

During the data collection, a standard marker set was used to capture the motion data. After gaining experience using the motion analysis system for different subsequent studies at Loughborough University, the number of the markers, the location of the marker attachment points and the way of estimating joint centre locations can now be adjusted regarding to the aim of the data collection. Using a better marker set would have improved the estimations of the joint centres.

During the data collection, pressure sensors were attached to the grip of the racket in order to measure grip force during backhand. However, due to a malfunctioning piece of equipment no satisfactory pressure data could be collected. Similarly, three axial accelerometers used to measure racket acceleration during impact did not work well for all trials. A successful grip pressure and racket acceleration measurement would make it possible to use these variables in the model evaluation.

8.3.2 Matching the Actual Performance

The Simulated Annealing (Corana et al., 1987) algorithm was used to vary the model parameters in order to find the best match. Although it is a robust algorithm to find global optimum points, it has relatively poor time efficiency. During the matching process, the most time consuming part was the interaction between the two software packages. For a single run, simulation of a complete backhand swing took 12-13 seconds in the ADAMS environment. When the simulation was run from MATLAB during optimisation, it took about 35 seconds for

a complete swing. Using another algorithm in the future (e.g. a genetic algorithm: (Chipperfield et al., 1994) may decrease the overall time to find a good set of parameters by decreasing the total number of simulations. Embedding a satisfactory optimisation routine in MSC.ADAMS may be another way of decreasing the optimisation time.

8.3.3 Model Complexity

The model in this study uses torque generators to drive the simulation model. Although torque-driven models are superior to angle-driven models allowing the user to simulate different conditions and answer 'what if' questions, they give information on the joint level i.e. net torques at a joint. However, a more complex model may include individual muscles and therefore information in the muscle level can be obtained. It is the intention to use individual muscles to drive the model in the future. The origin and insertion points of the all muscle groups associated with the arm motion have already been located and muscles were attached to the model. However, the muscle wrapping issue and the determination of the force-length-velocity relationship for each individual muscle have yet to be resolved. It is beyond the scope of the current study to fully implement them. Including individual muscles would give more information on the loadings at a specific muscle group such as ECRB, the muscle associated with 'tennis elbow'.

The motion of the thorax was determined from the performance data collection and used directly in the model. Since the focus was on the arm motion with respect to the body, the motion of the thorax was constrained to follow the performance data. For this reason, shoulder angles were calculated with respect to the thorax using performance data. The scapula orientation was assumed to be the same as the thorax orientation in order to make the model consistent with the performance data. In the future, it may be possible to drive these segments using torque generators in a whole body simulation model.

In the model, it was assumed that there was no damping in the joints. Although in reality every joint in the body has some damping regarding to their structure, the damping at the joints is generally active in the relative translation of segments via cartilages. The revolute joints used in the model do not allow any

translation in the joint. In the future, the effect of the damping could be investigated by implementing spring-damper systems at the joints or by adding a translational degree of freedom to the link segments.

The direct contribution of the wrist flexor muscles on the grip torque was omitted in the model since it was not an easy task to measure this contribution. In addition, the main focus of the current study was in the wrist extensors since the pain and injury has generally occurred in extensors during backhand strokes.

The racket frame was modelled with two segments to represent the fundamental vibration mode of the racket in and normal to the racket plane. Increasing the number of segments in the racket would improve the true mode shapes of the racket when it vibrates due to an impact. However, the penalty of additional computational load and so time overweight the benefit of improving the racket model accuracy.

Overall, the model complexity is sufficient to answer the research questions resulted from the aim of this study. In the future, incorporating individual muscles, for example, will allow additional questions to be addressed with a deeper insight.

8.4 Future Studies

The simulation model has been used to show the effects of different variables on the wrist and elbow loadings. During this process, the torque activation levels i.e. hitting technique remained at the level used in the matching simulation. However, for a critical variable, for example location of ball impact, a different technique having lower joint torques or moments may be possible. This technique can be compared to the original technique and later can be checked whether it is realistic technique or not. To this end, an initial attempt was made to minimize the maximum wrist extension torque value for an off-centre impact. Initially, the objective function was the magnitude of the torque and this resulted in very low torque values. However, the wrist flexed unrealistically. Therefore, a penalty was included for higher wrist flexion angles. Better results were obtained but this time the motion of the racket within the hand was not realistic. As a result, more specific bounds for the grip conditions and a better control of wrist flexion are needed. Once these problems are solved, the model could be used to investigate whether it is possible to reduce

loadings at the wrist and/or elbow. In a similar way, instead of considering maximum loadings a variable related to the performance could be used. For example, a technique to obtain maximum outbound velocity could be searched for.

The effects of different hitting techniques can also be examined using the model. The initial joint angles can be perturbed together or individually (as it has been done for the wrist flexion angle) to see the effects of different configurations at impact. In addition, the activation of several muscle groups can be altered to imitate fatigue or injury for that muscle group and the effects of this can be observed without changing the torque activation parameters of other muscle groups. Furthermore, a technique, compensating for the negative effects of injured muscle groups without increasing the severity of injury can be sought.

In the future, this subject-specific model can be used for different players either by collecting data for a number of players or by building a generic version of the model and scaling it. Then, different players and techniques could be easily compared.

Moreover, forehand or service strokes may be investigated with the model after supplying and matching necessary kinematic data.

8.5 Conclusion

The torque-driven simulation model developed in this study has been evaluated successfully and used to investigate the effects of several variables belonging to the racket and the player on the kinetics and kinematics of the wrist and elbow during one-handed backhand groundstrokes. A discussion of the results has been presented along with the limitations and possible improvements of the model. The results from the developed simulation model showed that off-centre impacts substantially increase the risk of injury by increasing the net torques at the wrist by up to seven times. The moment of inertia, the mass of the racket and grip tightness also had considerable effects on the loadings at wrist and elbow. In contrast, the racket frame flexibility and soft tissue movement in the arm had negligible influence on the wrist and elbow. This study suggests that due to high torques obtained in the wrist extensors, the off-centre impacts below the longitudinal axis of the racket may

be a substantial contributing factor for 'tennis elbow'. In the future, the model can be used for further investigations on the technique of the backhand stroke.

REFERENCES

Altchek, D. W. (2002). Shoulder injuries in tennis. *Tennis*. A. F. H. Renstrom, Blackwell Science: 248-261.

Anonymous (2008). Eletronic Code of Federal Regulations, GPO Access.

Bauer, J. A. and R. D. Murray (1999). Electromyographic patterns of individuals suffering from lateral tennis elbow. *Journal of Electromyography and Kinesiology* **9**(4): 245-252.

Blackwell, J. R. and K. J. Cole (1994). Wrist kinematics differ in expert and novice tennis players performing the backhand stroke: implications for tennis elbow. *Journal of Biomechanics* **27**(5): 509-516.

Brody, H. (1979). Physics of the tennis racket. *American Journal of Physics* **47**: 482-487.

Brody, H. (1981). Physics of the tennis racket II; the sweet spot. *American Journal of Physics* **49**: 816-819.

Brody, H. (1985). The Moment of Inertia of a Tennis Racket. *Physics Teacher* **23**(4): 213-216.

Brody, H. (1995). How Would a Physicist Design a Tennis Racket. *Physics Today* **48**(3): 26-31.

Brody, H. (1997). The physics of tennis. III. The ball-racket interaction. *American Journal of Physics* **65**(10): 981-987.

Brody, H. (2002). The tennis racket. *Tennis*. A. F. H. Renstrom, Blackwell Science: 29-38.

Brody, H., et al. (2002). *The Physics and Technology of Tennis*, Racquet Tech Publishing.

Brown, I. E. and G. E. Loeb (2001). *Toward the ultimate skeletal muscle model.* 25th Annual Meeting of the American Society of Biomechanics, San Diego, California.

Bruggeman, N. B., et al. (2003). Elbow, wrist and hand. *Textbook of Sports Medicine - Basic Science and Clinical Aspects of Sports Injury and Physical Activity*. M. Kjaer, M. R. Krogsgaard, et al, Blackwell Science: 739-772.

Carroll, R. (1981). Tennis elbow: incidence in local league players. *British Journal of Sports Medicine* **15**(4): 250-256.

Casolo, F., et al. (2000). On tennis equipment, impact simulation and stroke precision. *Tennis Science and Technology*. S. J. Haake and A. O. Coe, Blackwell Science Ltd: 83-90.

Challis, J. H. (1991) *Estimating Individual Muscle Forces in Human Movement.* PhD. Dissertation, Loughboroguh University of Technology.

Challis, J. H. and D. G. Kerwin (1992). Calculating upper limb inertial parameters. *Journal of Sports Sciences* **10**(3): 275-284.

Challis, J. H. and D. G. Kerwin (1993). An analytical examination of muscle force estimations using optimization techniques. *Proceedings of the Institution of Mechanical Engineers. Part H: Journal of Engineering in Medicine* **207**(3): 139-148.

Challis, J. H. and D. G. Kerwin (1994). Determining individual muscle forces during maximal activity: Model development, parameter determination, and validation. *Human Movement Science* **13**(1): 29-61.

Charlton, I. W. and G. R. Johnson (2000). *An interactive musculoskeletal model of the upper limb*. 3rd Conference of the International Shoulder Group, Newcastle upon Tyne, UK.

Cheng, E. J., et al. (2000). Virtual muscle: a computational approach to understanding the effects of muscle properties on motor control. *Journal of Neuroscience Methods* **101**(2): 117-130.

Chipperfield, A., et al. (1994). Genetic Algorithm Toolbox for use with Matlab. Users Guide. University of Sheffield, UK.

Chow, J. W., et al. (1999). Muscle activation during the tennis volley. *Medicine and Science in Sports and Exercise* **31**(6): 846-854.

Clarys, J. P. and M. J. Marfell-Jones (1986). Anthropometric prediction of component tissue masses in the minor limb segments of the human body. *Human Biology* **58**(5): 761-769.

Corana, A., et al. (1987). Minimizing Multimodal Functions of Continuous-Variables with the Simulated Annealing Algorithm. *ACM Transactions on Mathematical Software* **13**(3): 262-280.

Cordingley, L. P., et al. (2004). Measurement and modelling of hollow rubber spheres: surface-normal impacts. *Plastics, Rubber and Composites* **33**(2-3): 99-106.

Cross, R. (1997). The dead spot of a tennis racket. *American Journal of Physics* **65**(8): 754-764.

Cross, R. (1999a). Impact of a ball with a bat or racket. *American Journal of Physics* **67**(8): 692-702.

Cross, R. (1999b). Dynamic properties of tennis balls. *Sports Engineering* **2**(1): 23-33.

Davies, G. T. (2005) *Determination and Analysis of Dimensions of 'Feel' in tennis Ball Impacts*. PhD Dissertation, Loughborough University.

De Luca, C. J. (1997). The Use of Surface Electromyography in Biomechanics. *Journal of Applied Biomechanics* **13**(2): 135-163.

de Rugy, A. and D. Sternad (2003). Interaction between discrete and rhythmic movements: reaction time and phase of discrete movement initiation during oscillatory movements. *Brain Research* **994**(2): 160-174.

Delp, S. L. and J. P. Loan (1995). A graphics-based software system to develop and analyze models of musculoskeletal structures. *Computers in Biology and Medicine* **25**(1): 21-34.

Delp, S. L. and J. P. Loan (2000). A Computational Framework for Simulating and Analyzing Human and Animal Movement. *Computing in Science and Engineering* **2**(5): 46-55.

Dempster, W. T. (1955). *Space Requirements of the Seated Operator*. Wright Air Development Center, WADC-TR 55-159, Wright-Paterson Air Force Base, Ohio

Edman, K. A. (1988). Double-hyperbolic force-velocity relation in frog muscle fibres. *Journal of Physiology* **404**: 301-321.

Elliott, B. C. (1988). Biomechanics of the serve in tennis a biomedical perspective. *Sports Medicine* **6**(5): 285-294.

Epstein, M. and W. Herzog (2003). Aspects of skeletal muscle modelling. *Philosophical Transactions of The Royal Society of London. Series B, Biological Sciences* **358**(1437): 1445-1452.

Fairley, T. E. (1985). *Some measurements of tennis racket vibration and its transmission to the hand*. Human Response to Vibration, Derby, UK.

Flament, D., et al. (1999). Time course and temporal order of changes in movement kinematics during learning of fast and accurate elbow flexions. *Experimental Brain Research* **129**(3): 441-450.

Freund, H. J. and H. J. Büdingen (1978). Relationship between Speed and Amplitude of Fastest Voluntary Contractions of Human Arm Muscles. *Experimental Brain Research* **31**(1): 1-12.

Giangarra, C. E., et al. (1993). Electromyographic and cinematographic analysis of elbow function in tennis players using single- and double-handed backhand strokes. *American Journal of Sports Medicine* **21**(3): 394-399.

Glynn, J. A. (2007) *Investigation of Elbow Loading in One-Handed Tennis Backhand Groundstrokes Using Computer Simulation.* PhD. Dissertation, Loughborough University.

Goffe, W. L., et al. (1994). Global optimization of statistical functions with simulated annealing. *Journal of Econometrics* **60**: 65-99.

Goodwill, S. and S. J. Haake (2000). Modelling the impact between a tennis ball and racket using rigid body dynamics. *Tennis Science and Technology*. S. J. Haake and A. O. Coe, Blackwell Science Ltd: 49-56.

Goodwill, S. and S. J. Haake (2003). Modelling of an impact between a tennis ball and racket. *Tennis Science and Technology 2*. S. Miller, International Tennis Federation: 79-86.

Goodwill, S. R. and S. J. Haake (2001). Spring damper model of an impact between a tennis ball and racket. *Proceedings of the Institution of Mechanical Engineers Part C-Journal of Mechanical Engineering Science* **215**(11): 1331-1341.

Goodwill, S. R. and S. J. Haake (2004). Modelling of tennis ball impacts on a rigid surface. *Proceedings of the Institution of Mechanical Engineers Part C-Journal of Mechanical Engineering Science* **218**(10): 1139-1153.

Grood, E. S. and W. J. Suntay (1983). A joint coordinate system for the clinical description of three-dimensional motions: application to the knee. *Journal of Biomechanical Engineering* **105**: 136-144.

Gruber, K., et al. (1998). A comparative study of impact dynamics: wobbling mass model versus rigid body models. *J Biomech* **31**(5): 439-444.

Guler, H. C. (1998) *Biomechanical Modelling of Lower Extremity and Simulation of Foot during Gait.* PhD. Dissertation, Middle East Technical University.

Haake, S. J., et al. (2003a). Modelling of oblique tennis ball impacts on tennis surfaces. *Tennis Science and Technology 2*. S. Miller, International Tennis Federation: 133-137.

Haake, S. J., et al. (2003b). The dynamic impact characteristics of tennis balls with tennis rackets. *Journal of Sports Sciences* **21**(10): 839-850.

Hatze, H. (1976). Forces and duration of impact, and grip tightness during the tennis stroke. *Medicine and Science in Sports and Exercise* **8**(2): 88-95.

Hatze, H. (1983). Computerized optimization of sports motions: an overview of possibilities, methods and recent developments. *Journal of Sports Sciences* **1**: 3-12.

Hennig, E. M., et al. (1992). Transfer of tennis racket vibrations onto the human forearm. *Medicine and Science in Sports and Exercise* **24**(10): 1134-1140.

Herzog, W. (2000). Considerations on the Theoretical Modelling of Skeletal Muscle Contraction. *Skeletal Muscle Mechanics- from Mechanisms to Function*. W. Herzog, John Wiley & Sons: 89-94.

Hill, A. V. (1938). The heat of shortening and the dynamic constants of muscle. *Proceedings of the Royal Society of London. Series B, Biological Sciences* **126**: 136-195.

Hinrichs, R. N. (1985). Regression equations to predict segmental moments of inertia from antropometric measurements. *Journal of Biomechanics* **18**: 621-624.

Holzbaur, K. R. S., et al. (2005). A model of the upper extremity for simulating musculoskeletal surgery and analyzing neuromuscular control. *Annals of Biomedical Engineering* **33**(6): 829-840.

Hutchinson, M. R., et al. (1995). Injury surveillance at the USTA Boys' Tennis Championships: a 6-year study. *Medicine and Science in Sports and Exercise* **27**(6): 826.

Huxley, A. F. and R. Niedergerke (1954). Structural changes in muscle during contraction; interference microscopy of living muscle fibres. *Nature* **173**(4412): 971-973.

Huxley, A. F. (1957). Muscle structure and theories of contraction. *Progress in Biophysics and Biophysical Chemistry* **7**: 255-318.

Huxley, A. F. (2000). Cross-bridge Action: Present Views, Prospects, and Unknowns. *Skeletal Muscle Mechanics- from Mechanisms to Function*. W. Herzog, John Wiley & Sons: 7-31.

Huxley, H. and J. Hanson (1954). Changes in the cross-striations of muscle during contraction and stretch and their structural interpretation. *Nature* **173**(4412): 973-976.

Jenkins, D. B. (2002). *Hollinshead's Functional Anatomy of the Limbs and Back*, W.B. Saunders.

Jensen, E. J. (2002). Determination of discrete relaxation spectra using Simulated Annealing. *Journal of Non-Newtonian Fluid Mechanics* **107**: 1-11.

Karlsson, D. and B. Peterson (1992). Towards a model for force predictions in the human shoulder. *Journal of Biomechanics* **25**(2): 189-199.

Kelley, J. D., et al. (1994). Electromyographic and cinematographic analysis of elbow function in tennis players with lateral epicondylitis. *American Journal of Sports Medicine* **22**(3): 359-363.

Kibler, W. B. (2002). Pathophysiology of tennis injuries-an overview. *Tennis*. A. F. H. Renstrom, Blackwell Science.

King, M. A. (1998) *Contributions to Performance in Dynamic Jumps*. PhD. Dissertation, Loughborough University.

King, M. A. and M. R. Yeadon (2002). Determining Subject-Specific Torque Parameters for Use in a Torque-Driven Simulation Model of Dynamic Jumping. *Journal of Applied Biomechanics* **18**(3): 207-217.

Knudson, D. (1991). Forces on the hand in the tennis one-handed backhand. *International Journal of Sport Biomechanics* **7**: 282-292.

Knudson, D. and J. Blackwell (1997). Upper Extremity Angular Kinematics of the One-Handed Backhand Drive in Tennis Players With and Without Tennis Elbow. *International Journal of Sports Medicine* **18**(2): 79-82.

Kong, P. W. (2004) *Computer Simulation of the Takeoff in Springboard Diving*. PhD Dissertation, Loughborough University.

Lammer, H. and J. Kotze (2003). Materials and tennis rackets. *Materials in Sports Equipment*. M. Jenkins, Woodhead Publishing: 222-248.

Leigh, D. C. and W. Lu (1992). Dynamics of the interactions between ball, strings, and racket in tennis. *International Journal of Sport Biomechanics* **8**: 181-206.

Lemay, M. A. and P. E. Crago (1996). A dynamic model for simulating movements of the elbow, forearm, an wrist. *Journal of Biomechanics* **29**(10): 1319-1330.
Lewis, R. D. and J. M. M. Brown (1994). Influence of Muscle Activation Dynamics on Reaction-Time in the Elderly. *European Journal of Applied Physiology and Occupational Physiology* **69**(4): 344-349.
Lieber, R. L., et al. (1990). Architecture of selected wrist flexor and extensor muscles. *Journal of Hand Surgery [Am]* **15**(2): 244-250.
Lieber, R. L. and C. G. Brown (1992). Quantitative method for comparison of skeletal muscle architectural properties. *Journal of Biomechanics* **25**(5): 557-560.
Lieber, R. L., et al. (1992). Architecture of selected muscles of the arm and forearm: anatomy and implications for tendon transfer. *Journal of Hand Surgery [Am]* **17**(5): 787-798.
Lieber, R. L. (1993). Skeletal muscle architecture: implications for muscle function and surgical tendon transfer. *Journal of Hand Therapy* **6**(2): 105-113.
Lieber, R. L. and S. C. Bodine-Fowler (1993). Skeletal muscle mechanics: implications for rehabilitation. *Physical Therapy* **73**(12): 844-856.
Lieber, R. L. and J. Friden (2000). Functional and clinical significance of skeletal muscle architecture. *Muscle and Nerve* **23**(11): 1647-1666.
Lieber, R. L. and J. Friden (2001). Clinical significance of skeletal muscle architecture. *Clinical Orthopaedics and Related Search*(383): 140-151.
Lieber, R. L. (2002). *Skeletal Muscle Structure, Function, & Plasticity*, Lippincott Williams & Wilkins.
Liu, Y. K. (1983). Mechanical analysis of racket and ball during impact. *Medicine and Science in Sports and Exercise* **15**(5): 388-392.
Ljung, B. O., et al. (1999). Wrist extensor muscle pathology in lateral epicondylitis. *Journal of Hand Surgery [Br]* **24**(2): 177-183.
Maffulli, N., et al. (2003). Types and epidemiology of tendinopathy. *Clinics in Sports Medicine* **22**(4): 675-692.
Man, K. F., et al. (1996). Genetic Algorithms: Concepts and Applications. *Ieee Transactions on Industrial Electronics Ie* **43**(5): 519-534.
Maria, A. (1997). *Introduction to modeling and simulation*. Winter Simulation Conference, Atlanta, Georgia.
McLaughlin, T. M. and N. R. Miller (1980). Techniques for the evaluation of loads on the forearm prior to impact in tennis strokes. *Journal of Mechanical Design* **102**: 701-710.
Miller, S. (2006). Modern tennis rackets, balls, and surfaces. *British Journal of Sports Medicine* **40**(5): 401-405.
Mitchell, M. (1996). *An Introduction to Genetic Algorithms*, MIT Press.
Mitchell, S. R., et al. (2000a). Head speed vs. racket inertia in the tennis serve. *Sports Engineering* **3**(2): 99-110.
Mitchell, S. R., et al. (2000b). The influence of racket moment of inertia during the tennis serve: 3-dimensional analysis. *Tennis Science and Technology*. S. J. Haake and A. O. Coe, Blackwell Science Ltd.: 57-65.
Morrey, B. F. and E. Y. S. Chao (1976). Passive Motion of Elbow Joint - Biomechanical Analysis. *Journal of Bone and Joint Surgery* **58-A**(4): 501-508.
Murray, W. M. (1997) *The Functional Capacity of the Elbow Muscles: Anatomical Measurements, Computer Modelling, and Anthropometric Scaling*. PhD Dissertation, Northwestern University.

Needham, D. M. (1971). *Machina Carnis - The Biochemistry of Muscular Contraction in Its Historical Development*, Cambridge University Press.
Nelder, J. A. and R. Mead (1965). A Simplex-Method for Function Minimization. *Computer Journal* **7**(4): 308-313.
Neptune, R. R. and M. L. Hull (1999). A theoretical analysis of preferred pedaling rate selection in endurance cycling. *Journal of Biomechanics* **32**(4): 409-415.
Nesbit, S. M., et al. (2006). The effects of racket inertia tensor on elbow loadings and racket behavior for central and eccentric impacts. *Journal of Sports Science and Medicine* **5**: 304-317.
Nirschl, R. P. and E. S. Ashman (2003). Elbow tendinopathy: tennis elbow. *Clinics in Sports Medicine* **22**(4): 813-836.
Oreskes, N., et al. (1994). Verification, Validation, and Confirmation of Numerical Models in the Earth Sciences. *Science* **263**(5147): 641-646.
Pain, M. T. and J. H. Challis (2001). The role of the heel pad and shank soft tissue during impacts: a further resolution of a paradox. *Journal of Biomechanics* **34**(3): 327-333.
Pain, M. T. and J. H. Challis (2006). The influence of soft tissue movement on ground reaction forces, joint torques and joint reaction forces in drop landings. *Journal of Biomechanics* **39**(1): 119-124.
Pandy, M. G., et al. (1990). An optimal control model for maximum-height human jumping. *Journal of Biomechanics* **23**(12): 1185-1198.
Pandy, M. G. and R. E. Barr (2002). Biomechanics of the Musculoskeletal System. *Standard Handbook of Biomedical Engineering & Design*. M. Kutz, McGraw-Hill.
Pandy, M. G. (2003). Simple and complex models for studying muscle function in walking. *Philosophical Transactions of The Royal Society of London. Series B, Biological Sciences* **358**(1437): 1501-1509.
Pierrynowski, M. R. (1995). Analytical Representation of Muscle Line of Action and Geometry. *Three Dimensional Analysis of Human Movement*. P. Allard, I. A. F. Stokes and J. P. Blanchi, Human Kinetics.
Pluim, B. M., et al. (2007). Health benefits of tennis. *British Journal of Sports Medicine* **41**(11): -.
Raikova, R. (1992). A general approach for modelling and mathematical investigation of the human upper limb. *Journal of Biomechanics* **25**(8): 857-867.
Raikova, R. (1996). A model of the flexion-extension motion in the elbow joint some problems concerning muscle forces modelling and computation. *Journal of Biomechanics* **29**(6): 763-772.
Reece, L. A., et al. (1986). Injuries to elite young tennis players at the Australian Institute of Sport. *Australian Journal of Science and Medicine in Sports* **118**(4): 11-15.
Renstrom, A. F. H. (2002). Elbow injuries in tennis. *Tennis*. A. F. H. Renstrom, Blackwell Science: 233-247.
Retlig, A. C. (2002). Hand and wrist injuries in tennis. *Tennis*. A. F. H. Renstrom, Blackwell Science: 223-232.
Riek, S., et al. (1999). A simulation of muscle force and internal kinematics of extensor carpi radialis brevis during backhand tennis stroke: implications for injury. *Clinical Biomechanics* **14**(7): 477-483.
Roetert, E. P. (2000). Muscle activity in tennis. *Tennis Science and Technology*. S. J. Haake and A. O. Coe, Blackwell Science Ltd.

Runciman, R. J. and A. C. Nicol (1994). Modelling muscle and joint forces at the glenohumeral joint: overview of a current study. *Proceedings of the Institution of Mechanical Engineers. Part H: Journal of Engineering in Medicine* **208**(2): 97.

Santini, A. J. A. and S. P. Frostick (2002). How should you treat tennis elbow? *Evidence-based Sports Medicine*. D. MacAuley and T. M. Best, BMJ Books: 351-367.

Schnek, D. J. (1992). *Mechanics of Muscle*, New York University Press.

Scott, S. H. and D. A. Winter (1991). A comparison of three muscle pennation assumptions and their effect on isometric and isotonic force. *Journal of Biomechanics* **24**(2): 163-167.

Shier, D., et al. (2002). *Hole's Human Anatomy & Physiology*. New York, McGraw-Hill.

Snijders, C. J., et al. (1987). Provocation of epicondylalgia lateralis (tennis elbow) by power grip or pinching. *Medicine and Science in Sports and Exercise* **19**(5): 518-523.

Van der Helm, F. C., et al. (1992). Geometry parameters for musculoskeletal modelling of the shoulder system. *Journal of Biomechanics* **25**(2): 129-144.

Van der Helm, F. C. (1994a). A finite element musculoskeletal model of the shoulder mechanism. *Journal of Biomechanics* **27**(5): 551-569.

Van der Helm, F. C. (1994b). Analysis of the kinematic and dynamic behaviour of the shoulder mechanism. *Journal of Biomechanics* **27**(5): 527-550.

Van Gheluwe, B. and M. Hebbelinck (1986). Muscle actions and ground reaction forces in tennis. *International Journal of Sport Biomechanics* **2**: 88-99.

Van Soest, A. J., et al. (1993). The influence of the biarticularity of the gastrocnemius muscle on vertical-jumping achievement. *Journal of Biomechanics* **26**(1): 1-8.

Veeger, H. E. (2000). The position of the rotation center of the glenohumeral joint. *Journal of Biomechanics* **33**(12): 1711-1715.

Wang, L., et al. (1998). *Kinematics of upper limb and trunk in tennis players using single handed backhand strokes*. Proceedings of the XVI. International Symposium of Biomechanics in Sports, University of Konstanz, Germany.

Widing, M. A. B. and M. H. Moeinzadeh (1990). Finite element modeling of a tennis racket with variable string patterns and tensions. *International Journal of Sport Biomechanics* **6**: 78-91.

Wood, G. A. and L. S. Jennings (1979). Use of Spline Functions for Data Smoothing. *Journal of Biomechanics* **12**(6): 477-479.

Yeadon, M. R. (1984) *The Mechanics of Twisting Somersaults*. PhD Dissertation, Loughborough University of Technology.

Yeadon, M. R. (1990a). The simulation of aerial movement - II: A mathematical inertia model of the human body. *Journal of Biomechanics* **23**: 67-74.

Yeadon, M. R. (1990b). The simulation of aerial movement - I: The determination of orientation angles from film data. *Journal of Biomechanics* **23**: 59-66.

Yeadon, M. R., et al. (2006). Modelling the maximum voluntary joint torque/angular velocity relationship in human movement. *Journal of Biomechanics* **39**(3): 476-482.

Yue, Z. and J. Mester (2002). A model analysis of internal loads, energetics, and effects of wobbling mass during the whole-body vibration. *Journal of Biomechanics* **35**(5): 639-647.

Zajac, F. E. (1989). Muscle and tendon: properties, models, scaling, and application to biomechanics and motor control. *Critical Reviews in Biomedical Engineering* **17**(4): 359-411.

APPENDICES

A1 – Calculation of net joint torques at the torque generators

A2 – Definition and calculation of joint angles from Vicon data

A3 – Anthropometric measurements for segmental inertia parameters

A4 – Subject informed consent

A1 – Calculation of Net Joint Torques at the Torque Generators

```
      SUBROUTINE SFOSUB ( ID, TIME, PAR, NPAR, DFLAG,
     &                    IFLAG, VALUE )

!
!           el ve raket arasindaki torklar eklendi
!           written by Behzat B Kentel
!           last modified: 24/09/2007
!           gecici olarak vartor eklendi 18/10/07
!           ecc-conc ayriminda flexor ve extensor icin ayri ind eklendi. 04/12/07
!           write output torqdrive subroutine'i icine alindi
!           vart duzenlendi 27/12/07
!           varang yeniden duzenlendi 03/01/08
!           Varang tekrar duzenlendi 18/01/08
!           vart ve varang yeniden duzenlendi 26/03/08
!           varang duzenlendi 01/04/08
!           tut'a yay kuvveti eklendi 09/04/08
!           varang ve tut yeniden duzenlendi 18/04/08
!           varang duzenlendi sf ve ser icin carpma sonrasi yeni parametre eklendi. 27/05/08
!           vart'a yeni parametre eklendi. 12/08/08
!           tut'a her kuvvet icin tum k ve c'ler eklendi. 26/08/08
!
            implicit none
C
C === Type and dimension statements ==========================================
C
C Note: For machines with 60 or more bits per word,
C       substitute "REAL" for "DOUBLE PRECISION".
C
C --- External variable definitions ----------------------------
C
      INTEGER               ID
      DOUBLE PRECISION      TIME
      DOUBLE PRECISION      PAR( * )
      INTEGER               NPAR
      LOGICAL               DFLAG
      LOGICAL               IFLAG
      DOUBLE PRECISION      VALUE
C
C ID      Identifier of calling SFORCE statement
C TIME    Current time
C PAR     Array of passed statement parameters
C NPAR    Number of passed parameters
C DFLAG   Differencing flag
C IFLAG   Initialization pass flag
C VALUE   The SFORCE value returned to ADAMS
C
C --- Local variable definitions -------------------------------
C
            double precision tor,ang(2),angw,pi,ke(10),kf(10),wrcorr,
     *jang29(2),mange29(2),mangf29(2),mangwe29(2),mangwf29(2),tor29,
     *jang30(2),mange30(2),mangf30(2),mangwe30(2),mangwf30(2),tor30,
     *jang31(2),mange31(2),mangf31(2),mangwe31(2),mangwf31(2),tor31,
     *jang32(2),mange32(2),mangf32(2),mangwe32(2),mangwf32(2),tor32,
     *jang33(2),mange33(2),mangf33(2),mangwe33(2),mangwf33(2),tor33,
```

```
     *jang34(2),mange34(2),mangf34(2),mangwe34(2),mangwf34(2),tor34,
     *jang35(2),mange35(2),mangf35(2),mangwe35(2),mangwf35(2),tor35,
     *z29(2),z30(2),z31(2),z32(2),z33(2),z34(2),z35(2),inde(7),indf(7)

          integer acop(2)
          logical errflg

          common /m29/ jang29,mange29,mangf29,mangwe29,mangwf29,tor29,z29
          common /m30/ jang30,mange30,mangf30,mangwe30,mangwf30,tor30,z30
          common /m31/ jang31,mange31,mangf31,mangwe31,mangwf31,tor31,z31
          common /m32/ jang32,mange32,mangf32,mangwe32,mangwf32,tor32,z32
          common /m33/ jang33,mange33,mangf33,mangwe33,mangwf33,tor33,z33
          common /m34/ jang34,mange34,mangf34,mangwe34,mangwf34,tor34,z34
          common /m35/ jang35,mange35,mangf35,mangwe35,mangwf35,tor35,z35
          common /index/ inde,indf

C
C === Executable code ==========================================================
C
          if (iflag) then
                z29 = (/-2,-1/); z30 = z29; z31 = z29; z32 = z29
                z33 = z29; z34 = z29; z35 = z29
                jang29 = (/0,0/); jang30 = jang29; jang31 = jang29
                jang32 = jang29; jang33 = jang29; jang34 = jang29
                jang35 = jang29
                inde = (/1,-1,-1,-1,1,1,-1/)
                indf = (/-1,1,-1,1,-1,-1,1/)

!               open(29,file='output29.csv',form='formatted')
!               open(30,file='output30.csv',form='formatted')
!               open(31,file='output31.csv',form='formatted')
!               open(32,file='output32.csv',form='formatted')
!               open(33,file='output33.csv',form='formatted')
!               open(34,file='output34.csv',form='formatted')
!               open(35,file='output35.csv',form='formatted')
!               open(55,file='test.csv',form='formatted')
          end if

          pi  = 4*ATAN(1.0D0)

C
C Call SYSFNC to collect information for calculations
C below. Note: if IFLAG is true, these calls are
C actually setting functional dependencies.
C

          time = time+0.237    !start at the impact time


          select case (id)
          case (29)                              !elbow extension/flexion torque

                if (z29(2).eq.time) then
                      go to 129
                else if (z29(2).gt.time) then
                      z29(2) = time
                      mange29(2) = mange29(1)
                      mangf29(2) = mangf29(1)
                      mangwe29(2) = mangwe29(1)
                      mangwf29(2) = mangwf29(1)
```

```
                else
                        z29(1) = z29(2)
                        z29(2) = time
                        jang29(1) = jang29(2)
                        mange29(1) = mange29(2)
                        mangf29(1) = mangf29(2)
                        mangwe29(1) = mangwe29(2)
                        mangwf29(1) = mangwf29(2)
                endif

829             ang(1) = pi-jang29(1)
                call sysfnc('AZ',(/125, 123/),2,jang29(2),errflg) !joint angle from ADAMS
                call sysfnc('WZ',(/125, 123, 123/),3,angw,errflg)!j ang vel from ADAMS
                !125 = ej1.yrot; 123 = hum.ejc
                ang(2) = pi-jang29(2)  !converting angle and ang vel
                angw = -angw

                ke(1) = 51.953   !T0 (Nm)
                ke(2) = 72.734   !Tmax (Nm)
                ke(3) = 18.454   !wmax (rad/s)
                ke(4) = 5.549    !wc (rad/s)
                ke(5) = 0.234    !q
                ke(6) = 4.638    !thetaopt (rad)
                ke(7) = 0.927    !amin
                ke(8) = 0.031    !m
                ke(9) = -1.174   !w1 (rad/s)
                ke(10) = 280.3   !kt (Nm/rad)

                kf(1) = 75.817
                kf(2) = 106.144
                kf(3) = 18.095
                kf(4) = 5.428
                kf(5) = 0.026
                kf(6) = 0.325
                kf(7) = 0.96
                kf(8) = 0.16
                kf(9) = -1.527
                kf(10) = 651.5

                acop = (/1,0/)   !select agonist-antagonist

                call torqdrive(ang,angw,par,ke,kf,mange29(2),mangf29(2),
      *mangwe29(2),mangwf29(2),z29,tor29,acop,id)

129             tor = tor29

                ..................................................


        case (35)       !shoulder internal/external rotation torque

                if (z35(2).eq.time) then
                        go to 135
                else if (z35(2).gt.time) then
                        z35(2) = time
                        mange35(2) = mange35(1)
                        mangf35(2) = mangf35(1)
                        mangwe35(2) = mangwe35(1)
                        mangwf35(2) = mangwf35(1)
                else
```

```
                z35(1) = z35(2)
                z35(2) = time
                jang35(1) = jang35(2)
                mange35(1) = mange35(2)
                mangf35(1) = mangf35(2)
                mangwe35(1) = mangwe35(2)
                mangwf35(1) = mangwf35(2)
            endif

            ang(1) = pi/2 - jang35(1)
            call sysfnc('AZ',(/110, 109/),2,jang35(2),errflg) !joint angle from ADAMS
            call sysfnc('WZ',(/110, 109, 109/),3,angw,errflg)!j ang vel from ADAMS
            !110 = hum.sjc; 109 = sj2.hum
            ang(2) = pi/2 - jang35(2)  !converting angle and ang vel
            angw = -angw

            ke(1) = 42.665   !T0 (Nm)
            ke(2) = 59.73    !Tmax (Nm)
            ke(3) = 19.471   !wmax (rad/s)
            ke(4) = 9.711    !wc (rad/s)
            ke(5) = 0.048    !q
            ke(6) = 5.902    !thetaopt (rad)
            ke(7) = 0.786    !amin
            ke(8) = 0.17     !m
            ke(9) = 0.393    !w1 (rad/s)
            ke(10) = 603.1   !kt (Nm/rad)

            kf(1) = 33.748
            kf(2) = 47.248
            kf(3) = 18.0
            kf(4) = 7.2
            kf(5) = 0.1
            kf(6) = 0.896
            kf(7) = 0.9
            kf(8) = 1.0
            kf(9) = 0.0
            kf(10) = 113.7

            acop = (/0,1/)

            call torqdrive(ang,angw,par,ke,kf,mange35(2),mangf35(2),
     *mangwe35(2),mangwf35(2),z35,tor35,acop,id)

135         tor = tor35

        case default      !gripping torque around racket axes

            call tut(tor,time,par,id)

        end select
C
C Assign the returned value
C
    VALUE = tor*1000


    RETURN
    END
C
*****************************************************************
```

```
C
      subroutine tut(torq,time,cx,id)

      implicit none

      double precision torq,time,cx(13),pi,
     *rr(3),wr(3),tt(3),kt(3),cr(3),r0(3),dr(3),rri(3),wd(3),inv(3,3),
     *s1,c1,s2,c2
      integer id,ns,istat,i
      logical errflg

      pi = 4*ATAN(1.0D0)

      call vart(torq,cx,time)

!     if (id.eq.90) then
!     write (id,267) time,torq
!     end if

      CALL sysary ('RDISP',(/141, 447/), 2, rri, NS, ERRFLG)
      CALL RCNVRT ('EULER', rri, 'B213', rr, ISTAT)
      rr = mod(rr+pi,2*pi)-pi
      call sysary('RVEL',(/141, 447, 447/),3,wr,ns,errflg)



267   format(f14.12,1x,14f17.8)

      kt = cx(8:10)
      cr = cx(11:13)
c     r0 = (/-0.57505, -0.63539, -0.31542/)  ! it = 0.239
      r0 = (/-0.58583, -0.63194, -0.29585/)        ! it = 0.237
c     r0 = (/-0.6423, -0.6189, -0.2506/)    ! it = 0.237 actual vicon data

      s1 = sin(rr(1))
      c1 = cos(rr(1))
      s2 = sin(rr(2))
      c2 = cos(rr(2))
      inv = reshape((/(s1*s2/c2),c1,(s1/c2),1.d0,0.d0,0.d0,
     *(c1*s2/c2),-s1,(c1/c2)/),(/3,3/))

      wd = matmul(inv,wr)
      dr = rr-r0

      do i = 1,3
            tt(i) = -(kt(i)*dr(i)+cr(i)*wd(i)*abs(dr(i)))*-1
      end do

!     tt = -(kt*dr+cr*wd*abs(dr))*-1

      if (time.lt.0.237001) tt=0

!     if (id.eq.92) then
!           write(55,267) time,dr,wd
!     end if

      select case (id)
      case  (90,91)
            torq = torq-(tt(2)*cos(dr(1))+tt(3)*cos(dr(2))*sin(dr(1)))
      case  (88,89)
```

```
            torq = torq+tt(1)-tt(3)*sin(dr(2))
        case  (92,93)
            torq = torq-(tt(3)*cos(dr(2))*cos(dr(1))-tt(2)*sin(dr(1)))
        end select

        select case (id)
        case  (89,91,93)
            torq= -torq
        end select

        return
        end
C
*********************************************************************
C
    SUBROUTINE vart(f,cc,time)

    double precision f,cc(13),s1,s2,l1,l2,t1,t2,l3,time,angq,it

            s1 = cc(1)
            t1 = cc(2)
            l1 = cc(3)
            l2 = cc(4)
            s2 = cc(5)
            t2 = cc(6)
            l3 = cc(7)

            it = 0.237D0
            if (l3.eq.0) l3 = l2

            if (time.lt.it) then
                if (time.le.(s1+t1)) then
                    f = angq(s1,(s1+t1),l1,l2,time)
                    if (l1.le.l2.and.f.lt.l1) f = l1
                    if (l1.gt.l2.and.f.gt.l1) f = l1
                else
                    f = l2
                end if
            else
                if (time.le.s2) then
                    f = l3
                else if (time.le.(s2+t2)) then
                    f = angq(s2,(s2+t2),l3,0.d0,time)
                else
                    f = 0
                end if
            end if

        if (f.eq.0) f = 1D-8

    return
    end
c
*********************************************************************
C
        SUBROUTINE TORQDRIVE(ang,angw,par,ke,kf,mange,mangf,
    *           mangwe,mangwf,zz,tor,acop,id)

        implicit none
```

```
      double precision ang(2),angw,tor,zz(2),par(18),ce(9),cf(9),
     *ke(10),mange,mangwe,ketor,
     *kf(10),mangf,mangwf,kftor
            integer id,acop(2)

            ce = par(1:9)
            cf = par(10:18)

      call torque(ketor,ce,ke,ang,angw,mange,mangwe,1,acop(1),zz,id)
      call torque(kftor,cf,kf,ang,angw,mangf,mangwf,2,acop(2),zz,id)

      tor = ketor - kftor

c           write(id,215) zz(2),tor,ketor,kftor,ang(2),mange,mangf,
c     *angw,mangwe,mangwf
215   format(f14.12,1x,12f17.8)

            return
      end
C
*****************************************************************
C
      SUBROUTINE varang(f,cc,time,acop)

      double precision f,cc(9),s1,s2,s3,t3,l1,l2,l3,lx,t1,t2,f1,f2,
     *time,angq,it
            integer acop

            s1 = cc(1)
            t1 = cc(2)
            l1 = cc(3)
            l2 = cc(4)
            s2 = cc(5)
            t2 = cc(6)
            s3 = cc(7)
            t3 = cc(8)
            l3 = cc(9)

            it = 0.237D0

            if (acop.eq.1) then
                  if (time.lt.it) then
                        f1 = angq(s1,(s1+t1),0D0,l2,time)
                        f2 = l2-angq(s2,(s2+t2),0D0,l2,time)
                        if (s2.ge.(s1+t1)) then
                              if (time.le.(s1+t1)) then
                                    f = f1
                                    if (f.lt.l1) f = l1
                              else if (time.lt.s2) then
                                    f = l2
                              else if (time.lt.(s2+t2)) then
                                    f = f2
                              else
                                    f = 0
                              end if
                        else
                              if (time.le.s2) then
                                    f = f1
                                    if (f.lt.l1) f = l1
                              else if (time.lt.(s1+t1)) then
```

```
                                        if (f1.lt.l1) f1 = l1
                                        if (f1.le.f2) f = f1
                                        if (f2.lt.f1) f = f2
                                else if (time.lt.(s2+t2)) then
                                        f = f2
                                else
                                        f = 0
                                end if
                        end if
                else
                        if (l3.gt.0) then
                                lx = l3
                        else
                                if (((s1+t1).gt.it).and.((s1+t1).le.s2)) then
                                        lx = angq(s1,(s1+t1),0D0,l2,it)
                                else if (((s1+t1).gt.it).and.((s1+t1).gt.s2)) then
                                        lx = l2-angq(s2,(s2+t2),0D0,l2,it)
                                else if (s2.gt.it) then
                                        lx = l2
                                else if ((s2+t2).gt.it) then
                                        lx = l2-angq(s2,(s2+t2),0D0,l2,it)
                                else
                                        lx = 0
                                end if
                        end if
                        if (time.le.s3) then
                                f = lx
                        else if (time.lt.(s3+t3)) then
                                f = lx-angq(s3,(s3+t3),0D0,lx,time)
                        else
                                f = 0
                        end if
                end if
        else if (acop.eq.0) then
                if (time.lt.it) then
                        f1 = 1-angq(s1,(s1+t1),l2,1D0,time)+l2
                        f2 = angq(s2,(s2+t2),l2,1D0,time)
                        if (s2.ge.(s1+t1)) then
                                if (time.le.(s1+t1)) then
                                        f = f1
                                        if (f.gt.l1) f = l1
                                else if (time.lt.s2) then
                                        f = l2
                                else if (time.lt.(s2+t2)) then
                                        f = f2
                                else
                                        f = 1
                                end if
                        else
                                if (time.le.s2) then
                                        f = f1
                                        if (f.gt.l1) f = l1
                                else if (time.lt.(s1+t1)) then
                                        if (f1.ge.f2) f = f1
                                        if (f2.gt.f1) f = f2
                                else if (time.lt.(s2+t2)) then
                                        f = f2
                                else
                                        f = 1
                                end if
```

```
                end if
            else
                if (l3.gt.0) then
                    lx = l3
                else
                    if (((s1+t1).gt.it).and.((s1+t1).le.s2)) then
                        lx = 1-angq(s1,(s1+t1),l2,1D0,it)+l2
                    else if (((s1+t1).gt.it).and.((s1+t1).gt.s2)) then
                        lx = angq(s2,(s2+t2),l2,1D0,it)
                    else if (s2.gt.it) then
                        lx = l2
                    else if ((s2+t2).gt.it) then
                        lx = angq(s2,(s2+t2),l2,1D0,it)
                    else
                        lx = l
                    end if
                end if
                if (time.le.s3) then
                    f = lx
                else if (time.lt.(s3+t3)) then
                    f = angq(s3,(s3+t3),lx,1D0,time)
                else
                    f = 1
                end if
            end if
    endif

        if (f.lt.0.01) f = 0.01

!       f = 1   !only for full activation for all muscles

    return
    end
c
*****************************************************************
c
c    Subroutine angq:-
c    angq is the monotonic quintic on the interval t0, t1. Which
c    takes end-point values f0,f1 and which has zero first and
c    second derivatives at the end points.
c ==============================================================
c
    double precision function angq(t0,t1,f0,f1,time)
    double precision f0,f1,t0,t1,z,time

    z = (time-t0)/(t1-t0)
    angq = f0 + (f1-f0)*(z*z*z)*((6*z*z) - (15*z) + 10)

    return
    end
c
*****************************************************************
c
    SUBROUTINE  TORQUE(torq,cc,k,ang,w,angmi,wmi,opt,ao,zz,id)

        implicit none

    DOUBLE PRECISION torq,torm,tors,mact,dact,ang(2),w,angs,grad,
   *k(10),p(6),m(3),kt,zz(2),h,cc(9),
   *angm,wm,angmi,wmi,it,
```

```
      *pi,rtd,dtr,inde(7),indf(7),ind
       integer iii,iv,opt,id,n1,n2,ao

            common /index/ inde,indf

       PI  = 4*ATAN(1.0D0)
       dtr = PI/180.0D0
       rtd = 180.0D0/PI
       iii    = 0
       grad   = 4.3

            p(1:6) = k(1:6)
            m(1:3) = k(7:9)

            kt = k(10)
            it = 0.237

            if(zz(2).le.0) then

c     calculate initial muscle angle
c     assume muscle angular velocity = joint angular velocity
c
                        if(opt.eq.1) wm = w
                        if(opt.eq.2) wm = -w
                        inde = 1
                        indf = 1

                        call diffact(dact,wmi,m)
                        call varang(mact,cc,zz(2),ao)
                        call imang(ang(2),wmi,angm,p,kt,mact,dact,opt,grad)

!                       write (id,767) zz(2),mact
767                     format(f14.12,1x,12f17.8)

c                       call angsec(angs,ang(2),angm,opt)
c                       tors = angs*kt
c                       call torquem(angm,wm,p,mact,dact,torm,grad)

                        angmi = angm
c                       wmi = wm
c
c           t > 0.0
c
       else


c
c           integrate to calculate new muscle angle
c     calculate the tendon angle and torque
c
                        h = zz(2)-zz(1)
                        n1 = 5        !ratio of Adams timesteps to muscle mechanics timesteps
                        n2 = 20       !ratio of concentric timesteps to eccentric timesteps


                        if (opt.eq.1) ind = inde(id-28)
                        if (opt.eq.2) ind = indf(id-28)
                        if (ind.lt.0) then
c                               write (id,*) n1*n2 !x4 for all RK steps
                                h = h/(n1*n2)
```

```
                    do iii = 1,n1*n2
                        call rk4(angmi,wmi,ang,w,h,(zz(1)+(iii-1)*h),k,cc,
   *opt,ao,zz,id)
                    end do
                else
c                   write(id,*) n1      !x4 for all RK steps
                    h = h/n1
                    do iv = 1,n1
                        call rk4(angmi,wmi,ang,w,h,(zz(1)+(iv-1)*h),k,cc,
   *opt,ao,zz,id)
                    end do
                endif
c
c   prevent the muscle angular velocity from being to negative
c
!               if (wmi<-20) wmi = -20

                if (zz(2).eq.it) then
                    select case (id*opt)
                    case (29)
                        angmi=3.56913;wmi=1.98331
                    case (30)
                        angmi=4.47936;wmi=-11.27852
                    case (31)
                        angmi=3.67652;wmi=-0.51615
                    case (32)
                        angmi=4.58755;wmi=-13.52033
                    case (33)
                        angmi=5.37653;wmi=1.39877
                    case (34)
                        angmi=4.27375;wmi=5.60206
                    case (35)
                        angmi=3.09176;wmi=-6.01958
                    case (58)
                        angmi=2.61799;wmi=-3.08494
                    case (60)
                        angmi=1.45958;wmi=8.91431
                    case (62)
                        angmi=0.99062;wmi=-2.35607
                    case (64)
                        angmi=0.63439;wmi=2.92136
                    case (66)
                        angmi=0.85212;wmi=-0.71063
                    case (68)
                        angmi=1.97975;wmi=-5.50334
                    case (70)
                        angmi=3.10797;wmi=4.25798
                    end select
                endif

    endif

        call angsec(angs,ang(2),angmi,opt)
        torq = kt*angs

    RETURN
    END
c
**********************************************************************
c
```

```
      SUBROUTINE     TORQUEM(angm,wm,p,acte,act,torm,grad)

      IMPLICIT none
            double precision p(6),t0,tmax,wmax,wc,k2,thetaopt,
     *wm,tc,C,torm,we,E,grad,act,angm,acte,crit

            t0 = p(1)
            tmax = p(2)
            wmax = p(3)
            wc = p(4)
            k2 = p(5)
            thetaopt = p(6)

      if(wm.gt.0.0) then
                  Tc = (t0*wc)/wmax
                  C = Tc*(wmax+wc)
                  torm = (C/(wm+wc)) - Tc
      endif

      if(wm.le.0.0) then
                  We = ((tmax-t0)/(grad*t0))*((wmax*wc)/(wmax+wc))
                  E = -(tmax-t0)*We
                  torm = (E/(We-wm))+tmax
      endif
            crit = 1-k2*(angm - thetaopt)**2
            if (crit.le.0.1) crit = 0.1
            torm = torm*act*crit*acte

      RETURN
      END
c
**********************************************************************
c
      SUBROUTINE     ANGSEC(angs,ang,angm,opt)

      IMPLICIT none
            double precision pi,angs,ang,angm
      integer opt

      pi  = 4*ATAN(1.0D0)

      if(opt.eq.1) angs = (2*PI) - ang - angm
      if(opt.eq.2) angs = ang - angm

      if(angs.le.0.00000) then
                  angs = 0.0D0
                  if(opt.eq.1) angm = (2*PI)-ang
                  if(opt.eq.2) angm = ang
      endif

      RETURN
      END
c
**********************************************************************
c
      SUBROUTINE     DIFFACT(dact,wm,m)
c
c     calculate differential activation
c
      IMPLICIT none
```

```
      double precision m(3),amin,mm,w1,we,wm,a,b,c1,dact

            amin = m(1)
            mm = m(2)
            w1 = m(3)

      we = wm - w1
      a = 1.0
      b = (mm/(wm-w1))-(1+amin)
      c1 = amin-((mm/(2*(wm-w1)))*(amin+1))

      if(we.gt.0.0) dact = (-b+SQRT(b**2-(4*a*c1)))/(2*a)

      if(we.eq.0.0) dact = (1+amin)/2

      if(we.lt.0.0) dact = (-b-SQRT(b**2-(4*a*c1)))/(2*a)

      RETURN
      END
c
*****************************************************************
c
      SUBROUTINE      IMANG(ang,wm,angm,p,kt,acte,act,opt,grad)
c
c     calculate initial muscle angle
c
      IMPLICIT none
            double precision p(6),pi,t0,tmax,wmax,wc,k2,thetaopt,wm,tc,c,pt,
     *act,we,grad,e,aa,acte,bb,kt,cs,ang,angm
      integer         opt

      pi  = 4*ATAN(1.0D0)

            t0 = p(1)
            tmax = p(2)
            wmax = p(3)
            wc = p(4)
            k2 = p(5)
            thetaopt = p(6)

      if(wm.gt.0.0) then
                  Tc = (t0*wc)/wmax
                  C  = Tc*(wmax+wc)
                  PT = ((C/(wm+wc))-Tc)*act
      else
                  We = ((tmax-t0)/(grad*t0))*((wmax*wc)/(wmax+wc))
                  E  = -(tmax-t0)*We
                  PT = ((E/(We-wm))+tmax)*act
      endif

       aa = PT*k2*acte
       bb = -PT*2*k2*thetaopt*acte-kt

            if(opt.eq.1) then
                  cs = (2*PI-ang)*kt - PT*(1-k2*thetaopt**2)*acte
      endif

      if(opt.eq.2) then
                  cs = ang*kt - PT*(1-k2*thetaopt**2)*acte
      endif
```

```
      angm = (-bb - SQRT((bb**2)-(4*aa*cs)))/(2*aa)

      RETURN
      END
c
*****************************************************************
c
      SUBROUTINE ROOT(k,angj,angm,timex,cc,opt,ao,w,id)

      IMPLICIT NONE

      double precision k(10),mact,cc(12),angj,timex,
     *t0,tmax,wmax,wc,k2,thopt,amin,mm,w1,a0,kt,angm,angs,con1,con2,
     *C,tc,we,E,grad,Q,R,tt,pi,rt(3),p(6),m(3),dact,kmax,k0,fang,
     *pm0,pm1,pm2,pm3,w,torm,tors,inde(7),indf(7),ss,sm,ksm,bm,cm,
     *dm,em,rm1,rm2

      integer i,opt,id,ao

      common /index/ inde,indf

      t0 = k(1)
      tmax = k(2)
      wmax = k(3)
      wc = k(4)
      k2 = k(5)
      thopt = k(6)
      amin = k(7)
      mm = k(8)
      w1 = k(9)
      kt = k(10)
      grad = 4.3
      p(1:6) = k(1:6)
      m(1:3) = k(7:9)
      ss = 0

      pi = 4*atan(1.0d0)
      call diffact(a0,0.0d0,m)
      k0 = t0*a0
      kmax = amin*tmax

      call angsec (angs,angj,angm,opt)
      call varang(mact,cc,timex,ao)
      fang = 1-k2*(angm - thopt)**2
      if (fang.lt.0.1d0) fang = 0.1
      tors = kt*angs
      con1 = tors/(mact*fang)

      sm = 0.99999
      ksm = kmax*sm
      if (con1.gt.ksm) then
            if (opt.eq.1) then
                  bm = kt*angj-2*pi*kt
            else
                  bm = -kt*angj
            endif
            cm = k2*mact
            dm = -2*cm*thopt
            em = cm*thopt**2-mact
```

```
            if (fang.eq.0.1) then
                  angm = (-0.1*mact*ksm-bm)/kt
            else
                  rm1 = (kt-ksm*dm-sqrt((ksm*dm-kt)**2-4*ksm*cm*
     *              (ksm*em-bm)))/(2*ksm*cm)

                  rm2 = (kt-ksm*dm+sqrt((ksm*dm-kt)**2-4*ksm*cm*
     *               (ksm*em-bm)))/(2*ksm*cm)

                  if ((abs(angm-rm1)/abs(angm-rm2)).le.1.0d0) then
                        angm = rm1
                  else
                        angm = rm2
                  endif
            endif
            con1 = ksm
            ss = -1
      endif

      if (con1.ge.k0) then
            if (opt.eq.1) inde(id-28) = -1
            if (opt.eq.2) indf(id-28) = -1
            we = ((tmax-t0)/(grad*t0))*((wmax*wc)/(wmax+wc))
            E = -(tmax-t0)*we
            con2 = 2*(-con1**2+con1*tmax*(1+amin)-tmax**2*amin)

            pm0 = E**2*(2*amin*w1+mm*(1+amin))+
     *       we**2*(tmax**2*mm*(1+amin)-2*con1*mm*tmax-con2*w1)+
     *       2*we*E*(w1*(2*tmax*amin-con1*(1+amin))+
     *       mm*(tmax*(1+amin)-con1))

            pm1 = -2*E**2*amin+2*we*mm*tmax*(2*con1-tmax*(1+amin))-
     *       (2*E)*((we+w1)*(2*tmax*amin-con1*(1+amin))+
     *       mm*(tmax*(1+amin)-con1))+con2*(we**2+2*we*w1)

            pm2 = mm*tmax*(-2*con1+tmax*(1+amin))+
     *       (2*E)*(2*tmax*amin-con1*(1+amin))-
     *       con2*(2*we+w1)

            pm3 = con2

      else
            if (opt.eq.1) inde(id-28) = 1
            if (opt.eq.2) indf(id-28) = 1
            tc = (t0*wc)/wmax
            C = tc*(wmax+wc)
            con2 = -2*(con1**2+con1*tc*(1+amin)+tc**2*amin)

            pm0 = C**2*(2*amin*w1+mm*(1+amin))+
     *       wc**2*(tc**2*mm*(1+amin)+2*con1*mm*tc-con2*w1)-
     *       2*wc*C*(w1*(2*tc*amin+con1*(1+amin))+
     *       mm*(tc*(1+amin)+con1))

            pm1 = -2*C**2*amin+2*wc*mm*tc*(2*con1+tc*(1+amin))+
     *       (2*C)*((wc-w1)*(2*tc*amin+con1*(1+amin))-
     *       mm*(tc*(1+amin)+con1))+con2*(wc**2-2*wc*w1)

            pm2 = mm*tc*(2*con1+tc*(1+amin))+
     *       (2*C)*(2*tc*amin+con1*(1+amin))+
     *       con2*(2*wc-w1)
```

```
            pm3 = con2

        endif

        pm0 = pm0/pm3; pm1 = pm1/pm3; pm2 = pm2/pm3

        Q = (pm2**2-3*pm1)/9
        R = (2*pm2**3-9*pm2*pm1+27*pm0)/54

        if ((Q**3-R**2).ge.0) then
            tt = acos(R/sqrt(Q**3))
            rt(1) = -2*sqrt(Q)*cos(tt/3)-pm2/3
            rt(2) = -2*sqrt(Q)*cos((tt+2*pi)/3)-pm2/3
            rt(3) = -2*sqrt(Q)*cos((tt+4*pi)/3)-pm2/3

            do i = 1,3
                call diffact(dact,rt(i),m)
                call torquem(angm,rt(i),p,mact,dact,torm,grad)
                if (abs(torm-tors).le.0.001) then
                    w=rt(i)
                    exit
                endif
            end do

        else
            w = -sign(1.0d0,R)*((sqrt(R**2-Q**3)+abs(R))**(1.0d0/3.0d0)+
     *      Q/(sqrt(R**2-Q**3)+abs(R))**(1.0d0/3.0d0))-pm2/3
            rt(1:3) = 0

        endif

c       if (id.eq.31) then
c           write(id,555) timex,angj,angm,angs,con1,k0,mact,fang,
c     *inde(id-28),indf(id-28),ss
c       endif

c       call diffact(dact,w,m)
c       call torquem(angm,w,p,mact,dact,torm,grad)
c
c       if (id.eq.35) then
c       write(55,555) timex,mact
c       endif

555     format (12f17.8)

        RETURN
        END

c
*****************************************************************
c
        SUBROUTINE          ANGJ(ang,w,zm,angx,zz)

        implicit none
        double precision ang(2),zz(2),w,td,t,zm,disp,wi,alpha,angx

        td = zz(2)-zz(1)
        disp = ang(2)-ang(1)
        wi = 2*disp/td-w
```

```
      alpha = 2*(w*td-disp)/(td**2)
      t = zm-zz(1)
      angx = ang(1)+wi*t+0.5*alpha*t**2

      RETURN
      END

c
**********************************************************************
c
      SUBROUTINE          RK4(angmi,wmi,ang,w,h,zm,k,cc,opt,ao,zz,id)

      implicit none
      double precision  angmi,wmi,w,zm,k1,k2,k3,k4,h,
     *angmix,angx,k(10),cc(12),ang(2),zz(2)
      integer opt,id,ao

      k1 = h*-wmi

      angmix = angmi+k1/2
      call angj(ang,w,(zm+h/2),angx,zz)  !assuming cnst acc btw ang1 and ang2
      call root(k,angx,angmix,(zm+h/2),cc,opt,ao,wmi,id)
      k2 = h*-wmi

      angmix = angmi+k2/2
      call root(k,angx,angmix,(zm+h/2),cc,opt,ao,wmi,id)

      k3 = h*-wmi

      angmix = angmi+k3
      call angj(ang,w,(zm+h),angx,zz)

      call root(k,angx,angmix,(zm+h),cc,opt,ao,wmi,id)
      k4 = h*-wmi

      angmi = angmi+(k1+2*k2+2*k3+k4)/6
      call root(k,angx,angmi,(zm+h),cc,opt,ao,wmi,id)

c     if (id.eq.33) then
c     write(id,777) zm+h,angx,angmi,wmi
c     endif

777   format (6f17.8)

      RETURN
      END
```

A2 – Definition and Calculation of Joint Angles

```
{*VICON BodyLanguage (tm) model*}
{*copyright 1995-1999 Oxford Metrics Ltd*}

{*issued: November 1999*}
{*Model **NEW_NAME**.MOD*}
{*Use only with BodyBuilder V. 3.53 or later*}
{*Use only with **NEW_NAME**.MP parameters and **NEW_NAME**.MKR*}

{*This file is supplied to illustrate the normal operation of BodyLanguage.
Oxford Metrics and Vicon Motion Systems accept no responsibility for its
correct operation*}

{* The results should however mimic VCM very closely, though the feet are
modelled a bit differently and the static parameter values are different *}

{* There are also more advanced modelling options available, using more markers
on the feet, and the option to leave off the wand markers. *}


{*Start of macro section*}
{*==========================*}
macro REPLACE4(p1,p2,p3,p4)
{*Replaces any point missing from set of four fixed in a segment*}
s234 = [p3,p2-p3,p3-p4]
p1V = Average(p1/s234)*s234
s341 = [p4,p3-p4,p4-p1]
p2V = Average(p2/s341)*s341
s412 = [p1,p4-p1,p1-p2]
p3V = Average(p3/s412)*s412
s123 = [p2,p1-p2,p2-p3]
p4V = Average(p4/s123)*s123
{* Now only replaces if original is missing  11-99 *}
p1 = p1 ? p1V
p2 = p2 ? p2V
p3 = p3 ? p3V
p4 = p4 ? p4V
endmacro

{*End of macro section*}



{*Initialisations*}
{*================*}


OptionalPoints(LTIB,RTIB)

Gorigin = {0,0,0}
Global = [Gorigin,{1,0,0},{0,0,1},xyz]


{*KINEMATICS*}
{*===========*}
```

```
If ExistAtAll(LTHI,RTHI,LTIB,RTIB) Then
        VCM = 1
Else
        VCM = 0
EndIf


{*Thorax segment*}
{*==============*}
Replace4(C7,T10,CLAV,STRN)
UThorax = (C7+CLAV)/2
LThorax = (T10+STRN)/2
FThorax = (CLAV+STRN)/2
BThorax = (C7+T10)/2

TRX0 = CLAV+0.5*(C7-CLAV)
Thorax = [TRX0,LThorax-UThorax,BThorax-FThorax,zyx]

ISHO = 300
LSJC = LSHO+(ISHO*{0,0,0.2}+{0,-$LateralShoulderOffset,0})*Attitude(Thorax)
RSJC = RSHO+(ISHO*{0,0,0.2}+{0,$LateralShoulderOffset,0})*Attitude(Thorax)


{*Head Segment*}
{*============*}
Replace4(LFHD,RFHD,RBHD,LBHD)
LHead = (LFHD+LBHD)/2
RHead = (RFHD+RBHD)/2
BHead = (LBHD+RBHD)/2
FHead = (LFHD+RFHD)/2

If $Static ==1 Then
        $HeadSize = DIST(FHead,BHead)
        PARAM($HeadSize)
EndIf

CHead = BHead+$MarkerDiameter*(FHead-BHead)/(2*$HeadSize)
Head = [CHead,LHead-RHead,FHead-BHead,yzx]

If $Static == 1 Then
        HeadRef = [CHead,LHead-RHead,-3(Global),yxz]
        If $StaticHeadLevel == 1 Then
                $HeadFlexOS = 1(<HeadRef,Head,yzx>)
        Else
                $HeadFlexOS = 0
        EndIf
        PARAM($HeadFlexOS)
EndIf

Head = ROT(Head,2(Head),$HeadFlexOS+$HeadTilt)

HeadSize = $HeadSize
HeadScale = {1.2,1.2,1.2}
HeadShift = {0,0,-0.1}



{*Clavicle Segments*}
{*================*}
```

```
LClavicle = [LSJC,0(Thorax)-LSJC,-1(Thorax),zyx]
RClavicle = [RSJC,0(Thorax)-RSJC,-1(Thorax),zyx]

LClavicleSize = DIST(0(LClavicle),0(Thorax))
LClavicleScale = {1,1,1}
LClavicleShift = {0,0,0}

RClavicleSize = DIST(0(RClavicle),0(Thorax))
RClavicleScale = {1,1,1}
RClavicleShift = {0,0,0}


{*Humerus Segments*}
{*================*}
If ExistAtAll(LWRA,RWRA)
        LWRI = (LWRA+LWRB)/2
        RWRI = (RWRA+RWRB)/2
EndIf

ElbowOS = ($MarkerDiameter+$ElbowWidth)/2

LHumerus = [LELB,LSHO+ElbowOS*2(Thorax)-LELB,LWRI-LELB,zyx]
RHumerus = [RELB,RSHO-ElbowOS*2(Thorax)-RELB,RWRI-RELB,zyx]

LEJC = CHORD(ElbowOS,LELB,LSJC,LELB-500*2(LHumerus))
REJC = CHORD(ElbowOS,RELB,RSJC,RELB+500*2(RHumerus))

LRadius = [LWRI,LWRA-LWRB,LEJC-LWRI,xyz]
RRadius = [RWRI,RWRA-RWRB,REJC-RWRI,xyz]

WristOS = ($MarkerDiameter+$WristThickness)/2

LWJC = LWRI-$WristThickness/2*1(LRadius)
RWJC = RWRI+$WristThickness/2*1(RRadius)

Jono = [RSJC,RSJC-TRX0,UThorax-LThorax,zxy]
LHumerus = [LEJC,LEJC-LSJC,LEJC-LELB,zxy] {* y towards centre *}
RHumerus = [REJC,REJC-RSJC,RELB-REJC,zxy]


{*Radius (and Ulnar) Segments*}
{*============================*}
LRadius = [LWJC,LWJC-LEJC,LWRB-LWRA,zxy] {* y towards centre *}
RRadius = [RWJC,RWJC-REJC,RWRA-RWRB,zxy]


{*Hand Segments*}
{*=============*}


If ExistAtAll(LFIN,RFIN)
        HandOS = ($MarkerDiameter + $HandThickness)/2
        LHND = CHORD(HandOS,LFIN,LWJC,LWJC-500*1(LRadius))
        RHND = CHORD(HandOS,RFIN,RWJC,RWJC-500*1(RRadius))
{*      LHand = [LWJC,LWJC-LHND,-1(LWrist),zyx]
        RHand = [RWJC,RWJC-RHND,-1(RWrist),zyx]
Else
        LHand = LWrist
        RHand = RWrist
*}
```

```
Endlf

LHand = [LWJC,LHND-LWJC,LWRB-LWRA,zxy] {* y towards body centre *}
RHand = [RWJC,RHND-RWJC,RWRA-RWRB,zxy]


{*Tennis Racket*}
{*==========*}
Replace4(TRHDA,TRHDB,TRHDC,TRHDD)
Mid1=(TRHDB+TRHDC)/2
Mid2=(TRHDA+TRHDD)/2
MidHead=(Mid1+Mid2)/2
TennisRacket=[MidHead,Mid1-Mid2,Mid1-TRHDA,yxz]


OUTPUT(RSJC,REJC,RWJC,TRX0,TRHDA,TRHDB,TRHDC,TRHDD,TRHNA,TRHNB)



{*Joint Angles*}
{*==========*}
{* See Euler Angles document for a detailed explanation *}
{* of the use of the <> angle function *}

{* First, find the general progression direction of the subject *}
{*============================================================*}


{*Thorax: Global >> Thorax*}
ThoraxAngles = -<Global,Thorax,yxz>
ThxA123 = -<Global,Thorax,xyz>
JonoAngles = -<Global,Jono,zyx>
Clav123 = -<Global,Jono,xyz>
JSA = -<Jono,RHumerus,yxz>

{*Shoulders: Thorax >> Humeri*}
LShoulderAngles = -<Thorax,LHumerus,yxz>
RShoulderAngles = <Thorax,RHumerus,yxz>(-1)
AbsRSA = -<Thorax,RHumerus,yxz>
RSA123 = -<Thorax,RHumerus,xyz>

{*Elbows: Humeri >> Radii*}
LElbowAngles = -<LHumerus,LRadius,yxz>
RElbowAngles = <RHumerus,RRadius,yxz>(-1) {* all joint angles wrt flexion/pronation/int. rot. *}
AbsREA = -<RHumerus,RRadius,yxz>
REA123 = -<RHumerus,RRadius,xyz>

{*Wrists: Radii >> Hands*}
LWristAngles = -<LRadius,LHand,yxz>
RWristAngles = <RRadius,RHand,yxz>(-1)
AbsRWA = -<RRadius,RHand,yxz>
RWA123 = -<RRadius,RHand,xyz>

{*Tennis Racket: RRadius >> Racket)*}
RacketAngles= -<RHand,TennisRacket,yxz>
RackAng123= -<RHand,TennisRacket,xyz>
RackAng312=-<RHand,TennisRacket,zxy>
RAng321= -<RHand,TennisRacket,zyx>
RacketGlobal123= -<Global,TennisRacket,xyz>
RAG= -<Global,TennisRacket,zyx>
```

OUTPUT(ThoraxAngles,AbsRSA,RShoulderAngles,AbsREA,RElbowAngles,AbsRWA,RWristAngl
es,JonoAngles,JSA)
OUTPUT(RacketAngles,RacketGlobal123,ThxA123,Clav123,RSA123,REA123,RWA123,RackAng1
23,RAng321,RAG,RackAng312)

A3 – Anthropometric Measurements for Segmental Inertia Parameters

NAME	Jim May	AGE	22	DATE	14/05/04

All measurements are in millimetres

TORSO

Level	hip	umbilicus	ribcage	nipple	shoulder	neck	→	nose	ear	top
Lenght	0	173	221	403	549	620	0	73	139	246
Perimeter	946	840	815	910		380		476	586	
Width	348	296	296	319	350					
Depth					181					

LEFT ARM

Level	shoulder	midarm	elbow	forearm	wrist	→	thumb	knuckle	nails
Lenght	0		308	376	587	0	52	94	186
Perimeter	367	272	262	260	179		253	205	101
Width					62		105	85	47

RIGHT ARM

Level	shoulder	midarm	elbow	forearm	wrist	→	thumb	knuckle	nails
Lenght	0		289	371	585	0	52	91	186
Perimeter	375	272	265	281	171		261	215	105
Width					64		105	87	49

LEFT LEG

Level	hip	crotch	midthigh	knee	calf	ankle	→	heel	arch	ball	nail
Lenght	0	80		451	643	912	0	33		155	231
Perimeter		558	488	364	378	233		325	252	247	134
Width										102	61
Depth								129			

RIGHT LEG

Level	hip	crotch	midthigh	knee	calf	ankle	→	heel	arch	ball	nail
Lenght	0	78		461	655	919	0	34		152	234
Perimeter		555	480	361	359	229		324	248	238	148
Width										100	63
Depth								131			

Height (mm)	1860	Weight (N)	740.7

A4 – Subject Informed Consent

Purpose

To obtain kinematic, kinetic and EMG data during the performance of selected tennis backhand strokes. To obtain subject specific inertia, body composition and joint torque parameters.

Procedures

The kinematic, kinetic and EMG data of the tennis backhand strokes will be obtained using:

- An automatic data collection system and two high-speed video cameras
- Tennis rackets instrumented with accelerometers and grip pressure sensors
- EMG data using surface electrodes attached to the arm holding the racket

A number of trials will be requested with suitable breaks to minimise fatigue and boredom.

The subject specific parameters will be obtained from:

- Anthropometric measurements (using tape measures and specialist anthropometers)
- Body composition measurements (using skinfold callipers)
- Joint torque profiles (using an isovelocity dynamometer)

During the measurements, more than one researcher will be present, at least one of who will be of the same sex as you.

Questions

The researchers will be pleased to answer any questions you may have at any time.

Withdrawal

You are free to withdraw from the study at any stage without having to give any reasons.

Confidentiality

Your identity will remain confidential in any material resulting from this work. Video recordings will be stored in the video analysis room to which access is restricted to members of the biomechanics research team. On occasion, video images may be required. In such an instance we will seek your written permission to use such images and you are perfectly free to decline.

I have read the outline of the procedures that are involved in this study, and I understand what will be required by me. I have had the opportunity to ask for further information and for clarification of the demands of each of the procedures and understand what is entailed. I am aware that I have the right to withdraw from the study at any time with no obligation to give reasons for my decision. As far as I am aware I do not have any injury or infirmity, which would be affected by the procedures outlined.

Name .....

Signed ..... (subject) Date .....

In the presence of: Name .....